



Natural computation, much ado about nothing

Pierre Baudot

► To cite this version:

Pierre Baudot. Natural computation, much ado about nothing. Neurons and Cognition [q-bio.NC]. Université Pierre et Marie Curie - Paris VI, 2006. English. NNT : . tel-00203712

HAL Id: tel-00203712

<https://theses.hal.science/tel-00203712>

Submitted on 11 Jan 2008

HAL is a multi-disciplinary open access archive for the deposit and dissemination of scientific research documents, whether they are published or not. The documents may come from teaching and research institutions in France or abroad, or from public or private research centers.

L'archive ouverte pluridisciplinaire **HAL**, est destinée au dépôt et à la diffusion de documents scientifiques de niveau recherche, publiés ou non, émanant des établissements d'enseignement et de recherche français ou étrangers, des laboratoires publics ou privés.



UNIVERSITE PARIS VI - PIERRE ET MARIE CURIE

**Doctorat
Sciences Cognitives**

Pierre Baudot

Computation naturelle,
beaucoup de bruit pour rien ?

Natural computation,
much ado about nothing?

Thèse dirigée par Yves Frégnac
Soutenue le 29 septembre 2006

Jury :

Prof. Ad Aertsen

Dr. Yves Frégnac

Dr. Guillaume Masson

Dr. Jean-Pierre Nadal

Prof. Alain Trembleau

Rapporteur

Examineur

Rapporteur

Examineur

Examineur



« Je pense donc Je suis »

René Descartes ©

Un jour,

Un jour, bientôt peut-être,

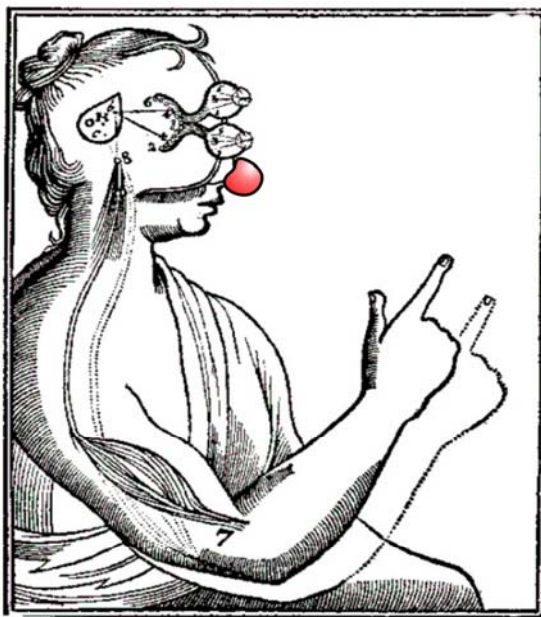
Un jour j'arracherai l'ancre qui
Avec la sorte de courage qu'il
Je lâcherai ce qui paraissait
Je le trancherai, je le
dégringoler.

D'un coup dégorgeant ma
combinaisons et
Vide de l'abcès d'être
nourricier.

A coups de ridicule, de
déchéance?), par éclatement.

Par vide, par une totale
j'expulserai de moi la forme
composée, coordonnée,
Et à mes semblables, si dignes,

Réduit à une humilité de
comme après une immense
Ramené au-dessous de toute



VISION Rene Descartes 1644

infime que je ne sais quelle idée-ambition m'avait fait désert.

Anéanti quant à la hauteur, quant à l'estime.

Perdu en un endroit lointain (ou même pas), sans nom, sans identité.

CLOWN, abattant dans la risée, dans l'esclaffement, dans le grotesque, le sens que contre toute lumière je m'étais fait de mon importance.

Je plongerai.

Sans bourse dans l'infini-esprit sous-jacent ouvert à tous, ouvert moi-même à une nouvelle et incroyable rosée.

A force d'être nul

Et ras

Et risible...

Clown.

tient mon navire loin des mers
faut pour être rien et rien que rien.
m'être indissolublement proche.
renverserai, je le romprai, je le ferai

misérable pudeur, mes misérables
enchaînements "de fil en aiguille"
quelqu'un, je boirai à nouveau l'espace

déchéances (qu'est-ce que la

dissipation-dérision-purgation,
qu'on croyait si bien attachée,
assortie à mon entourage
si dignes mes semblables.
catastrophe, à un nivellement parfait
trouille.

mesure à mon rang réel, au rang

« Maintenant, je m'encrapule le plus possible. Pourquoi ? Je veux être poète, et je travaille à me rendre Voyant : vous ne comprendrez pas du tout, et je ne saurais presque vous expliquer. Il s'agit d'arriver à l'inconnu par le dérèglement de tous les sens. Les souffrances sont énormes, mais il faut être fort, être né poète, et je me suis reconnu poète. Ce n'est pas du tout ma faute. C'est faux de dire : Je pense : on devrait dire : On me pense. - Pardon du jeu de mots. - Je est un autre. Tant pis pour le bois qui se trouve violon, et nargue aux inconscients, qui ergotent sur ce qu'ils ignorent tout à fait !

Car Je est un autre. Si le cuivre s'éveille clairon, il n'y a rien de sa faute. Cela m'est évident : j'assiste à l'éclosion de ma pensée : je la regarde, je l'écoute : je lance un coup d'archet : la symphonie fait son remuement dans les profondeurs, ou vient d'un bond sur la scène. Si les vieux imbéciles n'avaient pas trouvé du Moi que la signification fausse, nous n'aurions pas à balayer ces millions de squelettes qui, depuis un temps infini, ! ont accumulé les produits de leur intelligence borgnesse, en s'en clamant les auteurs ! En Grèce, ai-je dit, vers et lyres rythment l'Action. Après, musique et rimes sont jeux, délassements. L'étude de ce passé charme les curieux : plusieurs s'éjouissent à renouveler ces antiquités : - c'est pour eux. L'intelligence universelle a toujours jeté ses idées, naturellement ; les hommes ramassaient une partie de ces fruits du cerveau : on agissait par, on en écrivait des livres : telle allait la marche, l'homme ne se travaillant pas, n'étant pas encore éveillé, ou pas encore dans la plénitude du grand songe. Des fonctionnaires, des écrivains : auteur, créateur, poète, cet homme n'a jamais existé ! La première étude de l'homme qui veut être poète est sa propre connaissance, entière ; il cherche son âme, il l'inspecte, Il la tente, l'apprend. Dès qu'il la sait, il doit la cultiver ; cela semble simple : en tout cerveau s'accomplit un développement naturel ; tant d'égoïstes se proclament auteurs ; il en est bien d'autres qui s'attribuent leur progrès intellectuel ! - Mais il s'agit de faire l'âme monstrueuse : à l'instar des comprachicos, quoi ! Imaginez un homme s'implantant et se cultivant des verrues sur le visage. Je dis qu'il faut être voyant, se faire voyant. Le Poète se fait voyant par un long, immense et raisonné dérèglement de tous les sens. Toutes les formes d'amour, de souffrance, de folie ; il cherche lui-même, il épuise en lui tous les poisons, pour n'en garder que les quintessences. Ineffable torture où il a besoin de toute la foi, de toute la force surhumaine, où il devient entre tous le grand malade, le grand criminel, le grand maudit, - et le suprême Savant ! - Car il arrive à l'inconnu ! Puisqu'il a cultivé son âme, déjà riche, plus qu'aucun ! Il arrive à l'inconnu, et quand, affolé, il finirait par perdre l'intelligence de ses visions, il les a vues ! Qu'il crève dans son bondissement par les choses inouïes et innombrables : viendront d'autres horribles travailleurs ; ils commenceront par les horizons où l'autre s'est affaissé ! (...)

Donc le poète est vraiment voleur de feu. Il est chargé de l'humanité, des animaux même ; il devra faire sentir, palper, écouter ses inventions ; si ce qu'il rapporte de là-bas a forme, il donne forme si c'est informe, il donne de l'informe. Trouver une langue ; - Du reste, toute parole étant idée, le temps d'un langage universel viendra ! Il faut être académicien, - plus mort qu'un fossile, - pour parfaire un dictionnaire, de quelque langue que ce soit. Des faibles se mettraient à penser sur la première lettre de l'alphabet, qui pourraient vite ruer dans la folie ! Cette langue sera de l'âme pour l'âme, résumant tout, parfums, sons, couleurs, de la pensée accrochant la pensée et tirant. Le poète définirait la quantité d'inconnu s'éveillant en son temps dans l'âme universelle : il donnerait plus - que la formule de sa pensée, que la notation de sa marche au Progrès ! Enormité devenant norme, absorbée par tous, il serait vraiment un multiplicateur de progrès ! Cet avenir sera matérialiste, vous le voyez ; - Toujours pleins du Nombre et de l'Harmonie ces poèmes seront fait pour rester. - Au fond, ce serait encore un peu la Poésie grecque. L'art éternel aurait ses fonctions ; comme les poètes sont des citoyens. La Poésie ne rythmera plus l'action : elle sera en avant. »

Arthur Rimbaud, lettre du **Voyant** (à Paul Demeny, 15 mai 1871).

Acknowledgments

« Pour un tel inventaire
Il faudrait un Prevert »...

« ...Il faut aussi être très poli avec la terre
Il faut les remercier le matin en se réveillant
Il faut les remercier pour la chaleur
Pour les arbres
Pour les fruits
Pour tout ce qui est bon à manger
Pour tout ce qui est beau à regarder
A toucher
Il faut les remercier
Il ne faut pas les embêter...
Les critiquer
Ils savent ce qu'ils ont à faire
Le soleil et la terre
Alors il faut les laisser faire
Ou bien ils sont capables de se fâcher
Et puis après
On est changé
En courge
En melon d'eau
Ou en pierre à briquet
Et on est bien avancé... »
« En somme pour résumer
Deux points ouvrez les guillemets :
" Il faut que tout le monde soit poli avec le monde ou alors
il y a des guerres ... des épidémies des tremblements
de terre des paquets de mer des coups de fusil ...
Et de grosses méchantes fourmis rouges qui viennent vous
dévorer les pieds pendant qu'on dort la nuit. " »
Jacques Prévert, Histoires

Donc :

Donc merci à Yves Frègnac de m'avoir accueilli dans son laboratoire et de m'avoir supporté pendant ces 8 années.

Thanks Mr Aertsen, your scientific work has been guiding my labour all along my thesis. It is an immense pleasure and honour you accepted to read and comment the results.

Merci Mr Masson, pour l'interaction scientifique, l'accueil à Marseille, et d'avoir accepté de lire et corriger ma prose maladroite.

Merci Mr Nadal, pour m'avoir accueilli, aidé et avoir répondu présent gentiment, ainsi que pour vos travaux dont mon étude a essayé de s'inspirer. En espérant que ce document puisse vous intéresser.

Merci Mr Trembleau, de me faire l'honneur d'être dans mon jury, pour vos enseignements, votre franchise et votre compréhension.

Merci Cortico Magno, alias maître Fredo, pour m'avoir appris ce que je sais de l'électro et pis parce que t'es bo.

Merci Cyril pour ton exemple, ton aide, ta gentillesse et tes encouragements.

Merci Olivier et Manu, de m'avoir supporté et tant apporté (Belle et merveilleuse route à vous, en espérant que l'on se recroise sur d'autres bateaux).

Merci Gérard, merci mille fois, sans toi ce travail n'existerait pas, et tu as su en fondé les bases dans la gentillesse la douceur et l'humilité.

Merci Marc pour ton aide et ton amitié, faire ce bout de chemin avec toi fut plus qu'instructeur, ce fut un plaisir.

Merci à tous les zigotos, Alice la douce, Nazied la tigresse, Gilou le sioux, Christophe le dragon, Jo l'amazonien, GuiGui pop, Michèle the dark angel, Julien le quinquin, Vincent la ritournelle, Seb le grand, Peggy la souris (et tous les autres qui ont su rester du parti des Myosotis)... pour avoir mis le plein de ciel bleu, dans mes 3m² de plafond ou parfois il pleut. Vous rencontrer est ce qui pouvais m'arriver de mieux pendant mon séjour au laboratoire.

Merci Alain, Thierry, Dan, Michèle (la retraitée), Sylvie, Irina.

Merci Mr Atlan, de m'avoir accordé un peu de votre temps si gentiment (et pour le conseil)

Merci Mr Bennequin, toi qui m'as donné du feu quand... pour ton aide, ton soutien, et pour l'exemple (le plus beau bureau du monde !)

Merci Bruno pour l'enseignement de l'art de la bio et les petites fleurs du jura.

Merci aux chats pour leur bénévolat (en espérant qu'il ait servi à quelque chose)

Merci Meryou avant tout et pour tout !

Merci Papa & Maman Bodo sans qui rien n'aurait été possible (MERCI !!!!!!!)

Et merci à la musique d'être toujours là.

Contents

Acknowledgments.....	4
Contents.....	6
1. Abstract	10
2. Introduction	12
3. Results.....	16
3.1. Cortical Synaptic Receptive Fields: functional characterisation.....	16
3.1.1. Introduction	16
3.1.2. Spatio-temporal profile of visually evoked excitatory and inhibitory input... 16	
3.1.3. Synaptic integration field complexity	21
3.2. Orientation and direction selectivity of excitatory and inhibitory inputs in visual cortical neurons: a diversity of combinations produces spike tuning	30
3.2.1. Introduction	30
3.2.2. Results	33
3.2.3. Discussion.....	50
3.2.4. Experimental procedure	60
3.3. Center-surround interaction during apparent motion controls the timing of the responses and reveals a new motion direction selectivity in V1.....	64
3.3.1. Perceptual and cortical spatiotemporal interactions: the apparent motion paradigm	65
3.3.2. Center-surround apparent motion: protocol description.....	69
3.3.3. Excitatory effects of the apparent motion in the surround alone	71
3.3.4. Center-surround directional selectivity	73
3.3.5. Selective control of the timing of the responses by the Surround.....	75
3.3.6. Contrast dependency of the surround modulation and Surround impact on the SNR.....	79
3.3.7. Center-surround nonlinear control of the timing and contrast dependency..	84
3.3.8. Orientation selectivity of the surround-alone response and of the apparent motion center-surround modulation effect	87

3.3.9. Conclusion.....	89
3.4. Interlude: “What is the other 85% of V1 doing?” vs. “In praise of artifice”	102
3.5. Nature is the Code: reliable and efficient dissipation in V1	110
3.5.1. Computational principles in visual processing.....	111
3.5.2. A change in perspective: from information transfer to computation of complexity	112
3.5.3. Constrained dynamics in V1: low noise and temporal binary code	116
3.5.4. From dense input to sparse output through coincidence detection.....	121
3.5.5. Adaptation to external constraints reduces noise and redundancy.....	123
3.5.6. Recurrent network model of cortical computation.....	128
3.5.7. Material & Methods.....	130
3.5.8. Simulation of saccadic and fixational eye-movements scanpath	132
3.5.9. Time-frequency estimation of Signal-to-Noise Ratio	138
3.5.10. Evoked signal, noise, and total signal estimations as a function of the input complexity	143
3.5.11. Constrained cortical state and high SNR processing: a potential correlate to attentional and behavioral states	144
3.5.12. Ordered redundancies, computational capacity and structural complexity definition	147
3.6. Non-linear control of the temporal precision of the neural code by eye-movements dynamics in visual cortex.....	156
3.6.1. Summary	156
3.6.2. Introduction	156
3.6.3. Results	158
3.6.4. Conclusion.....	168
3.6.5. Methods.....	169
3.6.6. Supplementary figures	172
4. Conclusion.....	176
4.1. Much ado about nothing, still on the way of a thermodynamical theory of evolution and cognition: Knowledge is energy	176
4.1.1. Introduction	176
4.1.2. Systems information and complexity.....	176
4.1.3. Systems dynamic: Global “self-organisation” and local learning	192

4.2. Global conclusion: convergence and principles of cortical computation.....	206
4.2.1 Receptive field functional theory	206
4.2.2 Neural assembly theory and temporal binding (synchrony, β - γ oscillations)	209
4.2.3 Learning and adaptation theory	210
4.2.4 Efficient coding, informational theory and fluctuation-dissipation	210
4.2.5 Physical/thermodynamical theory of information and of cortical processing.....	212
4.2.6 Algorithmic and cybernetical theory	215
4.2.7 Active sensing theory	217
4.2.8 Conclusion.....	219
4.3 Redundancy and noise removing mechanisms in cortical areas.....	219
4.3.1 A generic neo-cortical code.....	220
4.3.2 Cortical areas as redundancy reduction modules	220
4.3.3 Cortical implementation of redundancy and noise reduction.....	224
4.3.4 Sharp neuronal assembly and redundancy reduction	227
4.3.5 Information, redundancy reduction and qualitative perception or attention.....	229
4.4 Natural computation: general self-organisation and adaptation physical laws ...	230
4.4.1 Redundancy, structure and organisational complexity (Logical Depth)	230
4.4.2 Toward a formal theory of evolution and cognition: reproducibility, differentiation, efficiency and diversity of living systems as a natural Maxent or Infomax process result	231
4.4.3 System computational capacity increase.....	235
4.4.4 Complex system modelisation and prediction	235
4.4.5 Living systems as a function: gain controls diversity and non-linear systems. So far from the line.....	236
4.4.6 Natural language and Human language: linguistic generalisation.....	237
4.4.7 Evolutionary Epistemology, history, and intelligence.....	238
4.4.8 Philosophical and epistemological debates	238
5. Bibliography.....	241

1. Abstract

The coding of the environmental information by the brain is subject to intense debate at the level of its biological implementation (functional properties) as well as at the level of its reliability, efficiency and precision. This study is based on *in-vivo* intracellular recordings of responses of primary visual cortex neurons to stimuli of various complexity including natural scene animated by eye-movements. We show that functional selectivity are generated by cortical recurrence notably by the excitation/inhibition balance expressed through a large diversity of combinatory of synaptic input functional selectivity. In natural condition with eye-movement, the observed code is highly reliable, binary and temporal and cortical computation is removing input redundancies. Nonlinearity or gain controls, which biphasic temporal profile sculpts the cortical responses, increase the temporal precision and reproducibility of the code. We propose a sketch of a statistical model of adaptation and self-organisation consisting in the maximisation of the mutual-information between the system and its environment. This model, based on a decomposition of entropy into ordered redundancy, is sufficient to account for some defining properties of living systems such as reliability, diversity/specialisation, and optimal or efficient coding.

Key words

Adaptation, cortex, reliability, nonlinearity, complexity, Receptive-field, neural assembly, efficient coding, perception, consciousness.

Résumé

Le codage de l'information environnementale par le cerveau est sujet à d'intenses débats tant au niveau de son implémentation biologique (propriété fonctionnelles) qu'au niveau de sa variabilité et de sa précision. Cette étude se base sur des enregistrements intracellulaires *in-vivo* des réponses des neurones du cortex visuel primaire à des stimuli de complexité variable incluant des images naturelles animées par des mouvements oculaires. Nous montrons que les propriétés fonctionnelles sont générées par la récurrence corticale, notamment par la balance excitation/inhibition exprimée au travers d'une grande diversité de combinatoire de sélectivité fonctionnelle des entrées synaptiques. En condition naturelle avec mouvement des yeux, nous montrons que le code est reproductible, binaire/temporel et que l'analyse corticale se traduit par une réduction des redondances présentes dans les entrées. Les interactions ou contrôles de gain corticaux, dont le profile temporel biphasique sculpte temporellement les réponses corticales, augmentent la précision temporelle et la reproductibilité du code. Nous proposons une ébauche de modèle statistique général d'adaptation et d'auto-organisation consistant en la maximisation de l'information mutuelle entre le système et son environnement. Ce modèle, basé sur une décomposition microscopique de l'entropie en ordre de redondance, est suffisant pour rendre compte des propriétés singulières de l'organisation du vivant (incluant la cognition) tel que sa reproductibilité, sa diversité, et son optimalité (en terme de codage).

Mots clefs

Adaptation, cortex, reproductibilité, nonlinéarité, complexité, Champ-récepteur, assemblées neuronales, codage efficace, perception, conscience.

2. Introduction

Le cerveau, notamment le cortex, est souvent désigné comme le système à la fois le plus complexe et le plus intelligent ou le plus performant du monde, soulignant par ce biais l'impuissance de nos investigations expérimentales et de nos théories pour comprendre, expliquer, prédire ou reproduire son comportement. Ce point de vue encore présent malgré les avancées théoriques et empiriques récentes, est motivé par l'irrégularité, la diversité et la multiplicité combinatoire des structures (morphologies, phénotypes, connectivités), et des fonctions (variabilité des champs récepteurs (CRs), des interactions, faible pouvoir prédictif des CRs, présence d'un bruit gigantesque). En effet, la connaissance empirique actuelle des structures et des fonctions corticales se résume à des descriptions moyennes ou macroscopiques avec beaucoup de variabilité. Se pose donc naturellement la question du statut de ces variabilités : ces fluctuations ont-elles un sens, une fonction ou ne sont elles que du bruit ? Ou autrement formulé, est-il possible d'intégrer cette variabilité et diversité dans un paradigme théorique général ? Les théories actuelles et les principes physiologiques d'intégration neuronale et de plasticité énoncés et précisés depuis plus d'un siècle d'étude, ne suffisent-ils pas à expliquer dans son ensemble la dynamique corticale et la cognition ? J'essaierai de vous convaincre que les avancées de la science nous permettent aujourd'hui d'affirmer que le neo-cortex est bien compris, et que cette compréhension est basée sur des principes simples reprenant et généralisant les mécanismes neuronaux depuis longtemps bien connus.

Plus généralement se dessine derrière ces questions la notion d'efficacité en science naturelle et en science physique. Les avancées de la biologie moderne ont montré à maintes reprises que les processus biologiques sont extrêmement efficaces, « fleuretant » avec les limites théoriques imposées par la physique. Anthropomorphiquement parlant, la science moderne, notamment grâce à l'avènement de la biologie, commence à reconnaître son statut de proluxe et optimal inventeur à la Nature. Mais nous ne sommes qu'au début de cette belle histoire ; histoire d'une science écologique des systèmes auto organisés dont l'avancement n'a jamais été aussi urgent compte tenu des besoins, des disparités et des gaspillages énergétiques actuels ; histoire dans laquelle je désirerais profondément inscrire ces travaux (à laquelle j'entends au moins essayer de participer).

Dans cette thèse, j'essaierai de démontrer que cette complexité, intelligence ou optimalité ainsi que la diversité et « variabilité » des structure-fonctions sous-jacentes peuvent être comprises comme la résultante d'un simple processus se basant sur une formalisation du bruit et de la complexité (inspirée des théories algorithmiques, de l'information, et du codage optimal dans le cerveau). Ce processus, bien connu en théorie de l'apprentissage, n'est autre que la maximisation de l'information mutuelle entre le système et son environnement, et constitue formellement une théorie de l'adaptation. Ce principe d'optimalité se décompose en deux effets fondamentaux, l'augmentation de la reproductibilité (minimisation du bruit) et la réduction des redondances (qui génère la diversité et la spécialisation-individuation). Ce processus peut être assimilé à une théorie de la connaissance ou science cognitive et formalise la propagation-diffusion des connaissances. En élargissant au principe de maximisation d'entropie, il apparaît que ce processus auto organisationnel n'est autre que le second principe de la thermodynamique énoncé par Boltzmann puis Gibbs, généralisé aux systèmes hors équilibre et se résume à un processus dissipatif. Il se dessine donc ainsi une sorte de Thermodynamique de la connaissance, mais aussi des problèmes plus délicats sur le statut du sujet et de son environnement : il n'y aurait rien d'autre que de la dissipation, un bruit, une

musique, qui n'aurait fait que s'amplifier jusqu'à nous ? Dans ce paradigme, le cortex et ses activités cognitives, ne se différenciant pas de l'évolution ou de la dynamique d'autres structures adaptatives, acquièrent un statut intrinsèquement naturel et deviennent un objet d'étude privilégié de la complexité et de l'adaptation. J'essaierai de montrer par ailleurs, que ce paradigme souligne un rôle singulier de la physique statistique par rapport aux autres physiques quantiques et relativistes, permettant peut être de nouvelles extensions théoriques.

Mais venons en aux expériences et aux résultats empiriques, fruit d'un travail d'équipe. Nos travaux sont basés sur des enregistrements intracellulaires des neurones du cortex visuel primaire (V1) effectués *in-vivo* chez le chat anesthésié et paralysé. Cette technique nous donne accès non seulement à la sortie supraliminaire (« spikante ») du neurone, mais aussi à ses entrées synaptiques excitatrices et inhibitrices (E/I). Combinée à des stimulations visuelles, elle nous permet de dresser la carte des fonctions « spikante » et sousliminaire excitatrice et inhibitrice ainsi que d'appréhender leur niveaux de corrélation et d'activité dans le réseau fonctionnel de la cellule, et leur reproductibilité.

En première approche, nous nous sommes intéressés à l'organisation spatiotemporelle des CRs synaptiques excitateurs et surtout inhibiteurs par le biais de stimuli impulsionnels (petits carrés de contraste positif ou négatif présentés statiquement) et de barres orientées statiques. Aussi bien les champs excitateurs, que les champs inhibiteurs s'étendent isotropiquement sur une large portion du champ visuel, au-delà du Champ de décharge (CMD). Les CRs synaptiques des cellules Simples (au sens de Hubel et Wiesel) présentent une organisation sousliminaire complexe avec un large recouvrement spatial des zones ON (de réponse au contraste positif) et des zones OFF (de réponse au contraste négatif), mettant ainsi en évidence le rôle déterminant de l'intensité relative entre l'excitation et l'inhibition dans la structuration spatiale et temporelle du champ de décharge. Ainsi que pour les champs excitateurs, la latence des réponses inhibitrices augmente avec l'excentricité du stimulus par rapport au centre du CR, avec une pente caractéristique de la propagation de la connectivité horizontale intracorticale. Ces CRs synaptiques illustrent l'existence d'une récurrence E/I intracorticale étendue, dont le rôle computationnel ainsi que dans les fonctions de sélectivité corticale constitue la suite de nos investigations expérimentales.

La participation de la récurrence corticale, notamment inhibitrice, à la genèse de la sélectivité à l'orientation et à la direction, les deux principales sélectivités émergentes dans V1, est un sujet intense de controverse. L'étude approfondie de ces sélectivités au niveau sousliminaire montre que les neurones présentent une grande variété de combinaisons de sélectivité E/I, que la sélectivité « spikante » résulte de la balance entre les sélectivités de ces deux composantes. De manière générale, les sélectivités sousliminaires sont larges comparées à la sortie spikante, l'inhibition est corrélée avec une chute de variabilité au travers des essais dans la trajectoire du potentielle de membrane signant ainsi probablement un effet shuntant. Ces résultats montrent l'origine corticale prédominante de la sélectivité à l'orientation et à la direction et suggèrent une diversité de circuits fonctionnels sous-tendant ces sélectivités.

Le champ d'intégration synaptique constitue un support probable pour les diverses interactions centre-pourtour jusqu'ici observées dans V1. Des expériences de psychophysique, conduites par l'équipe de Jean Lorenceau en collaboration avec nos travaux, montrent l'existence d'interactions latérales compatibles avec la propagation horizontale corticale. Ces interactions induisent une surestimation de la vitesse perçue pour des mouvements apparents de Gabors (patchs de luminance sinusoïdale atténuée par une Gaussienne) orientés colinéaires à grande vitesse. D'autre part, la sélectivité spatiale et orientationnelle, le rôle du contraste, ainsi que la nature facilitatrice ou suppressive des interactions centre-pourtour dans V1 reste sujet à débats. En reproduisant ce paradigme de mouvement apparent, nous avons montré l'existence d'interaction centre-pourtour sélective spatialement en moyenne pour l'axe colinéaire « Gestaltiste » des neurones de V1. Cependant, cette sélectivité spatiale présente

une large variabilité au travers des cellules. La stimulation du pourtour, en condition centripète (périphérie « silencieuse » stimulée avant le centre du CR) réduit la latence des réponses au centre seul par des mécanismes à la fois linéaires et nonlinéaires. Ces interactions dépendent du contraste et sont soit suppressives soit facilitatrices pour les conditions bas contraste dans le CR, et uniquement suppressives pour les conditions de haut contraste. Soulignant un peu plus leur origine intra-corticale horizontale, ces interactions centre pourtour sont sélectives à l'orientation du pourtour et non exprimées en condition centrifuge (centre du CR stimulé avant le pourtour).

Quel impact peuvent avoir cette récurrence corticale et leurs nonlinéarités sous-jacentes sur le codage de l'information dans V1, notamment sur la précision et la variabilité des réponses ? Une analyse préliminaire montre que quelque soit le type de stimulus utilisé (impulsionnel, barre en mouvement, mouvement apparent etc.) et pour au moins la partie de ces configurations recrutant le champ sousliminaire inhibiteur, la stimulation visuelle induit une diminution de la variabilité de la trajectoire du Vm au travers des essais. A l'opposé, le point de vue prédominant en neuroscience semble en faveur d'un rôle de la récurrence corticale dans la genèse de variabilité, bruit ou états corticaux spontanés, s'additionnant à la réponse visuelle. De nombreuses études montrent que la variabilité des réponses corticales est importante, d'amplitude égale ou supérieure à la moyenne de la réponse, définissant ainsi un comportement Poissonien, et ce indépendamment des caractéristiques du stimulus. Ce bruit impose que l'information du stimulus soit encodée dans la fréquence de décharge, et aussi une redondance de fonction et d'information entre neurones. Ce paradigme marque cependant une contradiction intuitive avec la théorie du codage optimal prenant ses racines dans les travaux de Barlow, qui préconisent que la redondance devrait être réduite de manière à utiliser optimalement la bande passante neuronale. En d'autres mots, le codage optimal énonce que le système nerveux devrait adapter ses processus et sa transmission d'information aux statistiques de son environnement naturel. Nous nous sommes donc demandés si en condition naturelle, le bruit ne pouvait pas être minimisé. Pour cela, nous avons construit une librairie de films de stimulation de complexité croissante allant du plus simple et « optimal », comme un réseau de luminance avec l'orientation du champ récepteur étudié et dérivant à la fréquence temporelle préférée, au bruit blanc dense, et incluant une image naturelle animée par une séquence de mouvement des yeux. Les résultats montrent que la reproductibilité du code neuronal est grande en condition naturelle et dépend de la complexité structurelle du stimulus. L'activité corticale présente des états dynamiques reproductibles reflétés au niveau du potentiel membrane et un code temporel binaire au niveau « spikant » en réponse aux conditions naturelles. A l'inverse, les réponses au réseau dérivant présentent une très grande variabilité et un code fréquentiel. Le contraste entre les entrées synaptiques temporellement denses et très informatives avec la sortie très éparse pour la condition naturelle démontre que le processus corticale retire les redondances de ces entrées par la détection d'assemblées synchrones précises. Cette réduction à la fois des redondances et du bruit peut être modélisée, en introduisant une définition hiérarchique ordonnée des redondances, comme une conséquence directe du principe de maximisation de l'information mutuelle entre les entrées et la sortie corticale, offrant par ce biais une formalisation universelle de l'adaptation. La modulation du code, par la pertinence des statistiques à la fois transitoires et globales de l'input sensoriel, jouant sur la balance entre les états spontanés internes et les états contraints par l'environnement, correspond à la propriété auto-générative bien connue des réseaux récurrents. Du point de vue computationnel, la dissipation des contraintes sensorielles par le cortex est interprétée comme le coût entropique à payer pour la formation de la mémoire ou plus généralement pour l'observation.

Du point de vue fonctionnel, les nonlinéarités et contrôles de gain sont des candidats sérieux pour implémenter cette réduction de redondance et de bruit. Par ailleurs, les mouvements des

yeux très souvent oubliés dans les études des réponses aux stimuli naturels, semblent indispensables pour obtenir le code contraint observé précédemment. Ces mouvements imposant une dynamique stéréotypée au flux optique à la fois pendant les saccades et les fixations sont aussi indispensables à la perception visuelle. Aussi leur impact sur le codage de l'information dans V1 et leur possible liens aux nonlinearités corticales, a constitué le dernier sujet d'investigation expérimental de cette thèse. Pour cela, nous avons construit des stimuli représentant différents niveaux de simplification du flux optique et analyser les précédents stimuli du point de vue fonctionnel. Les résultats montrent que les mouvements des yeux recrutent optimalement des nonlinéarités qui augmentent la reproductibilité et la précision temporelle des réponses sous liminaires et « spikantes ». Dans les conditions reproduisant les mouvements des yeux, le pouvoir prédictif du CR linéaire classique est quasiment inexistant, soulignant par ce biais la prédominance des interactions corticales en conditions naturelles. L'effet de ces nonlinéarités se manifeste notamment dans l'augmentation du ratio signal sur bruit dans les hautes fréquences (Béta-Gamma). Cette sélectivité accrue pour les statistiques naturelles, qui est associée à un recrutement de l'inhibition avec retard de phase, est amplifiée par le seuil de décharge. Ces résultats suggèrent que les nonlinéarités de V1 sont adaptées aux mouvement des yeux, et qu'elles agissent comme des contraintes sur le code notamment en réduisant la variabilité et en augmentant la sélectivité des réponses, générant le code optimal précédemment observé. Aussi, nous suggérons que la caractérisation des fonctions et des sélectivité corticales doivent tenir compte de la reproductibilité et de la précision temporelle des réponses plutôt que la simple intégrale ou amplitude de la réponse. L'ensemble de ces résultats ainsi que la vaste littérature physique et computationnelle, ont bien entendu suggéré le modèle général de complexité et d'adaptation décrit en début d'introduction.

3. Results

3.1. Cortical Synaptic Receptive Fields: functional characterisation

3.1.1. Introduction

As a first approach, we studied the spatiotemporal organisation of excitatory and notably inhibitory synaptic Receptive Fields (RFs) using impulsive and oriented bars stimuli. Both excitatory, as shown by previous results of the lab (Bringuier & al, 1999, Chavane, 1999, Monier, 2002), and inhibitory synaptic RFs extended isotropically over a visual spatial region much broader than the spiking RFs (or “discharge field”). Synaptic RFs in simple cells presented a complex organisation with large overlap between the On and Off subregions, pointing out the crucial role of the relative spatiotemporal Excitatory-inhibitory strength (E/I balance) in the shaping of spiking Spatiotemporal RF (STRF). In the same way as found for Excitatory RFs, the latency of the inhibitory responses increases with the eccentricity of the stimulus location relative to the center of the spiking RF, with a slope characteristic of the propagation speed measured for horizontal connectivity.

Those results demonstrate the existence and functional relevance of a widespread and important cortical E/I recurrence. A full article (Chavanne & al, 2000) integrating part of the data exposed in this section as well as psychophysical results from the team of Jean Lorenceau probing perceptual lateral interactions evoked by apparent motion at a speed corresponding to that of cortical horizontal propagation (Grinvald et al, 1994; Bringuier et al, 1999), is presented in annex.

3.1.2. Spatio-temporal profile of visually evoked excitatory and inhibitory input

One hundred and sixty two cortical cells were recorded intracellularly with sharp electrodes for periods ranging from 30 to 615 min. The average resting membrane potential was -66.1 mV (± 5.9 mV), input resistance between 10 and 70 M Ω , and spike height between 35 and 70 mV. In addition, twenty cells recorded using patch electrodes and whole-cell recording mode (Borg-Graham & al, 1998) were pooled with the sharp data base, leading to a total of 182 cells. Responses to three types of visual stimulation were compared, each stimulus recruiting a different level of spatial and temporal summation. The simplest stimulus, ‘sparse noise’, was a contrast impulsion (approximating a Dirac input) (Ratliff, 1965), of small spatial extent ($<0.5^\circ$ of visual angle) and duration (33–50 ms), of variable polarity (light or dark), and

a random walk was used to visit all possible locations in the explored visual field for the two possible contrasts (light ON, dark OFF). The neural response to such stimuli can be considered as the ‘impulse-response’ of the retino-thalamo-cortical pathway and the resulting 2D-maps established for each contrast characterize the linear ON and OFF components of the spatial transfer function (figure 3.1.1: A1, B1, A3, B3). Since cortical cells are best activated by correctly oriented static stimuli (Hubel & Wiesel, 1962), the second stimulus type consisted of contrasted bars with optimal orientation and length. These bars were flashed in random positions across the width axis of the RF, in order to obtain a 1D-map of the receptive field (figure 3.1.1: C1, C3). Finally, in order to optimize the synergetic activation of synaptic inputs, we also used compact (for the discharge field) and annular (for exploration of the “silent” surround) gratings whose orientation and spatial frequency were adjusted to optimize the evoked firing frequency (figure 3.1.1: D1).

Whatever the stimulus used and when the cell was initially at rest, significant depolarizing responses were evoked over regions much larger than the discharge field itself, unmasking in certain cells a very large responsive (at the subthreshold level) surround (D-field). For a given cell, the D-field size appeared to increase with spatial and temporal summation: on average, the equivalent diameter of the D-field was 2.5 times larger than that measured for the discharge field using sparse noise. This ratio increased to 3.3 for elongated bars and 5.6 for gratings. Whatever the stimulation protocol used to map the receptive field, we observed that the intensity of the response (measured by the peak or integral value) decreases as a function of the test stimulus eccentricity relative to the centre of the discharge field (figure 3.1.1: B1, C1, D1). In the case when a moderate depolarization of the membrane potential was imposed by an intracellularly injected current, the size of the discharge field increased, recruiting part or the totality of the previously measured subthreshold D-field.

The spatial extent of the synaptic integration field and its organization into a sensitivity gradient decreasing from the discharge field centre (figure 3.1.1: A1) suggests that membrane potential fluctuations regulate the recruitment of inputs effective enough to trigger spike activity. This is generally achieved by preserving the compact aspect of the responsive zone expressed at the spike level. More rarely, ectopic discharge regions can be revealed, sometimes as far as 10 degrees from the principal discharge zone measured at rest. The spatial extent of the discharge field, hidden by this ‘iceberg’ effect, can thus be considered as a dynamic variable dependent on the internal polarization state of the neurone and/or on the tonic synaptic bombardment by the rest of the network. Moreover, we also demonstrated that

subthreshold peripheral responses are orientation selective and, since orientation is not strongly expressed at the retinal or geniculate level, one can assume that they are most likely of cortical origin. The dependency of the time-courses of synaptic responses on the stimulus location relative to the discharge field centre suggests an indirect activation schema, consisting first of a serial retinotopic projection onto the cortex that will then be relayed to another distal cortical locus by the horizontal connectivity.

Our results show that, independently of the method used (figure 3.1.1, sparse noise B3, elongated bars C3, gratings (not illustrated)), the evoked latency of the subthreshold responses increases linearly with the stimulus eccentricity relative to the centre of the discharge field (delay of 10 to 50 ms for 3–10 degrees of eccentricity, in figure 3.1.1 A2). These latency increases are in agreement with the hypothesis of a spread of evoked action potentials travelling along intracortical axons across the cortical layer plane. We derived an estimate of the apparent speed of horizontal propagation by converting the distance separating two loci of stimulation in the visual field into the corresponding distance in the cortex between the focal zones of activation fired by the sole effect of the feedforward projection (Tusa & al, 1978). For this purpose, we used, for cat area 17, an average cortical magnification factor of 1 mm for 1 degrees in retinal space.

Our results show that stimuli flashed in the ‘silent’ surround of a given recorded cell receptive field evoke subthreshold responses which are relayed with the same velocity by the horizontal intracortical network (given by the slope of the spatial latency basin in figure 3.1.1, B3, C3). The apparent speed of horizontal propagation (ASHP) deduced from our *in vivo* experiments, although varying among cells between 0.02 and 2 m·s⁻¹, is in 75% of the cases lower than 0.4 m·s⁻¹, i.e. has a magnitude in the order of conduction speeds measured *in vitro* and *in vivo* along nonmyelinated horizontal axons (Hirsch & Gilbert, 1991, Moore & Nelson, 1998, Murakoshi & al, 1993, Nowak & Bullier, 1997). The value of the mode of the ASHP distribution remains at least one to two orders of magnitude lower than the conduction speeds reported for X- and Y-thalamo-cortical axons (8–40 m·s⁻¹, Hoffmann & Stone, 1971).

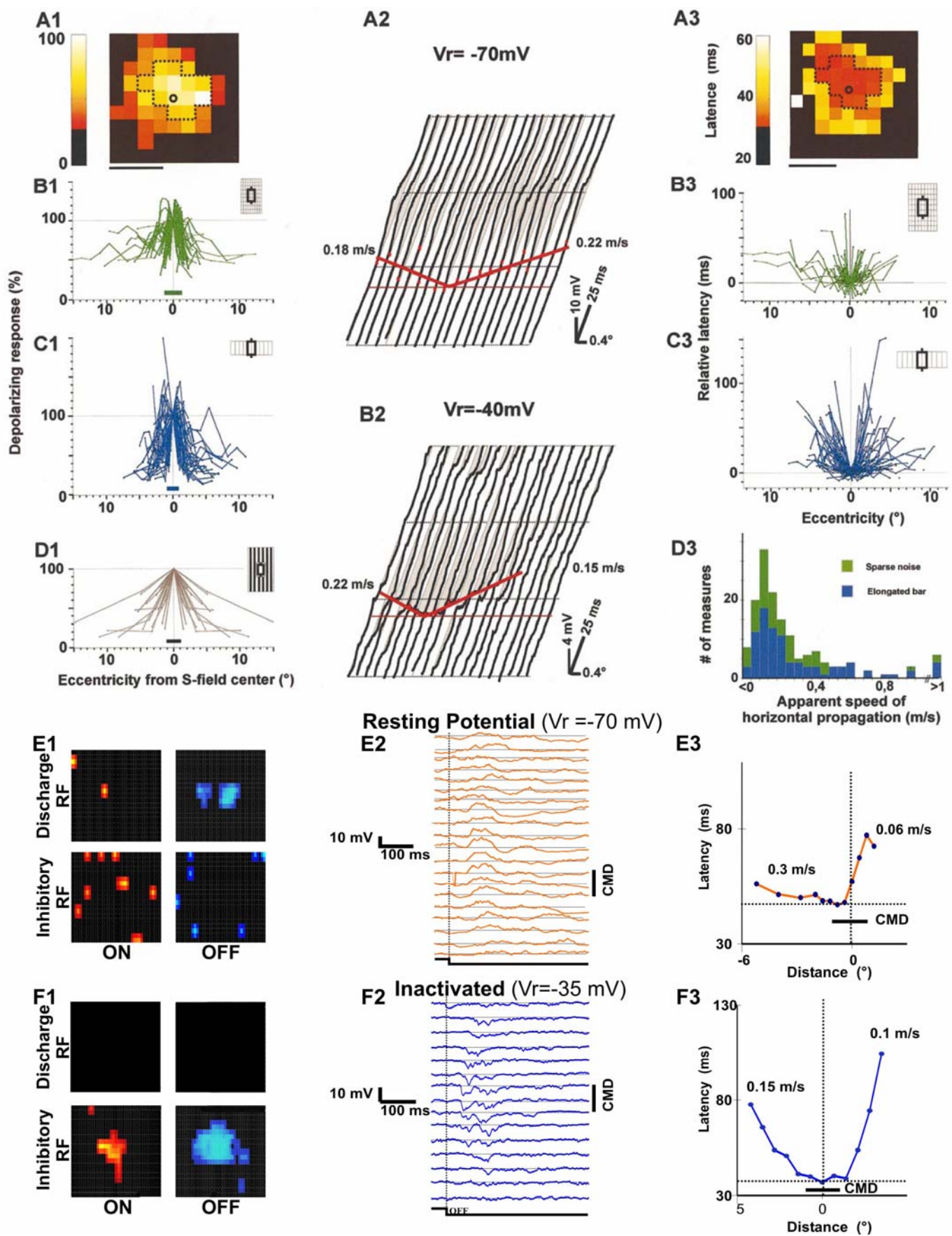


Figure 3.1.1. Spatial sensitivity profiles and latency basins of visually evoked synaptic responses. Left panel: **A1**: Map of the subthreshold response strength in a cortical neuron (D-field). The normalized intensity of the synaptic depolarization evoked in each pixel is colour-coded. The discharge field is outlined by a dotted contour, and the dot indicates which pixel elicited the highest discharge rate. Horizontal scale bar, 2°. **B1-C1-D1**: The strength of the visually evoked depolarizing response is normalized relative to that observed at the location eliciting the maximal discharge (circle). Each individual profile represents for a given cell the change in response strength across the width or length of the RF, expressed as a function of the eccentricity of the test stimulus from the discharge field centre. These different profiles have been superimposed together on the same graph, each corresponding to a particular mapping protocol (**B1**, 2-D sparse noise ($n=37$); **C1**, flashed bars ($n=21$); **D1**, flashed ($n=19$) or moving ($n=2$) sinusoidal luminance gratings). The average discharge field extent is indicated by a thick horizontal segment. In the case of annular stimuli (**D1**), the abscissa corresponds to the distance between the centre of the discharge field and the inner radius of the annulus. Central panel: **A2**: The waterfall representations illustrate the spatio-temporal profile of subthreshold depolarizing responses in a given cell at rest ($V_r = -70$ mV in **A2**) and in another cell during spike inactivation ($V_r = -40$ mV in **B2**, Section 2). The integral depolarizing and hyperpolarizing waveforms are indicated by shaded areas. Oblique lines indicate the best fit using a bi-linear regression accounting for the latency basin of synaptic responses. Similar AHSP values (0.15 to 0.22 m.s⁻¹) are derived from the slope measurements (in red) in the X-T plane for both dominant excitatory (**A2**) and dominant inhibitory (**B2**) subthreshold responses. Right panel: **A3**: Colour-coded latency basin map of depolarizing responses evoked on the visual field. Black pixels indicate the absence of significant changes in the onset slope of the postsynaptic response. The response latency is expressed as the absolute difference, in milliseconds, relative to the latency observed in the discharge field centre (dot in **A1-3**). **B3-C3-D3**: Change in the latency of the subthreshold response expressed as a function of eccentricity relative to the discharge field centre (abscissa in degrees of visual angle). Each cell is represented on a continuous graph, in response to sparse noise (**B3**) or to flashed bars (**C3**). Each latency basin is fitted by two linear regressions, and the slope of each fit, given in degrees per milliseconds in the visual field, is converted into m/s in the cortical layer plane (see text). The distributions of apparent speed of horizontal propagation (in m.s⁻¹), established for each stimuli class, are shown in **D3**. Discharge Field (**E1**, sparse noise map), D-field (**E2**, oriented bars), inhibitory field (**F1**: sparse noise map **F2**: oriented bars responses) and their respective latency profile (**E3**, **F3**) for another cell both recorded at rest (**E1**, **E2**, **E3**) and during spike inactivation (**F1**, **F2**, **F3**).

Our latency analysis suggests that the information received at one point in the cortex through the serial feedforward afferents is then propagated radially by the horizontal connectivity to neighbouring regions of the visual cortex over a distance that may correspond to up to 10 degrees of visual angle. Primary visual cortical neurons would thus have the capacity to combine information issued from different points of the visual field, in a spatiotemporal reference frame centred on the discharge field itself. This ability imposes precise constraints in time and in space on the efficacy of the summation process of elementary synaptic responses.

The contextual influence originating from the ‘silent’ surround is not limited to the transmission of excitatory intracortical input. Similar analysis and detection methods have been applied to hyperpolarizing responses that were revealed when the membrane potential was artificially maintained at a depolarized level (around -30 mV), away from the reversal potentials for chloride (-70 mV) and potassium (-90 mV) inhibitory synaptic currents. The goal of this protocol was to increase the visibility of subtractive inhibition by increasing the driving force of GABA_A and GABA_B currents and decreasing the AMPA/NMDA excitatory currents, and at the same time suppressing spike activity by inactivation of fast Na⁺

conductances. This method led to the same conclusion as for the excitatory events: a latency basin of hyperpolarizing events is observed, suggesting an intracortical propagation of inhibitory input with a velocity ranging between 0.1 to 0.3 m.s⁻¹ (examples in figure 3.1.1: B2, F1, F2, F3). The only difference with the spatial basin of latency observed for depolarizing responses is that the earliest onset inhibition following visual input is on average obtained for a point in visual space which is displaced by 1 to 2 degrees from the centre of the excitatory discharge field, as exposed in the two example cells.

Thus excitation and inhibition, although they may spatially overlap later in time, seem to take their origin in regions of the visual field which are spatially distinct. This result is reminiscent of extracellular observations made in layer VI cells in monkey V1 (Livingstone, 1998). Our electrophysiological data also agree with the recent description of a horizontal connectivity network of interneurons that can extend over several millimetres in the cortical layer plane, thus exerting suppressive influences over a cortical distance corresponding to several degrees of visual angle in retinal space (Kisvarday & al, 1997).

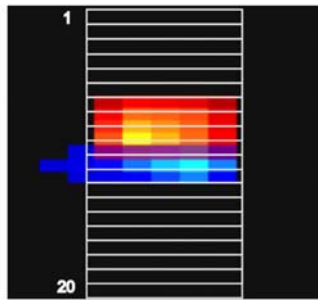
3.1.3. Synaptic integration field complexity

In the visual cortex, two major types of receptive field (RF) are classically defined, Simple and Complex, based partly on the degree of spatial overlap between ON and OFF spiking responses (Hubel and Wiesel, 1962; Dean & Tolhurst, 1983). Another criteria for simple and complex classification, more discriminative, consists in the comparison between the modulation amplitude with average response amplitude (Skottun & al, 1991). It is quantified by the ratio between the Fourier component of the preferred temporal frequency of the cell (F1) and its component zero (DC, average, F0). For this measure which quantifies the level of linearity of the response, simple cell are classically described as having a ratio $F1/F0 > 1$ ("linear"), whereas complex cells classically present a ratio $F1/F0 < 1$. In order to compare the RF organisation at the spiking and membrane potential level and thus to clarify the mechanisms explaining Spiking RF emergence, we have measured both criteria on each Vm and spike components (Chavane & al, 1998). A similar study has been recently published (Mechler & Ringach, 2002, Priebe & al, 2004) and presents results which are very similar to the ones presented here.

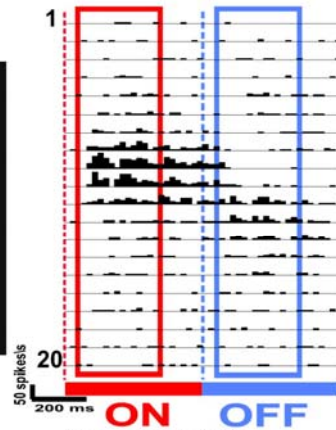
In a first approach, we will describe the overlapping of ON and OFF regions at the synaptic level and compare it to that seen at the spiking level. Sharp and patch electrodes have been used to record synaptic responses in response to optimally oriented light and/or dark bars flashed across the RF width (n = 70 cells, figure 3.1.2.1). A "discreteness" ratio (R_D) was

applied both to the spike rate and subthreshold potentials. R_D is defined as the absolute value of the difference between ON and OFF responses integrated over the stimulus duration, summed over all tested positions, and normalized by the sum of the absolute values of all responses. This ratio is bound between 1 (complete spatial segregation) and 0 (complete overlap of ON/OFF responses). We applied this measure both for the total integral of the responses and for the significant responses measured as the integral above a threshold calculated from the spontaneous activity (Z-score $P < 0.05$).

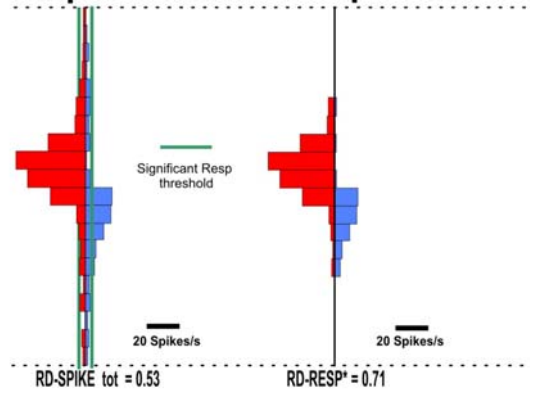
A1 MDF



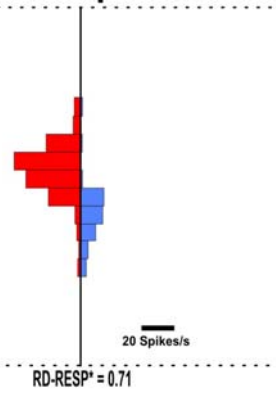
A3 PSTH



Spike

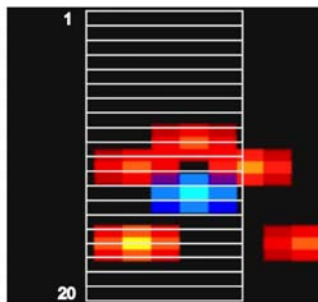


Resp*

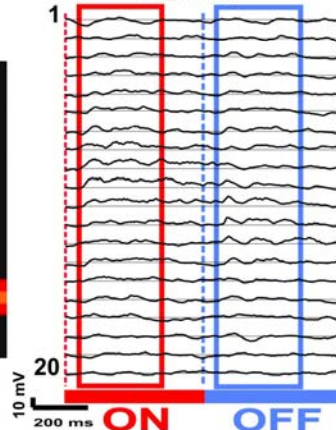


A5

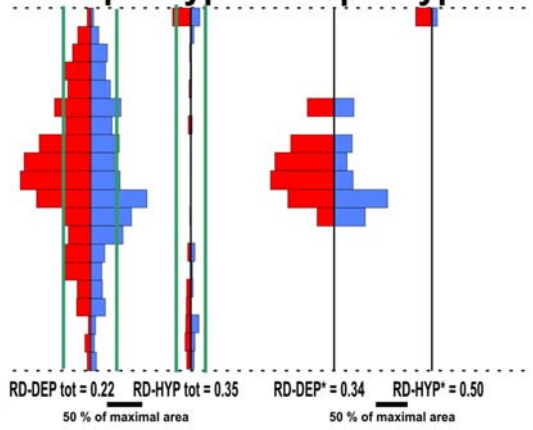
A2 D-Field



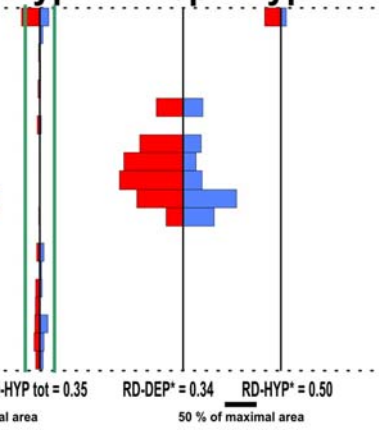
A4 PSTW



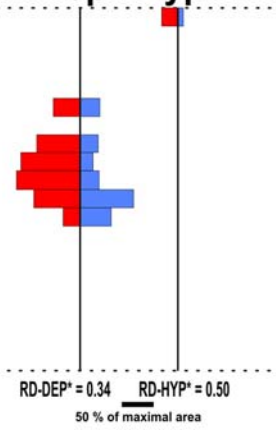
Dep



Hyp



Dep*

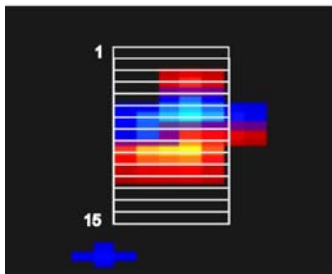


Hyp*

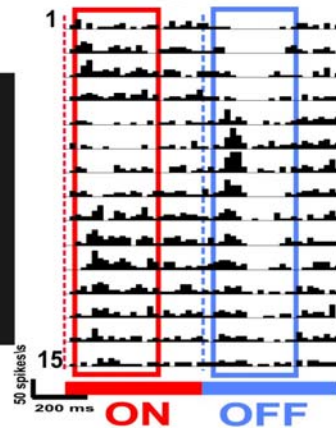


A6

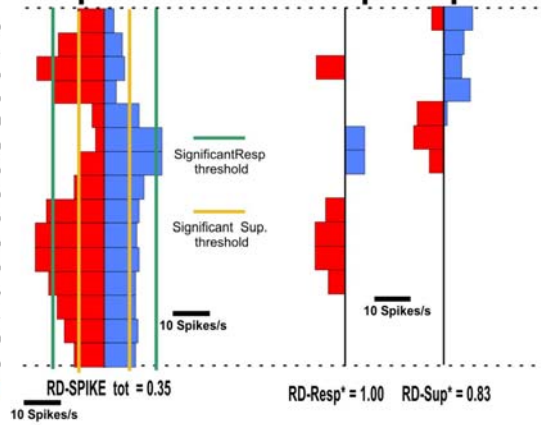
B1 MDF



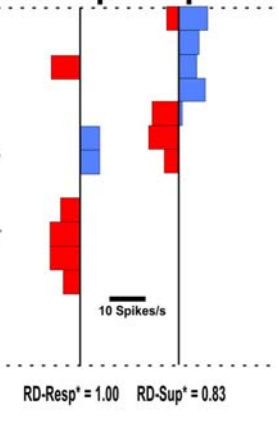
B3 PSTH



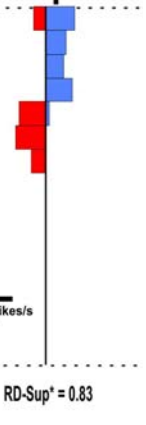
Spike



Resp*

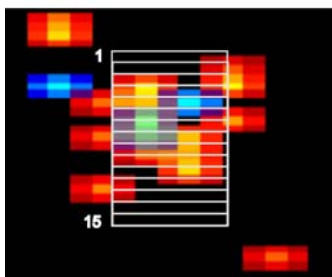


Sup*

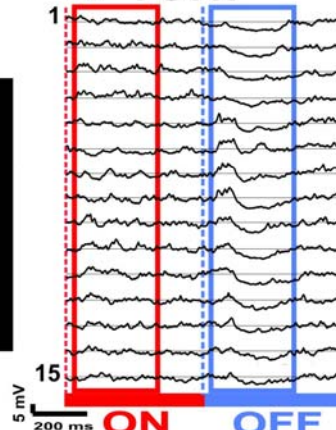


B5

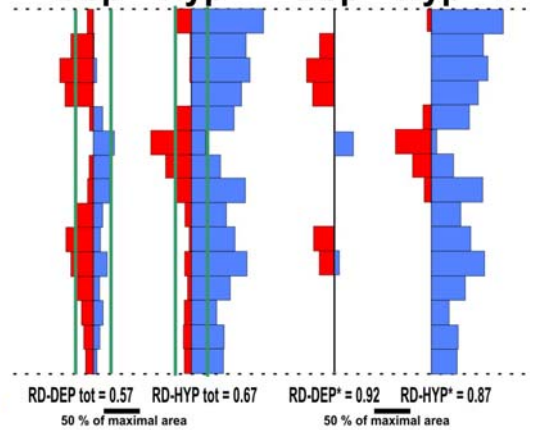
B2 D-Field



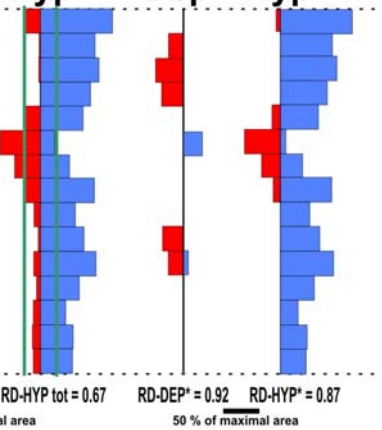
B4 PSTW



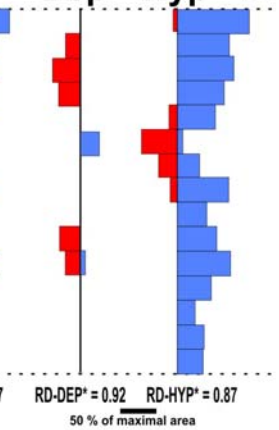
Dep



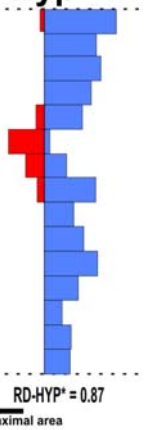
Hyp



Dep*



Hyp*



B6

Figure 3.1.2.1: Examples of a Complex-like organization of ON- and OFF- synaptic responses for two simple cells A & B. Sparse noise ON-OFF maps (ON Red - OFF blue color scale) for the discharge (**A1, B1**) and for the Depolarising Field(**A2, B2**) are presented in overlay with the position of the flashed bars stimuli used for further analysis (see other panels). The Peri-Stimulus-Time-Histogramms (PSTHs) of the spiking response (**A3 and B3**) and the PeriStimulus-Time-Waveforms (PSTWs) of the V_m response (**A4 and B4**) are illustrated in response to the ON (500 ms) and OFF (bar removal) transitions of these stimuli. The integral of either the total or only the significant component of those responses and the associated discreteness ratio (see R_D definition in the text) are quantified in **A5, A6, B5 and B6**. Cell **A** illustrates a complex Depolarising-field organisation whereas cell **B** a complex hyperpolarising-field organisation.

On the basis of spike activity, discreteness is continuously distributed between 0 and 1, with R_D larger for Simple RFs (figure 3.1.2.2). Discreteness derived from ON and OFF subthreshold response is about 70% that based on spike activity. When the depolarizing and hyperpolarizing parts of the responses are analyzed separately, hyperpolarizations are more spatially segregated ($R_D \sim 0.5$) than depolarizing responses ($R_D \sim 0.3$). A time-locked analysis of the evolution of the subthreshold discreteness shows a much richer dynamics that can be decomposed in two steps: most Simple cells start from a Complex-like state during the early part of the visual response and ON/OFF segregation increases during the later part of the response. Time-slice analysis of dominant and opponent responses indicate that both responses combine excitatory and inhibitory inputs. The dynamics of the discreteness ratio may thus provide detailed insights of the intracortical synaptic recurrence.

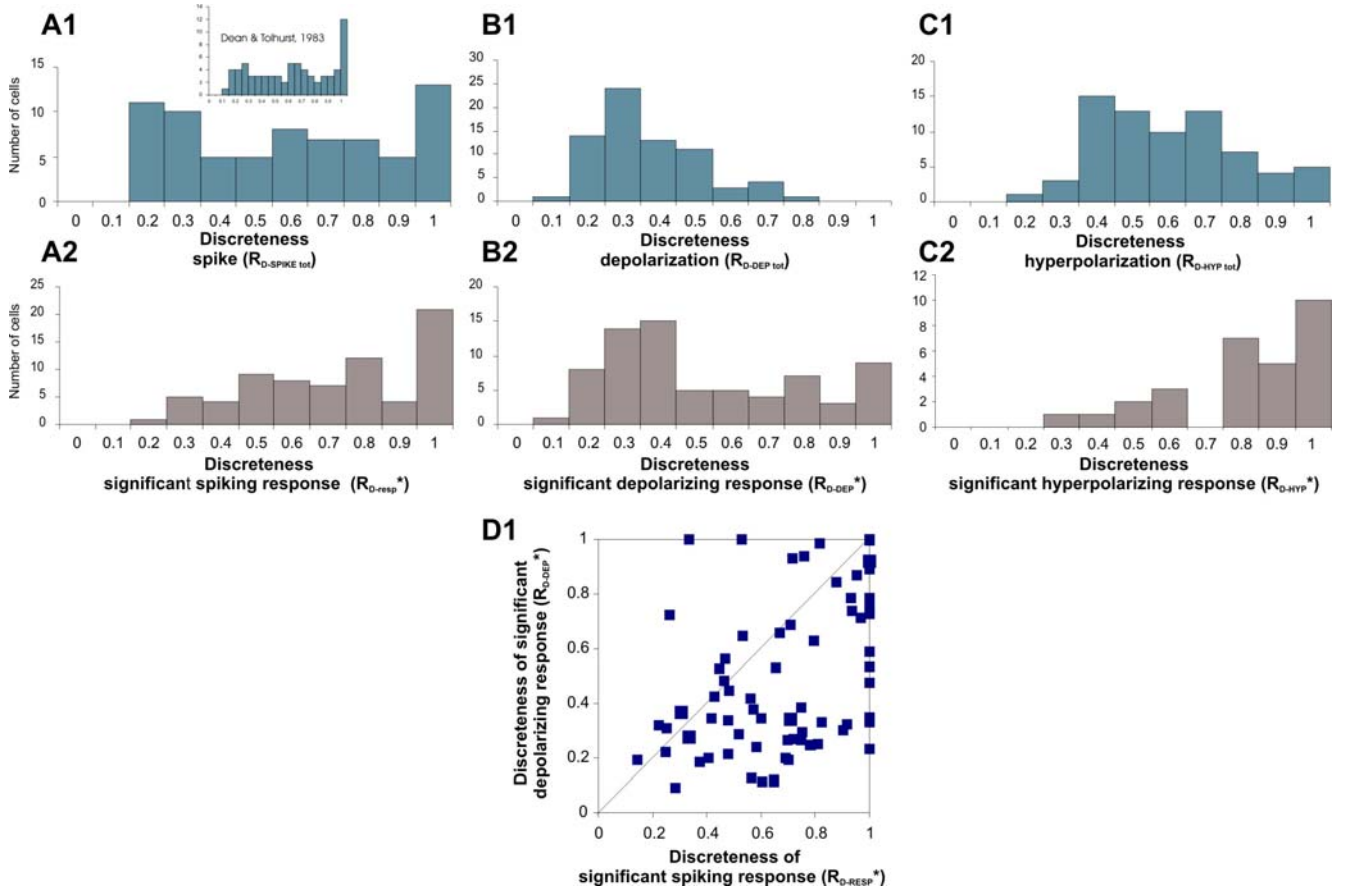


Figure 3.1.2.2: Population quantification of the spatial overlap of ON and OFF responses at the spiking (A), depolarising (B) and hyperpolarising (C) levels. The overlap extent is quantified by a discreteness ratio (see R_D in text), a value of 1 indicating an absence of overlap whereas a value of 0 a complete superposition. This ratio is calculated both for the total response integral (A1, B1, C1) and for the integral restricted to the significant component only (A2, B2, C2). The depolarising responses are found more in overlap than the spiking responses, as shown by the correlation plot of their respective discreteness ratios (D1).

In a second step, we quantified the modulation ratio $F1/F0$ of 13 cells recorded with sharp electrodes. The stimulation consisted in a full screen grating of sinusoidal luminance of optimal orientation and spatial frequency, drifting in the preferred direction at the optimal temporal frequency. The ratio between the $F1$ and $F0$ is quantified both at the spiking responses and membrane voltage (V_m) responses levels. On the 13 cells, 7 can be classified as simple and 8 as complex according to their spiking response $F1/F0$ ratio. In contrast, at the V_m synaptic level, this ratio decreases for most of the cells and some of the cells (4 of the 7 simple cells) classified as Simple based on their spiking modulation are falling in the Complex class from their synaptic activity observation (figure 3.1.2.3). Only 3 cells present a Simple-like modulation of the synaptic input, whereas 10 are complex. Examples of a Simple cell and of a Complex cell modulation both at the spiking level (PSTH) and at the V_m level (PSTW) are presented in figure 3.1.2.3.

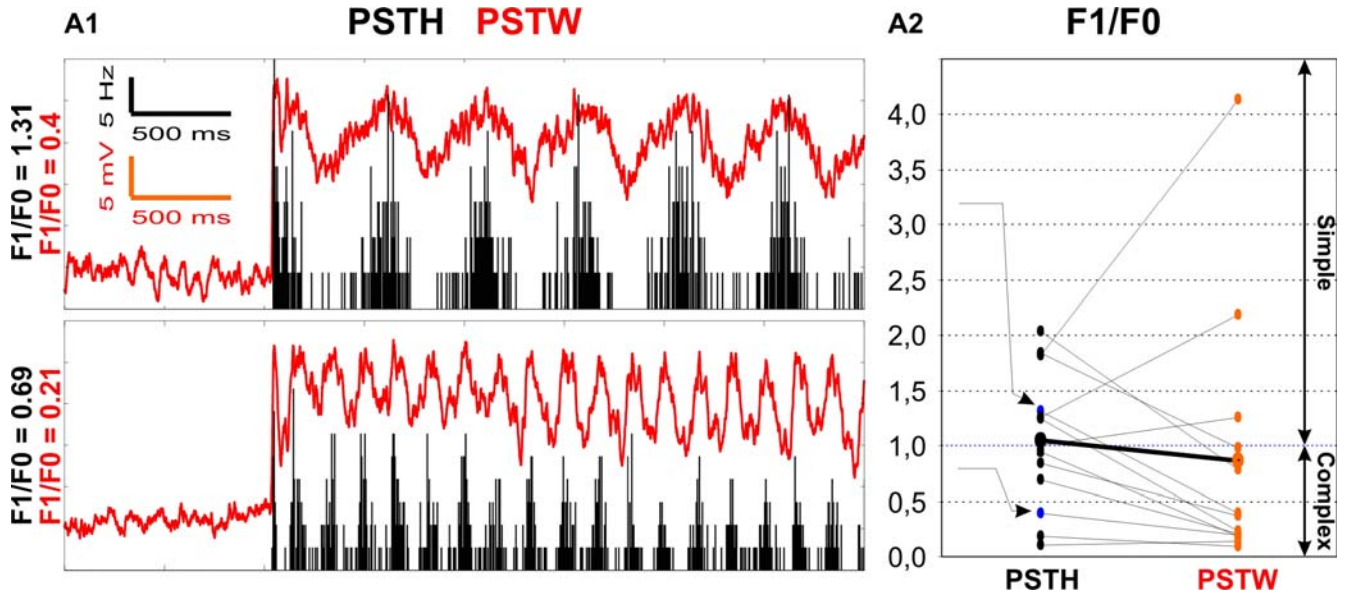


Figure 3.1.2.3: Spiking and Vm responses modulation in responses to optimal drifting grating and the quantification of the $F1/F0$ ratio. The spiking (PSTH) and Vm (PSTW) average responses are illustrated for two cells in A1. Note the strong DC component at the subthreshold level in both cells and the phase-independent transient firing at the stimulation onset. The top cell example is classified as Simple, whereas the bottom one as complex, according to the $F1/F0$ ratio of their spiking responses. The population quantification of the spiking and Vm responses $F1/F0$ ratio is presented in A2.

Our conclusions are that Simple and Complex cells, at least from their input organisation, lie on a continuum. Those results confirm the observation of Mechler & Ringach (2002) and Priebe & al, (2004) of subthreshold Complexity. Regarding this collection of convergent empirical results, the hierarchical model of receptive field originally proposed by Hubel & Wiesel (1962), which posits a hierarchical convergence of LGN cells to Simple cells and of Simple cells to Complex cells is no longer justifiable. Furthermore, those latter studies emphasized that the spike threshold nonlinearity is responsible for the difference between Simple and Complex RF organisation, which is partially true but not sufficient. We further point out that a single common synaptic connectivity scheme involving the Excitatory/inhibitory (E/I) balance, is accounting for RFs Simplicity and complexity organisation (figure 3.1.2.4). Combined with the excitatory and inhibitory large synaptic fields previously shown, it defines a generalised Simplex model which was originally proposed on the results that Hebbian supervised learning can balance V1 neuron responses from Simple-like to Complex-like (Shulz & al, 1999; Debanne et al, 1998). We propose that this balanced connectivity scheme between excitation and inhibition is modulated specifically for each cell (therefore lying on a continuum) and further segregated by the spike threshold nonlinearity.

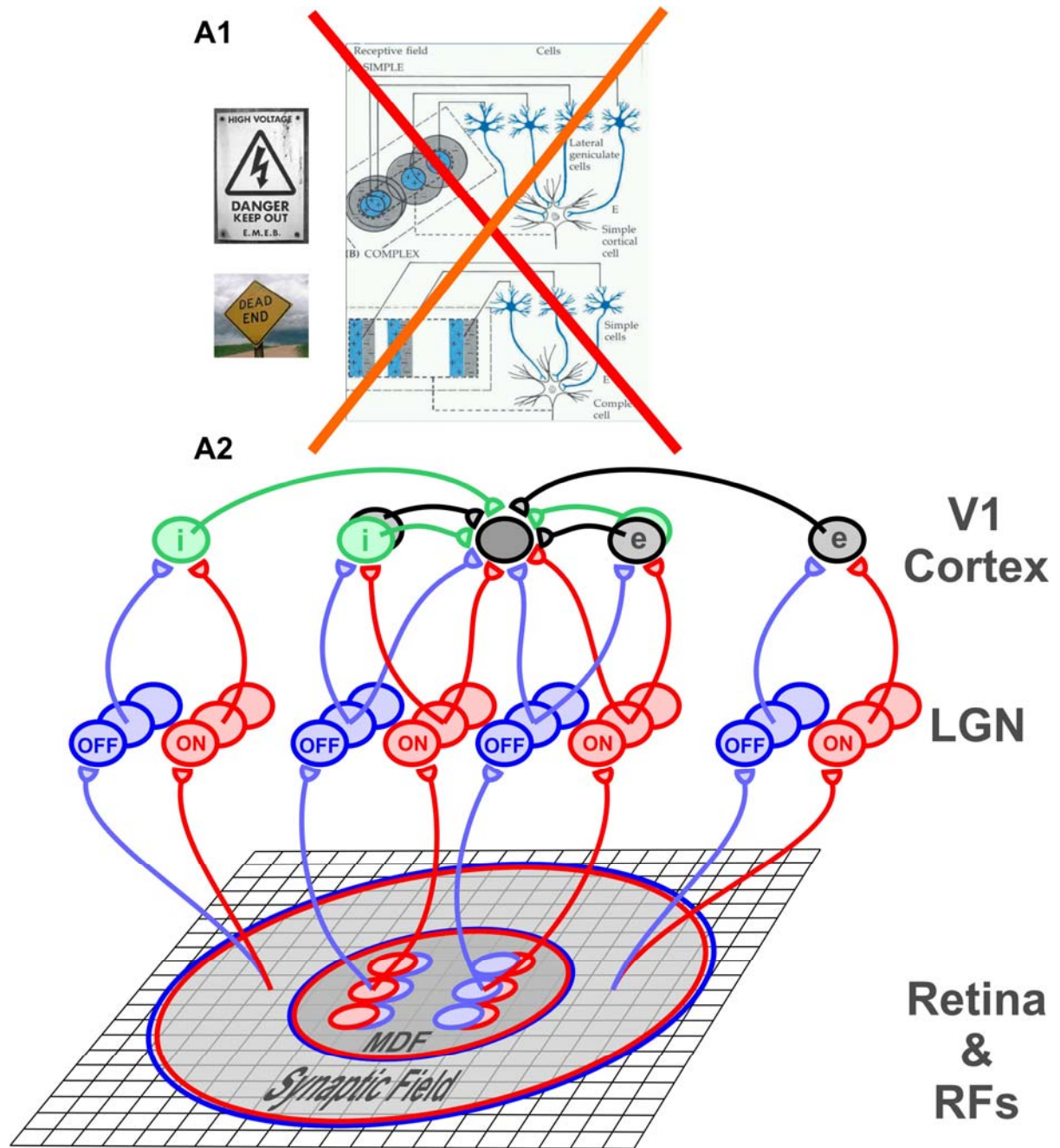


Figure 3.1.2.4: Generic cortical connectivity scheme for Simple and Complex Receptive Fields, and synaptic integration field generation. The Hierarchical model of Receptive Fields convergence does not account for the complexity of subthreshold responses and therefore loses its relevance (A1). The ON (red) and OFF (blue) channels are traced across the successive feed-forward visual integrative steps from the Retina, LGN, to cortex. Recurrent cortical connections either excitatory (black) or inhibitory (green) are deduced from our empirical results.

However, the convergent Hubel & Wiesel connectivity model is still supported by some recent results, which show that complex RF can be decomposed into a small number of Simple-like afferent units (Touryan & al, 2002, Touryan & al, 2005). The pertinence of those results can

be questioned, since they are based on the extraction of the second order covariance kernels imposing a biasing orthogonality on the subunit (Sharpee & al, 2006), and since the limited duration of their recorded data favours the detection of mostly “positive” excitatory subunits (Rust & al, 2005). In agreement with the model proposed here, a more sophisticated analysis mixing first and second order kernels and on larger data sample allowing the extraction of suppressive subunits have led to opposite results (Rust & al, 2005). The RFs, Simple as well as Complex according to this latest study, are composed of many significant subunits notably suppressive, presenting various types of spatiotemporal organisation (orientation, spatial frequency, phase etc...). However, such approaches only give a phenomenological description of the RF in term of multiple parallel filters which cannot be interpreted in terms of connectivity architecture or cortical machinery: the interpretative jump from functional suprathreshold RF subunits to physically defined afferent pathways has no direct reasonable foundation. At least, intracellular recordings of the membrane voltage input, and the identification of the excitatory and inhibitory spatiotemporal characteristics, allows an approximation of this functional/structural relation, and the result of our studies are incompatible with the classical functional convergence framework.

In conclusion, cortical E/I recurrence is strongly involved in the genesis of the receptive fields spatiotemporal characteristics, independently of the Simple or Complex dichotomy. The participation of cortical local recurrence, notably inhibition, to the genesis of orientation and direction selectivity, two of the main features of V1 selectivity, remains a subject of controversy. The functional role of those synaptic subthreshold RFs, indicating a dense and widespread E/I cortical recurrence, in the orientation and direction cortical selectivity is investigated in the next chapter.

3.2. Orientation and direction selectivity of excitatory and inhibitory inputs in visual cortical neurons: a diversity of combinations produces spike tuning

(published in Monier C, Chavane F, Baudot P, Graham LJ and Fregnac Y., Neuron. 2003, 20 [37(4)]: 663-80.)

Summary: This intracellular study investigates synaptic mechanisms of orientation and direction selectivity in cat area 17. Visually evoked inhibition was analyzed in 88 cells by detecting spike suppression, hyperpolarization and reduction of trial-to-trial variability of membrane potential. In twenty five of these cells, inhibition visibility was enhanced by depolarization and spike inactivation, and by direct measurement of synaptic conductances. We conclude that excitatory and inhibitory inputs share the tuning preference of spiking output in 60% of cases, whereas inhibition is tuned to a different orientation in 40% of cases. For this latter type of cells, conductance measurements showed that excitation shared either the preference of the spiking output or that of the inhibition. This diversity of input combinations may reflect inhomogeneities in functional intracortical connectivity regulated by correlation-based activity dependent processes.

3.2.1. Introduction

Brain computation, in the early visual system, is often considered as a hierarchical process where features extracted in a given sensory relay are not present in previous stages of integration. In particular, many response properties in visual cortex, such as orientation and directional selectivities, are not present at the preceding geniculate stage, and a classical problem is identifying the mechanisms and circuitry underlying these computations. In order to assess how much synaptic integration of the network activity at each neuron contributes to the genesis of cortical orientation and direction selectivity, it is necessary to provide reliable measurements of the input/output transfer function at the single cell level. In theory, a variety of combinations of excitatory and inhibitory input tuning can give rise to a given functional preference and tuning width in the spike response. Within this context an important issue is whether cross-oriented or null-direction intracortical inhibition is fundamental for stimulus selectivity, or rather only normalizes spike response tuning with respect to other features such as stimulus strength or contrast. After a long-standing debate, most recent models favor the

second possibility (see review in Ferster and Miller, 2000 and Douglas et al. 1999) largely because experimental support for the existence of inhibitory input in response to non-preferred stimuli has been somewhat contradictory.

The essence of the feedforward model, initially proposed by Hubel and Wiesel (1962), was that Simple cortical cells inherit their orientation preference from the anatomical convergence of thalamic inputs. In order to reproduce contrast invariance of orientation tuning (Sclar and Freeman 1982), this concept has been modified to include disynaptic intracortical inhibition acting in a so called “push-pull” manner (Troyer et al., 1998). This model predicts that the modulation of both excitatory and inhibitory input is largest for the preferred stimulus. However it is difficult to reconcile the apparent simplicity of feedforward schemas with the number and diversity of intracortical input sources impinging on cortical cells (Ahmed et al. 1994). Consequently, models of orientation tuning have been proposed, that rely on recurrent excitatory connections to amplify the optimal component of broadly tuned and weak thalamic input (Douglas et al., 1995, Somers et al., 1995; Ben-Yishai et al., 1995). In this scheme, a typical postulate is that intracortical inhibition acts non-specifically to maintain the selectivity of individual neurons by balancing intracortical excitation at the columnar level.

Nevertheless, a crucial role for inhibition has been indicated by pharmacological studies showing that GABA_A antagonists can modify or eliminate both orientation and directional selectivity in cat primary visual cortex (Sillito, 1979; Sillito et al., 1980, Eysel and Shevelev, 1994), although attempts to block GABA_A receptors intracellularly appeared not to change the qualitative orientation preference of the cell (Nelson et al., 1994). In addition, disinhibition experiments give strong evidence for an inhibitory shaping of orientation and direction selectivity by neighboring or distant columns (Eysel et al., 1990; Crook et al., 1997). Furthermore, these disinhibitory effects seem to be correlated with the anatomy of the intracortical inhibitory network (Crook et al., 1998, Roerig et al, 1999; Buzas et al., 2001). Some models of orientation and direction selectivity, incorporating non-specific or non-optimal inhibition, account partially for these different experimental results (Ferster & Koch 1987, Wörgötter & Koch 1991, Adojarn et al., 1999, McLaughlin et al., 2000, Ruff et al., 1987; Sabatini and Solari, 1999). However, currently available electrophysiological evidence supporting these models remains controversial. While intracellular recordings rather consistently show the presence of inhibition in response to the preferred orientation, as well as in some cases the direction opposite to the preferred one, no firm agreement has yet been reached concerning its presence for orientations outside the spike tuning range. Early

intracellular recordings (Benevento et al., 1972; Creutzfeldt et al., 1974; Innocenti and Fiore, 1974) showed strong hyperpolarizations in response to stimuli in the null direction and, occasionally, to cross-orientated stimuli. Later studies confirmed that prominent hyperpolarizations could be evoked by stimuli with nonoptimal orientations (Volgushev et al., 1993), depending of the laminar location of the cell (Martinez et al., 2002). However, other studies failed to reproduce these qualitative findings, reporting only iso-oriented hyperpolarisations (Ferster, 1986) or occasional hyperpolarizations for non-optimal orientations in some complex cells (Douglas et al., 1991).

Detecting inhibitory input on the basis of evoked changes in membrane potential may prove to be difficult since the reversal potential of GABA_A-controlled chloride channels is situated near the resting membrane potential of cortical neurons. This shunting inhibition may reduce the effect of concomitant excitation by evoking a large increase in input conductance while leaving the membrane potential relatively unaffected. Two strategies can be used to unmask this ‘silent’ inhibition: the first one is to depolarize the cell in current clamp, sufficiently to change the balance in the driving forces for inhibition vs. excitation. Using this method, Ferster (1986) reported that hyperpolarizing potentials recorded in the depolarized state had the same selectivity for orientation as depolarizing potentials.

The second approach is to estimate conductance changes during visual stimulation. First attempts using sample-based methods did not succeed in showing changes of synaptic conductance whether the applied stimulus feature was a preferred or a non-preferred one (Douglas et al., 1988, Berman et al., 1991, Ferster and Jagaadesh, 1992, but see Bush and Sejnowski 1994). In spite of these negative reports, we previously applied an *in vivo* whole-cell voltage clamping method to continuously track both the evoked conductance and the apparent synaptic reversal potential during visual responses of neurons in primary visual cortex. We demonstrated large transient shunting inhibition conductance increases for optimally oriented flashed stimuli (Borg-Graham et al, 1996, 1998). Using a similar method, but in current-clamp mode, a growing number of experimenters have since confirmed the presence of shunting inhibition *in vivo* (Hirsch et al., 1998; Anderson et al., 2000b). Furthermore, Anderson et al (2000b) reported that, for any given cell, the excitatory and inhibitory conductances had similar preferred orientations and tuning widths, highly correlated with that expressed by the firing tuning curve, whatever the laminar location of the post-synaptic cell.

Faced with the diversity of the experimental observations concerning the presence or not of inhibitory input evoked by non-preferred orientation or directions, we have re-addressed this issue with a quantitative comparative study combining several of the electrophysiological protocols mentioned above. Both sharp and patch electrodes were used in order to take advantage of complementary benefits provided by each technique applied in the same *in vivo* preparation.

3.2.2. Results

The approach we present here is to revisit, step-by-step, intracellular evidence for the presence of inhibitory input in non-preferred orientations/directions, and determine how the tunings of the excitatory and inhibitory inputs are related to that of the spiking output. Where possible, several complementary approaches were compared and combined in the same cell in order to compensate the limitations inherent to each method.

One set of protocols was based on passive measurement of intracellular potentials under current clamp. As a first step, at the resting membrane potential, we measured the tunings of evoked increases and decreases in spiking rate. We then measured the tunings of the depolarizing and hyperpolarizing components of the subthreshold synaptic activity. We also measured the inverse of the trial-to-trial variability ($1/\sigma$ of the stimulus-locked membrane potential waveform). Our hypothesis was that an increase in input conductance might produce a reduction in the trial-to-trial variability of the membrane potential trajectory independently of any change in the mean. Thus, an increase in $1/\sigma$ could signal the presence of shunting inhibition.

Since the presence of hyperpolarization can be masked by concurrent excitation, specially in the preferred orientation or direction, another set of protocols was aimed at increasing the visibility of synaptic input and allowing the quantitative measurement of this input. First, the inhibitory drive was amplified and the excitatory drive reduced by depolarizing the postsynaptic membrane potential in current clamp, sufficiently to fully inactivate spike-related currents. This method reveals visually evoked inhibition as hyperpolarizations. In the second approach, limited to low-access resistance patch recordings, we measured the continuous dynamics of the total synaptic conductance input and the associated reversal potential during the visual stimulation. Decomposition methods were then applied to dissect out the respective tuning of excitatory and inhibitory conductances (see Methods).

Orientation and direction tuning curves were measured using moving bars whose direction of motion was perpendicular to orientation, and which were swept across the full extent of the subthreshold visual receptive field (Bringuier et al., 1999). To facilitate comparison between the various response components presented above, we used the same quantifications in all cases, based on the integral calculated over the entire duration of visual stimulation. Statistical significance was tested against the non-stimulated condition. The optimal direction (OD), the tuning width (HWHH) and the nonorientation selective part ("Base") of each response component were estimated by fitting the response integral as a function of stimulus direction by two Gaussians forced to peak 180° apart. Importantly, the fit for each component was made independently of the other (see Discussion). Each response component was then classified into one of four categories depending on the comparison between its optimal direction and the preferred direction expressed by the spike response: "Iso-P" for angular difference ranging between [0°-30°], "Oblique" for differences between [30°-60°] or [120°-150°], "Cross" for differences between [60°-120°], and "Iso-N" for differences between [150°-180°].

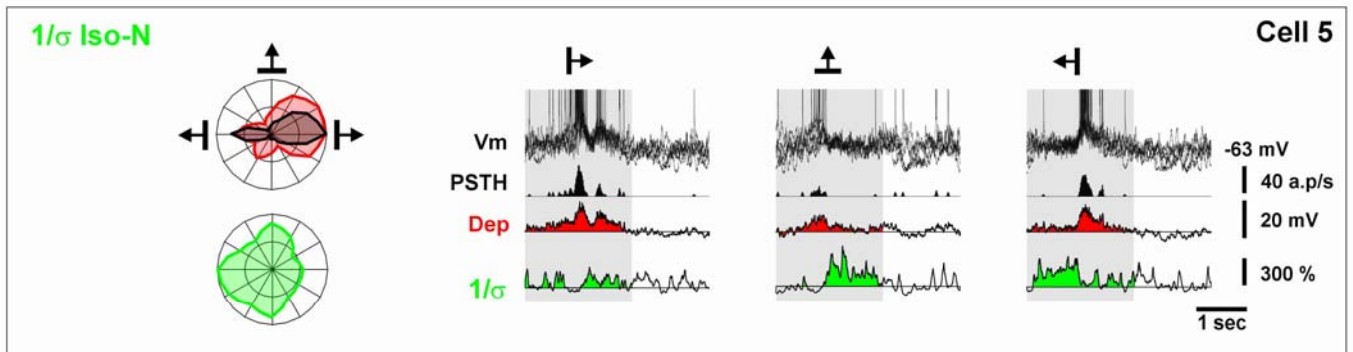
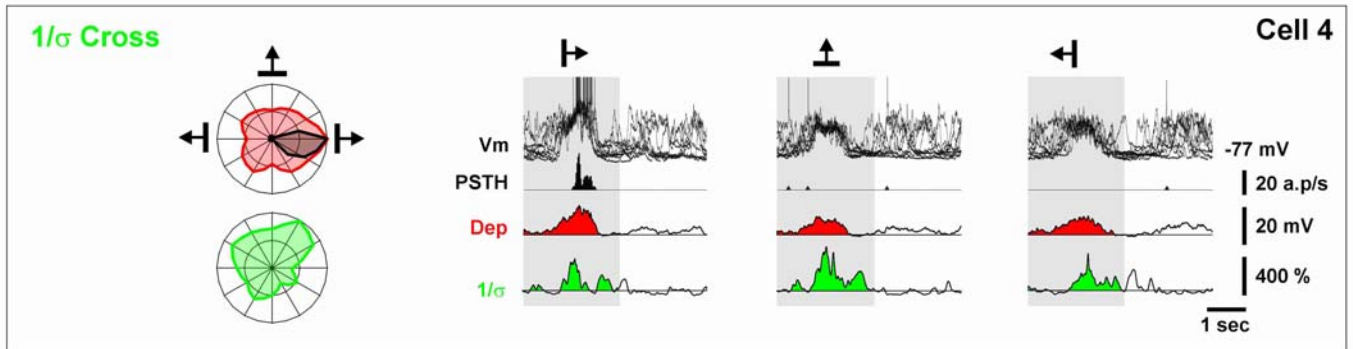
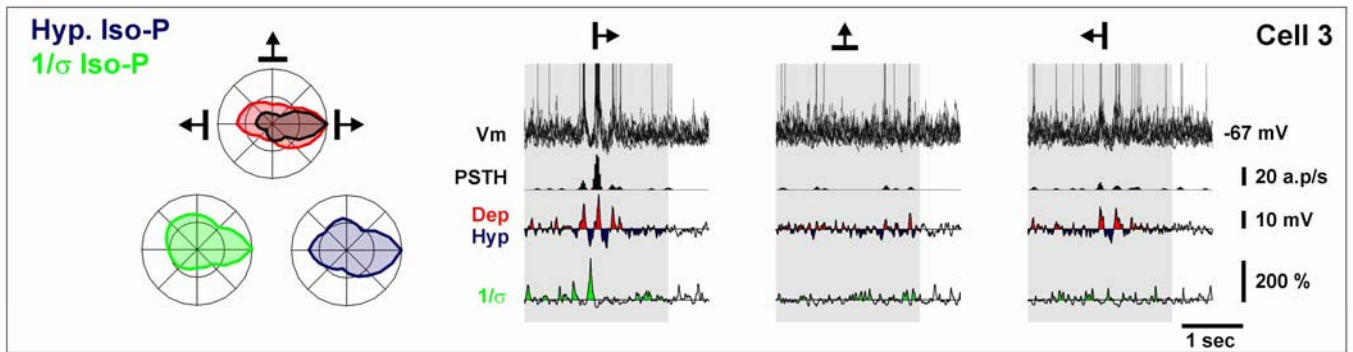
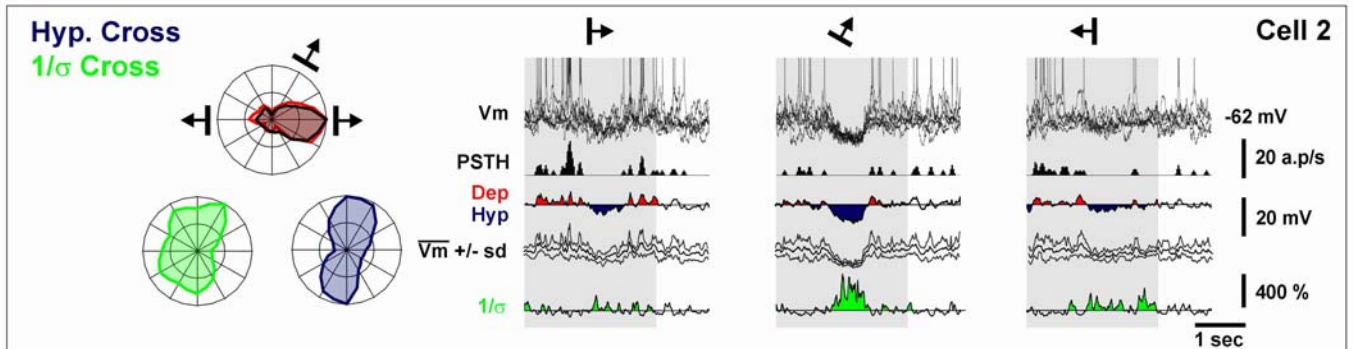
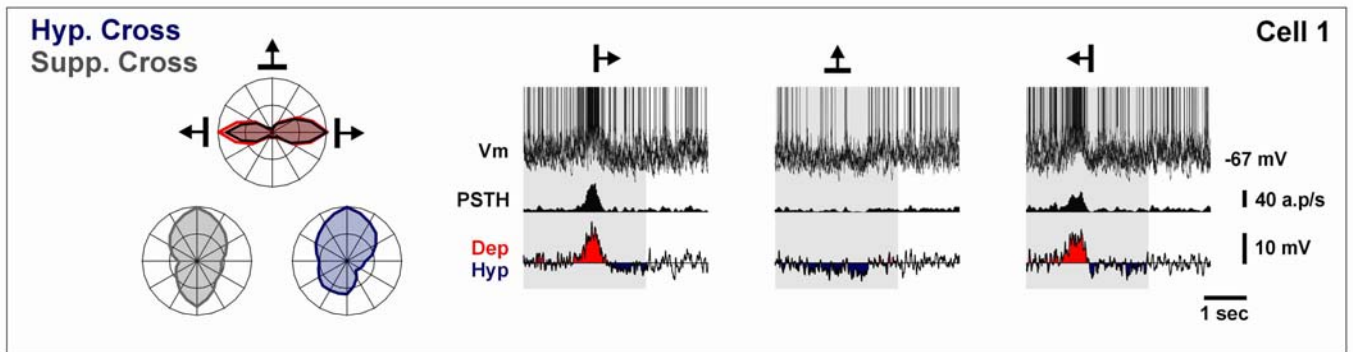


Figure 3.2.1: Measurements of visual activity, evoked from the resting state: This figure shows five examples of whole cell patch and sharp recordings, each row illustrating one cell. Each inset shows, from top to bottom, the time-course of evoked responses obtained at rest for the membrane potential (5 to 10 superimposed trials, truncated spikes), for spike counts (black: PSTH) and for subthreshold activity (depolarization in red (Dep); hyperpolarization in blue (Hyp)) for three particular stimulus directions (left, preferred direction (0°)); middle, cross-orientation [60° - 120° , 240° - 300°]; right, null-direction (180°)). The left column presents polar-plots of the different response components with their respective color codes. To facilitate comparisons in the polar plots of this and the subsequent figures, the direction eliciting the best spiking response was set to 0° for all cells, pointing to the right. For direct comparison, the tunings of the spike and depolarizing responses are overlaid on the same plot. Cross-oriented hyperpolarization and spike suppression are illustrated in **cell 1** (Sharp, Simple RF; optimal directions (OD): Dep. 1° , Supp. 88° and Hyp. 81°). Concomitant hyperpolarisation and $1/\sigma$ components are illustrated in **cell 2** (Patch, Complex RF; OD: Dep 0° , Hyp 80° and $1/\sigma$ 90°) and **cell 3** (Sharp, Simple RF; OD: Dep 5° , Hyp 0° , $1/\sigma$ 6°). Reduction of trial-to-trial variability associated with depolarizing or null mean response is illustrated in **cell 4**, which had a bistable behaviour (Patch, Complex RF; OD: Dep 9° and $1/\sigma$ 79°) and **cell 5**: (Patch, Simple RF; OD: Dep 5° and $1/\sigma$ 152°).

The present study is based on the quantitative analysis of 88 cells recorded using sharp ($n=39$) and whole cell patch ($n=49$) electrodes, for which the receptive field (RF) was characterized by sparse noise mapping (51 simple (25 S1 and 26 S2-S3), 32 complex and 5 unclassified) and the orientation selectivity of subthreshold and spiking activity was measured in response to moving bars. The spontaneous activity and the peak firing rates for the preferred stimulus were higher for sharp than for patch recordings (spontaneous activity: 3.8 ± 5 a.p./sec. ($n=39$) vs. 0.3 ± 0.5 a.p./sec ($n=49$), $p < 0.01$ and peak firing rate: 52 ± 28 a.p./sec. ($n=39$) vs. 32 ± 27 a.p./sec ($n=49$), $p < 0.01$). In about one quarter (20/88, 23%) of the cells, a clearly bimodal or two-state distribution of the spontaneous membrane potential was apparent in both patch and sharp recordings (see also Anderson et al, 2000a).

3.2.2.1. Spike and depolarizing responses

All cells presented a significant depolarizing response in at least one direction, with a mean peak depolarization amplitude for the optimal stimulus in the order of 10 mV (9.5 ± 4.8 mV, $n=88$). The orientation tuning of depolarizing responses was, on average, significantly wider than that of spiking responses (HWHH: $46 \pm 13^\circ$ vs. $30 \pm 9^\circ$, Base: $23 \pm 19\%$ vs. $5.6 \pm 8\%$, $p < 0.01$, $n=88$). However, the improvement in orientation selectivity between the depolarizing and the spiking responses (mean of the difference in tuning width: $15 \pm 13^\circ$, $n=88$) was highly variable between cells (range for the difference: -10° to 60° , see example in Figures 1, 3 and 4). As expected, the optimal direction derived from the subthreshold depolarizing response tuning and that expressed in the spike discharge tuning was similar for a large majority of cells (82% of Iso-P cases, shown in the red histogram (Dep.) of the left column in Figure 3.2.2). Nevertheless, some cases were observed where the largest depolarization (measured by its integral value) was obtained for non-preferred orientations (11%) or null-directions (7%).

Relative Optimal Direction

Tuning curve

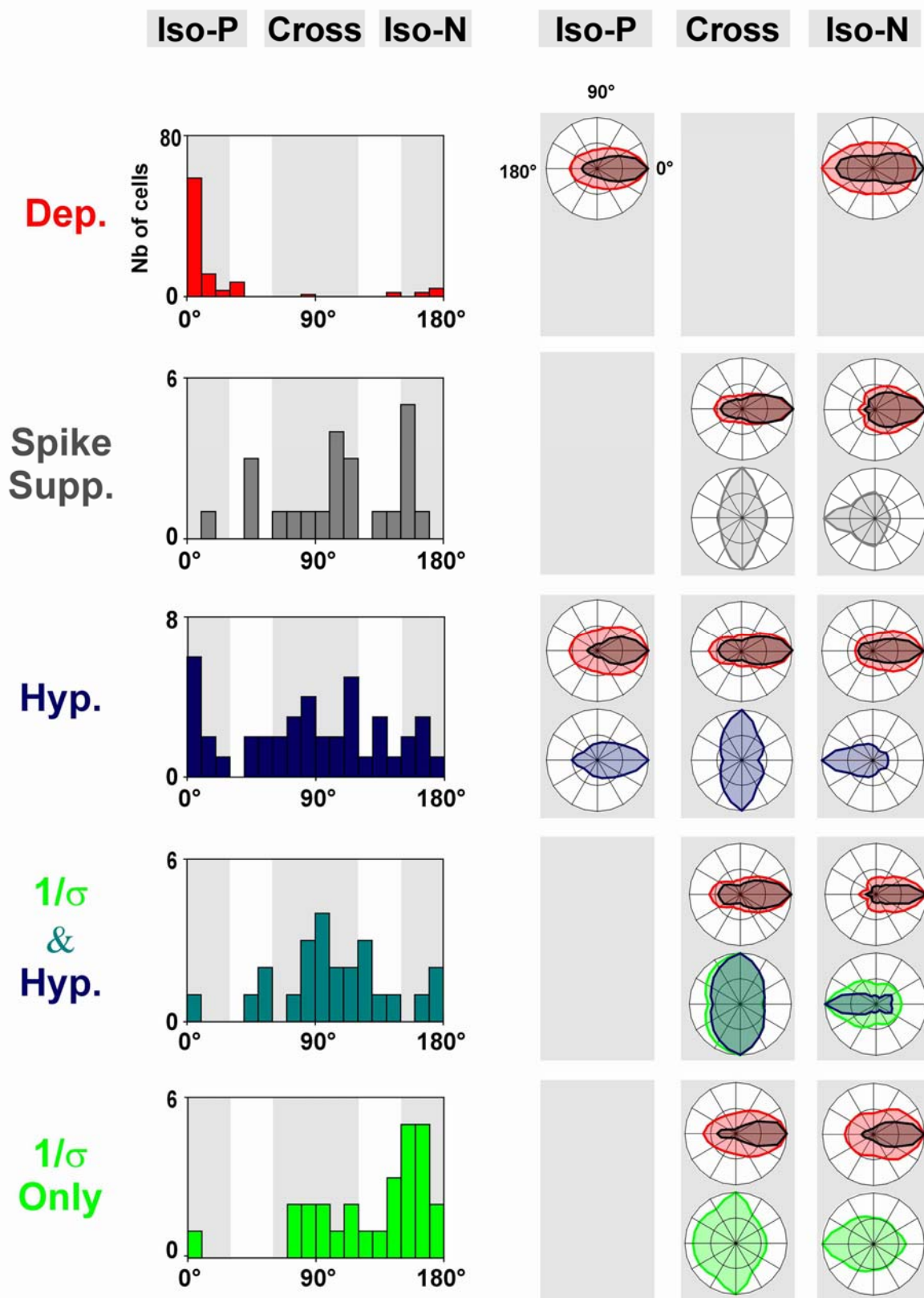


Figure 3.2.2: Measurements of visual activity, evoked from the resting state: Population analysis. The left column presents, for each component, the distribution of the optimal direction (OD) relative to the spike preferred (set to 0°): Spike suppression (Spike Supp.), Depolarization (Dep), hyperpolarization (Hyp), inverse of trial-to-trial variability concomitant with a significant hyperpolarisation (1/σ and Hyp) and without significant hyperpolarisation (1/σ only). The right panel presents the averaged tuning curves of the various components for different sub-populations of cells defined on the basis of their optimal direction relative to the preferred direction: Iso-P, Cross- or Iso-N. Cells with a component that had an oblique preference are not included in the averaged polar plots.

3.2.2.2. Suppression of spike discharge and hyperpolarizing responses

In one quarter of the cells (23/88, 26%) for which background activity was high enough to detect periods of significant spike rate decrease, it was possible to establish the range of orientations or directions for which a suppression of background activity (integrated only over the periods where it is detected during the whole stimulus exploration) was induced by the visual stimulus (shaded tuning curves in left column, for cell 1 in Figure 3.2.1 and cell 6 in Figure 3). The overall distribution of the optimal direction derived from the spike suppression component shows dominance for cross-orientation preference (Cross: 11/23, 48%) and null direction (Iso-N: 6/23, 26%). The tuning width of the suppression was generally broader than that of the spike (HWHH: $48.1 \pm 20^\circ$; base: $15 \pm 12\%$, $n=23$).

Significant hyperpolarizing responses from rest could be detected for at least one direction in half of the cells (42/88, 48%). The mean peak amplitude (calculated over a 25 ms period) of the hyperpolarization component was 3.7 ± 1.8 mV ($n=42$). The probability of detecting evoked hyperpolarizations appeared to depend on the initial resting potential, since the average resting potential of cells with significant hyperpolarizing responses was more depolarized than that of the remaining cells (-64 ± 4 mV ($n = 42$) vs. -69 ± 6 mV ($n=46$), $p < 0.01$). The hyperpolarizing component had a tuning width of $40 \pm 16^\circ$ with a base component equal to $11 \pm 12\%$ of the peak amplitude. The summary distribution (Hyp. in Figure 3.2.2) shows that the direction preference of the hyperpolarizing component differs from that expressed by the spike response. Almost two-thirds of the cells showed the optimal hyperpolarizing response for either cross-oriented (Cross: 18/42, 43%, see Figure 3.2.1, cells 1 and 2) or oblique directions (Oblique: 9/42, 21%, see cell 6 Figure 3). The remaining third of the cells had dominant hyperpolarizing responses for either the preferred direction (Iso-P: 9/42, 21%, see cell 3, Figure 3.2.1), or for the null direction (Iso-N: 6/42, 14% see cell 11 Figure 3.2.4). Of the 23 cells with significant background spike activity, 14 showed both significant spike suppression and hyperpolarizing responses, with similar optimal direction preference ($r^2 = 0.77$, $p < 0.01$, $n = 14$). Cells with a cross-oriented optimal hyperpolarizing

component were significantly less direction selective than cells with an iso-oriented optimal hyperpolarizing component (DI: 0.48 ± 0.27 (n=18) vs. 0.75 ± 0.24 (n=15), $p < 0.01$).

3.2.2.3. Trial-to-trial variability of the membrane potential

It was expected that the presence of a shunting inhibition might cause a significant reduction of trial-to-trial variability in the trajectory of the membrane potential independently of any significant hyperpolarization or depolarization during the visual response. We therefore calculated the inverse of the standard deviation of the membrane potential waveform synchronized with the stimulus onset (see $V_m \pm S.D.$ and $1/\sigma$, green trace in cell 2 in Figure 3.2.1) and compared this with the baseline level observed in the absence of visual stimuli.

A majority of cells (52/88, 59%) showed a significant reduction of trial-to-trial variability during visual stimulation in a least one direction. The mean peak amplitude of the $1/\sigma$ component was 183 ± 67 % (n=52) and was observed at similar membrane potential values in different cells (-66.4 ± 4.4 mV (n=52)). These cells exhibited a significantly higher trial-to-trial variability in their pre-trigger spontaneous membrane potential activity than the rest of the population (i.e., for $1/\sigma$: 0.3 ± 0.1 mV⁻¹ (n=52) vs. 0.8 ± 0.7 mV⁻¹ (n=36), $p < 0.01$), suggesting that a certain fluctuation level in the synaptic background activity has to be present in order to detect a significant reduction in evoked variability.

About half (24/52, 46%) of the cells that showed a significant reduction in trial-to-trial variability also showed significant evoked hyperpolarizations (see cells 2 and 3, Figure 3.2.1), and the orientation preferences of the two components were found to be correlated ($r^2 = 0.70$; $p < 0.01$ (n=24)). In spite of this similarity, and as summarized in the left column in Figure 3.2.2 (see Hyp and $1/\sigma$ rows), the tuning width of the $1/\sigma$ component was, on average, larger than that of the hyperpolarizing component (HWHH: $50 \pm 18^\circ$ vs. $41 \pm 19^\circ$; $p < 0.05$ (n=24)). For the majority of these cells, the largest reduction of variability was evoked for non-preferred directions or orientations (Cross and Oblique: 20/24, 83%).

We also recorded from cells in which a reduction in trial-to-trial variability during the visual response was seen without changes in membrane potential or with a concomitant depolarization of the mean membrane potential (Figure 3.2.1, cells 4 and 5). For these cells (28/52, 54%) the tuning width of the variability reduction effect was broad (HWHH: $61 \pm 19^\circ$, n=28), and the distribution of the direction preference derived from the $1/\sigma$ tuning curve (Fig 2, $1/\sigma$ only) showed a strong peak for the null direction. For the cells that showed a two-state behaviour (15/28, 54%), visual stimuli tended to clamp the membrane potential in the up-state

independently of the stimulus direction, resulting in a significant reduction in trial-to-trial variability associated with a strong depolarization. However the strength of this variability reducing effect still depended on stimulus orientation (compare the up-state variability observed for the cross and the null-directions in cell 4 of Figure 3.2.1).

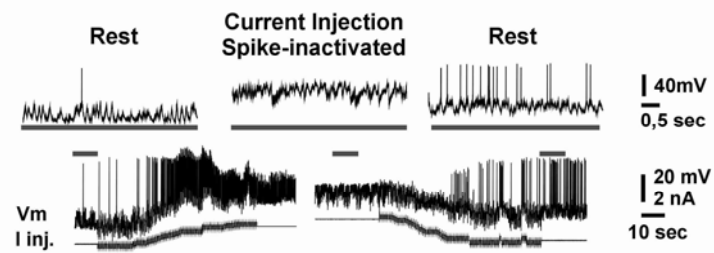
3.2.2.4. Unmasked inhibition by spike-inactivated protocols

The results presented above suggest the presence of inhibitory input for both preferred and non-preferred orientations. However, inhibition evoked by the preferred stimulus (i.e. that eliciting the strongest spike discharge) may be underestimated since it could be masked when concomitant excitation dominates and the cell fires. To address this possibility, as well as to improve the visibility of inhibitory inputs as hyperpolarizing events, we increased the inhibitory driving force by depolarizing the cell (Figure 3.2.3, see method panel) using intracellular injection sufficient to inactivate fast Na-channels and thus completely suppress spike activity. In this spike inactivated state, only hyperpolarizing responses were significant, giving a reliable indication that the holding potential was close to the reversal potential of excitatory input. This protocol was applied successfully and reversibly in nine cells, for which we could compare the tuning curves of the evoked hyperpolarizing responses observed in the spike-inactivated state (Inh: inhibitory component, in Figure 3.2.3), with the spike tuning curves established at rest (without current injection). Figure 3.2.3 illustrates five cells in which visually evoked spike and subthreshold responses were compared with the inhibitory response component. The main result is the striking diversity of the distribution of inhibitory input observed in different cells: one third of cells (3/9) had an inhibitory component with an optimal direction in the preferred direction, one third in the oblique- (1/9, see cell 6, Figure 3.2.3) or cross- (2/9, see cell 7, Figure 3.2.3) orientation preference and one third (3/9) in the null-direction (see cells 8 and 9, Figure 3.2.3). The HWHH of the tuning curves of the inhibitory component measured in the spike-inactivated state was on average of $43 \pm 16^\circ$ ($n=9$) with a base of $29 \pm 18\%$. The diversity in the respective tuning preferences of spike output and the inhibitory input revealed in the spike-inactivated state is further summarized in Figures 5 and 6. The hyperpolarizations evoked in the spike inactivated state were larger in amplitude and duration than that seen at the resting state, when this latter component was detectable. For cell 6 in Figure 3.2.3, the amplified evoked hyperpolarizations exhibited the same oblique preference as the hyperpolarizations at rest and the suppression of the spike component, but with a wider tuning due to the unmasking of inhibition for both the preferred and null directions. Cells 7, 8 and 9 (Figure 3.2.3) showed only depolarizing components under the

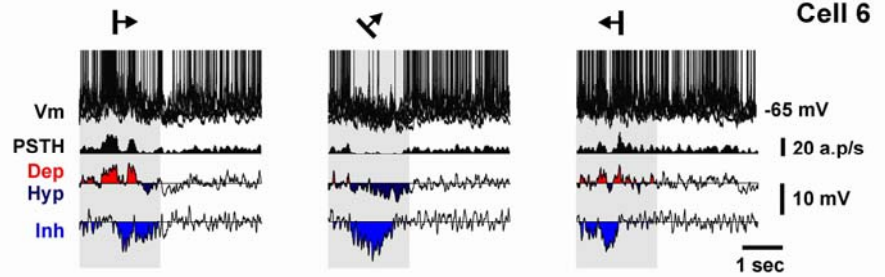
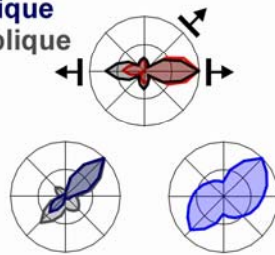
control condition, whereas the presence of an inhibitory component was revealed in all directions under depolarizing current, with either a cross-oriented (cell 7) or null-direction preference (cells 8 and 9). The time course of the inhibitory component waveform reproduced precisely that observed for the reduction in membrane potential trial-to-trial variability at rest, giving further evidence that the decrease of variability indeed reflects a dominant inhibitory input. The two cases where the orientation preference of the hyperpolarizing components was not the same at rest and in the spike-inactivated state corresponded to a shift from cross- to isoreference, and from oblique- to cross-preference, suggesting no systematic bias in the revealed component relative to the spike-based preference.

Figure 3.2.3: Inhibition revealed by spike-inactivated protocols: This figure presents four examples of sharp recordings for which a reversible spike-inactivated protocol was applied, each panel illustrating one cell. The method is summarized in the top inset. A depolarizing current was injected and its intensity level adjusted to inactivate spike initiation. The presence of IPSPs can be seen as hyperpolarizations in the membrane potential during current injection. The end of the trace illustrates the reversibility of the protocol. Inhibitory (Inh), hyperpolarization and spike suppression components with an oblique preference are illustrated in **cell 6** (Sharp, Simple RF; OD: Dep. 3°, Supp. 46°, Hyp. 46° and Inh. 41°). Cross-oriented inhibitory components are illustrated in **cell 7** (Patch, Complex RF; OD: Dep 2° and Inh 118°). **Cell 8** illustrates the case of an inhibitory component in the Null direction (Sharp, Complex RF; OD: Dep 12° and Inh 161°). A similar finding was observed for **cell 9**, for which both the time course and orientation tuning of the inhibitory and $1/\sigma$ components were highly correlated (Sharp, complex RF; OD: Dep 7°, $1/\sigma$ 159° and Inh 177°).

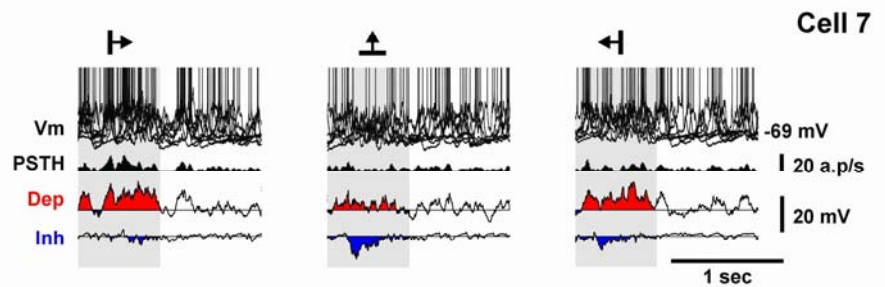
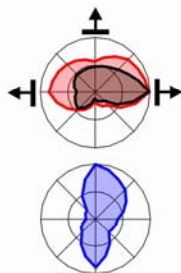
Method



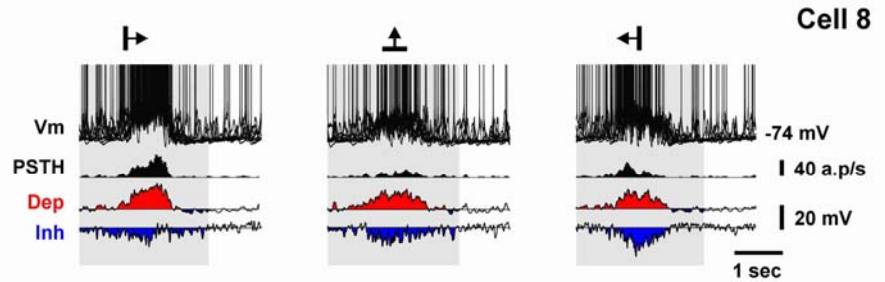
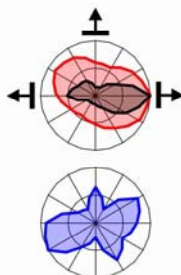
Inh. Oblique Hyp. Oblique Supp. Oblique



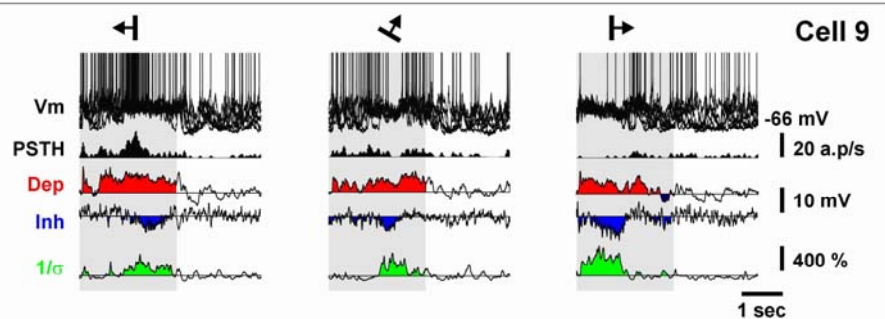
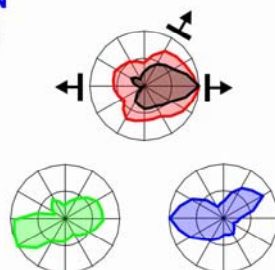
Inh. Cross



Inh. Iso-N



Inh. Iso-N 1/σ Iso-N



3.2.2.5. Excitatory and inhibitory conductances

The results obtained so far show that the tuning of inhibitory input can be unmasked and qualitatively studied in the spike-inactivated state. However these experiments do not provide a direct quantitative estimate of the excitatory and inhibitory tunings. The continuous measure of input conductance and the apparent reversal potential during the visual response advances one step closer towards the identification of the orientation or direction dependence of synaptic inputs (Borg-Graham et al., 1998, Borg-Graham, 2001). Voltage-clamp measurements of excitatory and inhibitory conductances and their orientation or direction tuning were successfully achieved with low access resistance for 12 cells (see example of VC recordings in cell 13, Figure 3.2.4). We also estimated conductance components in current-clamp mode in 7 cells. Since similar results were obtained with both methods when tested on the same cells ($n=3$), data were pooled for further population analysis (16 cells and 19 protocols in total).

The relative increase in global peak conductance was similar, on average, for different populations of cells when evoked by moving stimuli or by flashed stimuli ($110\pm60\%$ ($n=19$) vs. $113\pm58\%$, ($n=7$)), and the range (35% to 270%) was equally variable among cells. The relative contribution of excitation and inhibition in the input tuning was examined using a three-term decomposition algorithm to extract one excitatory (AMPA) and two inhibitory synaptic components ($GABA_A$ and $GABA_B$) of the evoked conductance change. Note that the possible implication of NMDA receptor activation was not taken into account by the decomposition model. Results show that in most cases the influence of the $GABA_B$ component was minor. The several examples shown in Figure 3.2.4, which illustrate only the AMPA and $GABA_A$ components of the conductance change, show a large diversity of tuning combinations for excitatory and inhibitory conductance increases.

Establishing the relative strength of conductances by integrating synaptic input for each stimulus direction may give only a partial understanding of the effectiveness of the interaction between excitation and inhibition. An additional key feature in the genesis of functional preference is the temporal overlap of both types of inputs, which act out of phase, or in-phase. To explore these temporal relationships, the waveforms of the excitatory and inhibitory conductances were crosscorrelated for each direction of the stimulus, and a normalized correlation index at zero-time lag was used to quantify their temporal overlap (TO: 0% for antiphase, 100% for in-phase, see Methods).

Over the whole population, only three major types of interaction between excitatory and inhibitory tuning were found for both orientation and direction selectivity on the basis of their similarity (“Preferred”: P) or dissimilarity (“Non-Preferred”: NP) to the spike output preference, distinguishing between 1) those cells in which excitatory and inhibitory input were tuned for the preferred direction or orientation (P-P), 2) those where the excitatory input was tuned for the preferred stimulus but the inhibition was tuned for the non-preferred stimulus (P-NP) and, finally, 3) those where excitatory and inhibitory inputs were tuned for the non-preferred stimulus (NP-NP). These different combinations (among four theoretically possible) were associated with particular modes of temporal overlap between the excitatory and the inhibitory conductances.

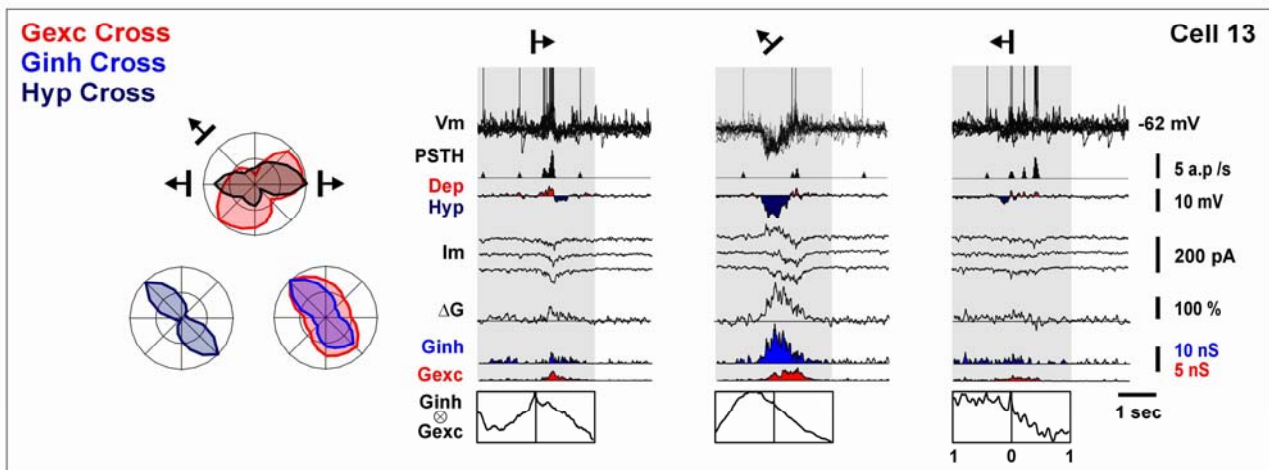
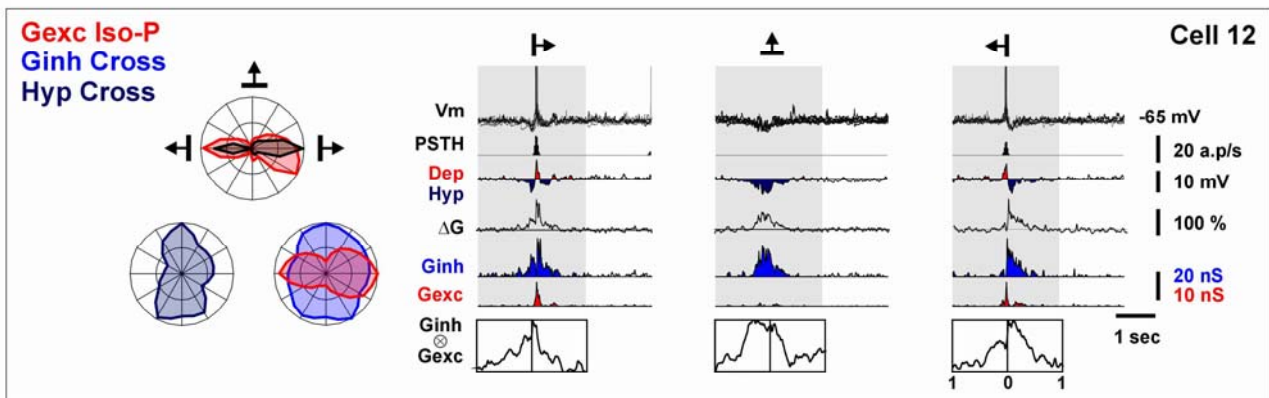
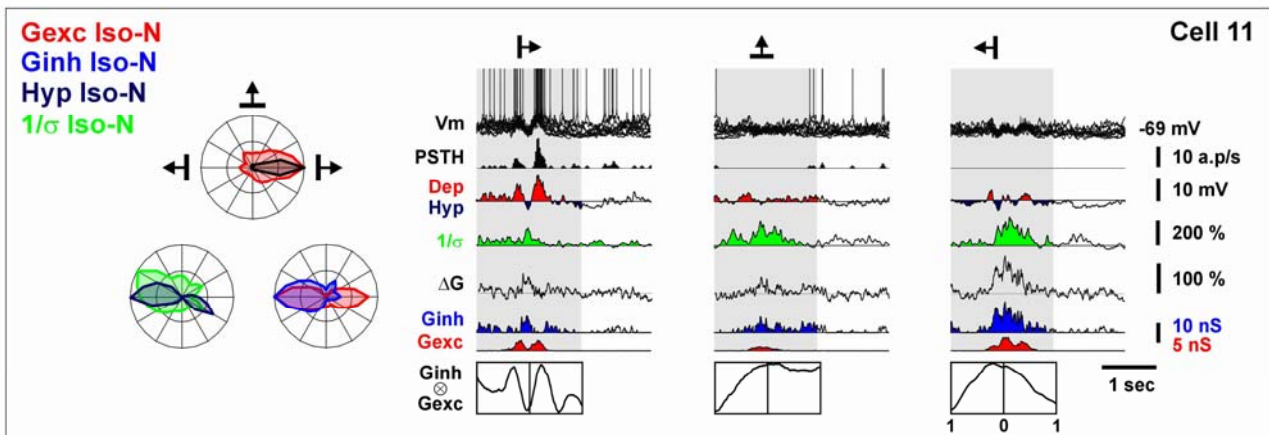
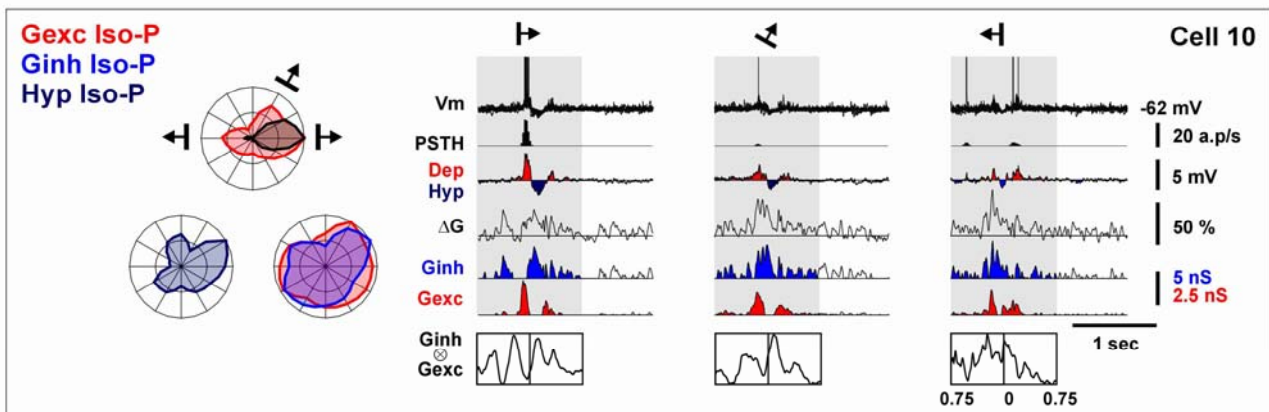


Figure 3.2.4: Excitatory and inhibitory conductances: This figure presents four examples of whole cell patch recordings, where measures of excitatory and inhibitory conductances were made in VC and CC modes (cell 13), each panel illustrating one cell. Excitatory conductances are in red and inhibitory conductances in blue. Note that the scale of excitatory conductance is double that of the inhibitory conductance. The case of iso-oriented excitatory and inhibitory conductances is illustrated in cell 10 (Patch, Simple RF, OD: Dep 2°, Hyp 9°, Gexc 19°, Ginh 25°) and cell 11 (Patch, Simple RF, OD: Dep 2°, Hyp 169°, $1/\sigma$ 172°, Gexc 180° and Ginh 179°). Both conductances were optimal in the preferred direction for cell 10 and in the null direction for the cell 11. Cell 12 (Patch, Simple RF) illustrates the case of a cross-oriented inhibitory conductance with iso-oriented excitation (OD: Dep 10°, Hyp 8°, Gexc 6° and Ginh 75°). Cell 13 (Patch: Complex RF) illustrates the case where both excitatory and inhibitory conductances were cross-oriented (OD: Dep 146°, Hyp 114°, Gexc 108° and Ginh 111°). The bottom insets give the normalized cross-correlation function between the excitatory and inhibitory conductance waveforms and the ordinate for a zero time delay is used to quantify the degree of temporal overlap (TO) between the two waveforms (see Methods).

In terms of orientation selectivity (summary in table 3.2.1 and Figure 3.2.6), in about two thirds of the cells, both excitatory and inhibitory conductance tunings were biased towards the preferred orientation (P-P class: 10/16, 62%, see cells 10 and 11, Figure 3.2.4). The tuning widths of excitatory and inhibitory conductances were, on average, broader than that of the spike output but similar to that of the depolarization component (see table 3.2.1 and Figure 3.2.6). On a cell-to-cell basis, however, the tuning widths of excitatory and inhibitory conductances were often different. The plot of the tuning width of excitation vs. that of inhibition shown in Figure 3.2.5, indeed illustrates that few data points lie on the diagonal and that no particular tendency is observed. The excitatory and inhibitory conductance tuning widths in cell 10 (Figure 3.2.4) showed poor selectivity but their temporal relationship (see cross-correlation graphs in Figure 3.2.4) was highly dependent on orientation (and direction): for the preferred direction both conductances were in anti-phase (temporal overlap (TO) index of 27%), whereas for the non-preferred orientations they were in-phase (TO of 77%). This observation seems to be the general case for cells of the type P-P (TO: $36 \pm 20\%$ for preferred direction vs. $71 \pm 18\%$ for non-preferred orientations, paired $p < 0.01$, $n=12$ (VC and CC recordings)).

For one fifth of the studied population (P-NP class: 3/16, 19%, see cell 12, Figure 3.2.4), the excitatory input was iso-oriented and the inhibitory input was cross-oriented. The tuning width of inhibition was wider than for excitation, but both were wider than spike tuning (see table 3.2.1 and Figure 3.2.6). A much higher level of temporal overlap between excitatory and inhibitory conductances was found than for the previous class of cells (P-P), independently of the orientation of the stimulus (table 3.2.1).

In the remaining cells (NP-NP class: 3/16, 19%, see cell 13, Figure 3.2.4) excitatory and inhibitory conductances shared the same orientation preference, either oblique (1/16) or cross-oriented (2/16), distinct from the spike-based preference (see the diagonal of figure 3.2.5). For

these cells, the tuning width of excitatory and inhibitory orientation tuning was broad (see table 3.2.1). As in the previous class, the two conductances were in temporal overlap (see table 3.2.1). The orientation selectivity of spiking activity (output tuning) results mainly from the broader tuning of excitation (higher base value), that predominates over inhibition for orientations away from the initial input preference (see cell 13, Figure 3.2.4 and table 3.2.1a).

In terms of direction selectivity, cells with an iso-oriented excitation and inhibition have a highly direction selective spike output ($DI=0.76\pm0.25$, $n=10$), whereas cells with non-optimally tuned inhibition are much less direction selective. This applies for cells with only cross-oriented inhibition ($DI=0.2$, $n=3$) and for cells where both excitation and inhibition are cross-oriented ($DI=0.23\pm0.13$, $n=3$). For simplicity and because cells with iso-oriented excitatory and inhibitory conductances present a high direction selectivity compared to others, only these cells (Iso-P or Iso-N) were considered for the study of direction selectivity. A classification for direction selectivity similar to that established for orientation preference was observed (summary in table 3.2.1b and Figure 3.2.6).

1.a. Orientation		Gexc			Ginh			Pref	N-Pref	Dep.	Spike	
Schema	# cells	PO	HWHH	Base	PO	HWHH	Base	TO	TO	HWHH	HWHH	DI
P-P	10/16	8±6°	47 ±11°	31±19%	17±9°	47±8°	27±14%	36±20%	71±18%	47±15°	26±6°	0.76±2
P-NP	3/16	7±5°	38 ± 6°	38±16%	82±17°	53±10°	43±21%	85±17%	94 ±4%	41±13°	24±10°	0.23±0.2
NP-NP	3/16	78±34°	49±14°	41±10%	81±24°	48±16°	27±10%	91±17%	94±5%	52±24°	35±12°	0.23± 0.1
1.b. Direction		Gexc			Ginh			Pref.	N-Pref.	Dep	Spike	
Schema	# cells	PD	DI		PD	DI		TO	TO	DI	DI	
P-P	7/10	9 ± 7°	0.22±0.1		17±8°	0.29±0.3		29±20%	61±19%	0.28±0.1	0.74±0.2	
P-NP	2/10	9 ± 9°	0.29±0.1		167±2°	-0.19±0.2		91±16%	92±8%	0.60±0.2	0.67±0.4	
NP-NP	1/10	179°	-0.2		180°	-0.36		32%	94%	0.65	1	

Table 3.2.1: Orientation & direction selectivity of excitatory and inhibitory conductances 1a: Orientation tuning: PO: preferred orientation; HWHH: half width at half height; Base: Basal fraction. TO: temporal overlap; DI: directional selectivity index; Gexc and Ginh: excitatory and inhibitory conductances. Dep: depolarizing component. Pref: spike-based preferred orientation. Non-Pref: oblique or cross-orientation. See text for further details. 1b: Direction tuning: This sub-table concerns the sub-population of cells where the optimal orientation for excitatory and inhibitory are iso-oriented (Iso-P and Iso-N). Pref: spike-based preferred direction. Non-Pref: Null direction. Same conventions as in Table 1. See text for further details.

A majority of cells showed both excitation and inhibition tuned to the preferred direction (P-P class: 7/10, 70%). These cells had a depolarizing response and input conductances with a lower direction selectivity index than that of the spiking output (see table 2). The temporal overlap between excitatory and inhibitory conductances seems to play a important role for the

spiking direction selectivity, the TO index being significantly lower for the preferred direction than for the null direction (TO: $29 \pm 20\%$ vs. $61 \pm 19\%$, $p < 0.01$, see table 2).

Two cells had excitatory conductances tuned to the preferred direction and inhibitory conductances tuned to the null direction (P-NP class: 2/10, 20%). The spiking and depolarization components were both moderately direction selective, whereas excitatory and inhibitory conductance inputs were not (see table 2). In contrast to the previous case, excitation and inhibition acted concomitantly and the temporal overlap between excitatory and inhibitory conductances was equally high for both directions (see table 2). In the last cell, both excitatory and inhibitory inputs peaked for the null direction (NP-NP class: 1/10, 10%). The same two processes (relative tuning and temporal overlap) can account for the spike output selectivity. First, inhibition was more tuned to the null direction than excitation, in such a way that excitation still evoked a depolarization for the preferred direction that was larger than that for the null direction (see table 2). Second, the temporal overlap between excitation and inhibition was much larger for the null (94%) than for the preferred direction (32%). In addition, a strong correlation was observed between the waveforms of the inverse of trial-to-trial variability and of the inhibitory input conductance (example in figure 3.2.4, cell 11: compare the green and blue traces). This correlation was also present in the polar plots for the two components.

We have extracted from the current clamp and voltage clamp recordings various measures that reflect to different extents the range and relative dominance of excitatory and inhibitory inputs to a cell. It is thus possible to compare the selectivity of subthreshold depolarizing and hyperpolarizing components measured at rest, with the tuning of inhibitory and excitatory conductances.

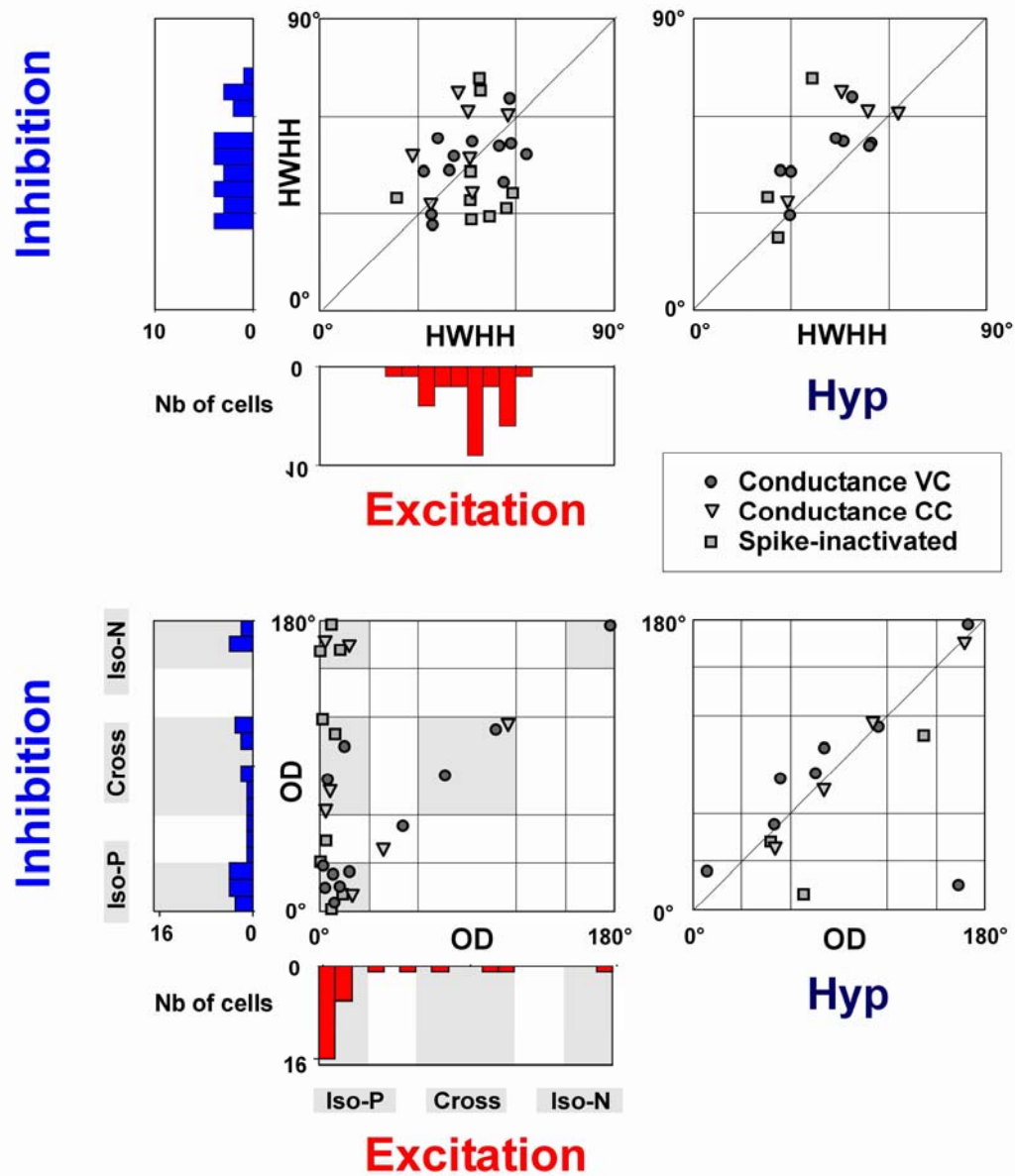


Figure 3.2.5: Excitatory and inhibitory input tunings: population analysis. This figure compares the tuning characteristics (HWHH and OD) of excitation and inhibition, revealed by two different methods. In the scatter plots, circles represent cases where the excitatory and inhibitory conductance tunings were measured in VC (12 cases), triangles the cases where these were measured in CC (7 cases). Squares represent cells where the inhibitory selectivity was explored with the spike inactivation protocol (9 cases). In these cases the tuning of the depolarizing component used to estimate that of excitatory input may partially mask the presence of excitatory input for non-preferred directions. TOP. Left, the tuning width (HWHH) of inhibition is compared with that of excitation on a cell-to-cell basis. The distribution of the tuning width for each component is represented along the corresponding coordinate axis. Right, the tuning width of inhibition is compared with that of the hyperpolarizing component (Hyp). BOTTOM. Similar plots of the optimal direction (OD) of inhibition versus that of excitation (left panel) or versus that of the hyperpolarizing component (right panel, Hyp). All direction preferences are expressed relative to that of the spike output. Filled red and blue symbols correspond respectively to the cases where excitatory or inhibitory orientation tuning was found statistically non-selective (index ratio lower than 0.10).

Nine cells in which input conductance dynamics were measured showed a significant hyperpolarizing response evoked at rest. The optimal orientation of the hyperpolarizing component was significantly correlated with that of the inhibitory conductance ($r^2=0.73$; $p<0.01$ ($n=12$); see Figure 3.2.4). This suggests that the integral of the hyperpolarizing component, when detectable, gives a gross, but nevertheless reliable, estimation of the optimal orientation for the inhibitory input. The tuning width of the evoked hyperpolarizations was, on average, sharper than that of the inhibitory conductance (mean of the difference: $8\pm10^\circ$). In contrast, the optimal orientation of the evoked depolarization was not significantly correlated with that measured for the excitatory conductance increase ($r^2=0.10$; n.s.). This implies, as illustrated in some examples (Figure 3.2.4: cells 11 and 13) that the optimal orientation of the excitatory input cannot be predicted from the integral of the evoked depolarization.

3.2.3. Discussion

This study represents a quantitative investigation of the role of the balance between excitation and inhibition in the emergence of orientation and direction selectivity in cat primary visual cortex. On the basis of conductance measurements, we report three different schemes of interaction between excitation and inhibition that underlie the genesis of orientation and direction selectivity.

For *orientation selectivity*, the P-P schema seems to be the most common. 62% of the cells, for which excitatory and inhibitory synaptic conductances were measured, fell in this category. With the spike inactivation method, we only have access to the selectivity of inhibition. However, as no NP-P cases were observed with conductance measurements, we can still classify cells with iso-oriented Inh component in the P-P schema (66% of cells). In contrast, the detection of significant evoked hyperpolarization or spike suppression for the preferred direction or orientation appear to be less sensitive indicators of the presence of iso-oriented inhibition, since these were noticeable in only a smaller proportion of cases (respectively 40% and 33% of the cells). This discrepancy could result from the fact that, in some cells, excitation and inhibition are in temporal overlap for the preferred stimulus: therefore their interaction will evoke a change in $1/\sigma$ without a hyperpolarization of the mean membrane potential (cell 5 in Figure 3.2.1). This interpretation is supported by the observation that 59% of cells that showed a significant decrease of trial-to-trial variability without significant hyperpolarization (Figure 3.2.2, $1/\sigma$ only) exhibited a $1/\sigma$ component tuned for the preferred orientation. In cells where both excitatory and inhibitory conductances were measured,

inhibitory tuning for non-preferred orientations was observed in 38% of cases (P-NP schema: 19%, and NP-NP: 19%). For the spike-inactivation protocol, 33% of cells had an inhibitory component tuned to a non-preferred orientation, (P-NP or NP-NP schemas). The other response components, hyperpolarization, spike suppression and $1/\sigma$ (only), were tuned for non-preferred orientations, in respectively 60%, 66% and 41% of cells.

In order to generalize our conclusions to the whole population of recorded cells, we extrapolated an estimate of the preferred orientation of the inhibitory input on the basis of the degree of correlation found between the different inhibitory-like components at rest (Hyp, Supp, $1/\sigma$) and the inhibitory component in the spike-inactivated state (Inh) or the inhibitory conductance (G_{inh}) when measured. The global picture remained the same as that established from the more restricted sample of conductance measurement: 60% of cells showed isooriented inhibition and 40% of cells showed crossoriented inhibition.

For *direction selectivity*, cells receiving a dominant inhibitory input, or showing an optimal hyperpolarizing response for non-preferred orientations were on average less direction selective than other cells (see Figures 2 and 6). Consequently, we considered only cells with an iso-oriented inhibitory-like component (i.e. either spike suppression, hyperpolarisation, or inhibitory component tuned to the preferred orientation). In a majority of these cells (70% on the basis of conductance measurement and 50% on the basis of the spike inactivation protocol), excitation and inhibition were tuned in the preferred direction (P-P schema). A comparable proportion of cells (60%) showed a hyperpolarizing component that was the largest for the preferred direction. In cells where synaptic conductances were measured, an inhibitory preference for the null direction was observed in 30% of cases (20% for P-NP and 10% for NP-NP schemas). When using the spike inactivation protocol, 50% of the cells showed inhibition tuned to a direction opposite to that of the spike preference (P-NP or NP-NP). In comparison 40% of cells exhibited a dominant hyperpolarization in the null direction.

In summary, our results argue against a single canonical circuitry underlying the genesis of receptive field properties within primary visual cortex. In the literature, the presence of inhibition evoked by non-preferred stimuli has been a controversial issue, with contradictory conclusions reached by several teams using intracellular protocols. In fact, the diversity of combinations of excitatory and inhibitory inputs observed in our data does account for the wide range of observations that have been previously reported. Before proposing hypothetical scenarios of cortical organization, we will compare our findings with those established from previous works.

3.2.3.1. Spike and depolarization

Similarly to two recent reports (Volgushev et al., 2000, Carandini and Ferster, 2000), we found that the tuning of depolarizing responses is, on average, wider than that of spike responses. However, as previously reported (Volgushev et al., 2000), we observed that the average difference masks a large diversity in the improvement in selectivity between the depolarizing component and the spike output. No correlation was found between this improvement and either the absolute or the relative spike threshold, but cells classified as receiving cross-oriented inhibition showed a significantly smaller improvement than those receiving iso-oriented inhibition. We conclude that the diversity in the tuning improvement reflects more the diversity in the combination of inputs than postsynaptic intrinsic properties.

3.2.3.2. Suppression and hyperpolarization

The presence of cross-oriented suppression has already been demonstrated on the basis of extracellular recordings and stimulus interaction protocols (Bishop et al., 1973; DeAngelis et al., 1992; Ringach et al., 2002). Early intracellular studies in visual cortex (Benevento et al. 1972, Creutzfeldt et al., 1974; Innocenti et al. 1974), whose findings were later replicated (Volgushev et al., 1993, Martinez et al., 2002), gave qualitative reports of diversity in the orientation tuning of visually evoked depolarizations and hyperpolarizations. In the present study, we present a quantitative analysis of the orientation and direction preference of the hyperpolarizing component explored over a large cell population based on explicit criteria of statistical significance. In addition, for some cells we have been able to compare the respective tunings of the depolarizing and hyperpolarizing components with those of the evoked inhibitory and excitatory conductance changes, which are expected to represent the actual synaptic input more faithfully. We observed a significant correlation between the optimal orientation of the inhibitory conductance and that of the hyperpolarizing component when detectable at the resting state, suggesting that indeed some of the cells reported in previous works did receive a cross-oriented inhibition.

3.2.3.3. Trial-to-trial variability of the membrane potential

Although the trial-to-trial variability in the evoked response has been a focus of attention in many extracellular studies, it has been only rarely analyzed in intracellular studies. Our hypothesis, that the reduction of the trial-trial variability is produced by the presence of a strong input dominated by inhibition, has been addressed in this study in a variety of ways. In many cells, the $1/\sigma$ component in the membrane potential was found to be correlated with the

presence of a significant evoked spike suppression and hyperpolarization. In other cells where a variability decrease was found concomitantly with a mean depolarization evoked at rest, the presence of inhibition was revealed during spike inactivation protocols (see cell 10). Furthermore, in cells recorded in voltage clamp, a strong decrease of variability was found to be correlated with a strong increase of the inhibitory conductance component (see cell 15). The method used here takes into account the time course of the trial-to-trial variability stimulus locked waveform. It differs from the approach used previously by Anderson et al. (2000c) where the trial-to-trial variability was averaged over the stimulus presentation period and considered as “a noisy component varying little with contrast and orientation”. However, despite averaging, their data did show a modulation on the order of 30% between preferred and cross-orientations, which is compatible with our own observations. From our results, we conclude that it is necessary to take into account the temporal waveform of the trial-to-trial variability for each orientation or direction in order to predict correctly the temporal spiking pattern on the basis of the mean visual response with a fixed threshold for spike initiation. We suggest that the addition of a constant noise, as proposed in the model of Anderson et al. (2000c) can only be relevant at the conductance level: the visually evoked dynamics of the mean global conductance modulates the trial-to-trial membrane potential variability. The spiking responses evoked *in vivo* are extremely variable from trial to trial (Heggelund and Albus, 1978; Dean, 1981). Nevertheless, a recent study (Melcher et al., 1998) shows that this variability depends on the type of stimuli used: drifting edges (transient stimuli), but not gratings (steady-state stimuli), generate responses with reproducible stimulus-dependent changes in the temporal structure of the spike train (temporal coding). In agreement with this study, we observed, using transient stimuli, the presence of reproducible stimulus-dependent changes in the trajectory of membrane potential, which affect the temporal structure of the spike train.

3.2.3.4. Unmasking inhibition by current injection

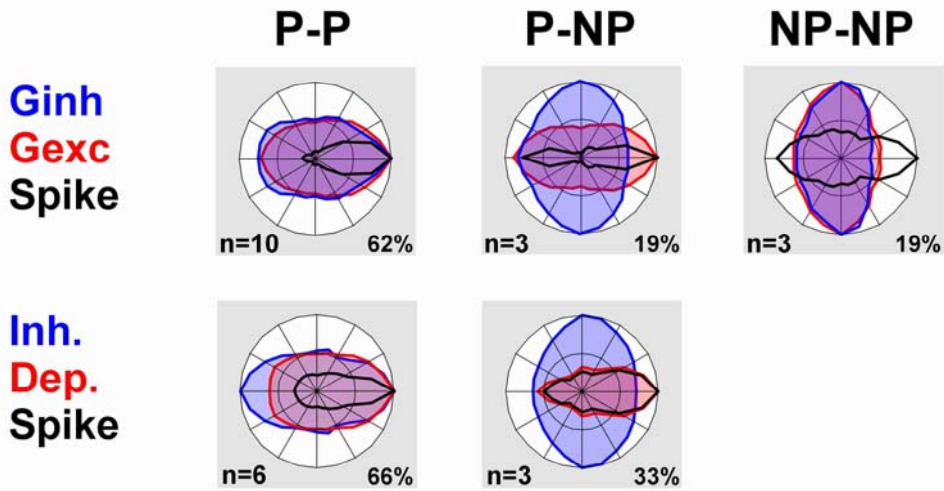
One possible way to detect inhibition *in vivo* is to study the voltage dependence of the evoked response through current injection (Innocenti and Fiore, 1974). The use of depolarizing currents to enhance the visibility of inhibition was applied in the earlier work of Ferster (1986) and Sato et al. (1991). Both groups concluded on the basis of a limited sample that the evoked hyperpolarization during positive current injection and the evoked depolarization with no current shared the same orientation preference and selectivity without quantifying the tuning curves of the detected inhibition. The reference criterion used in the present study was to use a

current strong enough to produce the total inactivation of the action potential, thus abolishing contamination by spiking activity. At this current injection level, evoked depolarizations were suppressed and only hyperpolarizations could be detected. This indicates that the cell membrane potential was maintained close to the reversal potential of excitatory synapses, thus minoring a possible masking of inhibitory components by NMDA-dependent responses that may dominate at intermediate levels of depolarization.

3.2.3.5. Excitatory and inhibitory conductance tuning

The present data confirm our previous observation that visual stimulation evokes strong conductance increases (Borg-Graham et al., 1998). The relative change in peak conductance (around 110%) is similar to values found by Anderson et al (128%). We also observed that the maximal conductance increase was quite variable from cell to cell. Our method of conductance decomposition differs partly from that of Anderson et al. (2000b). We decomposed the conductance into three components, excitation, inhibition dominated by chloride conductance (reversal potential of -80 mV) and by potassium conductance (-95 mV) instead of two components with an intermediate value for the reversal potential of the inhibition (-85 mV in Anderson et al., 2000b). This method tends to avoid both underestimating the chloride conductance, and obtaining a negative value for the excitatory conductance. Moreover, we estimated the total synaptic conductance, both evoked and spontaneous, based on an estimation of the leak conductance, whereas Anderson et al (2000b) derived only the evoked synaptic conductance increase.

Orientation selectivity



Direction selectivity

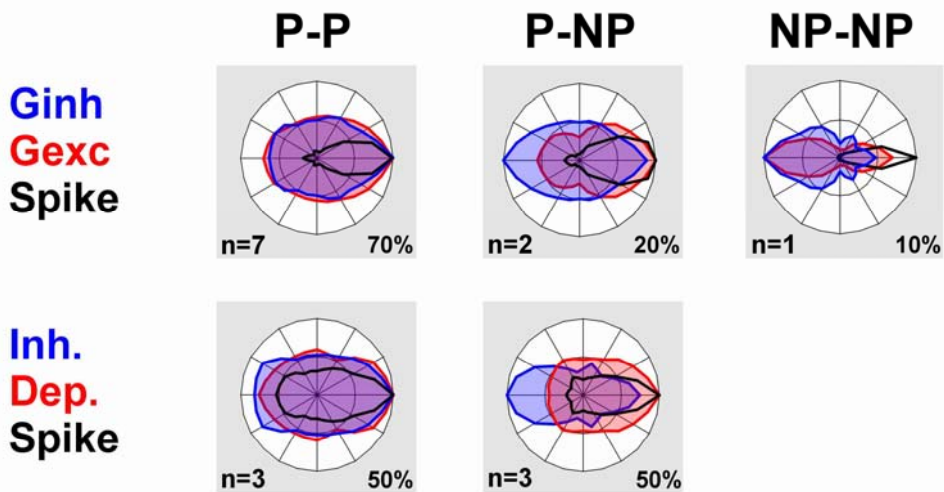


Figure 3.2.6: Diversity of combinations between excitatory and inhibitory input tunings. **A.** Averaged tunings of the excitatory and inhibitory inputs for cells grouped according to different schemes for orientation selectivity. Excitation-Inhibition: Preferred-Preferred (P-P), Preferred-Non Preferred (P-NP), Non preferred-Non preferred (NP-NP). The upper row of tuning curves is based on cells for which conductance measurements were made. In the lower row, tuning of the inhibition revealed in the spike-inactivated state can be compared with that of the depolarizing component observed at rest. **B.** Similar plots for the study of direction selectivity. Excitation-Inhibition: P-P (Iso-P-Iso-P), P-NP (Iso-P-Iso-N), NP-NP (Iso-N-Iso-N).

This allowed us to detect significant changes in the balance between the excitatory and inhibitory conductances even with small absolute evoked conductance increases. Both the two-term decomposition method used by Anderson et al (2000b) and the three-term

decomposition method used here do not take into account possible non-linearities introduced by NMDA receptor activation. Nevertheless, taking into account numerous immunological reports suggesting that, in neocortical neurons, inhibitory synapses are located more proximal to the soma than excitatory synapses, it seems unlikely that NMDA conductances mask inhibitory conductances, although the reverse situation may be true. Using drifting gratings in conjunction with current clamp recordings, Anderson et al. (2000b) concluded on the basis of steady-state responses that conductance was invariably maximal for a stimulus of the preferred orientation. These authors also concluded that orientation preference and tuning width on a cell-by-cell basis were similar for both excitatory and inhibitory input conductances. One reason for these apparent discrepancies with the present findings may be linked to differences in the fitting methods. In Anderson et al (2000b), in order to minimize the number of parameters, the mean and modulation of the input conductance were fitted together, forcing them to peak at the same orientation with the same tuning width. However, it is apparent in some of their examples that this constraint can lead to poor fits and that the respective tunings of the modulation and of the mean are uncorrelated (see for instance Figure 10 in Anderson et al (2000b): in cells 1 and 6 the increases in mean conductance are clearly cross-oriented with the spike preference whereas the modulation of conductance is iso-oriented). Thus, in spite of the apparent opposition between the conclusions of Anderson et al. (2000b) and our own, diversity in conductance tuning seems equally present in both studies. Differences in fact concern more quantitative issues: Anderson et al (2000b) concluded that the orientation tuning width is narrow and identical for excitation and inhibition (HWHH: 22°) whereas we report here that the tunings of excitation and inhibition are larger and less selective (HWHH: 45° ; base: 30%). We found also that the respective tuning widths of excitation and inhibition differ on a cell-to-cell basis (Figure 3.2.5), although these values averaged across all cells are comparable.

3.2.3.6. Principles for generating diversity

In summary, we conclude that, depending on the recorded cell, orientation and direction selectivity stem from a variety of combinations of excitatory and inhibitory synaptic tuning. We discuss below the implications of these findings for theoretical issues regarding the computational role of the visual cortical network architecture. Our data suggest that various computational solutions could be implemented locally and might coexist in the same network. We propose simple local connectivity rules based on neighbourhood relationships that, applied to the whole network, could explain such diversity.

Functional cortical maps of orientation selectivity present a high level of spatial heterogeneity with pinwheel loci exhibiting high spatial gradients in orientation preference, and iso-orientation domains with low orientation gradients (Bonhoeffer et al., 1995). However, whatever their positions within this heterogeneous map, cells present a high level of orientation selectivity (Maldonado et al., 1997). If we consider that intracortical connectivity distribution is governed mainly by the distance between cortical sites (Das and Gilbert, 1999), cells located at the pinwheel centers (position B, Figure 3.2.7) should receive a much broader range of orientation tuned input than cells in the middle of iso-orientation domains (positions A, Figure 3.2.7). This will create a first source of diversity, between cells receiving mainly inputs tuned to the same orientation and cells receiving inputs from a wide range of distinct orientation domains. In addition, differences between excitatory and inhibitory input selectivities can arise from the different extents of the axonal and dendritic arborizations of excitatory and inhibitory neurons (Somers et al. 1995, McLaughlin et al., 2000).

A second source of diversity in the cortical network could result from the shaping of intracortical connectivity by activity-dependent processes. Both theoretical models and experimental data suggest that correlated pre- and post-synaptic activities stabilize and strengthen the gain of excitatory connections and that uncorrelated activities reinforce inhibitory connections (review in Frégnac, 2002). Therefore cells with similar multidimensional functional preference (orientation, direction, phase and spatial frequency) will tend to excite each other reciprocally. In contrast, cells which differ in at least one of these functional preferences will inhibit each other. The final connectivity state stabilized in adult cortex will be the result of a local synaptic plasticity principle applied for various dimensions of the visual stimulus. It should be noted that in this correlation-based framework, the source of the anisotropy (thalamocortical vs. intracortical) cannot be identified since it will be propagated through synaptic changes distributed across the whole network.

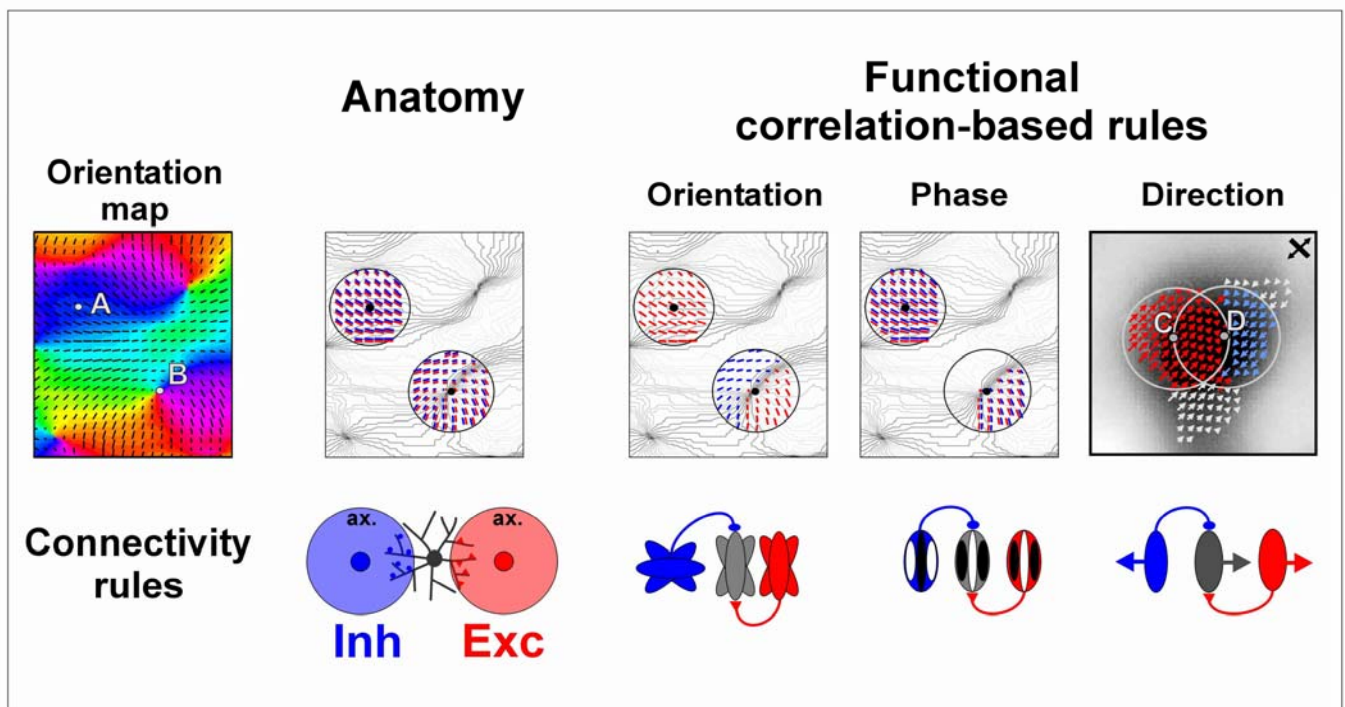


Figure 3.2.7: Principles for generating diversity. Connectivity principles applied in different locations of the cortical orientation/direction maps. Upper row, Left panel: iso-oriented domain (A) and pinwheel centers (B). Upper row, right panel: iso-directional domain (A1) and demarcation line between two opposite iso-directional domains (A2). Excitatory cells are in red, inhibitory cells in blue and the target cell in gray. Lower row: the left panel illustrates connectivity rules based on the anatomy: the intracortical connectivity distribution is governed only by the distance between cortical sites. The extent of the axon (ax.) afferent to a given postsynaptic cortical cell is schematized by a disk. The right panel illustrates connectivity rules based on functional correlation, with respectively excitatory and inhibitory synapses connecting cells with similar or dissimilar receptive field properties. Receptive field properties are symbolized by an oriented ellipse for **Orientation selectivity**, by a Gabor patch for **Spatial Phase** and an arrow for **Direction selectivity**. See text for further details. The schematized direction map was derived from the orientation map kindly provided with the courtesy of F. Chavane and A. Grinvald, Weizmann Institute of Science.

If we apply these hypothetical rules of plasticity to the orientation selectivity domain and the intracortical connectivity pattern defined previously, then cells located in the center of an iso-orientation domain will receive iso-oriented excitation from cells sharing similar receptive field properties, and inhibitory input from iso-oriented cells which differ in their phase or spatial frequency selectivity (akin to the push-pull model). The same reasoning predicts that cells located near pinwheel centers will receive, in addition, inhibition from cells which differ in their orientation preference from the target cell (hence oblique and cross-oriented input). In comparison, the model of Troyer et al. (1998), based on correlation rules dependent on the spatial phase between subfields, only considers excitatory and inhibitory connections between cells which share the same orientation preference, and does not generalize the plasticity principle to the orientation domain. According to our generalized schema, inhibitory

connectivity between neurons from different orientation columns provides a simple solution that will produce contrast invariance for both excitatory and inhibitory neurons (see also Adjoran et al., 1999).

For direction selectivity, the same reasoning can be applied. Optical maps established for direction preference show that iso-orientation domains appear divided into two contiguous regions exhibiting preferences for opposite directions (Shmuel et al., 1996; Kirsvarday et al., 2001). Cells close to the separation line will receive inhibitory inputs tuned to the preferred direction, whereas cells away from this line will receive only iso-preference inhibition. If, as predicted by our organization principle, cells near pinwheel centers receive cross-oriented inhibition, our data suggest in addition that these cells have weak direction selectivity.

This qualitative model, which accounts for part of our results, underscores sources of diversity. Restricting test stimulations to a spot or a contrast edge may significantly reduce the identification of visual signals that contribute, or have contributed in the past, to correlated activity in the cortical network. For example, center-surround experiments show the fact that at least some cells in the visual cortex respond maximally for cross-oriented bipartite stimuli, independently of the actual orientation of the stimulus (Sillito et al., 1995), in spite of the fact that they express normal orientation selectivity when tested with classical stimuli. This might explain our apparent paradoxical observation that some cells receive excitatory and inhibitory input for what we defined as non-optimal stimuli on the sole basis of a light bar stimulus. It may be that with different stimulus configurations or dimensions, the evoked synaptic input and the corresponding spike output might indeed share a similar specificity, with the connectivity obeying the same organization principle.

The arguments that we have presented so far concern the dependency of the input distribution on the location of the cell in the orientation and direction selective network, as visualized by optical imaging of superficial layers. Another source of input variability may be linked with the laminar position of the cell within the depth of the cortical column. A recent study combining intracellular recordings and biocytin labelling reports that the tuning preference of the hyperpolarizing component is correlated with the laminar location of cells (Martinez et al., 2002), inhibition being dominantly iso-oriented for granular and supragranular layers, and often exhibiting a cross-oriented preference in deep layers, most specifically in layer V. These authors conclude that this diversity in the inhibitory tuning seen across the cortical depth reflects hierarchical levels of integration in the serial flow of cortical processing. We propose here that the noticeable difference found between supragranular and granular layers on the

one hand and infragranular layers on the other hand could simply reflect a diversity in the input sampling in the laminar plane (Buzas et al., 2001; Kisvarday et al., 1994; Yousef et al., 1999).

In summary, the diversity of input combinations found across cells may reflect anatomical non-homogeneities in the lateral intracortical connectivity pattern. This diversity could result from topological irregularities in the lay-out of the orientation preference map and its functional impact may be up- and down-regulated by correlation-based activity-dependent processes. In favour of our view, several optical mapping experiments have shown that the position of the cell in the orientation map may influence the amplitude of the orientation change produced by a fixed orientation adaptation protocol (Dragoi et al., 2001; Schuett et al., 2001). We propose here that these regional anisotropies in plasticity in the developing cortex, or adaptation in the adult cortex, in fact reflect the regional dominance of different computational schemas for the genesis of orientation preference.

3.2.4. Experimental procedure

Cells in the primary visual cortex of anaesthetized (Althesin) and paralyzed cats (for details on the surgical preparation, see Bringuier et al., 1997; 1999) were recorded intracellularly using an Axoclamp 2A amplifier. Sharp electrode recordings (39 cells) were performed in bridge mode with 55-90 M Ω glass pipettes filled with 2M potassium methyl sulfate and 4mM potassium chloride. The average resting membrane potential was -67.5 ± 5 mV. Whole-cell patch recordings (49 cells) were made with 3-5 M Ω glass patch electrodes filled with a solution containing 140 mM K-gluconate, 10 mM HEPES, 4 mM ATP, 4 mM MgCl₂, 0.4 mM GTP and 0.5 mM EGTA (KOH), with pH adjusted to 7.3 with KOH and the osmolarity adjusted to 285 mosM. The seal resistance in attached mode was always above 1 G Ω . In whole cell mode, the average resting potential was -66.5 ± 6 mV. In voltage-clamp recordings, the access resistance was always lower than 40 M Ω . The estimate of access resistance was revised as necessary over the course of the experiment and, in some cases, off-line, by fitting the response to subthreshold hyperpolarizing current steps to the sum of two exponentials. A tip offset potential of 10 mV was subtracted from the voltage records off-line.

Data processing and visual stimulation protocols were done using in-house software (Gérard Sadoc, Acquis1-Elphy, Biologic CNRS-UNIC/ANVAR). Three millimeter artificial pupils were used and appropriate corrective optical lenses were added. The receptive field of each cell was quantitatively characterized using a sparse noise mapping. Receptive fields were

classified as Simple or Complex using classical criteria on the space-time separation between On and Off responses, including subdivision into S1 and C1 complex types for unimodal receptive fields, according to the presence or absence of antagonist hyperpolarization. Orientation and direction tuning curves were measured with moving bars (direction of motion perpendicular to orientation) swept across the full extent of the subthreshold receptive field, and using random sequences of 8 or 12 directions (angular step: 45° and 30° respectively) repeated 10 times.

For data analysis, we extracted the respective orientation and direction tuning curves of the following response components: spiking activity and spike suppression, membrane potential depolarization and hyperpolarization (without injection of current and during spike inactivation), trial-to-trial variability of the membrane potential and excitatory and inhibitory conductances. For the suprathreshold activity, PSTHs were computed with a 25 ms bin width, and the spike increase and spike suppression components were defined as the integral of firing rate, respectively above and below the mean pre-trigger background firing rate. For subthreshold activity, spike events were removed from the raw record and membrane potential was interpolated before and after each spike occurrence. The depolarizing and hyperpolarizing evoked components were defined on the basis of a quantitative amplitude selection criterion as the integral of voltage respectively above and below the mean depolarizing and hyperpolarizing fluctuations in the resting potential measured during spontaneous activity. Trial-to-trial variability was calculated as the inverse of the standard deviation ($1/\sigma$) of the time course of the stimulus-locked membrane potential response over all stimulation trials. The $1/\sigma$ component was defined by the integral above the mean background value. The $1/\sigma$ waveform is expressed as the percentage of change from the spontaneous reference level. Measurement of enhanced hyperpolarizations were made in a sample of cells recorded with sharp electrodes while applying depolarizing current sufficient to fully inactivate Na⁺ spike currents. The quantification methods used in the spike-inactivated state were the same as those applied from the resting state. To determine if responses calculated over the whole period of visual stimulation were significant, the mean of each component, defined by its integral normalized by the effective time during which its presence was detected (see above amplitude selection criterion), was compared with the normalized mean of this component during spontaneous activity, using a Student t-test. For polar plot measurements, the spontaneously expected component value was subtracted from the evoked component.

For whole cell patch-clamp recordings, the dynamics of the input conductance and its associated composite reversal potential were measured as described previously (Borg-Graham et al., 1998). In order to address the significance of the conductance measurement, a non-parametric bootstrap method was used, similar to that applied by Anderson et al. (2000b). The conductance waveform was decomposed to give the sum of a leak conductance (G_{leak}) and a global synaptic conductance (G_{syn}). G_{leak} was estimated as the lower boundary of the conductance waveform at rest and given by the threshold value corresponding to the 1% percentile of the cumulative distribution of conductance measures during spontaneous activity. The reversal potential E_{leak} was assumed to be in the order of -80 mV (Paré et al, 1998).

The synaptic conductance term was further linearly decomposed into three conductance components corresponding to the activation of one type of excitatory synapse and two types of inhibitory synapses, each associated with known, fixed reversal potentials. The value of the reversal potential of GABA_A receptor activation was measured by pharmacologically blocking other synaptic components in a slice preparation of rat visual cortex and estimated at -80 ± 3 mV ($n=20$) (Monier et al, in preparation). The other reversal potentials were fixed to 0 mV for excitatory and -95 mV for potassium conductances (associated with GABA_B receptors). We made the additional hypothesis that, depending on the actual value of the composite synaptic reversal potential, one or two out of three possible types of inputs contribute in a dominant manner to synaptic activation. Between 0 and -80 mV the synaptic conductance can be decomposed into excitatory and GABA_A conductances, and between -80 and -95 mV into GABA_A and GABA_B conductances. Above 0 mV and below -95 mV the synaptic conductance is thus equal respectively only to the excitatory or the potassium.

Similarly to the other measured components of the visual response, the evoked excitatory and inhibitory conductance components are given by the integral of the excitatory and inhibitory conductances above their mean values, calculated during pre-trigger and spontaneous activity. In order to determine the phase relationship and the degree of temporal overlap between excitation and inhibition, a normalized crosscorrelation function was calculated between the two stimuluslocked excitatory and inhibitory conductance waveforms. An index representative of the temporal overlap (TO) is given by the cross-correlation "contrast" ratio, defined as the difference between the amplitude at time 0 and the amplitude at the peak of the cross-correlation function, divided by the difference between the maximum and the minimum of the cross correlation function.

The mean of each component during spontaneous activity was then subtracted from the visual evoked response. Orientation and direction tuning curves were calculated when response components, for at least one direction, passed a preset significance level ($p < 0.01$) based on either paired t-tests or, in the case of conductance, on the bootstrap method. All components were averaged over the duration of the visual stimulation. Peak responses were calculated over a 25 ms bin. Direction tuning curves were fitted independently for each component by the sum of two Gaussians with the same width, whose peaks were 180° apart. The peak of the Gaussian determines the preferred (PD for spike output) or optimal direction (OD, for other components). The half-width of the tuning curve at half the height (HWHH) of the peak is given by the standard deviation of the Gaussian multiplied by $(2 \cdot \ln 2)^2$. The direction selectivity index (DI), which is independent of the fitting procedure, was defined as the difference in the responses obtained with stimuli of preferred and opposite directions, divided by the sum of those responses.

We also applied a spectral quantification method (S.D.O. analysis in Wörgötter and Eysel (1987)) which allows independent estimation of orientation and direction preferences and the computation of a selectivity index. An orientation index value of 0.1 or greater indicated that the circular distribution of the cell responses to moving stimuli was non-random ($p < 0.005$; Rayleigh test in Thompson et al, 1994; Zar, 1974). For tunings, a bootstrap method was applied to ensure that the standard deviation in the preferred orientation estimates ranged between 1 to 9° for the excitatory and inhibitory conductance components depending on the cell and its tuning selectivity, i.e. well below the discretization step used for orientation and direction distributions.

3.3. Center-surround interaction during apparent motion controls the timing of the responses and reveals a new motion direction selectivity in V1

The synaptic integration field is likely to support the various center-surround interactions observed in V1 and to be the biophysical substate of some perceptual binding or psychophysical biases. Psychophysical results conducted in collaboration with Lorenceau's team proves the existence of lateral perceptual interaction consistent with the intracortical propagation of visual activity relayed through the horizontal connectivity (Georges et al, 2002; Séries et al, 2002). This interaction are manifested in a perceptual speed overestimation for high speed apparent motions of collinear oriented Gabors configuration. On the physiological hand, the spatial and orientation selectivity of center-surround interactions, and even their facilitatory or suppressive nature, are still a matter of debate, and a diversity of results being reported.

In this study, we have intracellularly recorded the subthreshold and spiking neurons responses of V1 cells to high speed apparent motion of Gabor elements, during sequential stimulation of the “silent” surround and the discharge field center of the Receptive Field (RF). Our results show an important center-surround interaction selective to the collinear and iso-oriented “Gestaltic” configurations. This facilitatory and suppressive interaction presented a contrast dependent and biphasic temporal profile, leading notably for high contrast center to suppressive net effects, and to a drastic temporal reshaping of the center responses, shortening the latencies and duration of the synaptic responses.

These interactions demonstrate a center-surround directional selectivity of the RF for high speed motion along the collinear axis of V1 cells. This effect is expressed notably in the temporal dynamic modulation of the responses. Such kind of dynamic nonlinearity is likely to support a preliminary form of temporal coding in V1. Those results suggest a new model of classical and non-classical RF considering a suppressive as well as a facilitatory surround modulation, both modulated in space and time. Thus, two forms of motion selectivity can be distinguished in V1, namely the preference for low speed stimuli across the width axis of the classical RF and the preference for high speed collinear stimuli along the orientation axis of the RF demonstrated here. These two processes operate respectively on short and long spatial integration scale. Moreover, the remarkable fit of the spatiotemporal statistics of saccadic and fixational eye-movements, and these motion integrative paths suggest a general visuo-oculomotor model of multiscale and sequential analysis of the visual scene by V1.

3.3.1. Perceptual and cortical spatiotemporal interactions: the apparent motion paradigm

One of the major problems tackled by electrophysiologists and psychophysicists in the last decade has been to understand which mechanisms, at the synaptic, cellular and network level, underlie the emergence of a global and coherent perception. Such perception necessarily arises from the activity spatial and temporal pattern of the myriad of cortical neurons composing a cortical area, and from the coherence of those patterns among those neurons (Von Der Malsburg, 1981, Singer 2001, Engel & Singer, 2001 for review). A simplifying classic working hypothesis is to consider that the emergence of a unified percept allowing, for example, to identify an object independently of its spatial position in the visual field (spatial invariance), implies the existence of a binding process which links distinct neurones analysing different positions in space. The combinations of ‘parts’ into a global perceptual entity also require that this spatial binding operates at the same time between cells simultaneously activated by each of the components of the ‘whole’. Similarly, global motion perception is experienced even if the physical stimulus sequence is a composition of static individual spatial events which individually do not coexist temporally. In that case, as already pointed out by the Gestalt school, the commonality of fate (or destiny) decides of the binding in time.

The so-called perceptual “association field”, which has been extensively studied in humans, are usually defined by quantifying facilitatory or suppressive changes in the detectability of a central target when adding a contextual periphery (Field & al, 1993, Polat & Sagi, 1993, 1994). The largest interaction effects between the target and the lateral masks are found when the stimuli are oriented and co-aligned, suggesting that ‘lateral’ connectivity in visual cortex may participate in establishing such facilitation.

Numerous physiological studies support the view that the binding of visual contours into perceptually coherent objects involves long-range horizontal connections between V1 cortical neurons (Gilbert & Wiesel, 1989, Schmidt & al, 1997, Mallach & al, 1993, Yoshioka & al, 1996). Accordingly, surround facilitation has been described for stimuli of orientation similar to preferred orientation of the cell presented in the end-zone of the RF (iso-oriented collinear condition, Chen & al, 2001, Nelson & Frost, 1985, Polat & al, 1998, Knierim & Van Essen, 1992; Kapadia & al, 1995, Kapadia & al, 2000). These intra-cortical connections, best activated when the linked cells share similar orientation preference, may thus form the biological substrate of perceptual "association fields" (for review: Fitzpatrick, 2000, Series & al, 2004).

However, in contrast with this simple framework, a wide diversity of modulations effects and diversity of results have been reported in the literature. Most of center-surround interactions studies in V1 report that surround modulations are suppressive (end-stopping and side inhibition, length tuning), and present the same tuning characteristics as the center with less specificity (Series & al, 2004 for review, Cavanaugh & al, 2002, DeAngelis & al, 1994, Knierim & Van Essen, 1992, Levitt & Lund, 1997). Surround facilitation has been reported for cross-oriented surround conditions (Jones & al, 2002, Sillito & al, 1995). The amplitude and even the facilitatory or suppressive nature of those interactions appear to be dependent on the stimulus center contrast (Toth & al, 1996, Polat & al, 1998, Mizobe & al, 2001, Levitt & Lund, 1997).

Surprisingly, very few studies have addressed the underlying temporal specificity and dynamics of the center-surround cortical interactions. In psychophysics also, the temporal dependence of the surround facilitation has only received little attention (Hess & al, 2001, Polat & Sagi, 2006). However, it is long known that a visual, auditory or tactile stimulus presented sequentially in neighbouring locations elicits a vivid perception of apparent motion or binding, even over broad “distance” of integration (Wertheimer, 1912, Burt, 1917a, 1917b, Braddick, 1980). In the visual system, this perception is correlated with the activity of motion selective neurons in area MT that receive predominantly direct inputs from area V1 (Mikami & al, 1986, Newsome & al, 1989, Maunsell & Newsome, 1987).

Classically, in primary visual cortex, where the first direction selective responses arise, the integration (both linear and nonlinear) of the visual motion is observed on small spatial distance (around 0.5° on average for the second order interaction, Pack & al, 2006), is selective for low speed (optimal frequency 2-6Hz, optimal velocity 2-20°/s, De Valois & al, 1982, Movshon 1975, Pack & al, 2006), and is expressed in the axis perpendicular to the preferred orientation of the cell (parallel axis). Geisler & al (2001) have shown that V1 cells are direction selective for motion in the collinear axis of the RF and that this collinear motion detection is preferentially expressed for high speed motions (compared to the parallel axis), defining a gain control of a new type. However, their study, restricted to the classical RF, could not assess the involvement or not of center-surround interactions in this effect.

A second important reason to address the temporal specificity and dynamics of the center-surround cortical interactions is that, according to temporal characteristics of the synaptic fields described previously, the surround stimulation is likely to modulate the timing and temporal profile of the neuronal responses, with a dependency on the relative timing of the

stimulation in the center and the surround. Classical contrast gain controls have shown to have an important effect on the timing and latency of the responses and thus may sustain a basis of a temporal code (Gawne & al, 1996, Victor & Pupura, 1996, Mechler & al, 1998, Reich & al, 2001) or derivated latency code (Thorpe & al, 2001). Thus, the surround stimulation may play a critical role in the timing of the neuronal responses, by imposing a temporal control on the gain of response.

We conjectured that the spatiotemporal structure of V1 synaptic fields (cf. chapter 3.1), notably imposed by intra-cortical axons conduction properties, might influence the center-surround interaction expression (figure 3.3.1.1), and in turn, the perception of motion by modulating the expression of a perceptual bias for a specific range of speed and for specific level of orientation invariance along the motion path.

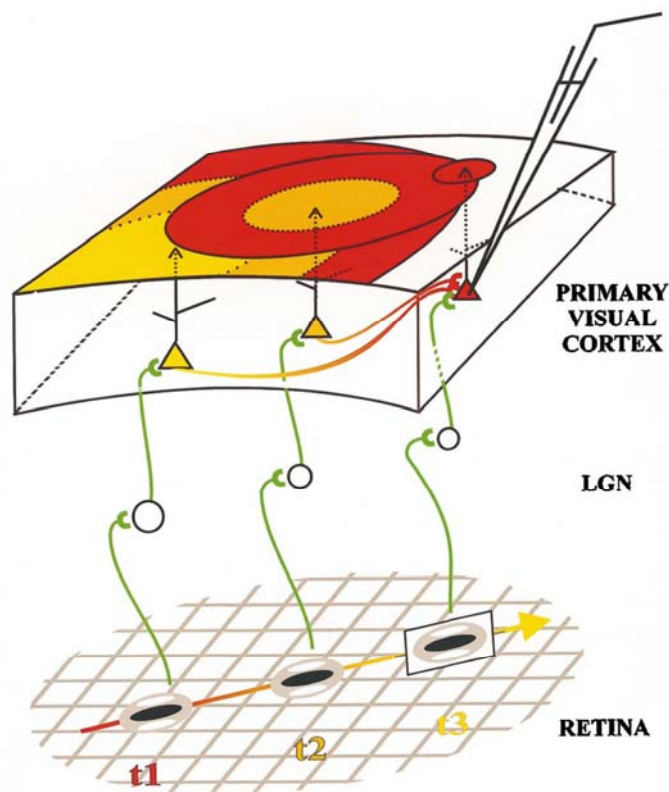


Figure 3.3.1.1: High speed apparent motion and its possible recruitment of horizontal cortical connectivity. This cartoon depicts the intra-cortical propagating waves of visually evoked spiking activity triggered by the sequential presentation of three Gabor patches on the retina. The respective orientations of those three stimuli are co-aligned with the motion axis of the 'association pathway', i.e. the orientation preference axis of the classical RF. The presentations of the Gabor patches are done sequentially (t_1 then t_2 then t_3), and the inter-stimulus interval ($ISI=t_3-t_2=t_2-t_1$) is adjusted so that the serial retino-thalamo-cortical feedforward input reaching the intracellularly recorded cell (red triangle) rides in phase the evoked 'horizontal' intracortical waves. The position of the 'horizontal' activity wave as a function of the time elapsed from the presentation of the first stimulus (t_1) is colour-coded.

In collaboration with our research group, Lorenceau's team explored the psychophysical effects of apparent motion. For this purpose, the stimulus used were Gabor patches namely oriented sinusoidal luminance gratings whose modulation is weighted by a bi-dimensional Gaussian function. The form, the spatial frequency and the anisotropy along the main orientation axis precisely reproduce the spatial sensitivity profiles of cortical discharge fields (Daugman, 1985, Jones & Palmer, 1987). The results show that the apparent speed of motion induced by a sequential presentation of Gabor patches in different positions of the visual field was estimated faster by the subject when the orientation of each Gabor patch was collinear to the axial direction linking the different positions than when they were orthogonal to the 'association' pathway.

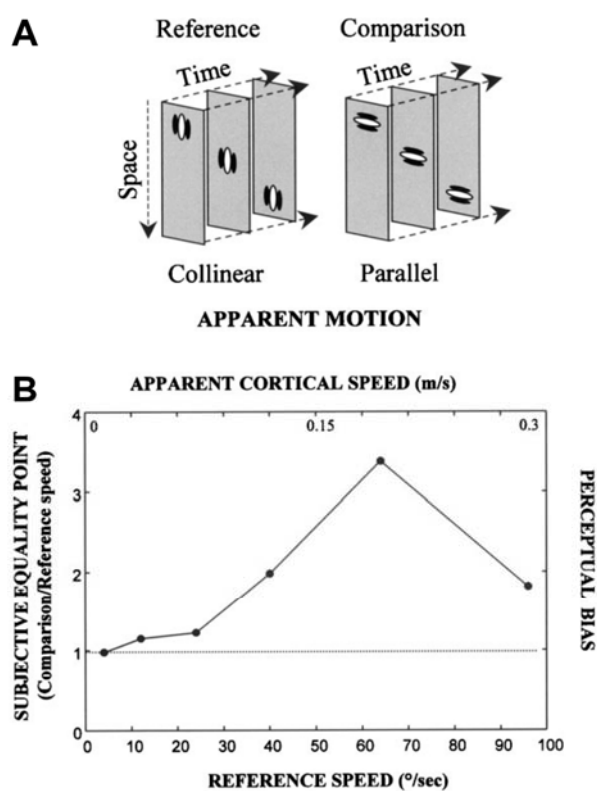


Figure 3.3.1.2: High speed collinear apparent motion biased the perception of speed: Psychophysical results. **A** Space-time plots of the apparent motion sequences. A trial consisted of the successive presentation of two short apparent motion sequences of a vertical (left cartoon, reference Collinear Sequence) and a horizontal (right cartoon, comparison Parallel Sequence) Gabor patch moving along a vertical axis. In a 2-Interval Forced-Choice design, observers indicated which sequence appeared faster. **B** The speed of the parallel sequence eliciting a subjective equality (50% probability) in choice when compared with the reference sequence was measured for six different reference speed values, ranging from 4 to $96^{\circ}.\text{s}^{-1}$. The ratio of both speeds (comparison:reference) quantifies the perceptual bias experienced for collinear contours. This effect peaks for an absolute reference speed of $64^{\circ}.\text{s}^{-1}$, corresponding to an apparent intracortical 'horizontal' speed of $0.2 \text{ m}.\text{s}^{-1}$. (Georges & al, 2002, Chavane & al, 2000).

This effect, summarized in figure 3.3.1.2 (see also paper in annex Chavane & al, 2000, and Georges & al, 2002), may be quantified by the ratio between the speed of the comparison ‘parallel’ sequence over that of the ‘reference’ collinear sequence for which the subject reports equality in speed. The perceptual bias can be as strong as 3-fold, and its strength explains why observers find in more than 80–95% of cases that ‘parallel’ sequences are faster than ‘horizontal’ even if both composite stimuli have the same physical speed. The physical reference speed for which the effect is maximal corresponds to $64^{\circ} \cdot s^{-1}$ in the visual field, which would be equivalent for parafoveal tests to an apparent ASHP propagation speed of $0.2 \text{ m} \cdot s^{-1}$ in man V1 cortex. Remarkably, and as predicted, this value extrapolated in human cortex is well within the range of those we measured electrophysiologically in cat area 17. If one assumes an average magnification factor in primary visual cortex of 1 mm in cat and 3 mm in monkey for 1° of solid angle in parafoveal regions, the propagation of activity through horizontal connections corresponds to fast retinal motion ranging from 50 to $500^{\circ} \cdot s^{-1}$ in cat (Tusa & al, 1978) and 15 to $170^{\circ} \cdot s^{-1}$ in monkey (at an eccentricity of 2 to 4° , the cortical magnification factor in monkey V1 is 2.5-3.5 mm by degree of visual solid angle, Dow & al, 1981). These speeds are strikingly similar to those for which we observed the largest effects in the psychophysical experiments, since the perceptual bias revealed in humans is best expressed at a speed of $64^{\circ} \cdot s^{-1}$.

3.3.2. Center-surround apparent motion: protocol description

In order to characterize at the synaptic level the orientation/direction motion center-surround interaction process that has been hypothesized in V1, we looked for possible electrophysiological correlates in cat area 17. The same contextual stimulus sequences as those used in the psychophysical experiments were applied in the "silent" surround of the discharge field of V1 cells, while postsynaptic responses to a test stimulus flashed in the center of the discharge field were recorded intracellularly.

The receptive field was first measured quantitatively using a sparse noise of impulsion-like ON and OFF stimulation and classical stimulus/response correlation method. The resulting impulsional transfer function defines the Minimum Discharge Field (Barlow, 1967), or the first order kernel (exempt of any interaction), and its spatial extent is used to define the center stimulus position, length and width. The preferred orientation of the discharge field was established on the basis of the response tuning to light and dark bars moving at optimal velocity, thus defining the parallel axis (orthogonal to the orientation axis) and the collinear axis of the discharge field. Optimal Gabor patches were defined by applying variable phase,

spatial frequency and contrast tuning protocols in the MDF. We then flashed those optimal Gabor patches in the periphery in various sequences along collinear and parallel axes and looked at the modulatory effect such sequences could produce on the response to a test stimulus flashed within the MDF. The apparent motion direction selectivity, that we suspect to be constrained by the horizontal propagation, is studied along the orientation or width axis of the discharge field by applying randomly interleaved stimulation sequences moving away from the receptive field center ("centrifugal" condition), or from the "silent" surround to the center ("centripetal" condition). The orientation of the peripheral stimuli could be either that preferred by the cell in its discharge field or orthogonal to it, thus defining in the periphery of the recorded cell "iso-oriented" or "cross-oriented" sequences. In order to evoke a sizeable synaptic "horizontal" response the contextual flashed sequence was always presented at high contrast, whereas the test stimulus was flashed in the MDF either at low or high contrast (values depending on the contrast tuning curve of the cell, low contrast mean = 0.25, high contrast mean = 0.75) to assess the contrast dependency of the interaction. The distance between patches was set at 120% of the MDF length and the duration of presentation of each patch was 16 ms. The resulting apparent speed ranged from 175 to 500 °.s⁻¹, and these values, when chartered in cortical space, fit with the speed of intracortical horizontal propagation measured in the cat (figure 3.3.2.1).

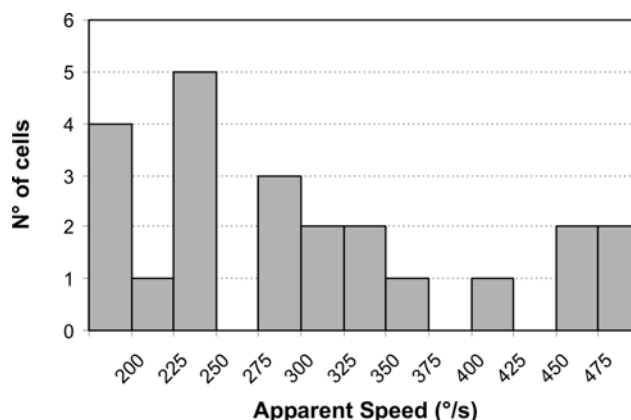


Figure 3.3.2.1: Distribution of apparent motion speed used for our population of recorded cell ($n = 23$). The average speed is $329^{\circ} \cdot s^{-1} (\pm 101 \text{ Stddev})$.

The impact of the association field stimulation is studied by comparing the response to the full apparent motion sequence (3 patches) i) to the response to the test center-only stimulus to reveal the overall modulatory effect of the surround ii) to the addition of the center alone and surround alone test stimuli to assess the strict nonlinear component of the surround interaction.

3.3.3. Excitatory effects of the apparent motion in the surround alone

The use of an apparent motion stimulus was found to be an efficient way to recruit the so-called “silent surround” responses. A first result on the “silent” surround stimulation effect is obtained by studying the characteristics of the responses to the sequence of the two Gabor patches apparent motion presented only in the surround while leaving the discharge field center unstimulated (figure 3.3.3.1). Such configuration usually triggered much stronger responses than those evoked by sparse noise impulsional stimuli, and often even lead to supraliminal response (59 % of the cases). A significant depolarising response was recorded in 66% (76% in collinear condition, 55% in parallel condition).

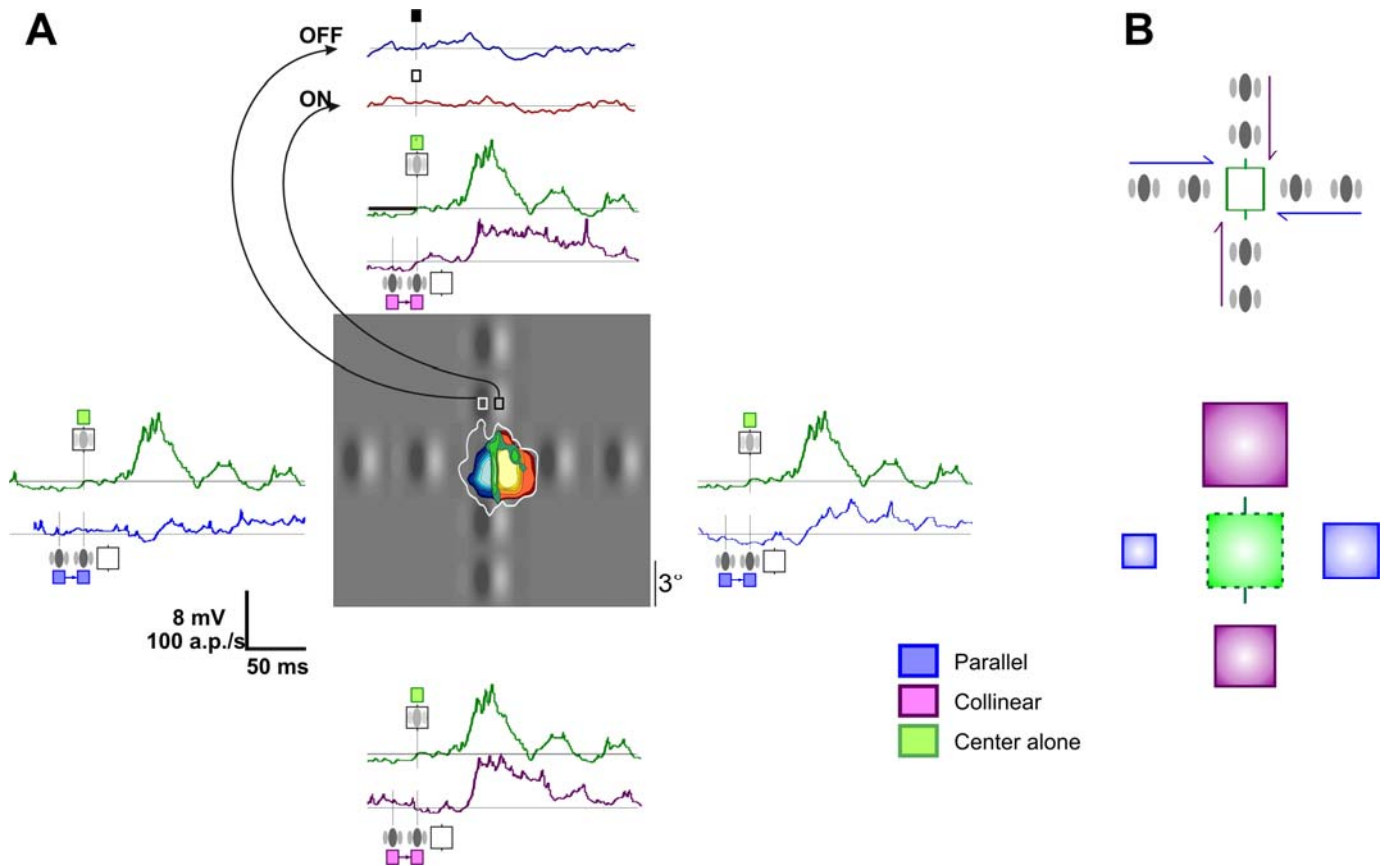


Figure 3.3.3.1: Spatial selectivity of subthreshold responses to an apparent motion stimulus in the “silent” surround. A: A simple cell example of surround responses for apparent motion stimuli along the 4 polar axis, compared with impulsional stimuli responses (top ON and OFF PSTWs). The cell MDF is represented in the central picture (ON spiking responses in Red colour scale, OFF spiking responses in blue colour scale), the significant depolarising field extent (z -score $P < 0.05$ against spontaneous activity) is symbolized by the white contour, and the respective positions of the Gabor stimuli flashed in the surround are presented for sake of comparison. B: Quantification of the mean significant depolarising response averaged across all recorded cells, induced by the surround stimulation (purple: along the collinear axis, Blue: along the parallel axis) compared to the low contrast center alone stimulus condition (in Green). Responses are measured as the integral of the V_m average response above a significance threshold (z -score $P < 0.05$ against spontaneous activity, see Methods).

Those surround supralimnar responses are attributable to nonlinear visual processes since the nearest peripheral Gabor was flashed at a distance (from center to center) of 120% of the maximal length of the MDF defined with impulsional stimuli, corresponding on average to a distance of 5.9 visual degrees. This general suprathreshold effect can be included in the broad class of receptive field dependencies on the stimulation context and is likely to be modelised by a classical power law nonlinearity, that determine the instantaneous discharge rate output in response to a linearly stimulus dependent input voltage (Albrecht and Geisler 1991; Albrecht and Hamilton 1982; Anzai et al. 1999; Carandini et al. 1997, 1999; Gardner et al. 1999; Heeger 1992, 1993; Sclar et al. 1990).

However this nonlinear effect is also present at the Vm level: most of the depolarizing response evoked by the peripheral sequence can be attributed to nonlinear processes since in most of the cases the nearest Gabor patch was flashed outside the detectable significative depolarising field. This simple observation further stress the restriction to a phenomenal but not structural description of the Linear-NonLinear model (and other derived models): L-NL models formalise a global cortical computation covering and averaging a wide range of cortical mechanisms, of specialised neuronal nonlinearities.

Consequently the resulting response map can be distinguished from the classical synaptic integration field and considered as an elementary form of the "association field" of the cortical unit. As described earlier, this association field extend far beyond the subthreshold map revealed by impulse-like stimuli, as illustrated here by the respective location of the Gabor patches and the subthreshold Depolarizing field of the cells illustrated in Figure 3.3.3.1 A.

Furthermore, this association field was found to be dependent on the directional axis, revealing a spatial selectivity and anisotropy not present in the MDF impulsional response (which presented a spatial length to width ratio of 1.2). Collinear peripheral stimuli evokes a depolarising response in average 2,6 times more important than in the parallel configurations. In most cases, one of the polar end-zones of the discharge field was inducing a stronger depolarizing response than the other in the same axis defining a surround associative directional selectivity. The index of polar axis selectivity we thus could calculate, was in average of 0.5 in the collinear axis of the cell (selectivity index = $((\text{max}-\text{min})/\text{max})$ for centripetal conditions).

In summary, probing the "silent" surround with apparent motion stimuli pairs showed that the periphery elicit excitatory responses in most of the cases for all the cardinal directions of

motion, and that the nonlinear "association field" cortical mechanisms favor input collection along the collinear axis, resulting in the emergence of some form of motion direction selectivity for high speed stimuli. The more detailed analysis of center-surround responses that follows further emphasizes those preliminary results.

3.3.4. Center-surround directional selectivity

The first important effect of the apparent motion stimuli consisted in the spatial anisotropy revealed by the strength of the responses to center-surround apparent motion sequences. This effect is particularly apparent in the low contrast center condition, and is revealed by a simple comparison of the full apparent motion sequence with the center alone probe condition (figure 3.3.4.1 A&B). Thus, we will restrain the analysis to those two levels of observation, before the next chapter investigation on nonlinearity and contrast dependency.

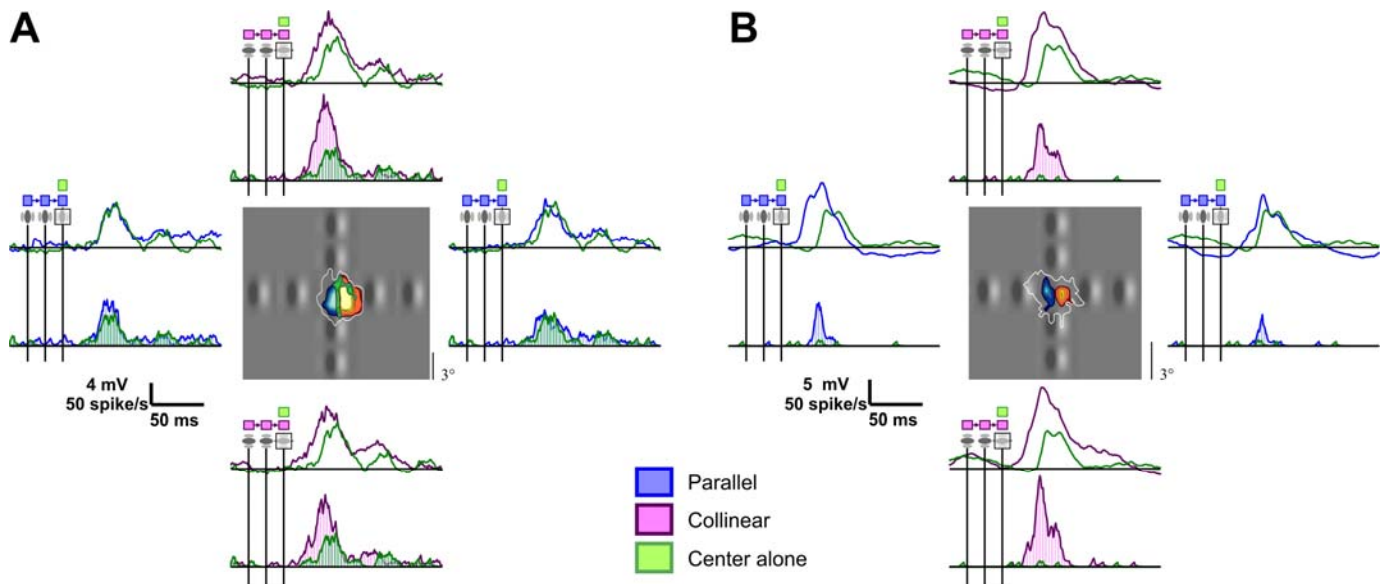


Figure 3.3.4.1: Examples of apparent motion modulation of the center alone response (for the low contrast center and centripetal condition). **A & B:** Example of center-surround apparent motion responses compared to the center alone condition in two simple cells. PSTWs (top) and PSTHs (bottom) of the full sequence responses axis are represented for the four apparent motion (purple: along the collinear axis, Blue: along the parallel axis) in superimposition with the response to the center alone stimulation (green). A cartoon of the apparent motion stimulus, MDF, and the depolarising field extent is illustrated with the same conventions as in figure 3.3.3.1.

The full sequences of three Gabor patches, two being flashed in the "silent" surround and one in the discharge field center allowed us to quantify the impact of surround stimulation when combined to a center alone condition. We expressed the modulatory global effect of the surround stimulation as a gain measured by the ratio of the response to the full apparent motion sequence divided by the response to the center alone condition (figure 3.3.4.2 A). In both conditions, the responses are quantified by the integral of the evoked average PSTHs and PSTWs responses above a significant threshold determined by the spontaneous activity (z-

score $P < 0.05$). Surprisingly, most of the conditions either parallel or collinear, in most of the cell, elicited a facilitating effect. A facilitation by the surround stimulation could be observed at the depolarising response level in 84% of the tested conditions (respectively 95% for collinear and 69% for parallel conditions), and at the spiking response levels in 75% of cases, (respectively 84% for collinear and 66% for parallel conditions).

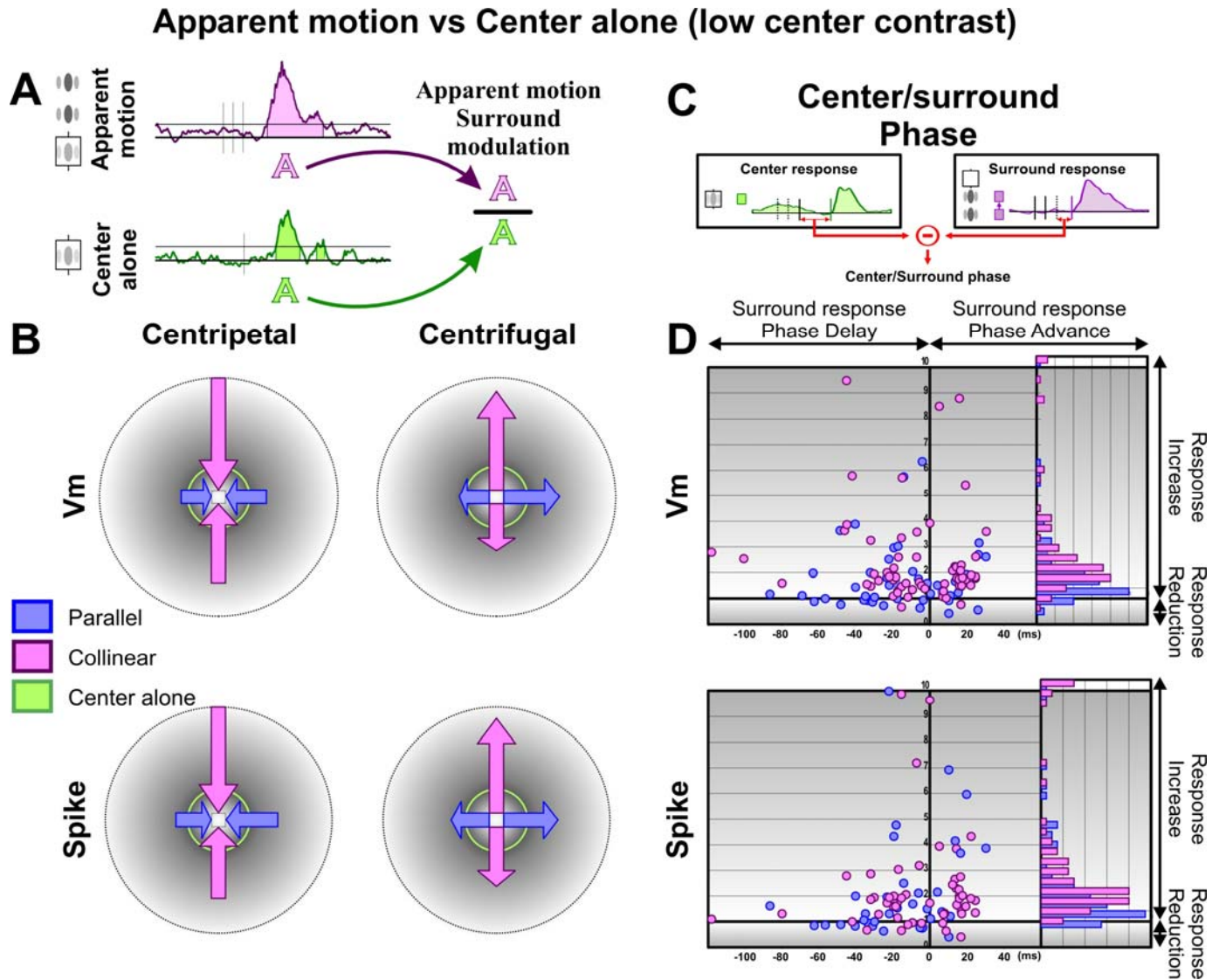


Figure 3.3.4.2: Apparent motion modulation of the center alone response: directional and spatial selectivity (for the low contrast center conditions), Population analysis. **A:** principle of measure of apparent motion surround modulation ratio: The modulation by the surround apparent motion stimulation is defined by the ratio between the significant synaptic response (its integral value) evoked by the full sequence center+surround and that evoked by the center-alone stimulus. These ratios are computed for spike and subthreshold Vm fluctuations (Z-score against spontaneous activity $P < 0.05$). **B:** Population analysis ($n = 23$) of the apparent motion modulation ratio. The length of the arrows is proportional to the mean ratio value averaged across the population of recorded cells. The green circle represent the center-alone response integral (or modulation ratio = 1). **C** Principle of measure of the center/surround phase relationship, both center-alone and surround-alone Vm responses are measured (cf. methods) and subtracted. **D:** Apparent motion surround modulation as a function of the center/surround phase plotted both for the centripetal and centrifugal conditions. On the right panels are presented the distribution histograms of the apparent motion surround modulation for collinear (purple) and parallel condition.

This nearly ubiquitous surround effects present a directional selectivity for the collinear axis: surround stimulations in the collinear axis are evoking in most of the cells a much stronger facilitation effect on the center-alone response than in the parallel axis (figure 3.3.4.2 B). 91 % of the cells presented this collinear bias in the depolarising response, 95 % in the spiking response (mean on the two directions of the axis). In the collinear axis, the apparent motion stimuli evoked a depolarising response on average 2.6 times more important and a spiking response 2 times more important, than in the parallel sequence condition. Furthermore, most of the cells presented a clear selectivity for one directional axis vs the opposite one. For example, the “directional-like” selectivity index we could measure for the collinear axis was of 0.3 for the depolarizing response and of 0.38 for the spiking response (meaning that the surround effect is about 1.5 times larger in the preferred collinear axis than in the non-preferred collinear axis, figure 3.3.4.2 B).

Although a significant difference in the distribution of the apparent surround modulation of the depolarizing and spiking responses is found between parallel and collinear conditions, no significant difference could be revealed when comparing the centripetal vs. centrifugal conditions. On average, centripetal depolarizing and spiking responses were respectively 1.1 and 1.2 times larger than centrifugal responses (figure 3.3.4.2 B). A simple explanation to this apparently surprising result, taking into account the duration of the responses and the relation of phase between the surround-alone and the center-alone responses, will be given in the temporal analysis of the result in the following chapter.

3.3.5. Selective control of the timing of the responses by the Surround

In the previous analysis, we showed that with an apparent motion stimuli, the surround stimulation modulated the amplitude of the center alone response. A simple observation of the two examples in figure 3.3.3.1 shows that this surround modulation is expressed also crucially in the temporal profile or timing of the response. In this chapter, we will focus on the description of those temporal modulation and their dependency on the stimulus configuration (centripetal vs. centrifugal, collinear vs. parallel).

Two main goals guided us to study the temporal characteristics of those effects:

_ First of all, center-surround interactions may impose a specific temporal control of the gain of response, possibly sustaining both a temporal code, and the perceptual bias observed in psychophysics. The model elaborated by Series & al (2002) binding our electrophysiological results and the psychophysical results, relies critically on such temporal effects. It simulates

the facilitatory effect of the collinear configuration by the orientation dependent recruitment of a slow wave of intra-cortical activity propagating through long-range horizontal connections. The phase advance in the firing of V1 neurons resulting from the optimization of the temporal overlap between horizontal and feed-forward activation is shown to bias the spatiotemporal correlation performed at a second stage by MT-like motion selective cells or Reichardt detector (1961).

_ Secondly, as the amplitude of the global facilitation did not seem to express an important specificity on the temporal characteristics of the stimulation (cf. centripetal vs. centrifugal, figure 3.3.4.1.), we are expecting the temporal structure of the response and of the non-linearity to do so.

In order to characterize the relative timing of synaptic input depending on its origin, we used a method consisting in determining and subtracting the onset latency of the postsynaptic potentials evoked independently by the center alone and the surround-alone stimulation (see figure 3.3.4.2 C). The result of this latency subtraction will be referred in the rest of the text as the center/surround phase. The interest of such quantification is to give an objective measure which allows the direct comparison of the effects of different associative sequences realized for a given cell as well as across various cells.

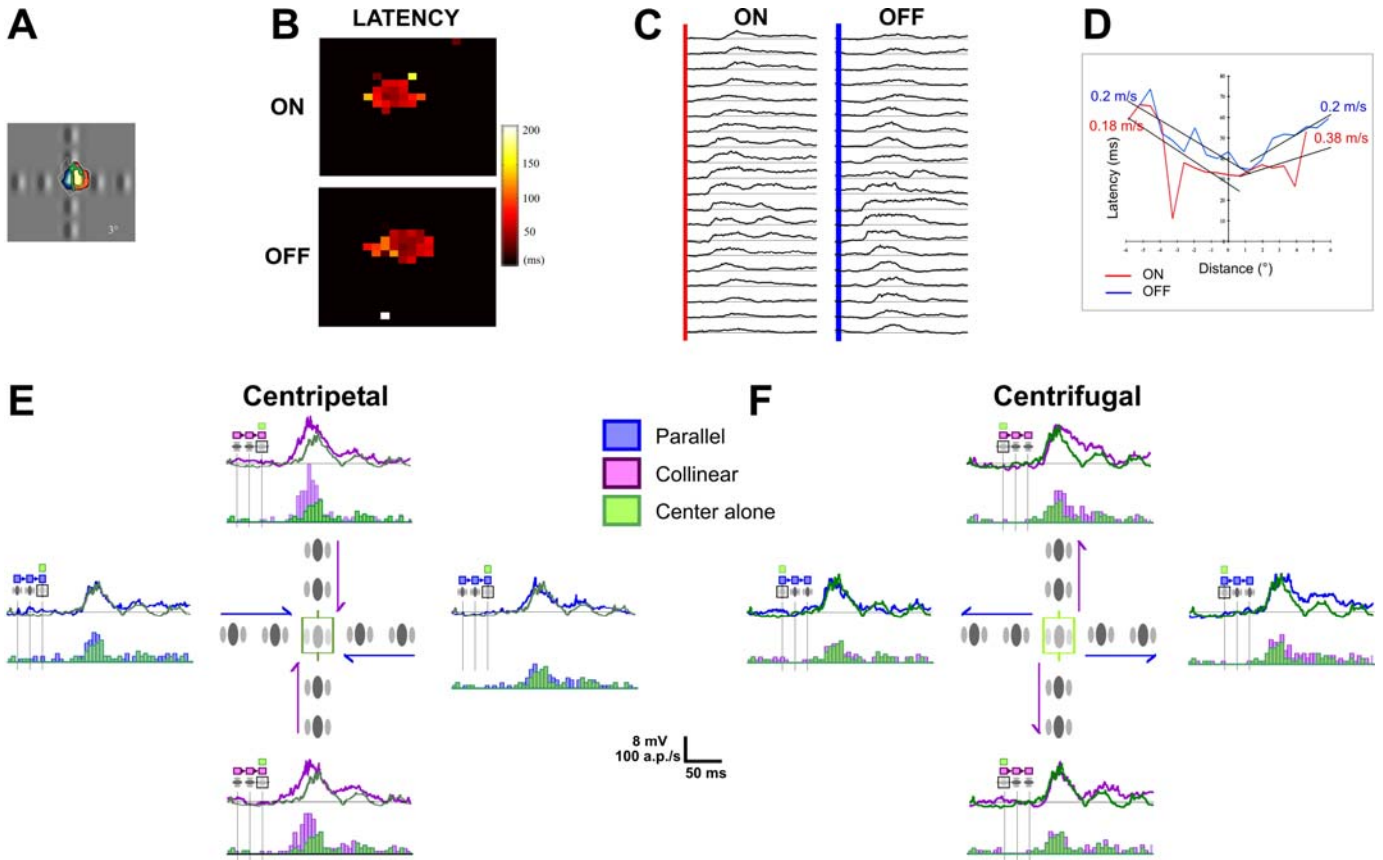


Figure 3.3.5.1: Importance of the temporal order of the center-surround apparent motion on the timing of the surround facilitation and latency decrease of the center-alone response (low contrast center condition): Example of the same Simple cell as in figure 3.3.4.1. **A, B, C & D** : characterisation of the temporal profile of the Depolarising Field (**A**: receptive field map) using classical static stimuli: sparse impulsional noise (**B**, Latency maps), elongated bars of optimal orientation flashed in various position along the parallel axis (**C**, ON and OFF PSTWs) and the latency quantification to their subthreshold responses (**D**). **E** and **F** illustrate respectively the Centripetal (**E**, see also figure 3.3.4.1) and Centrifugal (**F**) apparent motion responses with the same conventions as in figure 3.3.4.1.

As the protocols involve surround responses which display a temporally constrained profile in latency basin, and also the time order of the sequential stimulation (centripetal & centrifugal), two parameters having potentially a crucial influence in the responses latency (figure 3.3.5.1), the recorded results explore a large range of phase relationship between the surround-alone responses and the center-alone responses. The global center/surround phase distribution shown in figure 3.3.5.2 C (bottom diagram) shows the full range of phase relationship from -80 of phase lag to $+35$ ms of phase advance which have been applied. The analysis was restricted to instances where both latencies of surround-alone and center-alone responses could be determined (58%). As expected, a strong bias in the distribution was observed in favour of the surround phase advance for the centripetal sequences (orange distribution) and in favour of the surround delay for the centrifugal sequences (blue distribution).

The plot of the apparent motion surround modulation (as measured previously) in function of this center/surround phase (figure 3.3.4.2 D) allows us to explain the lack of difference observed previously between centripetal and centrifugal conditions. The peripheral gain effect appears to express a facilitatory effect (>1) for a wide time window of phase relationships, ranging from -40 ms to $+40$ ms, in which both centripetal and centrifugal conditions are highly represented. This large temporal window of center/surround coincidence showing a center-alone response facilitation by the surround stimulation can be related to both center and surround's responses broad duration (mean center response duration: 100 ms, mean peripheral response duration: 130 ms). The temporal overlap between the center-alone and surround-alone responses whatever their phase relationship is sufficient to induce on average a facilitation by the surround. However, the timing of this facilitation appears crucially dependent on their phase relationship, a latency decrease of the responses being only observed for centripetal condition (cf. example in figure 3.3.5.1 E vs. F), i.e. when the periphery is activated before the center.

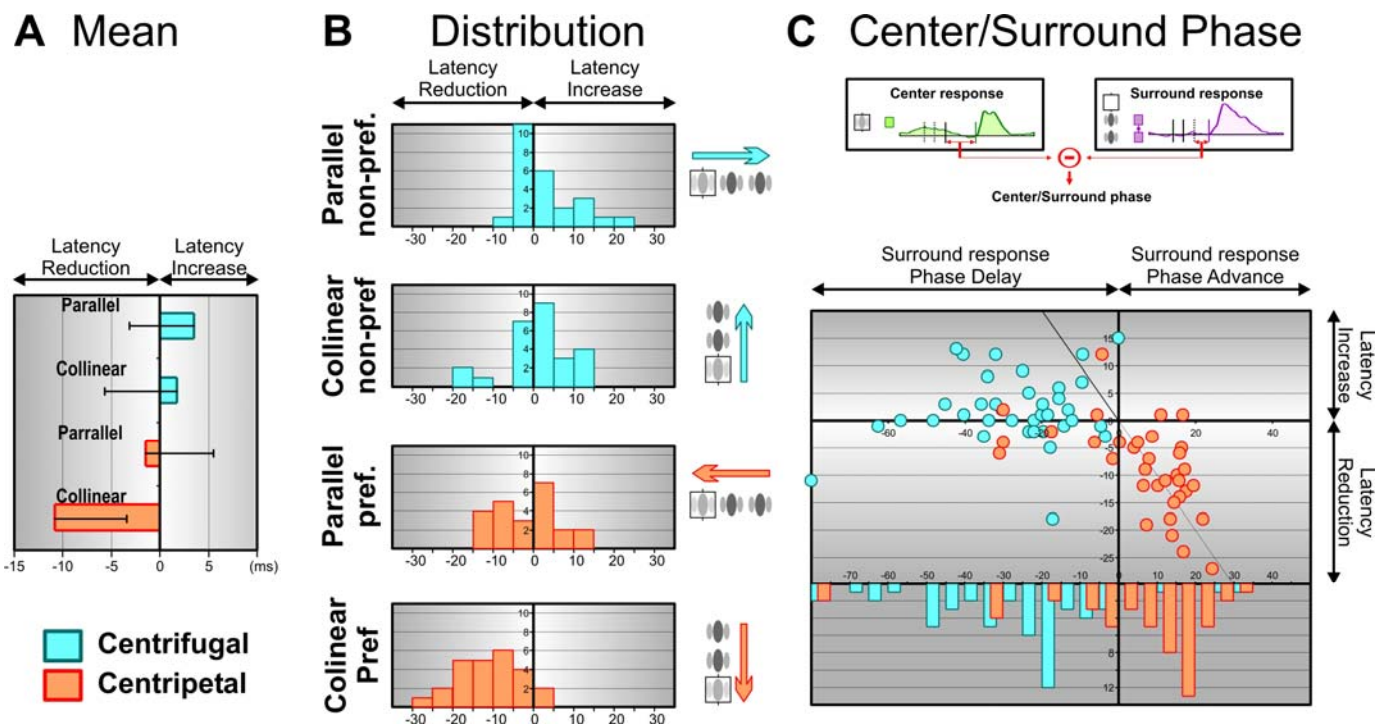


Figure 3.3.5.2: Population analysis of the surround modulation of the timing and latency of the center response as a function of the apparent motion centripetal (orange) or centrifugal (blue) conditions ($n = 23$). The average and distribution of the latency increase or reduction for the various conditions are presented in **A** and **B** respectively. **C Top:** Measure principle of the center/surround phase relationship, both center-alone and surround-alone V_m responses latency are measured (cf. methods) and subtracted. **Bottom:** Apparent motion's surround modulation of the center-alone spiking latency as a function of the center/surround phase plotted both for the centripetal (orange) and centrifugal (blue) conditions. On the bottom panel is presented the distribution histograms of the center/surround phase for centripetal and centrifugal conditions.

We could test the validity of one of the key hypothesis of the model (Séries et al, 2002) explaining the psychophysical experiments with a modulation of the spiking latency of primary visual cortex cells, by subtracting the center-alone latency from the center/surround composite stimulation latency. The mean and the distribution of this difference are plotted in figure 3.3.5.2 A and 3.3.5.2 B. The striking result is that apparent motion sequences could induce significant phase advances, as large as 30 ms for the spiking response, only when they were properly timed (centripetal) and moving along the collinear axis. The latency reduction observed for the collinear axis during a centripetal stimulation was on average of 10.8 ms (\pm 7.8 ms StdDev). In the other conditions, either centrifugal or centripetal along the parallel axis, no significant latency reduction could be seen. If a linear model (L-NL), or the more sophisticated interaction model proposed by Series & al (2002) appear to be corroborated by those results, they are not sufficient to explain the entire effect observed electrophysiologically. Indeed, the examination of the surround-alone depolarizing latencies reveals a bias for shorter latencies when the motion path is along the collinear axis. The depolarizing wave evoked by a collinear pair of stimuli flashed in a centripetal sequence in the “silent” periphery was arriving on average 9 ms (\pm 5.2 ms SE) earlier than when the stimuli were oriented orthogonally to the width axis path (parallel condition). This effect was significant in 65% of the cells showing significant depolarizing centripetal peripheral response for parallel and collinear conditions. A first raw argument allow us to attribute, in the same way as seen before with the spatial anisotropy, this peripheral latency reduction specific of the collinear axis and the centripetal direction, to an associative facilitatory effect between the pair of peripheral stimuli: no anisotropy related to collinear axis could be found in the latency basin of the depolarizing field of the cells. The next analysis demonstrates the involvement of strong nonlinearities responsible for these effects.

3.3.6. Contrast dependency of the surround modulation and Surround impact on the SNR

Until now, we have focused our analysis on apparent motion responses with a low contrast in the center, which revealed a facilitatory effect of the surround on the amplitude and latency of the center response. The experimental litterature on center-surround interaction using static framework presents however conflicting reports concerning their contrast dependency: some studies showed that facilitatory effects for low contrast become suppressive for high contrast (Polat & al, 1998), whereas others found only suppression or facilitation even at high contrast (Kapadia & al, 1995). In our own experiments, when the apparent motion sequence is

presented with a high contrast in the center, the previously observed surround facilitation of the center response decreases drastically and even becomes suppressive in some cases as shown for an example cell in figure 3.3.6.1 A & B. We applied the same quantification of the apparent motion surround modulation ratio, which shows that the surround effect on the integral of the center response is very low (figure 3.3.6.1 C). A latency reduction could be observed but with a much lower amplitude than at low contrast, as shown by averaging PSTHs across cells (figure 3.3.6.1 D). These results can simply be explained by the fact that the high contrast stimulation saturated the response both in its amplitude and latency reduction. Note that as expected from Gwane & al (1996), the increase of the contrast of the Gabor-test stimulus has reduced the center-alone latency response by about 5ms.

The response variability is classically considered as proportional and as important as the average responses, independently on the stimulation characteristics. Those observations will be reconsidered in detail in the next chapter of the thesis, and we propose here just a preliminary analysis introducing the effects of cortical interaction on noise and more pertinently on the signal to noise ratio.

We thus wondered if the center-surround interactions could not solely affect the amplitude and time course of the synaptic responses but also their variability across trials. To do so, we applied a time frequency complex wavelet analysis on each trial and measured both the signal as the modulus of the average response vector and the noise as the average distance of the individual trial vectors to the average signal vector. As noise is classically considered as a multiplicative constant to the signal, we have only presented in the following study the relevant Signal to Noise ratio results. Furthermore, SNR measure is related to the information brought by the response about the stimulus and represents the part of the signal that is available for the next processing steps. This technique is detailed in the chapter 3.5, and the related results are analysed more in depth in the next part of the thesis. When applied to the apparent motion responses (figure 3.3.6.1 A & B), it shows that the concomitant stimulation of the surround amplifies the SNR of both the Spike and Vm responses in most conditions. At least even when the surround did not present any modulation on the average center response (figure 3.3.6.1 A 2nd column), the SNR could present an important amplification, pointing out the importance of the surround modulation on the variability of the response.

An other important remark can be done from the simple comparison of the time-frequency SNR(Vm) and SNR(Spike) to their corresponding averaged PSTWs and PSTHs: the SNR increase only corresponds to the initial part of the response whereas latter response

depolarizing components are not associated with significant increase of the SNR. This result can be generalised to any type of flashed or impulsional stimuli (as revealed by further investigation): the initial component of the response is bringing more information about the stimulus whereas the latter component corresponds to less informative and more variable responses, presumably representing the relaxation phase of the network recurrency.

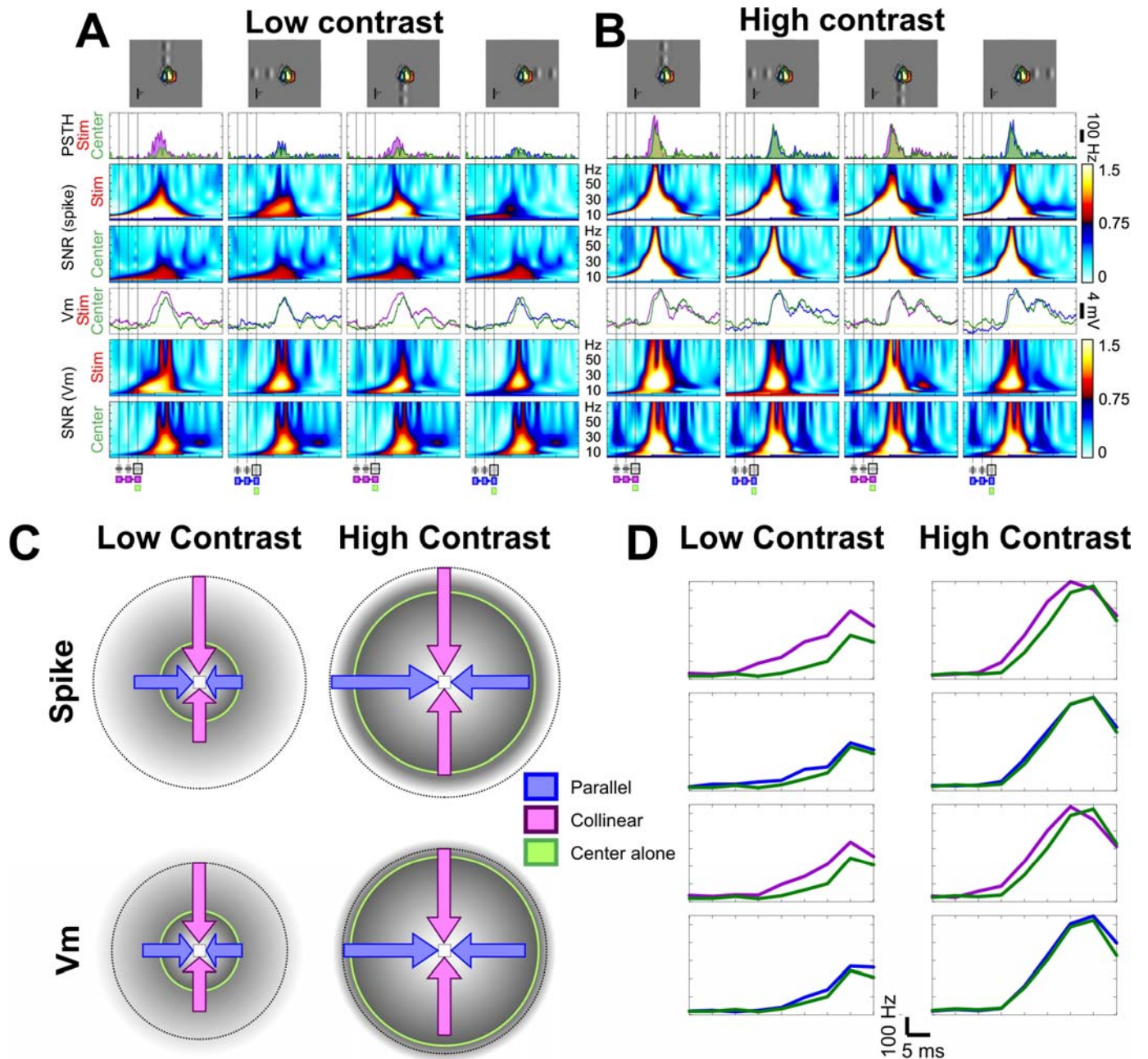


Figure 3.3.6.1: The contrast dependency of the apparent surround modulation of the amplitude and latency of the center response: example and population analysis ($n = 23$). Responses of the same simple cell as in figure 3.3.4.1 and 3.3.5.1 to the centripetal apparent motion in the four cardinal axis of the cell at low contrast center (A) and high contrast center (B). The PSTHs, PSTWs and SNR(spike), SNR(Vm) time-frequency analysis of the pool of 20 trials per condition (see methods) are presented for all conditions. C: Population analysis ($n = 23$) of the apparent motion surround modulation ratio for both low and high contrast center condition. The length of the arrows is proportional to the average ratio across the population. The green circle represent the center alone response integral (or modulation ratio = 1) and is normalised at the same value for spike and Vm at low contrast. D: Average latency reduction for low and high centre contrast condition: average PSTHs across cells for from top to bottom the preferred collinear axis, the preferred parallel axis, the non-preferred collinear axis, and the non-preferred parallel axis (bin = 5 ms).

In order to reveal variations of SNR amplitude during the time course of V1 responses, we have compared the temporal profiles of the PSTHs and PSTWs, averaged across cells, respectively to the frequency-time patterns of SNR(spike) and SNR(Vm) (also averaged across cells (figure 3.3.6.2 A)). The energy of the SNR time-frequency spectra is more concentrated in the initial phase of the response than in the latter, as shown by the phase shift of the averaging of the matrices across frequencies (blue traces). We then wondered what was on average the effect of the surround on the time course and on the SNR of the center responses as a function of the contrast. We have therefore subtracted the various temporal responses (PSTWs, PSTHs, SNR(spike), SNR(Vm)) recorded for the full apparent motion sequence to the one obtained for the center-alone probe condition. We then have averaged these differences as well as the responses (PSTWs, PSTHs, SNR(spike), SNR(Vm)) across all conditions and cells, to obtain the surround average temporal modulation (figure 3.3.6.2 B). The four axis stimulation presented the same profile of modulation but with various amplitude depending on the cells and the conditions, justifying the global averaging.

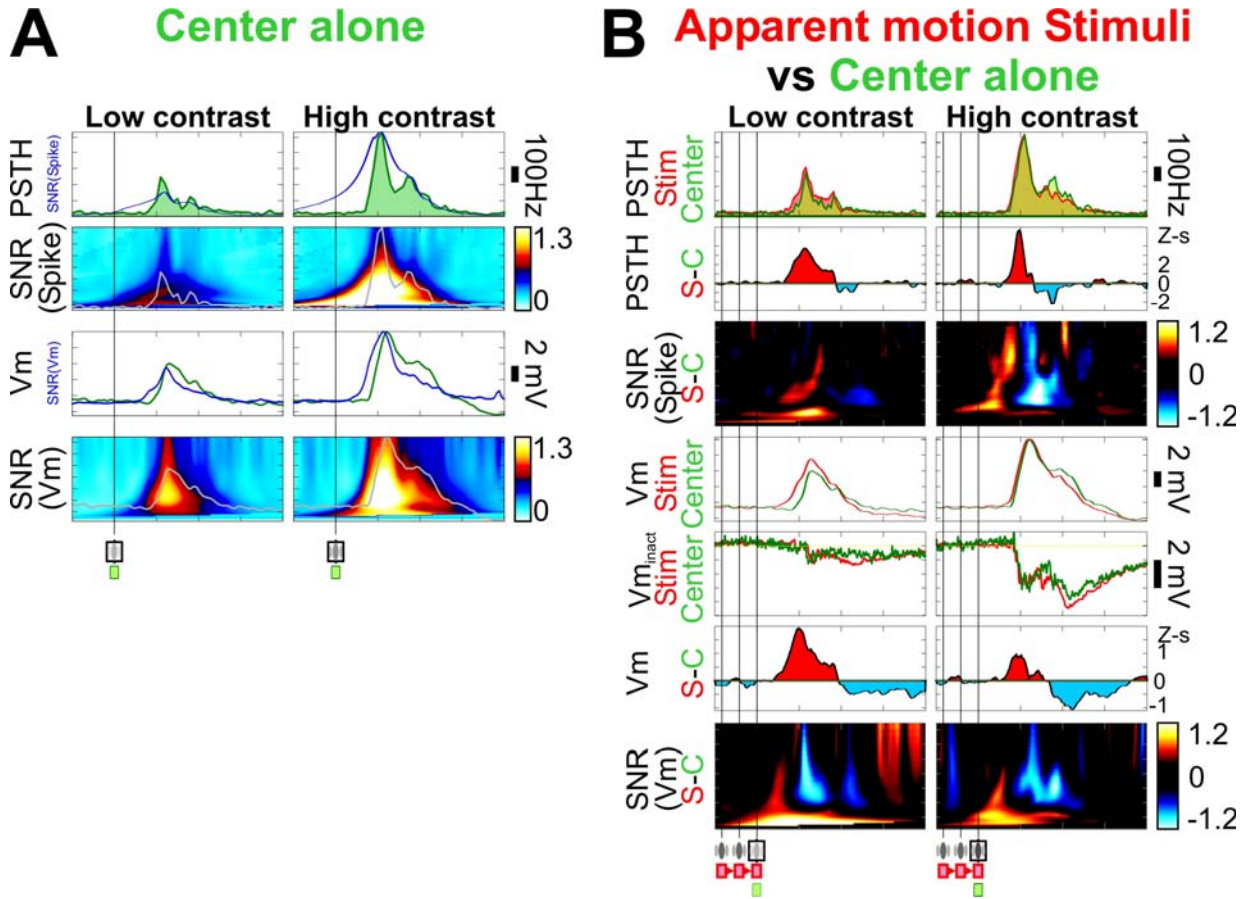


Figure 3.3.6.2: The biphasic modulation of the center response by the surround facilitate the initial high SNR response and suppresses the late poorly informative (variable) response tail. A: SNR increases mostly during the initial phase of the Vm and spiking response. From top to bottom: cell averaged for the center only condition, PSTHs superimposed with the integral across frequency of the SNR(spike), SNR(spike) superimposed with the PSTHs, PSTWs superimposed with the integral across frequency of the SNR(Vm), and SNR(Vm) superimposed with the PSTWs. B: Surround average biphasic modulation of the center responses by the surround. The measures presented are the average across cells for all the centripetal conditions (for the four cardinal of axis). From top to bottom: **i)** center-alone condition (Green) and apparent motion (Red) PSTHs, **ii)** the average across cells of the difference between center-alone and apparent motion PSTHs expressed in z-score of the spontaneous activity, **iii)** The average across cells of the difference between the apparent motion and the center alone SNR(spike) expressed in z-score of the spontaneous activity (calculated independently for each frequency). **iv), vi) & vii)** The same measures are presented at the membrane voltage level (for PSTWs). **v)** The averaged across condition PSTWs responses to center alone and apparent motion stimuli of one cell recorded in inactivated state ($V_m = -43$ mV), revealing the inhibitory response, is shown in the 5th row.

The effect of the surround is biphasic with an initial facilitatory phase followed by a later suppressive effect. It is observed whatever the signal considered, either Vm or spikes, and this finding applies both to the average responses or their SNR. The contrast mainly shortens the initial facilitatory phase. In conclusion, surround stimulation is removing part of the late, low informative and noisy, component of the center alone response whereas it facilitates transiently the early high SNR phase of the response. Thus surround stimulation “concentrates” in time the information about the stimulus. We recorded the responses for one cell in the spike-inactivated state (cf. methods) where action potentials are suppressed and the

inhibitory inputs become identifiable by stimulus-locked hyperpolarizations amplified by the imposed change in driving force. The surround stimulation increases slightly the inhibition during the late suppressive phase, confirming the suspicion of its inhibitory origin.

3.3.7. Center-surround nonlinear control of the timing and contrast dependency

It is possible to assess the nonlinearity of the apparent motion center-surround interactions by considering the difference between the responses recorded to the full apparent motion sequence to the sum of the individual responses to the center and surround alone condition. Of course, as we previously emphasized in chapter 3.3.3 and 3.2, the individual responses are already themselves a result of a nonlinear mechanisms and process, but the present aim is to uncover the supplementary nonlinearity brought by the center-surround interaction.

Thus we have directly added up either the Vm average waveforms (PSTWs) or the Spiking average responses (PSTHs) of the center-alone and surround-alone conditions in order to effectively obtain a linear predictor of the apparent motion response. We then applied the same measure of significance for the integral value of depolarising responses (z-score compared with mean spontaneous activity: $p < 0.001$) both to the apparent motion response and to its linear predictor. The two resulting values were divided to obtain the global apparent motion nonlinear gain (we did not include in this study the stimulation conditions which were ineffective in evoking subthreshold responses). The same technique, but on each trial, was applied to obtain a linear predictor and the nonlinear component of the SNR time-frequency measure. We summed all trials corresponding to the center-alone condition with those corresponding to the surround-alone condition to obtain a pool of linear predictor trials, on which we could apply the same SNR time-frequency analysis. The global nonlinear SNR gain evoked by the apparent motion is then calculated by the ratio (real/predicted SNR) of the integral of the matrices values significantly different from the spontaneous activity (significant threshold calculated independently for each frequency z-score $p > 0.001$).

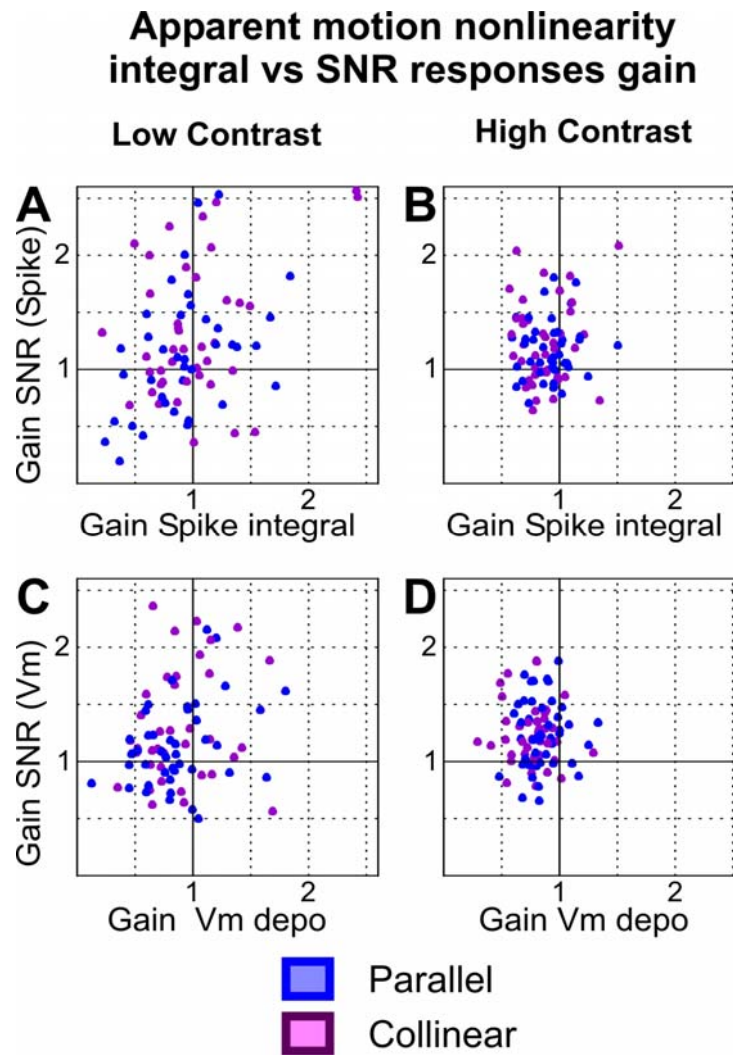


Figure 3.3.7.1: Center-surround nonlinearity are globally suppressive at high contrast and increase the SNR of the response (for centripetal apparent motion conditions, $n = 23$). The nonlinear gain of the integral of the responses is plotted as a function of the nonlinear gain of the SNR responses, for the Vm (bottom panels) and the spiking responses (top panels) at high and low contrast.

The resulting measures are presented in figure 3.3.7.1, where the response amplitude global integral nonlinear gain is plotted against the response SNR global integral nonlinear gain, for the voltage membrane and spiking response at high and low contrast. At low contrast, the apparent motion non-linear effect displays a large diversity of amplitude and sign, and demonstrates the existence of both globally facilitatory and suppressive nonlinear interactions depending on the stimulation condition and the cells. At high contrast, the apparent motion center-surround interaction was globally suppressive in the vast majority of conditions. Considering the SNR global integral nonlinear gain, the apparent motion has a facilitory effect in most of the cells both at low and high contrast although this increase is more

ubiquitous in this last condition. Moreover, no noticeable difference was observed between the collinear and the parallel axis of the cells using these global time average measures. These latter observations are reminiscent of the facilitation/suppression contrast dependency reported by Polat & al (1998) among others. However this previous work did not fit with our observation of a latency reduction observed also at high contrast. The global selectivity to the direction of the apparent motion previously reported suggested us that these averaged measures may occult a complex temporal effect and led us to investigate the precise time-course of the nonlinearity.

To reveal the time course of the amplitude and sign of the nonlinearity, we subtracted the linear predictor to the real response waveform observed in response to the full apparent motion sequence (figure 3.3.7.2). To reduce the non specific across-cell variability, we expressed for each cell this temporal nonlinear waveform in z-score values of its spontaneous activity and then averaged the normalized waveforms across cells (the raw waveforms were presenting the same behaviour but amplified).

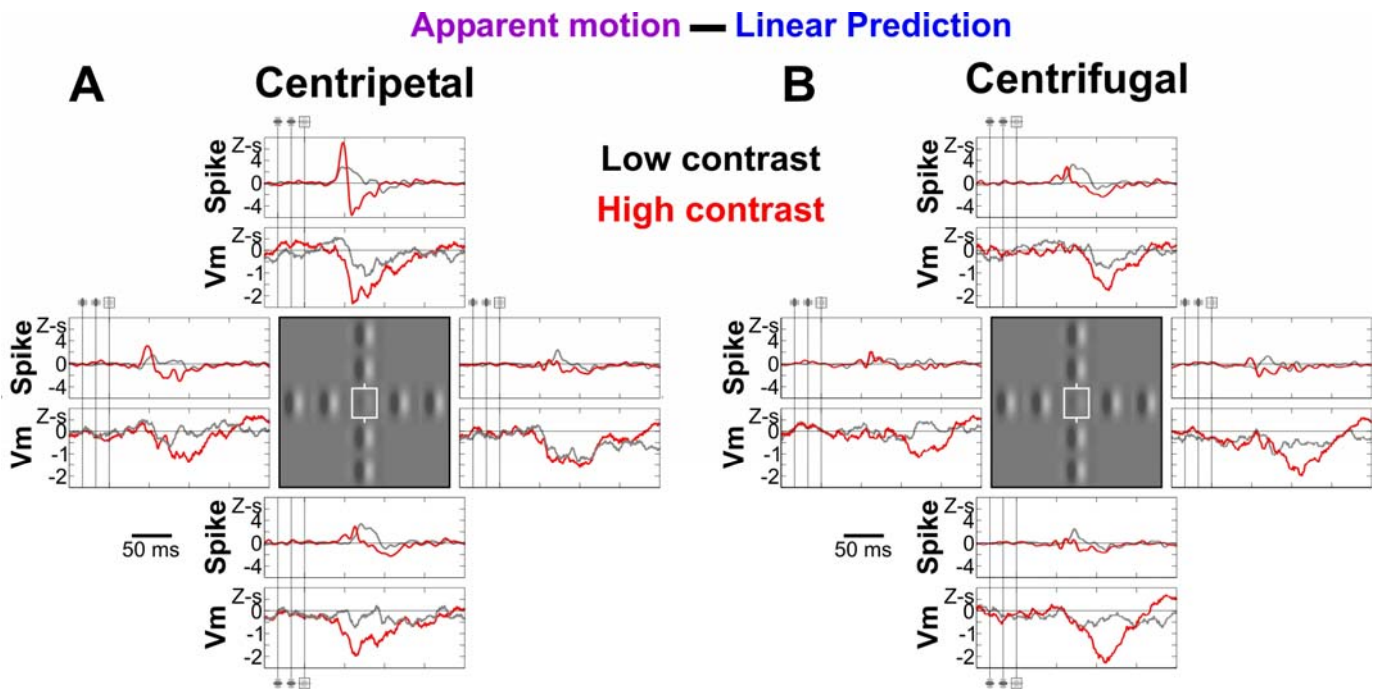


Figure 3.3.7.2: The biphasic temporal profile of the center-surround apparent motion nonlinearity, and its directional selectivity and modulation by the contrast (population analysis for the centripetal conditions, $n = 23$). The temporal waveforms of the nonlinearity are calculated for each cell by subtracting the linear predictor (Center alone + surround alone responses) from the real response to the full apparent motion sequence, both at the spiking level (top panels) and at the Vm level (bottom panels). Here, we present the average z-score waveform (relative to the mean spontaneous activity). The temporal profile of the nonlinearity is given for the low contrast center (grey colour) and the high contrast center (red colour) conditions both for centripetal (A) and centrifugal (B) directions of apparent motion.

As expected, this analysis revealed that the center-surround interaction probed by the apparent motion presents a strong temporally biphasic effect (figure 3.3.7.2 A top panel), with an initial transient facilitation interrupted by a strong and long-lasting suppression observed also at the Vm level. This nonlinear temporal profile is modulated by the contrast : increasing the center contrast amplifies the biphasic behaviour of the waveform and increases its suppressive component. This nonlinearity is highly specific for the collinear axis of the cell and furthermore, seems specific of one of the two possible motion direction axis. This demonstrates a strong directional selectivity of the center-surround nonlinear interaction. In contrast, along the parallel axis, the apparent motion did not trigger detectable nonlinearity at the spiking level nor a long-lasting suppressive nonlinearity at the Vm level. Note also that this nonlinearity is selective to the centripetal direction of the apparent motion, since nonlinear effects are mostly absent in the centrifugal condition at the spiking level and expressed in a late and delayed suppressive phase at the Vm input level (figure 3.3.7.2 B).

3.3.8. Orientation selectivity of the surround-alone response and of the apparent motion center-surround modulation effect

In order to assess the dependency of the center-surround interaction on the local orientation cues shown in the surround we designed protocols of surround-only apparent motion and center-surround apparent motion for which the surround Gabors were flashed with an orientation orthogonal to the preferred orientation of the cell (Cross-oriented conditions). We then compared the recorded responses to those cross-oriented conditions to the previously described iso-oriented conditions (figure 3.3.8.1 A & B).

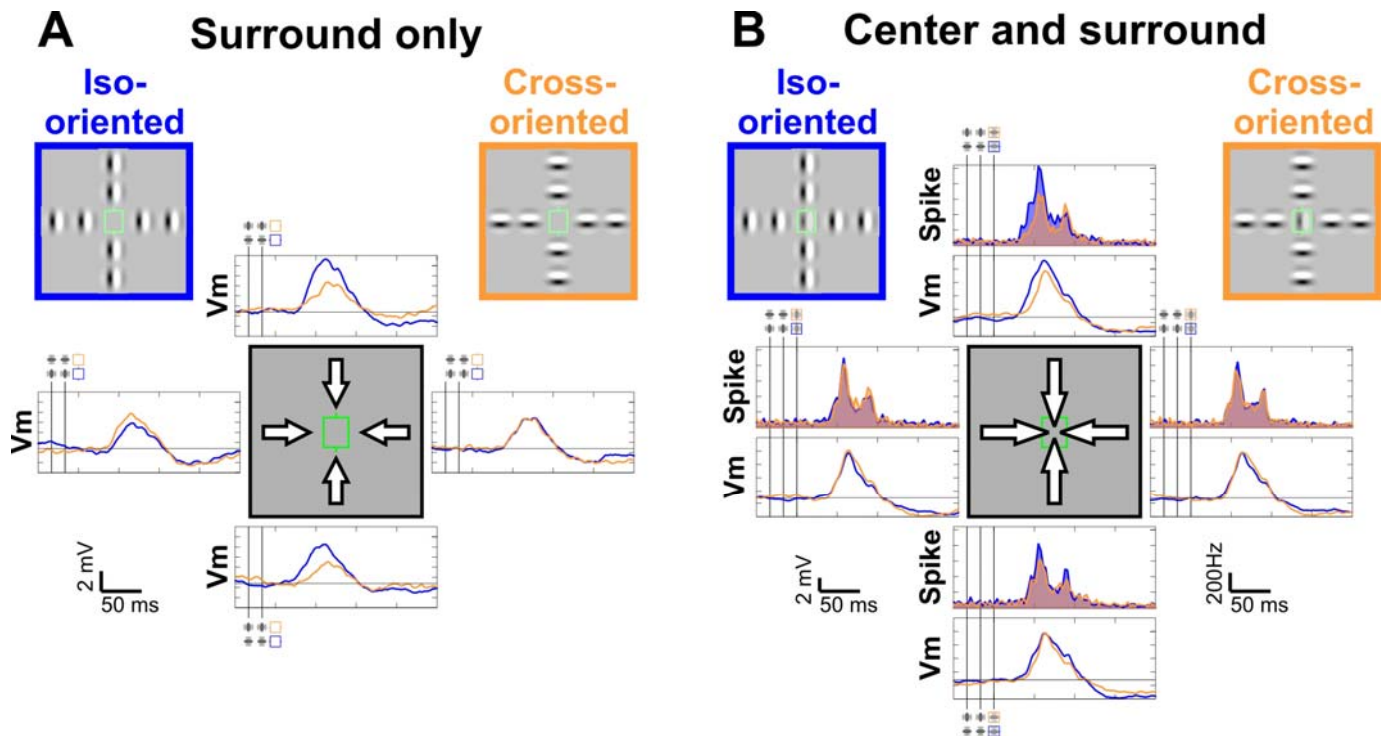


Figure 3.3.8.1: Orientation selectivity of the apparent motion responses in the surround-only and in the surround-center conditions: (population analysis for centripetal and low contrast center conditions, $n = 13$). A: Surround orientation selectivity: Responses to apparent motion restricted to the surround-only. The effect produced by Gabor elements whose local orientation is the preferred orientation of the cell (iso-oriented configuration, in blue) are compared with those produced by Gabor elements flashed with an orientation orthogonal to preferred orientation of the cell (cross-oriented configuration, in orange). The PSTWs of the responses are averaged across the 13 cells for which both conditions were applied. B: Same comparison but with the full center-surround apparent motion sequence.

The surround-only condition reveal a preference for the iso-oriented condition, and this bias was seen best for one of the two collinear axis. A similar trend was found also in the responses to the full center-surround apparent motion sequences. These results further point out both the intra-cortical origin of the observed center-surround apparent motion effect. They also further demonstrate the selectivity of center-surround apparent motion effect for the “Gestaltic” iso-oriented collinear configuration, allowing to V1 neurons to detect selectively for one direction, high speed motions in the visual field respecting isofeature binding and spatiotemporal good continuity laws (similarity (for orientation), common fate and spatial good continuity (for motion)).

3.3.9. Conclusion

3.3.9.1. Two cortical processes of motion detection

Our results point out a remarkable correlation between the psychophysical and electrophysiological data which in turn both similarly conclude to a stage of motion integration dependent on the congruence of the motion axis with orientation detection. This step, probably preliminary to the disentanglement of motion from form attributes by higher cortical areas, seems to operate as early as in the primary visual cortex. This process operates for high speed slips on the retina, that induce for real motion strong motion streaks (Geisler, 1999), and seems to be carried out by primary visual cortex in a functional way distinct from that engaged during the classical local form analysis. Indeed, depending on the absolute speed of oriented contours, area 17 cells in the cat show two distinct behaviours (figure 3.3.9.1):

_ for directional apparent motion sequences as fast as $500^\circ/\text{sec}$, they respond selectively along the orientation or collinear axis of their receptive field, and this integrative process concerns long-range spatial interactions.

_ for speeds which are two order of magnitude slower, V1 cells fire preferentially for iso-oriented stimuli displaced along the width axis of the receptive field and code the motion component orthogonal to the orientation of the moving contours. This selectivity is expressed for short-range spatial interactions.

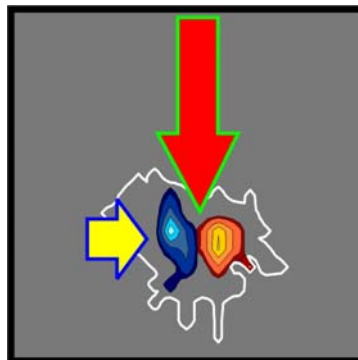


Figure 3.3.9.1: Schematic representation of the two motion axes of direction selectivity in V1 neurons. Red arrow: long spatial range and high speed motion selectivity along the collinear axis of the cells. Yellow arrow: classical motion selectivity for short spatial range and low speed motion along the width (or “parallel”) axis of the cells. The minimal discharge field of a Simple cell (MDF) is represented with ON- and OFF-subregions respectively in red and blue (colour coded response scales). The spatial extent of the depolarizing subthreshold field is depicted by a white curve.

Our findings at the intracellular level partially corroborate the hypothesis made by Orban in the 90s who proposed in primary visual cortex an orthogonal shift of preferred motion axis for high velocity. The noticeable difference is that the stimulus used here is an optimally oriented Gabor patch whereas most previous reports (Worgötter & al, 1989, Crook, 1990, Crook & al 1994) typically used a non-oriented spot which produce responses with a higher cut-off velocity than that observed for bars and contain equal Fourier component at each orientation.

Our findings confirm Geisler's team results (Geisler, 1999, Geisler & al, 2001) of the existence of specific motion mechanisms in the collinear axis of the RF and that this collinear motion detection is preferentially expressed for high speed motions. Our results further demonstrate the crucial involvement of center-surround interactions in this effect and its relevance for a speed range in fact much higher than that to which they limited their study (4-8°/sec).

Futhermore, our results find a strongly supportive correlate in a recent optical imaging study (Basole & al, 2003) showing that the highest activation domains coding for "slow" and "fast" motion flip from the isopreference representation to the complementary cross-oriented domain for a specific critical speed situated between the values used for our apparent motion sequences (equivalent to their "fast" motion condition) and those reported as the preferred velocity of V1 cells for oriented stimuli ("slow" motion condition). At slow speed, vertical motion activates horizontal columns whereas, above 20 °/sec, it activates vertically oriented columns.

3.3.9.2. Apparent motion and center-surround cortical integration: proposition of a spatiotemporal E/I balance model of cortical gain

Physiologically, the biphasic temporal profile of the center-surround nonlinearity is reminiscent of Hirsch and Gilbert's (1991) results who showed *in-vitro* that horizontal long range connectivity stimulation evoked a transient voltage-dependent (nonlinearly amplified) excitation probably mediated by AMPA like receptors interrupted/followed by disynaptic inhibition.

The observed global nonlinear suppressive effect, emphasized for the high contrast condition, can be compared to the classically reported surround suppression. Our results point out that a global averaged suppression, classically measured by studies using gratings and harmonic

analysis of the response, can occult a temporal transient facilitation followed by consecutive important suppression.

Classical phenomenological models of center-surround interaction consider that the receptive field can be modelled by two spatial Gaussian envelope input distributions, one excitatory and one inhibitory considered of larger width, either interacting linearly to form a modulatory pattern with a global shape reminiscent of a mexican hat (Sceniak & al, 1999, figure 3.3.9.1 A) or divisively (Cavanaugh & al, 2002, figure 3.3.9.1 B). The latest form of interaction is just a generalisation to the center-surround interaction of the standard model with divisive normalisation and represents the effect of a pool of unselective inhibitory cells recruited by the surround stimulation (Albrecht and Geisler 1991; Albrecht and Hamilton, 1982, Anzai et al. 1999; Carandini et al., 1997, 1999; Gardner et al., 1999, Heeger 1992, 1993, Sclar et al. 1990). This model accounts only for suppressive surround effects and for the contrast dependency of the center-surround interaction by playing on the gain of the inhibitory Gaussian component (figure 3.3.9.1 B).

Our results, showing transient surround facilitation even for high contrast imply that a more sophisticated center-surround model has to be considered. According to our results, the temporal profile of the center-surround nonlinearity is modulated by the contrast. Moreover the selectivity presented here originates from an anisotropy in space as well in time of the nonlinear receptive field. We propose, in addition to the spatial classical renormalisation model, center-surround interaction to involve also a balance between facilitation and suppression in space as well as in time, and that contrast play on this balance (figure 3.3.9.1 D). The resulting model consider center and surround part of the receptive as a single component E/I, function of space and time.

This new model can account for an average facilitatory surround interaction at low contrast, as exhibited by some of our recorded cells and as shown by Polat & al (1998). The resulting contrast response, attributable to the low contrast surround facilitation, presents the remarkable property to give rise to responses which are nearly contrast invariant (figure 3.3.9.1 D bottom). It has to be noticed that this model can account for the latency reduction observed in our study. Moreover, the finding of a directional selectivity of the center-surround interactions requires another supplementary modification of the standard model consisting in a spatial anisotropy (a spatial shift between the excitatory and inhibitory Gaussians). This proposal generalise to the non-linear RF kernels the excitatory/inhibitory push-pull model (Troyer & al, 1998) which is consistent with hebbian network self-organisation and accounts

for contrast invariance of orientation selectivity. It is also consistent, at the linear kernel level, with the spatial shift in position observed between the depolarizing excitatory and the inhibitory subthreshold receptive fields (Chavanne, 1998).

To account for both the linear (cf. for example chapter 3.3.3) and nonlinear center-surround effects we observed, we propose a complete model combining the two (Figure 3.3.9.1 D bottom model). To fully account all the properties of V1 cells for example the oriented gabor shape of the linear spiking RF, one has to consider not Gaussian but more specific spatiotemporal functions $f(x,y,t)$. Considering this functional generalisation, this model appears in the direct spirit of the general Volterra-Wiener kernels decomposition, and further underlines the involvement of both intracortical excitation and inhibition in the neurons responses properties. More generally, we propose that the spatiotemporal anisotropies of the E/I balance both at the linear and non-linear level (association field) to generate the output neuron's selectivity. Of course, one aim of such spatiotemporal E/I balance model is to try to be structurally as well as a phenomenologically relevant.



Figure 3.3.9.2: Classical phenomenological models of center-surround interaction (A & B) and a proposition of a generalised phenomenological and structural spatiotemporal model (C & D). Classical phenomenological models taken from the literature are presented in the top rows, and their implementations for low and high contrast are illustrated below. The resulting contrast gain function are depicted in the bottom rows (purple) and compared to the classical contrast function for the center-alone condition (black). A: The Difference of Gaussians (DoG) and B: the Ratio of Gaussians (RoG) models, proposed respectively by Sceniak et al (1999) and Cavanaugh et al (2002), consisting in a generalisation of the standard divisive normalisation model. In both cases, the model considers the excitatory Receptive Field and the suppressive surround-only as two overlapping Gaussians of different spatial extent and predict only suppressive effects by the surround at the level of the spiking response. Whereas the DoG model assumes that the center and surround mechanisms interact linearly, the RoG model posits that the influence of the surround is divisive and leads to a better fit of the contrast dependency of the center-surround interactions (Cavanaugh et al, 2002). The contrast modulates in both cases the suppressive Gain KS of the surround and thus the apparent extent of the MDF. C and D present our generalisation to the spatiotemporal domain, decomposed for illustrative purpose into spatial (C) and temporal (D) components. To account for the facilitatory effect of the surround observed, an excitatory function is ascribed to the surround. The resulting contrast dependency can be then described by a simple modulation of the Excitatory/Inhibitory balance as stressed by structurally realistic models (Stemmler, 1995, Somers & al, 1998). To account for the temporal modulation of the response by the center-surround interactions, notably the latency reduction (green arrow), this model is applied also in temporal domain with a phase delay (temporal anisotropy) of the inhibitory component. To explain both the linear and nonlinear observed effects of the surround stimulation, we propose a general linear-nonlinear spatiotemporal model, where each Excitatory and Inhibitory components can be considered as a specific function of X , Y , T , leading to a unified center and surround output selectivity genesis framework.

An advantage of this type of model is that it can account for quite complex spatiotemporal properties of the RF and considers center and surround as a single component. One definite disadvantage if such a model is that it is hard to be applied and fitted to empirical data (at least, probably impossible on the small data sets imposed by intracellular recordings).

Structurally realistic models of V1 including long range horizontal connections (Stemmler, 1995, Somers & al 1998, Series & al, 2002), have shown that the contrast dependency of center-surround interactions can be modelled by various mechanisms playing asymmetrically on excitation or inhibition, and thus modulating the E/I balance. Similarly, our result, in agreement with those models, further underline the temporal dimension of the E/I balance, as more deeply investigated more in depth in the next chapters.

Furthermore this observation of a temporally biphasic nonlinearity may explain partly the diversity of results concerning the suppressive or facilitatory nature of the center-surround interactions. Depending on the stimulation characteristics (static or dynamic such as drift or counter-phase), and the type of measure used to quantify the response (average integral over time or harmonic modulation, maximum amplitude) one can expect to find very different and even opposite conclusions.

On conclusion, nonlinearities in V1, notably center-surround, are dynamic, they have an intrinsic temporal profile; and this profile is sustained notably by the intra-cortical connectivity characteristics. We further want to stress the crucial importance of "time" in

cortical processing, a factor whose impact is too often neglected: cortical receptive fields, including the surround, are spatiotemporal functions or memories.

3.3.9.3. Active sensing and the hypothesis of a visuo-oculomotor computation in V1

One can ask legitimately when in natural viewing those high speed long range motion occur, or, in other terms, what kind of motion during natural viewing presents those peculiar spatiotemporal characteristics. Intuitively, natural environment present very rarely high speed motion. This intuition is further demonstrated by a spatio-temporal analysis of natural movies (Dong & Atick, 1995) showing that in the environment, motion is very rare and all the more rare so that the speed of the motion is high.

These spatiotemporal statistics arising from the natural environment do not include the additional “perturbations” or motion in the sensory input flow imposed by the subject motor behaviour. In fact, as a general rule, the subject own motion and behaviour increase and reshape drastically the environmental statistics. This is particularly true for visual signal, for which notably the eye-movements drastically reshape the temporal statistics of the optic flow, as shown in next chapter. Considering the organism own motion, the eye-movement in our particular case, the high speed long spatial range motion used in our experience to probe center-surround apparent motion selectivity find a natural and obvious correspondence with the saccadic component of the eye-movement. More fundamentally, in the sensory-motor dependencies lies the only information available for a system to define a “self”, and those sensory-motor dependencies are sufficient to infer the dimensionality of the environment (Philipona & al, 2002). The idea that perception and system knowledge are based on the sensory-motor dependency extraction and production (O'Regan & Noë, 2001) may take its roots, according to our intuition, to the relativity principle in physic.

First, saccades are highly frequent movement: they occur in average 3 times per second in Human (Harris, 1988) as well as in the Cat (Collewyn, 1977). Second, they are spatially long range (distribution mode 2° , distribution median 13° in the feely behaving cat, Collewyn, 1977, figure 3.3.9.3) and high speed, ranging from few degrees per second up to $800^\circ/\text{s}$. The apparent motion speed values used in our empirical investigation fall approximately in those temporal and spatial characteristics of saccades (see figure 3.3.2.1 and chapter 3.3.2), leading us to propose that the center-surround interactions observed should be expressed during saccades.

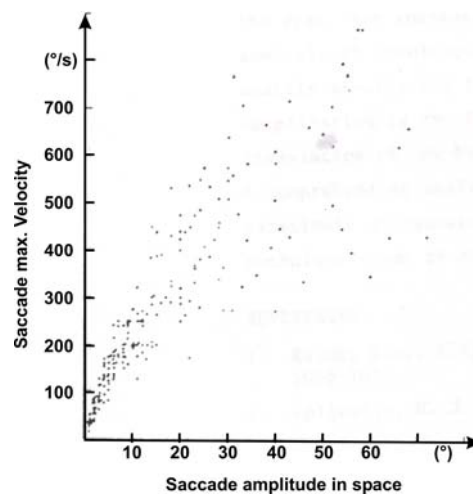


Figure 3.3.9.3 : Saccade velocity as a function of its spatial amplitude (redrawn from Collewyn, 1977). The graph represents 200 individual saccade measurements in the freely behaving cat. The measures take into account the head movement that classically accompanies the saccadic movement. Removing this head component gives slightly lower values Collewyn (1997).

It is classically considered that the information of the visual environment is blurred by the saccadic motion, due notably to the integration time of the retinal neurons, leading to the idea that no information about the environment can be gained from at the time of the saccade. The saccadic blurring is in reality a bit more complex, and may reveal much more information about the environment than previously expected. In fact, the motion blurring, which is also present for speeds lower than that reached during saccades and gives rise to the more general concept of motion streak effect (Geisler, 1999), only concerns the spatial frequencies which are not iso-oriented with the direction of the motion, as shown by Barlow & Olshausen (2004, figure 3.3.9.4). The faster the image motion is, the more selectively and precisely the spectrum of the iso-oriented components of the image will be extracted. We can thus propose that saccadic motions are selecting precisely some components of the visual information, those that are iso-oriented with the direction of the saccade, and erases all the other. This simple and low level observation may point to a more general conclusion on a possible role of eye-movements during perception: they reduce the dimensionality of the environment by extracting peculiar relevant features of the visual scene.

This automatic selection may be of important physiological and psychophysical relevance, since the ballistic trajectories of saccadic eye-movements have been shown to be highly correlated with orientated features in the visual scene. In humans, during active identifications of faces, Yarbus noted that the oculomotor search pattern and the positions of the fixation

anchor points formed the elementary skeleton of a perceptual sketch of the recognized object (Yarbus, 1967, figure 3.3.9.5 B).

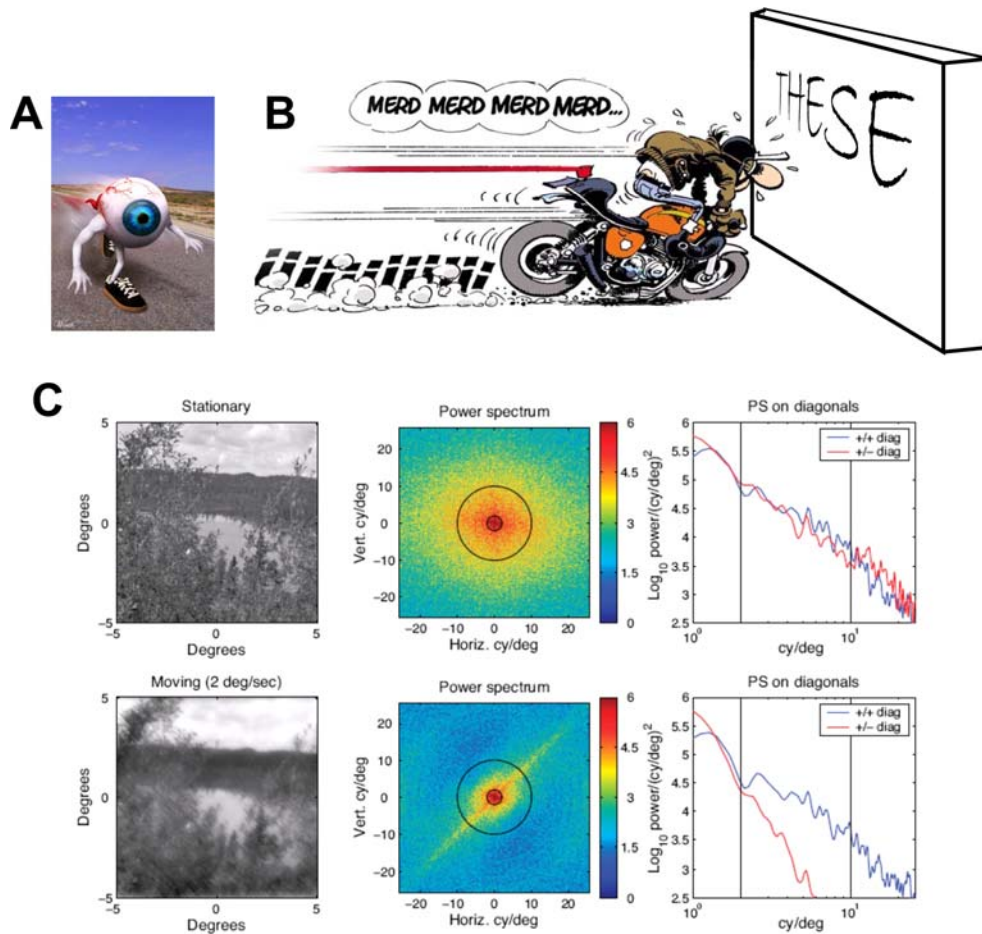


Figure 3.3.9.4: Saccades blur the visual image but streak the elements or contours presenting an orientation iso-oriented with the direction of the saccade. **A:** a rapid eye movement, probably saccadic given its following blurring. **B:** High speed motion streaks iso-oriented contours owing to temporal integration in the retina (Drawing from Christian Debarre, 2003). **C :** For moving images, the spatial power spectrum is distorted by becoming steeper in the directional axis corresponding to the modulation of the retinal flow in the direction of motion. “The influence of motion on the effective power spectrum and appearance of an image, assuming that the whole image subtends a visual angle of 10×10 degrees and moves diagonally down and to the left at 2 deg/sec. The top row shows the original static image, its 2-D spatial powerspectrum, and sections through this power spectrum along the two diagonals. The lower row shows the corresponding three figures for the moving image, obtained by attenuating the 2-D spatial Fourier Transform of the static image by factors derived from the contrast sensitivity measurements of Koenderink and van Doorn. The effect of motion on the power spectrum is brought out by the cross-sections (right pair of figures) along the diagonals in the direction of motion (red) and orthogonal to it (blue). Circles in the center pair and lines in the right-hand pair are drawn at 2 and 10 cy/deg to indicate the range where contrast sensitivity is high in the human visual system, and it will be seen that motion at 2 deg/sec severely attenuates spatial frequencies in the upper part of this range” (from Barlow & Olshausen, 2004).

The correlation of the saccadic path with the image contours suggests that the selective blurring is used as a strategy by the visual system to analyse and explore spatiotemporally the

environmental scene. During such exploration, one can imagine the center-surround effects demonstrated here as being of a primordial importance, as illustrated by the figure 3.3.9.5 C.

Moreover, the saccade induces a shrinkage of distances between stimuli, mostly in the direction corresponding to the saccadic path as well as an underestimation of temporal intervals between stimuli (Morrone & al, 1997, Kaiser & al, 2004, Morrone & al, 2005). In other words, the perception of time and distance during and around a saccade is compressed. It would not be a surprise for us if this compression was found to be related to the speed overestimation observed with apparent motion, and dependent on the orientation of the stimuli compared to the direction of the saccade.

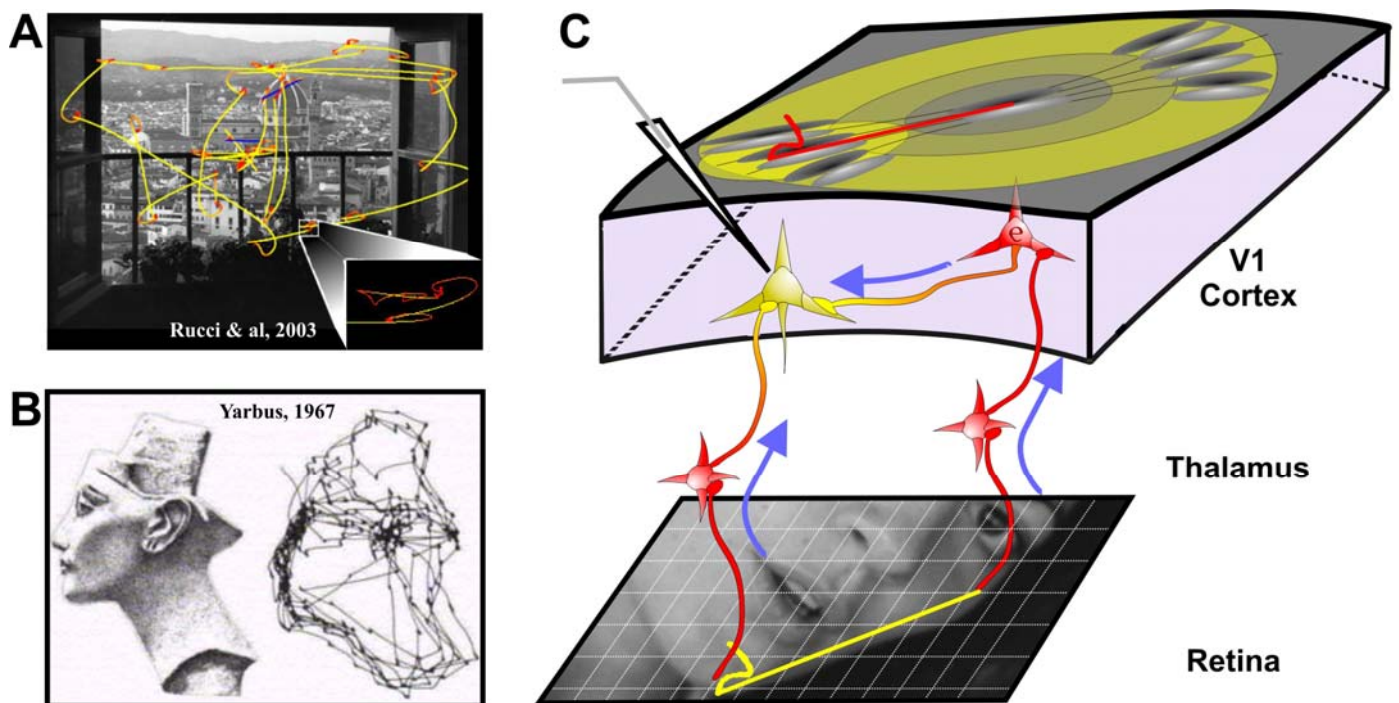


Figure 3.3.9.5: Active sensing in V1: the hypothesis of a visuo-oculomotor global and local sequential processing of the visual scene in V1. **A:** Eye-movement continuously explore the visual scene. The eye-movement scanpath of a monkey is superimposed with the corresponding scene (taken from Rucci & al, 2003), the speed of the eye motion is depicted using a colour code varying from red (for low speeds) to yellow (for high speeds) colour. The oculomotor pattern corresponds roughly to alternance between fixational drifts and saccades respectively. Eye blinks are symbolised by the blue lines and an enlargement of a fixational period is given in the bottom right insert. Note the systematic directional shift of the scan-path following a saccade and corresponding to the drift fixational movement. **B:** The eye-movement scan-path is correlated with the image features, notably the contours (for the saccadic path in this image exploration) and to higher order relevant features (for the saccadic target and fixation regions in this exploration). The cartoon, taken from Yarbus (1967), presents the exploration oculomotor pattern of a Human observer (right panel) and the corresponding photography of the object to be recognized (left panel). **C:** Schematic representation of the model of visuo-oculomotor processing in V1, sequentially integrating spatial long range and short range visual information. During saccadic high speed long range movement, V1 neurons integrate selectively the visual information iso-oriented to the saccadic motion along their collinear axis by the mean of their spatiotemporal association field (cf. figure 3.3.94), whereas during fixation they integrate the visual information on low spatial scales and low speed across the discharge field axis (corresponding to their classical direction selectivity).

A more detailed observation of the eye-movement paths may help to go a step further in the thought. Eyes never stop moving: even during the periods of fixation, a dynamic component in the visual flow remains due to the continuous scanning of the visual field with small involuntary stereotyped movements. Those fixational eye-movements can be decomposed in 3 different categories according to very different kinetic characteristics: drifts, tremor and microsaccades (Martinez-Conde & al, 2004 for review). Each of these movements have been shown to evoke response in the primary visual cortex, and have been proposed to sustain distinct and various functions (microsaccade, Martinez-Conde & al, 2002, and drift: snodderly & al, 2001, tremor: hennig & al, 2002). These movements are critical to maintain perception (Coppola & Purves, 1996, Martinez-Conde & al, 2006) and contribute for an important part to the power content of the temporal spectrum of the retinal flow.

Microsaccades present the same spatiotemporal characteristics as macrosaccades, and only differ by their non-voluntary origin, and their smaller average amplitude.

Tremors are extremely small aperiodic movements at high frequency 40-100 Hz (typically of an amplitude equal to the photoreceptors distance, and to visual hyperacuity resolution). Their function may be related to a fine grain spatiotemporal visual sampling.

Drifts are following temporally the saccade motion and are present during most of the fixation period (except during the rare microsaccades). They consist in a drift in space but also in the direction of the eye path, notably compared to the direction of the preceding saccade (figure 3.3.9.5 A and C). Drifts are of particular interest since their spatiotemporal characteristics make them very likely to activate the classical motion selectivity in V1. They are movement of small spatial amplitude ($1.21^\circ \pm 0.63^\circ$ in the cat (Olivier & al, 1993), to compare to the classical width of simple cell discharge zone: $1.1^\circ \pm 0.6^\circ$ (Palmer & Davis, 1981) or to the spatial scale (0.5°) of second-order directional interaction (Pack & al, 2006). The drift mean speed ($14.9^\circ/\text{s}$, according to Olivier & al, 1993) is within the range of the preferred speed of cortical cells (mean $2.2^\circ/\text{s}$ with responses up to $20^\circ/\text{s}$ for simple cell (as further shown in natural context of stimulation the speed selectivity of simple cell is increased) and $18.8^\circ/\text{s}$ for complex cell, Movshon, 1975). Drift speed fits also quite nicely with that deduced from the slant in the spatio-temporal receptive fields, meaning that such movement will activate cortical RFs mostly when executed across the width axis of cortical cells shall elicit approximately classical directional optimal response in V1.

The remarkable fit between the spatiotemporal characteristics of the two main eye-movement components, saccades (including microsaccades) and drifts, and the two main direction

selectivity mechanisms occurring in V1 (width axis and orientation preference axis), lead us to propose a simple visuo-oculomotor model of V1 cortical processing and function. According to this model, V1 operates a sequential and multiscale (local short range and global long range) analysis of the visual scene thanks to the convolution of environmental features with the eye-movement ballistics. In more classical terms, we propose that V1 implements a visuo-oculomotor representation and analysis of the environment.

Moreover, since the Superior Colliculus is one of the main V1 output target, and since microstimulation of V1 cells induce saccade that terminate in the RF location of the stimulated cell (Tehovnick & al, 2004, for review), V1 may be included in a first low-level sensory motor loop. As we will argue more in depth in the next chapter, this framework is intrinsically in agreement with the general idea that the cortical processing is adapted to the statistics of its extrinsic and recurrent inputs. According to the efficient coding hypothesis, RF functional properties and therefore connectivity in the network shall reflect the statistical bias in the visual input flow, which is strongly and predominantly sculptured by the eye-movements. From this point of view, it is not a surprise to find that the two most important motion selectivity mechanisms observed in V1 are related to the omnipresent eye-movement dynamics.

3.3.9.4. Center-surround interaction and cortical computation

Interpreting our result from a computational point of view, the center-surround spatiotemporal nonlinearity can be interpreted as specifically detecting and amplifying temporally precisely coincident center and surround “horizontal” inputs (figure 3.3.7.2). It allows the neuron to behave as a directional selective detector for high speed collinear motion and to thus reduce the redundancy or correlations in the optic flow, according to our hypothesis imposed by saccadic like movement. Such kind of nonlinearity or gain control is likely, in this interpretative framework, to give a first primary form of eye-movement invariance response as early as in V1. In agreement with the idea that redundancy reduction can account for visual response adaptation to eye-movements and removing, the thalamic model of efficient coding proposed by Dong (2004) reproduces saccadic-like suppression (without motor efferent signal) by triggering fast contrast adaptation.

Furthermore, the temporally biphasic profile of the apparent motion nonlinearity constrains temporally the spiking response by imposing a transient facilitation. This time-dependent nonlinearity modifies the timing of the responses, notably by reducing spiking latency and is

likely to improve the spike timing precision and sparseness of the discharge. These points will be further emphasized in the next chapters of the thesis.

3.4. Interlude: “What is the other 85% of V1 doing?” vs. “In praise of artifice”

This section aims at uncovering some basic ideas arising from the cortical physiology literature interpreted in the light of our previous results, and to further introduce the following chapters that will discuss the cortical code. We will notably argue in an intuitive way on how to define a function in “self”-organised biological systems, some cortical organisation principle such as specialisation and diversity already suggested by physiological results, and more generally about some trails that may allow a better understanding of cortical dynamic and function.

In their reasonable but pessimistic critic of the actual knowledge of V1 functioning, Olshausen & Field (“What is the other 85% of V1 doing?”, 2005), five main problems on the current view of V1 are identified:

- **Biased sampling of neuron:** only spontaneously active and visually responsive neuron are recorded by the experimentalist. This bias does not hold for intracellular recordings and blind impalement techniques, and, from our experience, not highly relevant for V1 neurons: the only visually non-responsive neurons we recorded were correlated with EEG deeply synchronized, and with bistable unflappable intracellular membrane potential dynamics, pointing out the cortical state irrelevancy to visual computation. At least, a selection of visually responsive neurons would only bias toward responses perceptually relevant states (a non visual cell in V1 is a glia, in fact, and even glia present Vm responses).

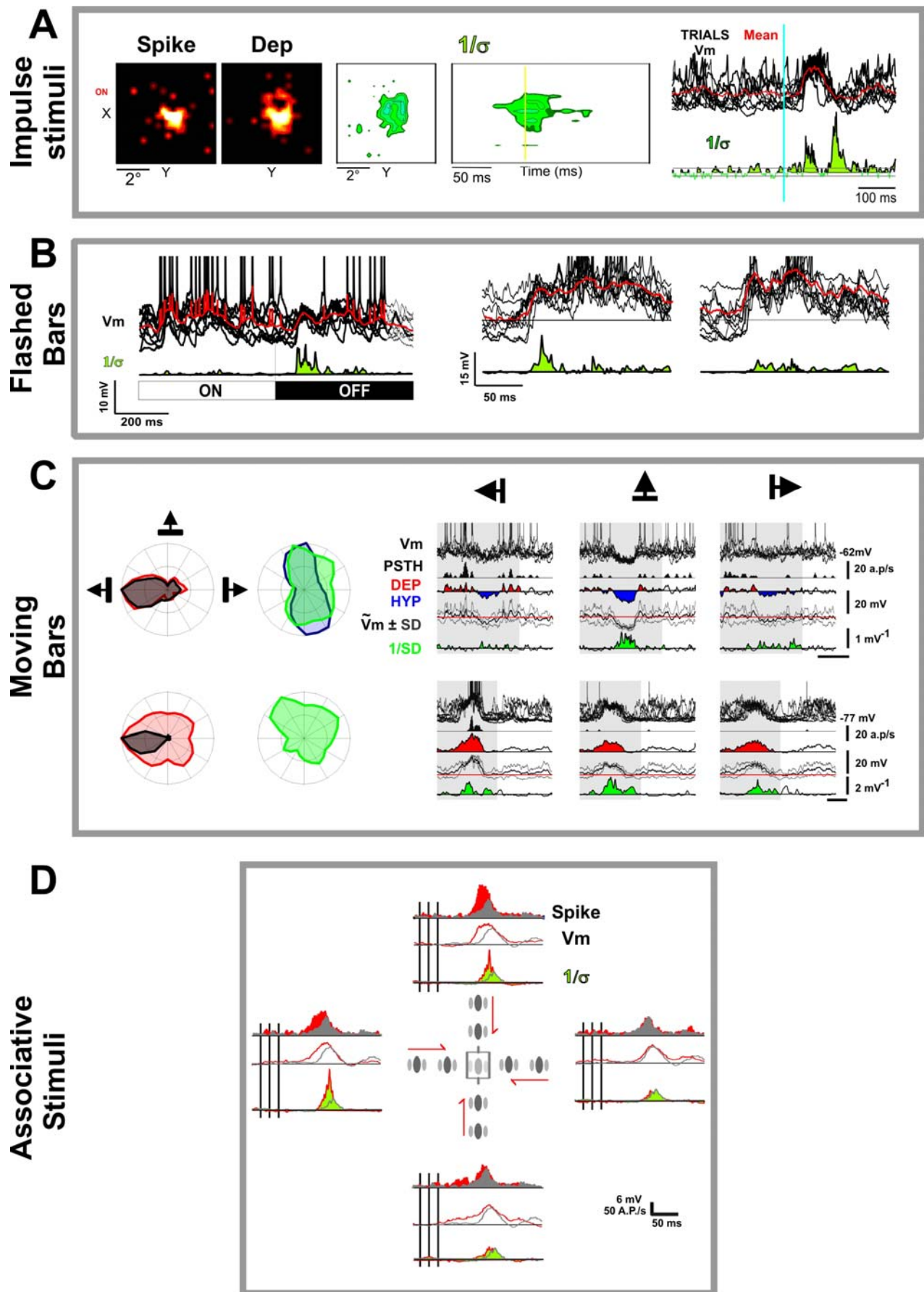
- **Biased stimuli:** most of the studies concerning V1 have been assessed using oversimplified and ecologically non-relevant stimuli such as sinusoidal luminance grating, that may fall outside the selectivity range of cortical nonlinear mechanisms. In fact, considering that the cortical system can be intrinsically nonlinear renders its investigation extremely difficult given the explosive number of combinatory to test. This point is still debated. As a response, Rust & Movshon (“in praise of artifice”, 2005), defending a much more optimistic point of view and a new sophisticated version of the standard model containing an undefined number of linear boxes rectified by nothing but 6 nonlinearities (Rust & al, 2005), claim that important part of V1 mechanisms has already been uncovered and that artificial stimuli is a

necessary simplification step toward functional investigation. A crucial outcome of such a debate resides in the capacity of V1 models not only to account for average selectivity or gain function but also and mainly in their capacity to predict precisely the real recorded responses (Bialek & al, 1991, Rieke & al, 1997). Unfortunately, the new standard model has not been tested against this real response prediction benchmark, and furthermore against responses recorded in responses to a natural stimulus.

- The 3 next criticisms are directly linked to the latest. **Biased theories:** The authors argue about the irrelevance of simple and complex segregation and the purely Fourier view of the cortical function. **Contextual dependency of the responses:** this point is intrinsically included in the dimensionality and nonlinearity of the neuronal function. **Ecological deviance:** the author argue about the interest of not only the models successes but also and equally of the models failures.

Here, we will preliminary propose, a supplementary bias, that may account and allow to quantify all the previous ones: the response variability. As shown in introduction, cortical responses variability, notably in V1, is considered to be huge. This noise account for about 50% of the response and is either considered as an irreducible and computationally noxious component, or as reflecting “States of Mind” expressing the brain's autonomous internal context (Arieli, 2003, Fiser & al, 2004). One has to include and/or add to the 85% of the unknown V1 emphasized by Olshausen & Field, a minimum of 50% of noise.

Figure 3.4.1: Visual stimulation decreases the trial-to-trial stimulus-locked variability in the Vm responses trajectory for all type of tested stimulus (impulse stimuli, oriented flashed bars, oriented moving bars, and apparent motion center-surround associative stimuli). **A:** spiking MDF and depolarising Field maps (left) compared to the $1/\sigma$ map (right) obtained for one cell in response to impulse stimuli. Note the large spatial extent of the significant $1/\sigma$ map. The superposition of ten individual Vm trial responses (black) to the ON stimulation of a predetermined pixel in the X-Y map and the temporal profiles of the average depolarization (red) and of the corresponding reduction in stimulus-locked variability ($1/\sigma$) are presented in the right panel. **B:** Two examples, for two different cells, of ON and OFF responses to an optimally oriented bar. The trials Vm responses (black), their average (red) and $1/\sigma$ waveforms (green) are presented. **C:** The decrease of variability observed during responses to oriented moving bars, for two example cells (cells 2 and 4 of figure 3.2.1) illustrated in each row. Polar tuning curves of the spiking, depolarising, hyperpolarising and $1/\sigma$ components are presented on the left, and their respective waveforms on the right. These waveforms correspond to responses to preferred (left), cross-oriented (middle) and non-preferred direction (right) are illustrated with the same conventions as in figure 3.2.1. **D:** A cell example of Vm variability decrease in response to center to surround apparent motion stimuli (red colour, cf. chapter 3.3) and in response to the center alone control (grey colour). PSTHs (top panels), PSTWs (middle panels) and $1/\sigma$ waveforms (bottom panels, green colour) are presented for the four cardinal axis of centripetal stimulation.



One striking result, which has been previously presented, lies in the increase of trial-to-trial reliability of the Vm trajectory evoked by visual stimulation. It is quantified by the measure of the inverse of the standard deviation of the Vm trial-to-trial trajectory. This effect, that we have preliminary observed for oriented flashed bars stimulus, and quantified in the oriented moving bar study of chapter 3.2 (Monier et al, 2003), can be generalised to the whole set of visual stimulation we've been testing as illustrated in figure 3.4.1. This variability decrease is present for a broad range of tested stimuli condition (where the experimenter varies its position, orientation, apparent motion axis), proving a general low selectivity of the effect. Moreover, in most of the cases, this variability decrease is predominantly observed for the conditions outside of the range of the output selectivity. This relation holds in the temporal domain: decreases of variability are observed before and/or after the bulk of the spiking response. This out-of-phase relationship between spiking responses and variability decrease corresponds to the well known correlation between the Vm variability and the discharge rate output for low dimensional stimuli (Carandini, 2004).

Those results show that the variability decrease of Vm trajectories can be observed either during depolarising or hyperpolarising periods, and even in some cases without any net effect on the average amplitude of the Vm compared to spontaneous activity (cell 5 figure 3.2.1, cell 11 figure 3.2.4), is signaling the presence of input. In conclusion, the observation of variability decrease probes the presence of inputs arising from a very broad range of selectivity domains. These inputs arising from large and even very distant domains of selectivity are likely to sustain the cortical computation, and more complex and nonlinear process than classically admitted.

A second general remark can be drawn from our previous results: inhibition is generally correlated with the Vm trial-to-trial variability decrease, and the relative balance between excitation and inhibition is controlling the spiking cell response expression and thus selectivity, both in the spatial and temporal domains.

We could also generalise the observation of the correlation between inhibition and trial-to-trial variability decrease for all the range of stimulus type we used (figure 3.4.2). Part of this correlation is likely to emerge from a simple cellular shunting effect. The visually induced increase of inhibitory conductances, (Borg-graham & al, 1998), but also excitatory conductances, decrease the impact on the voltage of the synaptic inputs leading to a more or less strong clamp of the membrane potential, and thus may reduce the amplitudes of the trial-to-trial fluctuations as well as the amplitude of the averaged responses. A paper, reviewing the

importance of shunting inhibition in cortical processing notably in the orientation and direction V1 selectivities, is presented in annex (Fregnac & al, 2004).

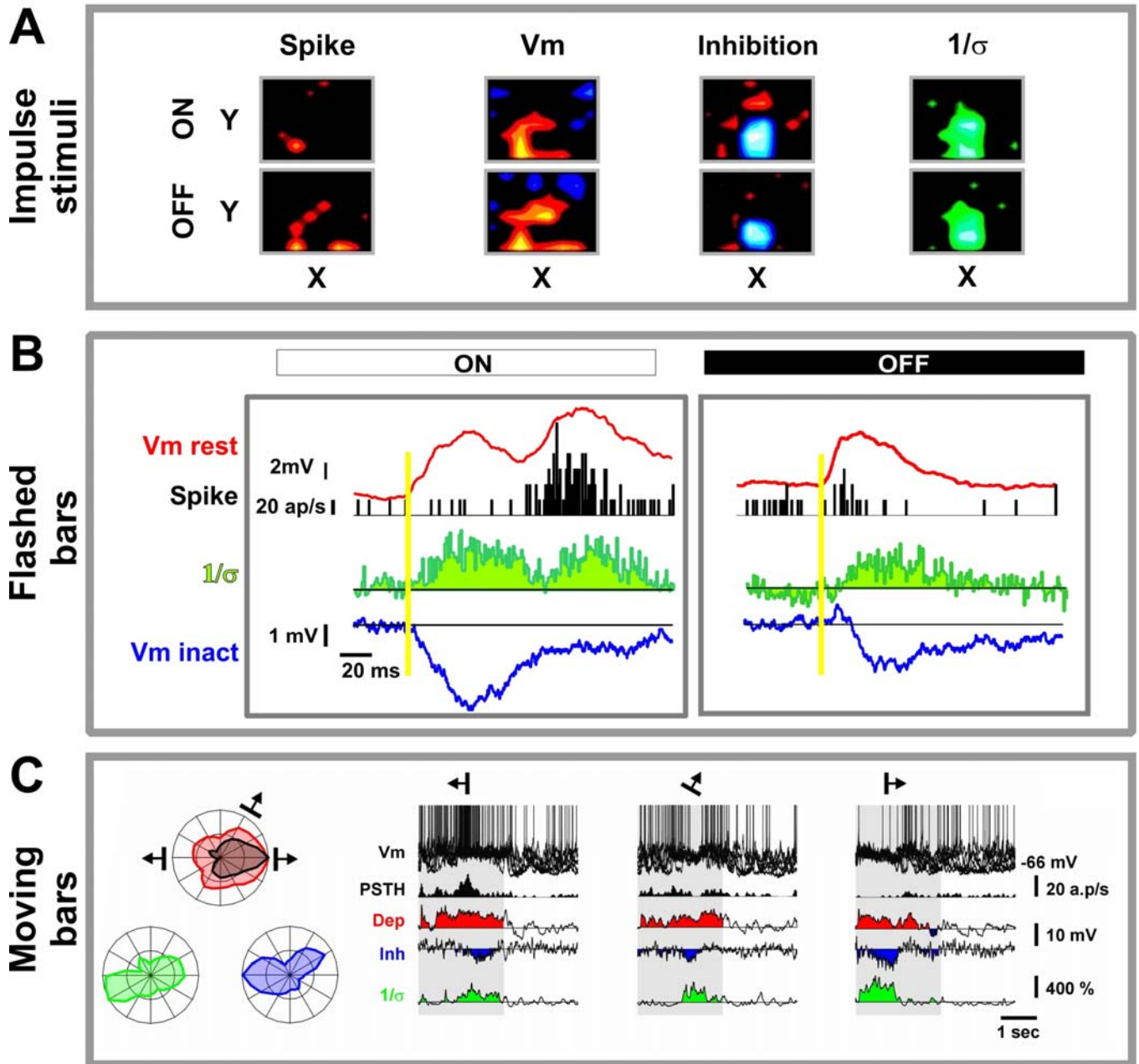


Figure 3.4.2: The decrease of the trial-to-trial variability in the Vm responses trajectory is correlated with the increase of the inhibition for most of the tested stimulus (impulse stimuli, oriented flashed bars, oriented moving bars). **A:** from left to right: spiking MDF, depolarising Field (both measured at rest), inhibitory field obtained during current-induced spike inactivation protocol and $1/\sigma$ map (measured at rest) obtained in the same cell in response to impulse stimuli. Note the spatial overlap between the extent of the significant $1/\sigma$ map and the extent of the “inhibitory” field. **B:** ON and OFF responses to an optimally oriented flashed bar. The trials Vm responses (black), their average (red), the Vm average waveforms in the current-induced spike-inactivated condition revealing inhibitory input (blue) and $1/\sigma$ waveforms (green) are presented for one cell. Note the mirror profile and same time course for the blue and green signals. **C:** Example of correlation between the decrease of stimulus-locked variability and the increase of inhibition evoked by oriented moving bars (cell 9 of figure 3.2.3). Tuning curves of the spiking, depolarising, inhibitory and $1/\sigma$ components are presented on the left, and their corresponding waveforms responses on the right with the same convention as in figure 3.2.3.

A third remark concerns the functional diversity of excitatory and inhibitory input across cells. In chapter 3.2, we have shown using simple low dimensional stimuli that the broad functional diversity of excitatory and inhibitory inputs can lead to similar spiking output selectivity such as orientation and direction. As an introduction to the following chapters, we now ask whether this functional diversity of inputs could support a diversity of output spiking selectivity in the context of more complex and informative stimuli than the elementary one previously and classically used.

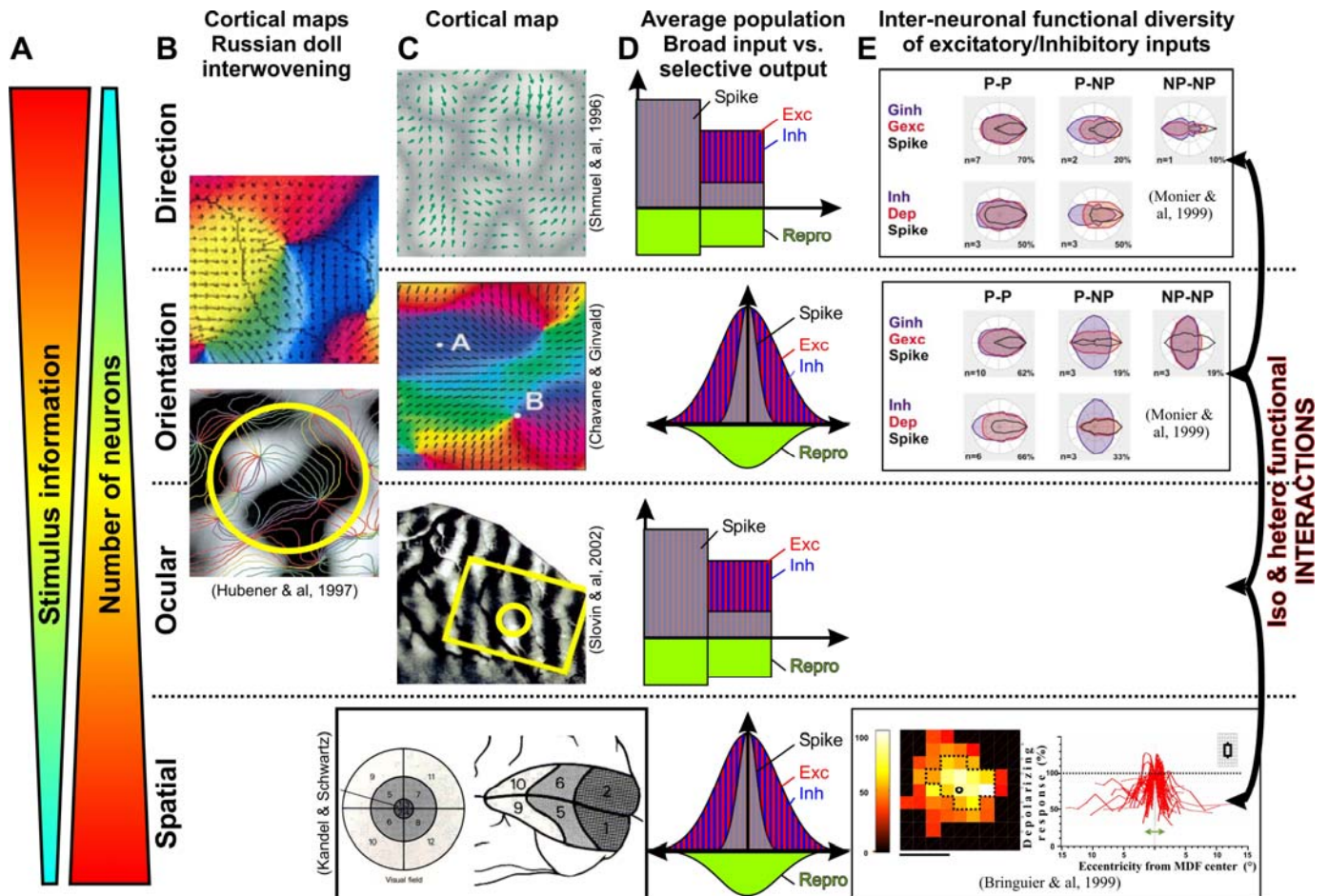


Figure 3.4.3: Proposition of a principle of apparent functional diversification and specialisation in V1 with stimulus complexification **A:** the two opposite axis proposed to explain physiological results and cortical maps organisation: the number of neurons implied in the cortical representation is inversely proportional to the "information content" (or dimension/complexity) of the stimulus. **B:** The functional cortical maps Russian doll organisation : a spatial position is represented for the two eyes, all orientations are represented for each eye, the two directions are represented for each orientation. **C:** the various functional cortical maps observed by optical imaging in V1: from bottom to top: spatial retinotopic maps, ocular dominance bands, orientation and direction maps. **D:** Schematic illustration of the average broad synaptic input selectivity vs. the sharp spiking output selectivity of V1 neurons for the various classical selectivity dimensions. The respective tuning of the synaptic excitatory and inhibitory inputs and spiking output deduced from our results or extrapolated in the case of ocular dominance selectivity. The abscissa represent the whole possible range of the explored dimension (space, orientation, etc...) and the ordinate represents the mean amplitudes of excitatory, inhibitory and spiking responses averaged across cells, occulting the inter-neuronal diversity of E-I selectivity combinations presented in **E** (cf. chapter 3.1 & 3.2).

The physiological literature already provides some trails of answers to this question. First, in agreement with the “efficient coding” hypothesis, the stimulation of the “non-classical” RF surround with natural complex stimuli tends to increase the decorrelation between neurons when compared to the condition where the same stimuli are restricted to the classical RF center (Vinje & Gallant, 2001). Second, the relative organisation of the various cortical functional maps, visualized notably by optical imaging techniques, presents an obvious Russian doll interwoven structure, revealing a hierarchical increase in specialisation as a function of the stimulus complexity (cf. figure 3.4.3, complexity will be further defined).

For simplicity we will not take into account the “time” dimension in the following intuitive reasoning. Starting with the simplest minimal spatial information (x,y), the V1 cortical map presents the well known retinotopic organisation: two neighbouring neurons respond for neighbouring visual regions. The spatial information can stem from the two eyes and specifying from which eye stem the visual information segregates the cortical representation into 2 distinct territories: the ocular bands: for each spatial position the two eye information is represented (figure 3.4.3 B & C). The orientation bias of the spatial information (and of the stimulus) can be specified, which in turn segregates each ocular band into orientation domains structured around pinwheels (Hubener & al, 1997): for each spatial position and each eye, all the orientations are represented (figure 3.4.3 B). Considering dynamic stimuli (and all stimuli are dynamic thanks to eye-movements) the direction of the oriented motion (and of the stimulus) can be specified, segregating “orientation domains” in two directional domains (Schmuel & al, 1996): the two directions of motion are represented for all orientations, for both eyes for each spatial position (figure 3.4.3 B). From this point of view the Russian doll functional organisation appear a bit trivial and this functional structure seems in some way to be imposed by the dimensionality of the explorative stimuli applied by the experimenter.

Informally speaking, increasing the “information” present in the stimulus (we will further define more rigorously this information in term of redundancy), decreases the size of the responding cortical territory, and thus the number of activated cells (figure 3.4.3 A): In other very intuitive word; the more information the stimulus offers, the more selective the cortical response is, and the more specialised cortical territories appear. Of course, an interesting question would be to determine if any functional subterritories exist under the direction selectivity level.

These functional territories observed in optical imaging, even the smallest ones dedicated to directional selectivity, reflect the activity averaging of thousands of neurons. One important question is then to wonder if these neurons have all the same activity, function and relay the same information. It is known that neighbouring neurons can display various and even opposite spatial phases (DeAngelis & al, 1999). Reich & al (2001) assessed the question more precisely, and showed that pooling the responses of small population of neighbouring neurons leads to an important decrease of the information available when compared to the information carried by neurons individually.

Our results shows two important principles potentially supporting a diversity and a further specialisation of function:

- On average, the excitatory and inhibitory inputs are coming from a broad range of functional domains (space, orientation, direction etc...figure 3.4.3 D)
- The organisation of those excitation and inhibition functional selectivity appears specific for each cell, offering the substrate for a diversity of higher-order associative computations combining those various domain of selectivity (figure 3.4.3 E). Indeed, using more complex stimuli combining various dimensions of the input, physiological studies have probed various interactions occurring in V1. The apparent motion center-surround interactions presented in the latest chapter is one example (spatial – orientation). Interactions between spatial and ocular information from which depth analysis arises, between orientations and ocular information, between direction (motion) and ocular information (depth) (Anzai & al, 2001), among others, have also been demonstrated. Since simple low dimensional stimulations evoke transient decrease of stimulus-locked variability in Vm trajectories for a broad range of conditions, one can also wonder what would be the variability of V1 responses to complex dynamic stimuli like those experienced during natural sensory-motor experience, presumably implicating additional interaction constraints as mentioned above.

3.5. Nature is the Code: reliable and efficient dissipation in V1

(to be Submitted, Baudot, P., Marre, O., Levy, M. and Frégnac, Y.)

‘If the eye were not sun-like, the sun’s light it would not see.’ Plotin, Goethe.

Summary: The specificity of sensory network organization in living systems, achieved through evolution, development and short-term plasticity, can be viewed as an ultimate form of memory collection resulting from the adaptation to different scales of the environmental statistics. According to the metaphor of a global “fit between mind and world” (James, 1890), our sensory neural systems can be thought of as encoding a highly compressed version of the informational content of our natural environment. Here we show that the reliability of the neural code in adult primary visual cortex (V1) reflects in a mirror way the complexity and natural relevancy of the sensory input statistics.

Using intracellular recordings in the anaesthetized mammal, we find that the activity evoked in V1 during exposure to natural scenes continuously updated by eye-movements, displays highly reproducible dynamical states at the subthreshold membrane potential (V_m) level and a temporal impulsional code at the spiking output level. In contrast, responses to simple artificial stimuli (“optimal” gratings) are highly unreliable, which supports the prevalence of rate coding for low-dimension or unknown stimuli. In natural-like conditions, the contrast between the temporally dense informative synaptic input and the sparse spiking output shows that cortical computation removes input redundancies by detecting transient precisely coactive assemblies.

Introducing a statistical definition of complexity and ordered redundancies, we show that both noise and redundancy reduction observed in natural-like conditions are a direct consequence of the principle of mutual-information maximisation, suggesting a general framework for environmental adaptation. This modulation of the code by the relevancy of both the transient and global inputs statistics, expressed as a balance between externally imposed states and internal ongoing states, may correspond to the well known self-generative property of recurrent networks. From the computational point of view, the irreversible dissipation of the input constraints operated by the cortex is interpreted as the entropic cost to pay for observing and engraving (or forgetting) the information present in the environment.

3.5.1. Computational principles in visual processing

Following the original impulse given by Attneave (1954) and Barlow (1961), the reduction of redundancy in the evoked neural activity pattern, also referred as sparsening, has been proposed as a computational principle in sensory processing (Atick & Redlich, 1992, Atick 1992, Redlich, 1993, Olshausen & Field, 1996). Maximization of mutual information between sensory input and the response of a single neuron (Laughlin, 1981, Brenner & al, 2000) or of a perceptron network (Linsker, 1988) was demonstrated to be equivalent respectively to an adaptative process and to a Hebbian self-organizing principle which also results in a general decrease in response redundancy (Nadal & Parga, 1994, Bell & Sejnowski 1995, 1996). The adaptative processing of neural network, has been proposed to rely on a cascade of multiple temporal scale mechanisms (Fairhall & al, 2001, Fusi & al, 2005). Because of the reduction of the informational capacity of the visual channel from the retina to the thalamus, redundancy reduction appears necessary to preserve visual information, a prediction which has been confirmed experimentally (Dan & al 1996). At the cortical level, the concomitant stimulation of the receptive-field (RF) surround has been shown to increase the sparseness and efficiency of the code (Vinje & Gallant, 2000, 2002). However, the final impact on information representation in V1 remains yet to be understood, in view of the massive increase in the number of cortical neurons ($161n^{3/2}$ in primate (Stevens, 2001)) when compared to that of thalamic input fibers. The prevailing view posits that the resulting gain in informational capacity allows averaging activity across large neuronal assemblies and the redundancy imposed by the overcompleteness gives to the cortical network some form of invariance relative to noise (Barlow, 2001, Doi & Lewicki 2004). Consistently with this theoretical schema, a high variability in evoked firing has been reported in primary visual cortical neurons, corresponding to a Poissonian or supra-Poissonian behaviour (variance \geq mean) independently of the stimulus characteristics (Schiller & al, 1976, Heggelund & al, 1978, Arieli & al, 1996, Wiener & al, 2001, Britten & al, 1993, Buracas & al, 1998). This noisy behaviour appears as a computational nuisance since information has to be integrated over time and averaged across highly redundant population of neurons with broad selectivity tuning (Georgopoulos 1994, Series & al, 2004), which implies a rate based code (Shalden & Newsome, 1998). Since the transfer function of neurons in-vitro is highly reliable under realistic current somatic injection (Mainen & Sejnowski 1995, Nowak & al, 1995), the origin of visual response variability has to be found in the cortical recurrence (or “shared” Noise (Deweese & Zador, 2004)). Recent electrophysiological and imaging studies have shown that

the spontaneous activity observed just prior to the stimulus can predict to a large extent the response variability, leading to an additive model of Signal and Noise (Arieli & al, 1996, Azouz & Gray, 1999) where evoked responses are linearly corrupted by spontaneous cortical ongoing states. This global internal Noise pattern is spatially and temporally organised into coherent activity waves spreading across the entire V1 (Tsodyks & al, 1999, Kenet & al, 2003).

3.5.2. A change in perspective: from information transfer to computation of complexity

This study, considering cortex and environment as complex dynamical systems, investigate the cortical processing as a diffusion process, by the estimation of the propagation and dissipation of the input fluctuations in the nervous system media. The working hypothesis of the present paper is that the code operating in V1 is in fact dynamically regulated by the ever changing input statistics, and that visual response reliability or noise, should be studied not only with elementary visual stimuli, as done most classically, but with ecologically relevant features. Indeed, the complexity of our natural visual world, and moreover of living systems, resides in its “aperiodic crystal” structure (Schrodinger, 1944), that makes it lie between “crystal”-like order and “smoke”-like disorder (Atlan, 1979) and which can be considered as a consequence of their global far from equilibrium state. This particularity, neither reflected in Algorithmic nor Shannonian information that quantifies randomness and uncertainty, is referred to as structural complexity, physical complexity (Adami & Cerf, 2000) sophistication (Atlan, 1979, Atlan & Koppel, 1990) or logical depth (Bennet 1985, 1988, cf. chapter 3.5.12.3).

In order to explore experimentally the contextual input-dependency of the neural code, we opted for intracellular recordings in the primary visual cortex in the anaesthetized cat and compared in the same cell the response reliability for different visual stimulation conditions. The interest of intracellular techniques is to give access not only to the spike output activity but also to the network-driven dynamics (monitored by the continuous fluctuations of the membrane potential, V_m) and the synchrony state of the effective functional assemblies in which the recorded cell is embedded (Bringuier & al, 1999, Monier & al, 2003). We took also advantage of the blockade of eye-movements in the paralysed preparation to externally impose reproducible changes in the retinal flow through a sequence of eye-movement simulation composed of virtual saccades, micro-saccades, drifts and tremor (cf.

supplementary information chapter 3.5.8). The resulting retinal image animation thus mimics in a realistic way the visual effect of natural eye-movement scanpaths recorded in the freely behaving animal (Collewijn, 1977 in cat; see also Rucci et al, 2003 in humans). For each recorded cell, we tailored a library of four visual stimuli of increasing informational complexity, consisting in the full field presentation, at a high screen refreshing rate (150Hz), of the following 10s movie clips: 1) a drifting grating (a point in the Fourier space) of optimal orientation direction spatial and temporal frequency, 2) the same optimized grating animated by a modeled eye-movement sequence, 3) a natural image animated by the same eye-movement virtual path, 4) a binary dense white noise (high rate high definition) corresponding to the highest complexity condition.

Global statistical cues of this structural complexity are given by scale invariance or $1/f$ spectrum property, already probed for natural scenes (Field, 1987, Ruderman & Bialek, 1994). In natural viewing conditions, eye-movements continuously reshape the spatiotemporal statistics falling on the retina and the temporal luminance profile feeding one pixel of the retina displays a $1/f$ spectrum (cf. supplementary information chapter 3.5.8), intermediate between the spectra of a drifting grating at a fixed temporal frequency (one peak spectrum) and of dense noise (flat). Moreover, most of the structural complexity of the visual input, relevant for perception, resides in the higher order statistics (or phase spectrum, Bell & Sejnowski, 1996) when considered globally, and in the spatial and temporal fluctuations or statistical non-stationarities of the signal when considered locally. At the time scale of a visual percept, the convolution of eye-movements dynamics with natural scenes imposes some more non-stationary to the input, i.e. a continuous update in the input autocorrelation function (cf. supplementary information chapter 3.5.8).

In order to detect local transient correlations and the possible phase locking of response fluctuations between individual trials (reliability), a time-frequency wavelet analysis was applied to both the recorded Vm and spike trains. The resulting filtering through an array of complex Gabor wavelets ranging from 1 to 75 Hz provides a time-frequency-dependent measure of signal, noise and Signal-to-Noise Ratio (SNR, cf. supplementary information chapter 3.5.9). This time-frequency measure can be understood as the best local temporal multi-scale estimation of SNR, reflecting the mutual information between stimulus and response. When applied to spike train, SNR can also be considered as an extension of the measure of the temporal precision of spikes (Mainen & Sejnowski, 1995) at any precision scale (1-75 Hz roughly corresponds here to a temporal scale ranging from 6.6 to 500 ms) and

reflects both the absolute spike timing precision and the spike probability across trials. This frequency-time representation best illustrates the contrast (exemplified in Figure 3.5.1 and the top left panel in Figure 3.5.2) between a classical “rate code”, whose SNR energy is found restricted to the low frequency domain, and a precise “spike timing code” where SNR remains highly significant in the high frequency band (hence the red peaks in the frequency-time plots shown in Figures 1 and 2).

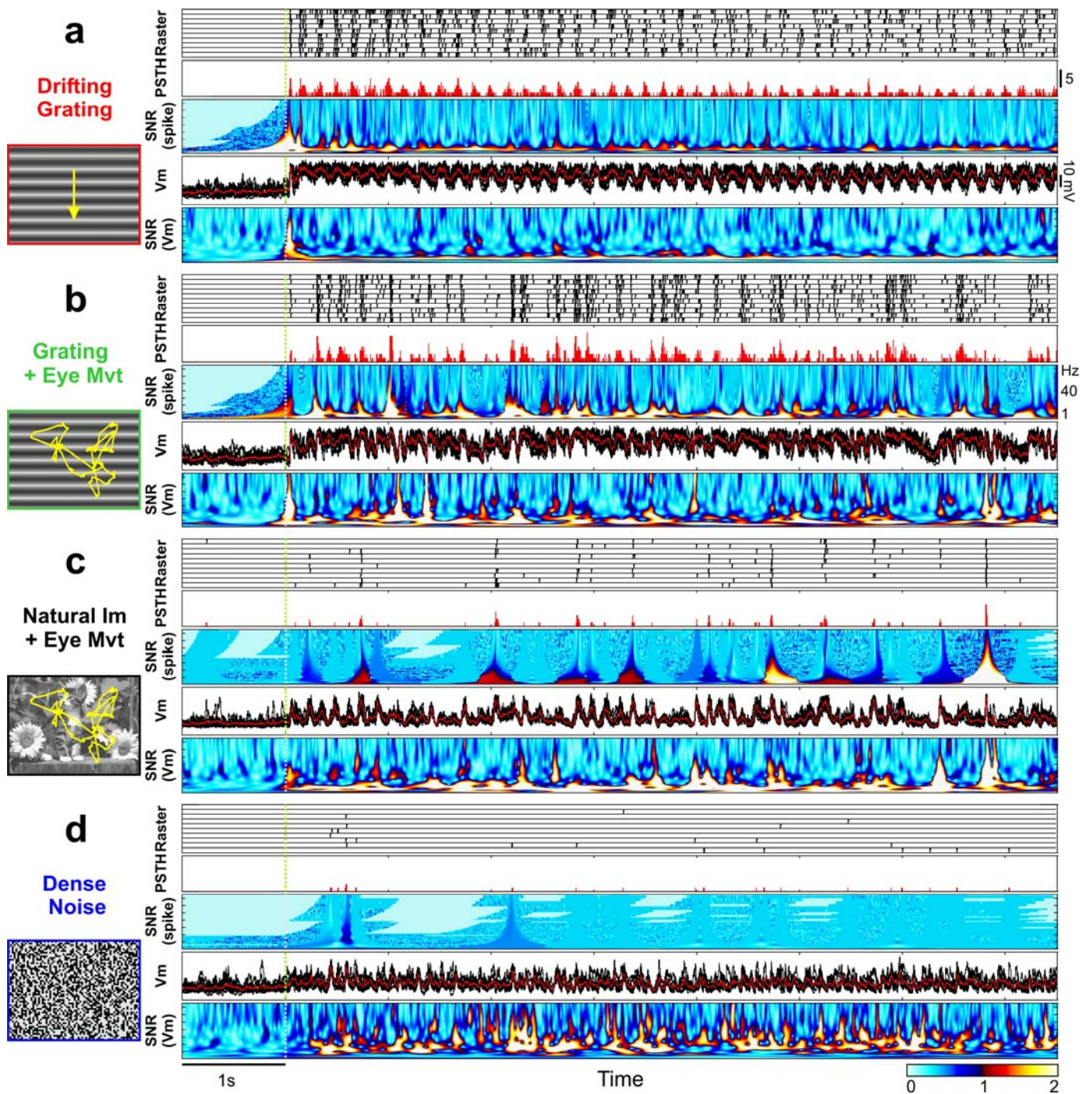


Figure 3.5.1: Reliability and dynamic of the evoked Spiking and Vm responses as a function of visual input complexity. Responses of a Simple cell to 4 types of full screen stimulus animations: **a**, optimal sinusoidal luminance grating, drifting at 6 Hz; **b**, same grating animated by saccadic and fixational eye-movements; **c**, natural image animated by the same sequence of eye-movements; **d**, dense binary white noise. Panels represent 1 second of spontaneous activity followed by 7.5 seconds of evoked activity of (from top to bottom): i) raster of trials spike patterns ii) Post Stimulus Time Histogram (PSTH, 3 ms bin width, red); iii) time-frequency Signal to Noise Ratio (SNR) of the spiking responses (between 1 and 75 Hz); iv) superimposed trials (black) and average (red) Vm trajectories after spike removal; v) time-frequency SNR of the Vm responses.

3.5.3. Constrained dynamics in V1: low noise and temporal binary code

Twenty-two cells were submitted to the four sets of stimulus conditions. Twelve of them, recorded long enough to apply the complete series of protocols, were used for the comparative quantitative analysis presented below. The dynamics observed either in the input membrane potential trajectory or the output spike train in response to the four classes of stimuli are illustrated in Figure 3.5.1 in the case of a Simple cell ($F1/F0=1.26$) and are representative of the mean behaviour observed at the population level (see additional illustrations of Signal, Noise and SNR in eight other cells, ranging from Simple to Complex, in supplementary information chapter 3.5.13 (in attached PDF file)). The first result of our study (seen on all 22 cells) is the repeated observation that response reproducibility across trials increased as the input statistics became closer to natural conditions of viewing. In the « natural-like » condition, spiking responses displayed a sparse precise spike timing code, allowing for most trials the replication of single spikes or sometime doublet or triplet unitary pattern events, which occurred at fixed dates during the time course of the movie. A second general observation in our data is that the more « natural-like » the input statistics became, the more transient the postsynaptic events were and the more temporally irregular the Vm dynamic regime was.

spectrum is obtained by integrating SNR values for each frequency channel over the whole movie duration and averaging the individual power spectra across cells (right panel in Figure 3.5.2). The temporal frequency domain where the contextual input dependency was found to be the most striking lies in the beta/gamma range. The average spike-based SNR power measured for the « natural scene » condition, in spite of the strong dilution of the measure by the sparsening of the discharge, still presents a significant increase in the 10-30 Hz band when compared to the « drifting grating » condition. This increase extends, both for EcoG and for Vm dynamics, to all the upper range of investigated frequencies (10-75 Hz), i.e. well beyond the classical high cut-off frequency of the temporal frequency tuning (around 20 Hz). As a general rule, SNRs of Vm and spiking activity (upper panel in Figure 3.5.2), as well as for EcoG (bottom panel), are found maximal for the stimuli animated with the rich temporal dynamics of eye-movements (« natural scene » and « grating with eye-movements » conditions). The key effect, most apparent when one switches from the « grating » to the « natural scene » condition is that the increase in the Signal power component is accompanied by a concomitant decrease in the Noise component (cf. supplementary information chapter 3.5.10). For natural-like environments, the trajectory of the membrane potential of single neurons become clamped across trials and varies in time in an almost deterministic way for several hundred of ms, even for periods when the cell is not spiking (see example in Figure 3.5.2). A straightforward quantification, obtained by integrating the Noise power spectrum between 1 and 75 Hz, gives a divisive ratio of 4.1 ± 3.6 for spike train and 1.9 ± 1.2 for Vm, when comparing both conditions.

In the « dense noise » condition, although responses display reliable subthreshold dynamics notably in the high frequency range, a high probability of spike failure observed across trials results in some cells in the almost complete suppression of spike activity and thus in an unreliable behaviour. The most likely interpretation is that « dense noise » does not produce enough synergic excitatory correlation to drive the network, and/or triggers dominant suppressive shunting effects between excitation and inhibition. This observation supports the hypothesis of a cortical filtering mechanism removing uncorrelated noise and preventing its accumulation across serial or recurrent processing stages (Deweese & Zador, 2004).

From this descriptive analysis we reach already two conclusions: 1) V1 network processes and encodes visual information across a wider temporal bandwidth than classically admitted. 2) Furthermore, our data show that Noise is not an independent additive neither a multiplicative component to the Signal. Rather, SNR appears to be modulated both transiently

over time and on average by the global input statistics: at the Vm level, the closer the input statistics to natural ones, the larger the Signal and the lower the Noise.

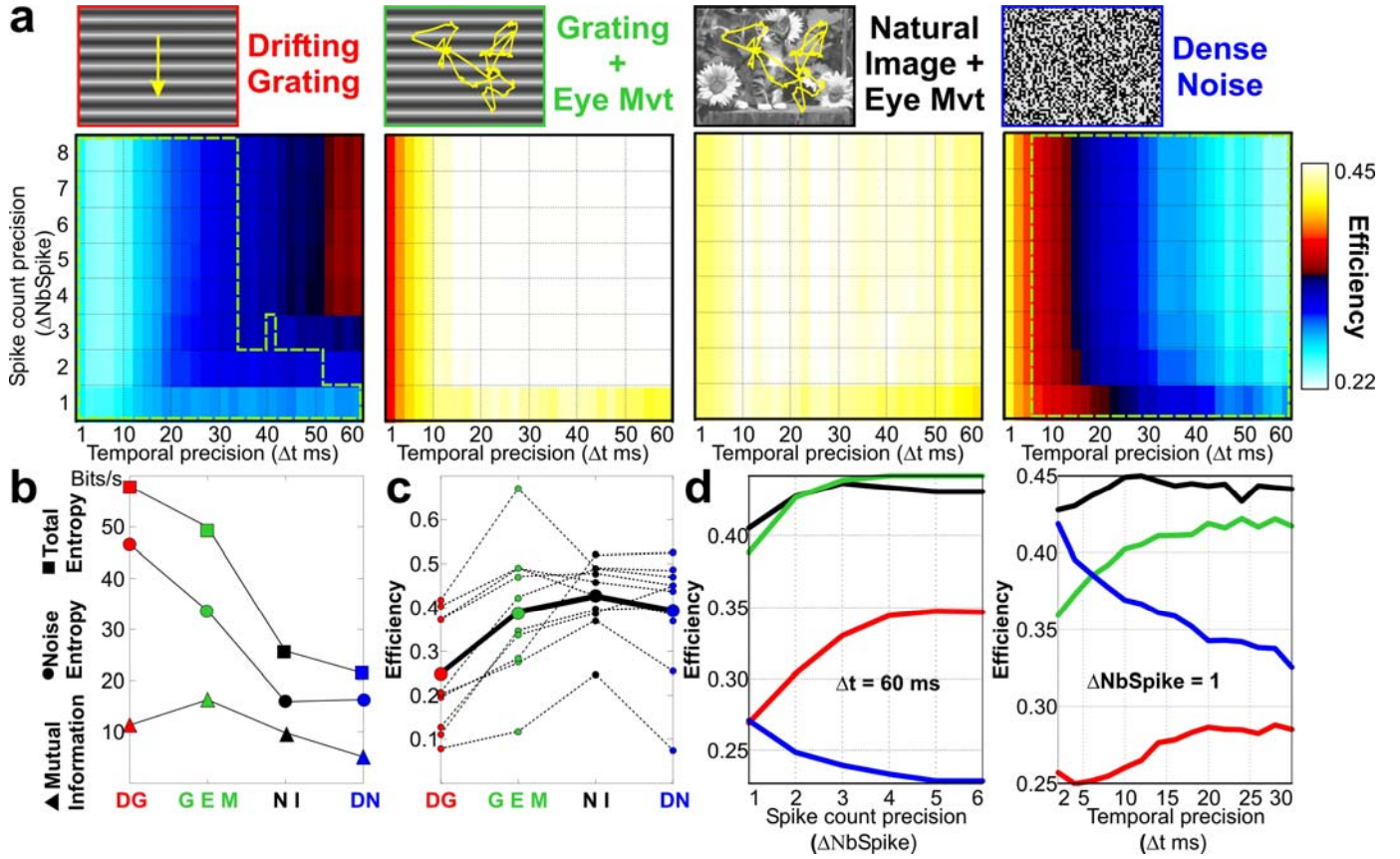


Figure 3.5.3: Efficiency, temporal and spike count precision of the code in V1 as a function of visual input statistics. Classical information measures^{35,36} based on the spiking responses are averaged across the cells ($n=10$). A direct information measure is applied to quantify Total Entropy, Noise Entropy, Mutual Information and Efficiency, in the single letter word case, for different durations of time bins (Temporal precision, Δt), and for different spike count precision of the bin value content ($\Delta NbSpike$). **a**, Efficiency values as a function of Δt and $\Delta NbSpike$ for the 4 different stimulus conditions. Areas surrounded by a green dotted contour represent domains where the efficiency value is significantly lower than that measured for the Natural Image condition (Wilcoxon paired test: $p < 0.05$). **b**, Total Entropy, Noise Entropy and Mutual Information estimates, averaged across cells, for the 4 different stimulus conditions (for $\Delta t = 2$ ms and $\Delta NbSpike = 1$ (exact spike count value)). **c**, individual cell (dotted line and small symbols) and mean (bold line and large symbol) Efficiency values for $\Delta t = 2$ ms and $\Delta NbSpike = 1$. **d**, mean Efficiency values are plotted as a function of spike count precision (left, $\Delta t = 60$ ms) and of temporal precision (right, $\Delta NbSpike = 1$).

To further quantify the precision of the neural spiking code and its efficiency, we have used direct classical measurements of information (Rieke & al, 1991, De Ruyter Von stevenink & al, 1997, Borst & Theunissen, 1999). Efficiency is computed here as the mutual information

normalised by the total entropy of the spike train (Rieke & al, 1991, Borst & Theunissen, 1999), which differs from the Shannonian definition (mutual information normalised by the channel capacity), but rather quantifies the computational efficiency (cf. model and cf. supplementary information chapter 3.5.12.2). In our one-letter implementation, this measure, studied here as a function of the temporal and amplitude precision of the measure of spike activity, allows to estimate the temporal scale and fuzziness under which the code operates (Rieke & al, 1991). It represents the fraction of the overall information present in the spike train that is available for the system and can be used in the next processing stages. In this study, spike-based efficiency is expressed in Figure 3.5.3 as a matrix, function of the temporal precision of the sampling of the spike train (bin-width ranging from 2 ms to 60 ms) and of the amplitude precision of the spiking response (binned modulo 1 up to modulo 8 events, rather than keeping the ad hoc classical single spike event resolution). Entropy, ambiguity, mutual information are calculated considering the simplest assumption of a memoryless code, i.e. the single letter word case allowing measures on our very small data samples (see Methods).

In the drifting grating condition, the efficiency is low (ranging from 0.25 to 0.29 for a spike precision of 1 as shown in Figure 3.5.3d) and decreases when both the temporal and amplitude precisions of the measure increase. This behaviour is expected from previous studies on visual cortical code (Kara & al, 2000) and reflects the noisiness associated with the rate code: neuronal responses have to be integrated over time and averaged over a population of cells coding for the same feature to obtain an efficient (reliable) code. In the natural-like condition, efficiency is found to be high (ranging from 0.41 to 0.44 for a spike precision of 1, Figure 3.5.3d) and is roughly constant across the different time and response amplitude precisions of the measure. This indicates that the precise arrival time of a single spike carries most of the information and that the code is almost binary. The grating with eye-Movement condition displays also high efficiency values but presents a slight decrease when the temporal precision becomes high. Responses in the white dense noise condition present an opposite behaviour to that observed in the drifting grating condition. Efficiency increases with the temporal and response amplitude precision of the measure, which is supportive of a temporal binary code, somehow less efficient because of a lack of reliability than for the natural-like condition.

3.5.4. From dense input to sparse output through coincidence detection

The comparison of the Vm input and spiking output dynamic allows us to uncover the various mode of information propagation and dissipation imposed by our stimuli set, and by the way how the sparse reliable cortical code is generated. The analysis of the mean Vm trajectory preceding and following the spike (detailed in Figures 2 and 4) shows that in the natural-like condition, the emission of a spike is always correlated with a fast transient depolarizing subthreshold event (see $\langle V_m \rangle$ spike trigger averaging (STA), lower panel in Figure 3.5.4d) and an increase in the higher frequencies of the spectral content of SNR(Vm) values (Figure 3.5.4c). In the natural-like and the drifting grating with eye-movement conditions, the neuron is acting like a temporally precise and reliable coincidence detector, whereas in the drifting grating condition the neuron works in a firing rate-based integration regime. This conclusion is strengthened when looking at a larger spatial scale of integration, as shown in the EcoG signal, simultaneously recorded in close vicinity or in the homotopic site in the ipsilateral cortex. The SNR(ECOG) is also modulated by the statistics of the visual stimulation and extends its significance peaks to higher frequencies for the natural-like condition (lower panel in Figure 3.5.2, see also similar evidence based on LFP recordings in the awake cat in Kayser & al, 2003). Its variations across conditions reflect mostly the influence of coherent synchronous activity in the network whereas uncorrelated activities sources cancel each other out (see also Fiser & al, 2004).

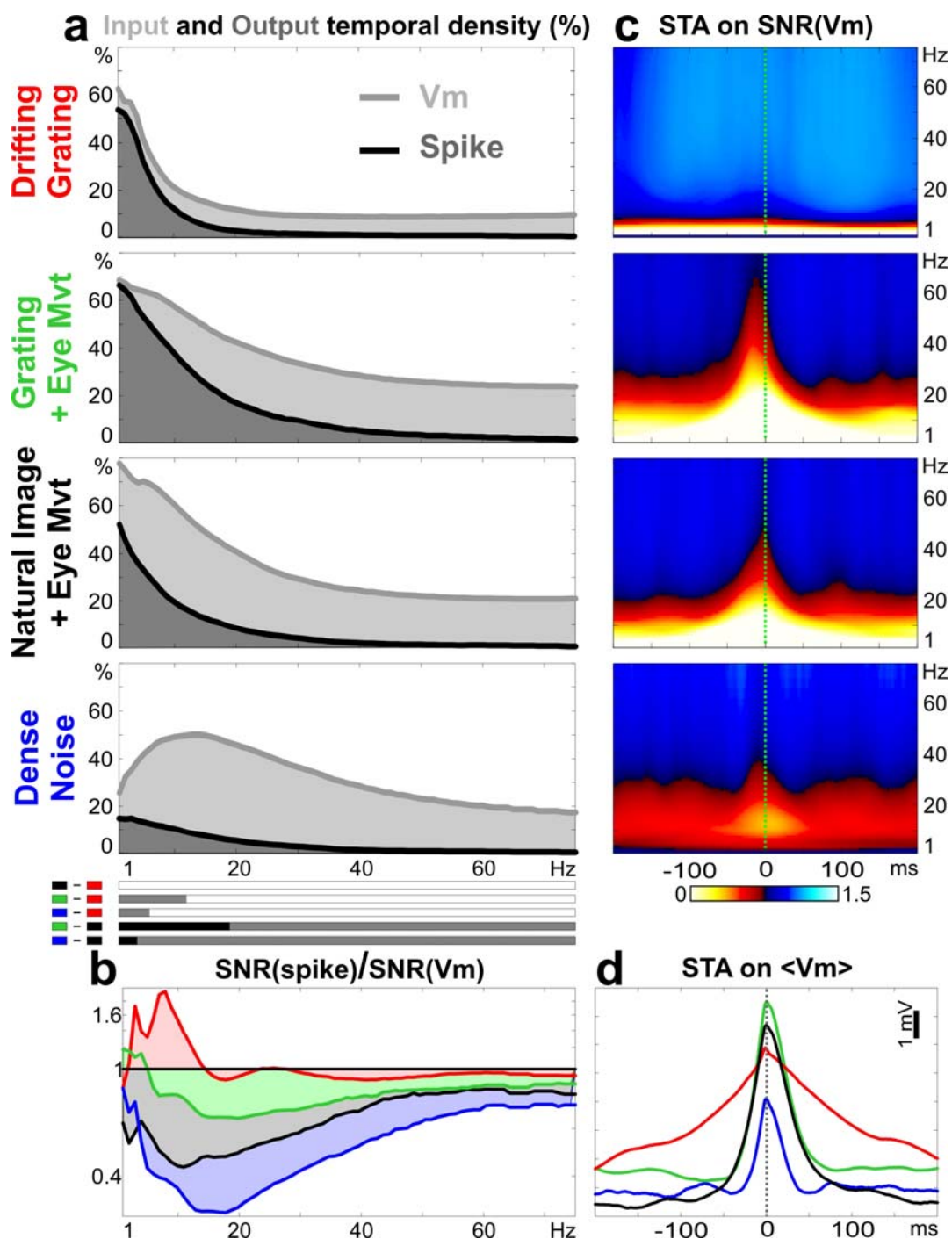


Figure 3.5.4: Output temporal sparseness vs. input temporal density, and neuronal redundancy removing process. *a*, frequency-dependent measure of temporal sparseness (or density) for each stimulus condition measured as the percentage of frame occurrences where a significant evoked SNR activation is observed (significance compared to a Rayleigh diffusion process, $p < 0.05$) for Vm and spike responses and for each stimulus condition (population analysis, $n=12$). The bottom indicator shows the results of a non-parametric Wilcoxon paired test (significance level: $p < 0.05$), applied for each frequency with same convention as figure 3.5.2. *b*, correlation removing of the cortical process measured as the ratio between SNR(spike) vs SNR(Vm) (population analysis). *c*, Spike trigger averaging (STA) on SNR(Vm) time-frequency analysis averaged across cells ($n=12$). *d*, Spike trigger averaging of the mean Vm profile (population analysis).

An important observation in the natural-like condition is that, whereas the spiking output response is sparse (meaning that a neuron responds selectively to a very low proportion of stimuli frames), neurons exhibit Vm responses to almost each movie frame. This finding corroborates previous results on orientation and direction selectivity demonstrating diverse and much broader synaptic tunings when compared to the spiking output (Monier et al, 2003). It can be generalised also to the domain of temporal frequency tuning as shown in the companion paper (Baudot al, 2006). This contrast between dense input (signalled by the evoked PSPs) and sparse output (spike), illustrated at the single cell level in Figures 1 & 2, is confirmed at the population level, as shown in Figure 3.5.4a : the temporal density or sparseness of the response was quantified both at the spiking and membrane potential level by the percent of frames eliciting a significant SNR response compared to a Rayleigh diffusion process which corresponds to a complete signal scattering ($P < 0.05$, SI. 2).

SNR reflects the amount of stimulus-driven correlations at the input (seen in the Vm recording) and the spike train output levels. The comparison of the cortical informational transfer between the different stimulation conditions is illustrated in Figure 3.5.4b, by measuring the ratio between the SNR(spike) vs. the SNR(Vm) spectra. Whereas, for the drifting grating condition, a synergetic (Schneidman & al, 2003) amplification is observed for harmonic frequencies from 3 to 13Hz, in contrast, for natural-like and even more for dense-noise conditions, cortical processing is strongly acting as a nonlinear filter removing input higher-order redundancies, at least the second-order statistics (see companion paper, baudot & al, 2006). This redundancy removal process observed at the single neurone integration scale can be generalised to the global processing performed by a whole cortical area: since, apart for the grating conditions, the presented movie clips were the same for each cell, we cross-correlated the activities between different cells. This calculus demonstrates that the correlations of the input dynamics between recorded cells is higher than the correlation between their spiking output in natural-like conditions (data not shown).

3.5.5. Adaptation to external constraints reduces noise and redundancy

In this section, we reexamine the implications of our observations in the wider framework of the computational literature by introducing a formal definition of ordered redundancies. Our results invalidate the view that neurons are independent channels with signal and noise considered as independent components, for two reasons. First, noise is an intracortical emergent component modulated by the input statistics. Second, the mutual information between the neuronal response and the input is equal or even lower in the natural-like

condition when compared with the drifting-grating condition, in spite of the fact that the information content is much higher in the former than in the latter. This paradox implies that cortical inter-neuronal redundancies change as a function of the stimulus context (Reich & al, 2001).

Let us consider V1 network activity as the state of a system S , defined by the sampling of n_1 individual neuron responses during n_2 discrete time bins, hence the n variables S_1, S_2, \dots, S_n (with $n = n_1 * n_2$) taking M possible values (1 or 0 for a spike based code). The Shannonian entropy of the system (V1) is given by:

$$H(S) = H(S_1, S_2, \dots, S_n) = \sum_{i=1}^{M^n} P_i(S) \log_2(1/P_i(S))$$

The entropy of a system is less or equal to the sum of the entropies of its constitutive elements. Following Shannon and Weaver (1949) and Atlan (1979), we define: $H(S) = H_0(S)(1 - R(S))$ (1), where $H_0(S) = n \log_2 M$ and $R(S)$ is the redundancy present in the system. $H_0(S)$, the system capacity, a constant which depends only on the intrinsic dimensions of the system S and is the maximum possible entropy of the system. The development of equation (1) allows to decompose redundancy into first and higher order terms (see Atick, 1992):

$$R = (H_0 - \sum_{i=1}^n H(S_i)) / H_0 + (\sum_{i=1}^n H(S_i) - H(S)) / H_0 = R_1 + R_H = R_1 + R_2 + \dots + R_n,$$

where each $R_{i>1}(S)$ can be expressed independently of the total entropy as a renormalized sum of mutual information between i elements of S given the others (cf. supplementary information chapter 3.5.12.1 & 2 and figure 3.5.5b). Entropy can thus be intuitively understood as quantifying the whole world of possible microscopic states minus each constraints imposed by elementary interactions (elementary mutual informations, ponderated as a function of the level of sharing of this interaction in the whole population). For simplicity, those elementary interactions can be understood as elementary knowledge, monade or beliefs, whereas the rest is just uncertainty. A fundamental interest of this decomposition is to stress the microscopic nature of entropy under the reasonable discrete assumption, whereas it is classically considered as a macroscopic variable.

This formalism can be applied to any system, physical or biological, that can be decomposed into elementary probabilistic quantized constituents. It allows to compare the photon flow

structure falling on the retina to the cortical activity structure. $H(S)$ quantifies the number of degrees of freedom of the system, its uncertainty, whereas H_0R quantifies the constraints present in the system. The redundancy component H_0R_H accounts for the spatiotemporal statistical dependencies and the structure of the environment, and minimising this “contrast” function is the general aim of ICA algorithm (Jutten & Herault, 1991, Comon, 1994). It provides the only information available in order for the system to learn, to evolve and to « perceive ». H_0R_H is also equivalent to negentropy: to paraphrase Schrödinger’s adage (1944), “organism feeds upon environment redundancy”, which allows the system to dynamically maintain its inner order/structure in a homeostatic way. Furthermore, H_0R_H gives a formal definition of spatial and/or temporal memory (Ashby, 1967).

Nevertheless the definition of entropy does not catch the intuitive concept of structural complexity, relevant in biology and perception, for which several complementary measures have been proposed (Chaitin, 1977, Bennett, 1985, 1988, Bialek & al, 2001). We propose in the supplementary results a statistical measure of structural complexity similar to Algorithmic Logical Depth (Bennett, 1985, 1988), which naturally arises from the redundancy decomposition and measures the dispersion of the redundancy across different orders (cf. supplementary information chapter 3.5.12.3 & 4).

Mutual information $I(E;S)$ characterizes the interaction between the system S and its environment E , and is defined by:

$$I(E;S) = H_{0S} - H_{0S}R_S - H(S/E) = \sum_{i=1}^n H(S_i) - H_{0S}R_{HS} - H(S/E).$$

The maximisation of Mutual information may provide a logical and general formal definition of adaptation, applicable to the interaction between biological systems and their environment. Indeed, this measure is a statistical approximation of the average mutual Algorithmic complexity ($\langle K(E:S) \rangle_S \approx I(E;S)$, Adami & Cerf, 2000). When applied to the genomic code, this complexity measure increases while the genome of a given species adapts to its environment (Adami et al, 2000). Considering the present case of cortical systems, the maximisation of mutual information has already been proposed as a principle of unsupervised self-organisation and adaptation (Laughlin, 1981, Linsker, 1982, 1988, Atick, 1992, Nadal & Parga, 1994, Bell & Sejnowski 1995, 1996). We propose that this principle result in the progressive build-up of environmental memory by progressively maximizing the determinism or reproducibility of the system dynamics conditional to its environment ($\min(H(S/E))$).

The second direct signature of this process is the reduction in redundancy, which is synonymous of a specialisation of the constitutive entities and of genesis of functional diversity (e.g. maximally diverse and selective RFs). Both correlates are the core of our experimental findings.

The redundancy reduction sustained by the adaptation to the sensory input implements a computation that can be described phenomenologically, on the basis of our empirical results, in two steps:

- First, the sparse code observed in natural-like condition imposes that the R_I component is huge, and thus suggests that the redundancy increase imposed by V1 overcompleteness affects only the R_I component. In contrast R_H which can be interpreted as the signature of cortical assemblies (see also Martignon & al (2000)) and for at least its second order statistic component, appears to be selectively reduced in natural-like conditions (figure 3.5.4). As originally proposed by Field (1987), this reduction reflects a simple dissipative computational mechanism, supported by the neuronal RFs function, that transfers R_H (analogous to free energy) into R_I (analogous to internal energy). The companion paper (Baudot et al, 2006) details some of the neural RFs mechanisms responsible for this filtering process.

- Second, the cortical transfer function filters out independent sources, and thus also the R_I component, by signalling only at the spiking output level the coincidences (notably high-order) present in the input.. A correlate can be found in our data by the observation of quasi silent spiking states evoked by white-noise input. This R_I component of the input becomes a lost information since it is no longer represented in the output. Consequently, this results in equivocation in the information transfer, and represents the entropic cost of observation or memory formation or erasing (Figure 3.5.5). It further point out the fundamental irreversibility of cortical sensory computation, and the apparent *natural* Maxwell-demon process operated by the cortex (Bennett, 1982, 2003, Adami and Cerf, 2000)

We propose that this process, which can be seen as a dissipation of input constraints ($H_0 R_H$), operates iteratively across successive cortical processing steps, and thus achieves a spatiotemporal progressive simplification (and abstraction) of the structural complexity of the visual scene representation (see conclusion and Figure 3.5.5c). Of course, given the colossal logical depth of natural environments, cortical representations always present some R_H component or remaining correlations (Fiser & al, 2004), which may be reflected in the EcoG

signal and SNR increase notably in the Beta-Gamma range found for natural scenes (figure 3.5.2, Kayser & al, 2003).

Moreover, as already advocated by Olshausen & Field (1996), a representation of the input in an overcomplete basis using an individual low entropy code leads invariably to a minimization of R_H . Since R_H depends on the low entropy individual code (sparseness) and is inversely proportional to the cortical capacity of V1. ($R_H = (\sum_{i=1}^n H(S_i) - H(S)) / H_0$), we propose that cortical capacity H_0 is a R_H removing capacity, thus defining a computational capacity. This mean that in order to model reliably the real cortical processing, a computational power far over those currently used is probably necessary. This computation intrinsically implement a cognitive process as logically emphasised by G. Chaitin who proposed that “understanding is compressing”, or discovering the structure, that encompass Gestalt’s simplicity and Helmholtz’s likelihood principles of perception (Chater & Vitanyi, 1996, Chater, 1996). In the field of perception, achieving through computation the less redundant and less noisy representation of our intrinsically probabilistic environment (which can be thought has a hard optimisation problem) could be the correlate of “percept” emergence. We emphasize that this adaptation framework encompasses the concept that functional redundancy confers noise resistance properties (Von Neumann, 1956), and stochastic resonance paradigm (Collins & al, 1995). Noise is not a nuisance; it’s a prerequisite for adaptation, and given the finite capacity of living systems, there is an apparent compromise between specialisation and adaptability.

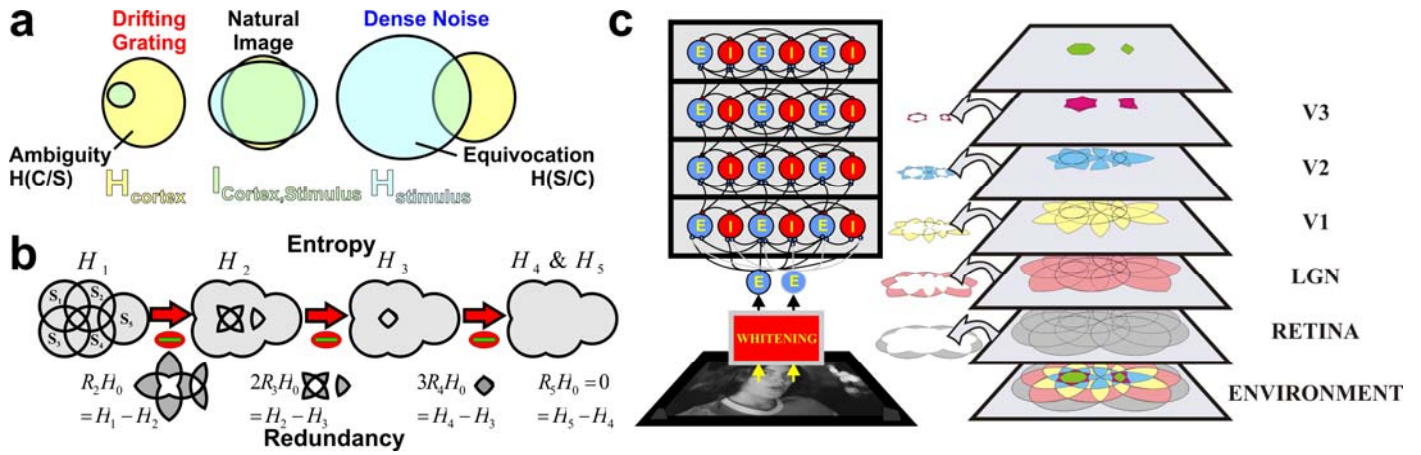


Figure 3.5.5: Model of cortical computation and dissipation of input-driven complexity. *a*, Schematic interpretation using Venn diagrams of the entropies and mutual-information between the stimulus and V1 response for the different experimental conditions. V1 entropy, represented by the Yellow disk is arbitrarily maintained constant across conditions. The interpretative value of the diagram is limited to the variation across conditions of Noise, Mutual Information and stimulus Entropy (blue disk). Ambiguity (noise) or equivocation (representational failure) respectively arise if the dimension of the stimulus is lower (left, "grating") or larger (right, "dense noise") than the network capacity. *b*, Representation using Venn diagrams of the decomposition of entropy and ordered redundancies. Each R_i is a renormalized sum of mutual information between i elements knowing the others. *c*, Model of cortical computation and dissipation of complexity along a hierarchy of visual cortical processing steps⁷⁵. At each stage of integration, higher order redundancies are transferred into first order redundancies that, because of their statistical independency, do not propagate further to the next cortical area. This dissipation process represents the entropic cost of the cortical computation. Note the decrease in the logical depth of the environmental representation across cortical stages.

3.5.6. Recurrent network model of cortical computation

Our observations in natural-like conditions validate the prediction made by De Ruyter Von Steveninck & al (1997) based on the observation of low noise spiking responses to Brownian velocity stimulus in the fly H1 neuron. Further more, since reliable responses have already been observed in subcortical structures (Aertsen & al, 1979, Rieke & al, 1995, Reinagel & al, 2000, Jones & al, 2004) as well as in the auditory primary cortex (Aertsen & al, 1979, Machens & al, 2004), we propose that a precise temporal code and highly reproducible constrained network dynamics may be the general signature of active adapted cortical states. This principle may generalise to motor cortex, since ultra-sparse reproducible code has been found for complex highly reproducible (logically deep) motor pattern in bird motor cortex (Hahnloser & al, 2002). This principle may generalise to motor structures in birds and mammals, since ultra-sparse reliable code has been found for complex (high logical depth) and highly reproducible patterns in motor and song production areas (Vaadia et al, 1995;

Hahnloser & al, 2002). Further more, this principle holds for macroscopic spatiotemporal scales of cortex activation observed using fMRI on Human, where complex natural scene induce reliable responses dynamics, distributed over the whole cortical visual and auditory cortical areas (Hasson & al, 2004).

Applying the logic of Entropy maximisation under external constraint (Dewar, 2004, 2005), we interpret the highly reproducible dynamic states code we found in V1 as the result of evolution/adaptation in a highly structured environment. The only source of constraints and information is the environment itself, and the code operating in V1 can be considered as an external code. The novel interpretation that we give of Noise is that its contextual dependency should be taken as an indicator of the number of cortical states that are authorized by the external environmental constraints. In natural-like conditions, the cortex can only occupy a low number of states, and the fixed Vm trajectories observed here directly reflects reliable microscopic network states. Those reliable microscopic states are further probing the functional relevance of the highly specialised V1 microcircuits or "cortical songs" described in spontaneous activity in-vitro and in-vivo (Ikegaya & al, 2004). Attention and reward expectancy processes, which have been shown to promote the visibility of synfire chain patterns (Vaadia et al, 1995; Riehle et al, 1997), can be considered as a form of contextual constraints that may modulate the SNR and the information propagation (SI. 5).

In contrast, in the case of low-dimension input such as drifting gratings, the variability observed in subthreshold dynamics and spiking activity reflects the large number of states made possible by the lack of constraints in regards with the computational capacity of the network. In the absence of external constraints, the ongoing activity pattern reflects the inner structural connectivity of the network. In the absence of external drive, the ongoing activity pattern will span the ensemble of microstate which averaging reflect the dominant relational recurrency in the network (i.e., the horizontal connectivity and orientational maps, Arieli et al; Kenet et al, Tsodyks & al, 1996).

Several additional theoretical arguments can be made which strengthen the pivotal role of network recurrence in modulating ongoing activity and extracting progressively redundant components from the environmental input. First, our study demonstrates that internal ongoing activity is not an additive component to the signal, but is in competition with externally imposed states. The dependency of this balance on the level of previous adaptation to environment is a well known property of recurrent networks. Recurrent architectures (Hopfield, 1982), such as in Boltzmann nets (Hinton & Sejnowski, 1986) or Helmholtz machine (Dayan, Hinton, Neal, Zemel, 1996), implementing a distributed non-linear

dissipative memory, present the remarkable capacity of self-generating spontaneously learned states in absence of input or in presence of unlearned input.

Second, recurrent architecture can account for the temporally dense Vm synaptic input activity that we have observed in natural-like conditions.

Third, models of recurrent excitatory-inhibitory networks endowed with plastic Hebbian-antiHebbian connections implement an input redundancy reduction leading to the emergence of realistic Gabor-like receptive fields (Foldiak 1990, Harpur & Prager, 1996, Deco & Para , 1995, Amari & al, 1995).

Fourth, the observed deterministic neural assemblies integrating input in coincidence detection mode and responding using a temporal code are directly predicted from a generalisation of the infomax principle to the temporal domain in recurrent network (Wennekers & Ay, 2005, with time dependent plasticity).

Given the fact that inhibitory circuits remain intrinsic to a given area, the global topology of the visual cortical network (Felleman, Van Essen, 1991) offers multiple instantiations of recurrent E/I generic modules able to learn the input structure/code and deliver a less redundant simplified and more abstract representation available for the next processing step (Figure 3.5.5c). The information maximisation may provide a computational substrate to the language of thought and modularity of mind hypothesis (Fodor 1987, Fodor & al, 1988), and overcome the old nature vs nurture debate. Indeed, the mechanisms of efficient dissipation exposed here suggest a unified unsupervised statistical framework for genetic adaptation and cognition ensuring living system's stability and enduring. We'll see in the last chapter, that this computation is compatible with (and probably intrinsically the result of) the quantum decoherence and einselection phenomena that is governing system/environment interactions (Zurek, 2003).

3.5.7. Material & Methods

3.5.7.1. Preparation and recordings.

Cells in the primary visual cortex of anesthetized (Alfathesin) and paralyzed adult cats were recorded in vivo using sharp electrode recordings (n=12, average $V_{rest}=-67\text{mV}$, 0nA) as described in chapter 3.3. The electrocorticogram (EcoG) was simultaneously recorded using silver electrodes positioned homotopically or close to the recording site. Data processing and visual stimulation protocols used in-house software (G. Sadoc, Elphy, Biologic CNRS-UNIC/ANVAR).

3.5.7.2. Visual stimulation.

Stimuli were displayed on a 21" CRT monitor with a 1024*768 pixels definition and a 150 Hz refreshing rate, with a background luminance of 5 cd/m². RFs were mapped using sparse noise reverse correlation analysis and classical tunings were determined by automated exploration. spikes. The mean luminance and contrast of each movies were equalized (so that each conditions only differ in their higher order statistics). Each full field movie was presented at least 10 times (except in 2 cells rejected for direct information measure) for a 10 second duration and interleaved by 2 seconds. For natural-like condition we used a high definition natural image (2048*1536 pixels) animated virtual eye movement sequence (chapter 3.5.8). White noise consisted in a high rate sequence (13.3 ms refresh) of high definition full field (50*50 shaker board of 0.39° pixels) binary dense noise. To measure the first-order receptive field kernel, each trial lasted for 80 seconds.

3.5.7.3. Stimulus-locked time-frequency analysis.

Spike trains and Vm waveforms are convolved for each trial with an array of complex-valued normalized Gabor function (two period) ranging in frequency from 1 to 100 Hz (1 Hz steps). This time-frequency decomposition allows to extract relevant signal/noise measures: Noise power, Signal power, Total Signal power, Signal to Noise Ratio (SNR), Coherence, and a time-dependent local estimation of an upper bound of Mutual Information rate (chapter 3.5.9). For a given frequency (f) and a given time (t), the time-frequency signal spectra is defined as $S_{est}(t, f) = \left| \langle S_i(t, f) \rangle_i \right|$, noise spectra as $N(t, f) = \left| \langle S_i(t, f) - \langle S_i(t, f) \rangle_i \rangle_i \right|$, and SNR spectra as $SNR(t, f) = S_{est}(t, f) / N(t, f)$ (angular brackets $\langle \rangle_i$ indicate the average across all trials i, and straight brackets $| |$ indicate the modulus). Signal(f), Noise(f), and SNR(f) power spectra are obtained by integrating the respective squared functions over time.

3.5.7.4. Direct information measures:

Direct informational measures were computed using the classical estimation technique (Rieke & al, 1997, de Ruyter von Steveninck, 1997, Strong & al, 1998, Borst, A. & Theunissen, 1999, Vinje & Gallant, 2002). Spike trains were discretised with different bin temporal size (Δt =temporal precision) and with an additional new parameter, i.e. the spike count precision (ΔN_{bSpike}). Classical finite data bias correction and extrapolation for an infinite number of repeats were applied to entropy computation (Strong & al, 1998, Vinje & Gallant, 2002), and

we checked resulting values against the Ma entropy lower bound estimate (Strong & al, 1998, Vinje & Gallant, 2002).

3.5.8. Simulation of saccadic and fixational eye-movements scanpath

3.5.8.1. The modeled scanpath spatiotemporal dynamic

In order to simulate in a realistic way the continuous changes in the retinal flow imposed by eye-movements during a natural scanning of visual scenes, we built a model of the retinal image displacement whose kinematic parameters were fitted on the basis of measurements previously made in the freely behaving cat (Collewijn, 1977; Olivier & al, 1993, Eizenman & al, 1985). Eye-movements are classically decomposed in intermittent ballistic movements, saccades, of large but variable amplitudes, separated by fixation episodes (figure 3.5.6).

During fixation, the eyes are not still, their mean position drift slowly in time with superimposed high frequency and very low amplitude tremors (in the 40-100hz range), as well as microsaccades (although the latter type of movement occurs rarely in the cat (Kording et al, 2001)). These micromovements avoid bleaching of photoreceptors, maintain visual perception from fading (Martinez-conde & al, 2004, 2006), and may even serve to increase visual acuity (Rucci et al, submitted). One characteristic of fixational drift and tremor dynamics is the $1/f^2$ shape of the temporal power spectrum (Eizenman & al, 1985), which is reproduced by our model (Data not shown).

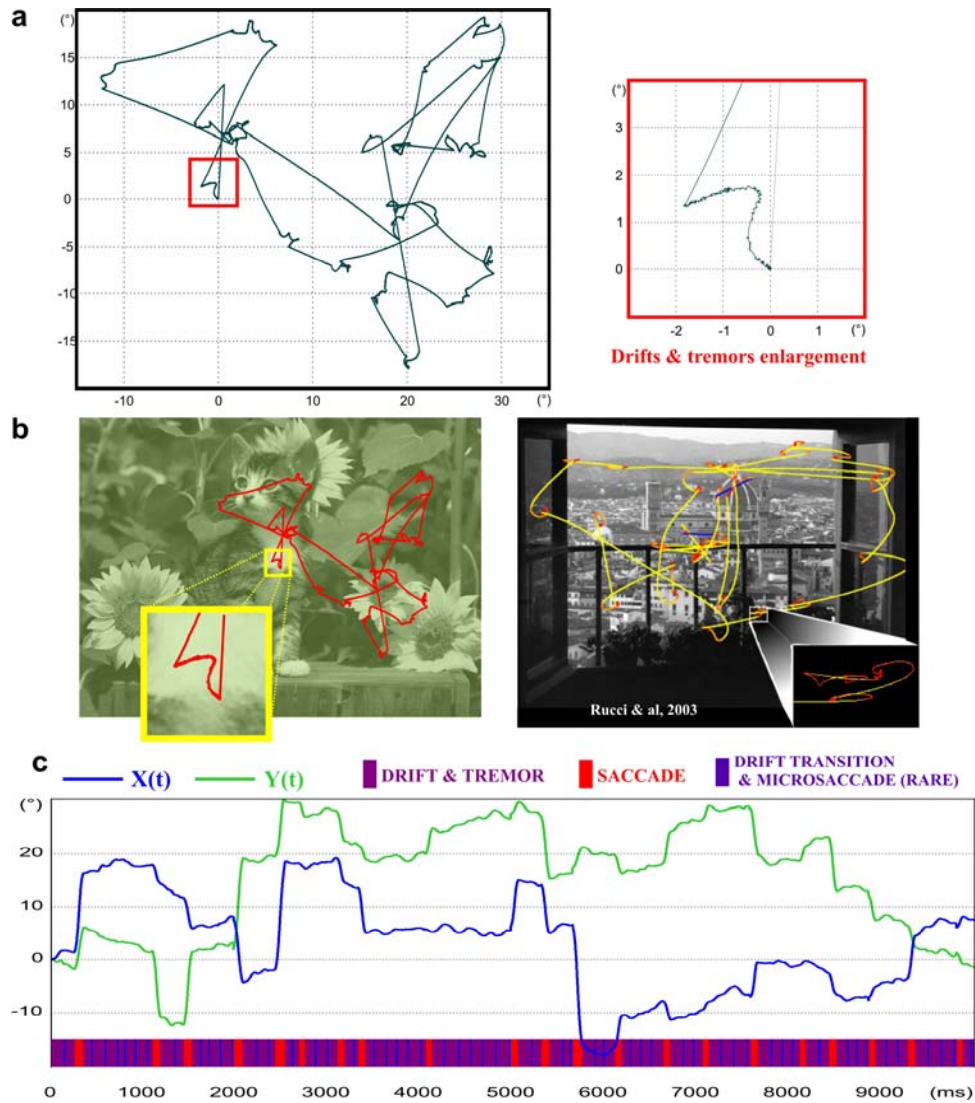


Figure 3.5.6: Spatial and temporal profile of the modeled eye-movement scanpath. *a*, Spatial trajectory of the modeled eye movement sequence with an enlargement presenting drifts and tremor fixational movements. *b*, Comparison of the modeled spatial scanpath with one eye-movement scanpath obtained in Human (taken from Rucci & Desbordes, 2003). *c*, Temporal profile of the modelised eye-movement sequence and the various eye-movement components temporal succession (bottom).

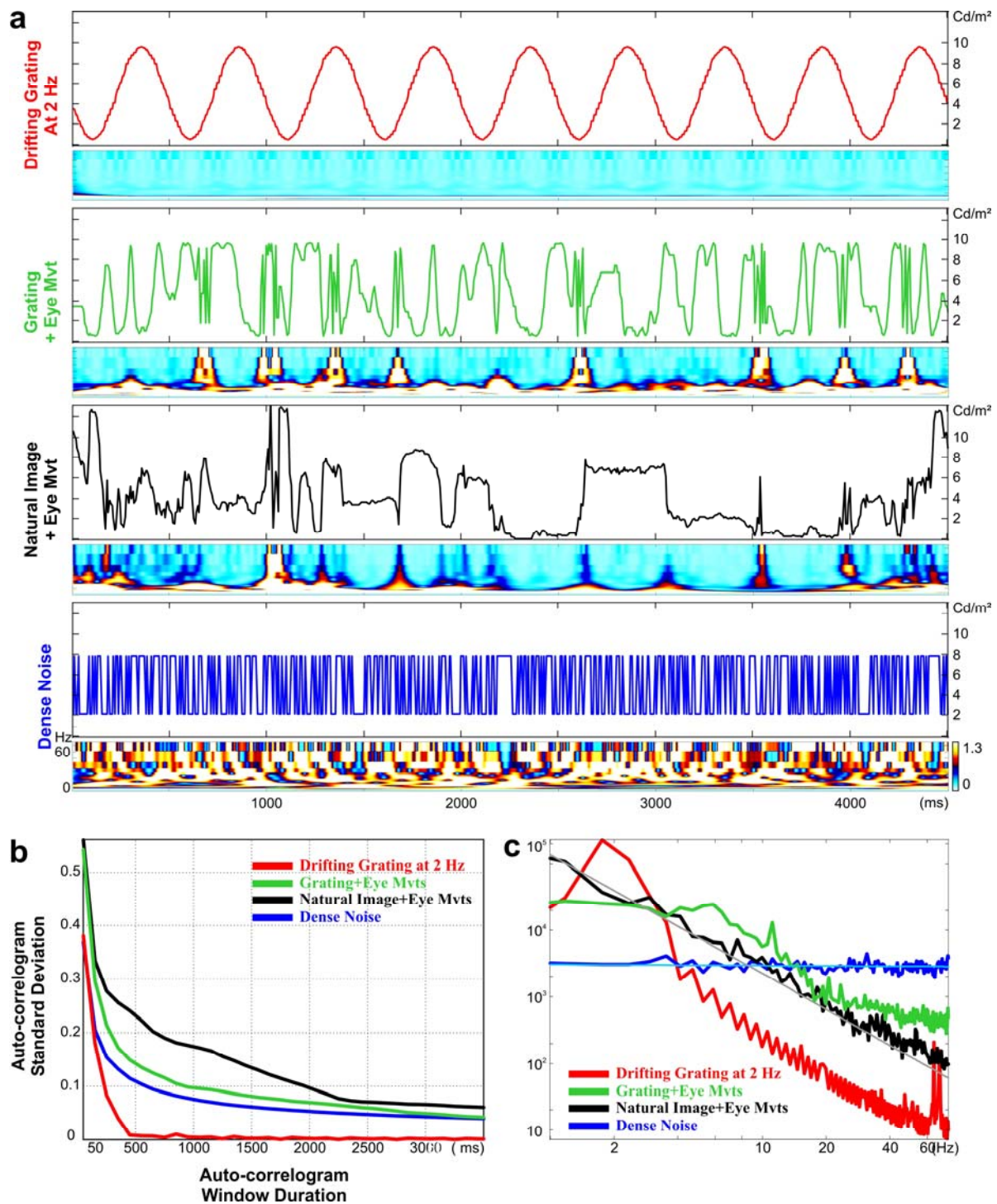


Figure 3.5.7: temporal profile, spectra and non-stationarity of the luminance falling on the retina in the four conditions of stimulation. *a*, Temporal profile of the luminance of one screen pixel representing roughly the luminance waveform falling on one photoreceptor in our four conditions and their respective time-frequency spectra (1-75Hz). *b*, Stationarity of the luminance profile: the mean standard deviation of the autocorrelograms calculated at various multiple epochs of the luminance profile (window sliding every ms) as a function of the window duration used to calculate the autocorrelograms. Stationarity (of 2nd order statistics) is achieved when the graph reach the 0 value. *c*, Power spectrum of the temporal profile of luminance obtained for the four condition of stimulation (calculated by time-frequency wavelet analysis for one example pixel).

The eye-movement animation of the natural environment have a drastic effect on the spatiotemporal statistics of the luminance profile falling on the retina, which, as a result, strongly departs from the ones classically imposed by experimentalist in neurophysiology (drifting grating and dense noise condition in figure 3.5.7a,b,c). The temporal statistic modulation by the eye-movements can be exemplified by two very global affected parameters: the temporal spectra of the luminance falling on one retinal photoreceptor (approximated to one image pixel figure 3.5.7) and the stationarity (or the level of fluctuations) of the spectra (figure 3.5.7b). The temporal spectrum of the luminance of eye-movement animated stimuli present a $1/f^\gamma$ shape falling between the flat spectra of the white noise and the one impulsion spectra of the drifting grating. The γ values obtained for natural-like condition are around -1.8 (-1.79 in figure 3.5.7b) which is close to a Brownian signal value, although, as detailed notably in the following chapter, this signal originate from a more structured mechanisms (or algorithm), and probe the existence of long-time correlations (or memory) in the visual natural-like input signal. The peculiar non-stationarity (wide-sense) of natural-like input signal, roughly demonstrated in figure 3.5.7b showing that autocorrelation function (or spectra) has to be measured on very long time windows ($>3s$) in order to be approximately reproducible, is further indicating the probable existence of inner fine structure (or higher order redundancies) in the signal.

3.5.8.2. Model of saccades

Saccade amplitudes: the amplitude A_s was chosen randomly from the distribution established for saccadic and head gaze movements by Collewyn (1977) in the freely behaving cat (Figure 3.5.8a).

Inter-saccadic intervals: The duration between two successive saccades was chosen randomly from the distribution of intersaccadic intervals reported by Collewyn (1977) (Figure 3.5.8b).

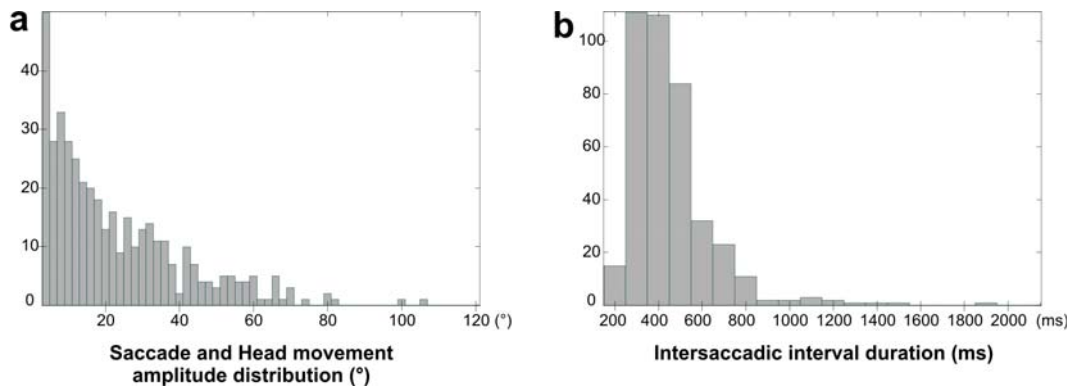


Figure 3.5.8: Saccade and head movement amplitude and intersaccadic interval duration distributions. Redrawn from Collewyn (1977).

Saccadic duration: an estimate of the duration of the saccade (D_s) was predicted on the basis of Collewyn's observations, by using the best linear fit between saccadic amplitude and duration (Pearson correlation $r = +0.81$): $D_s = 1.9 * A_s + 63$ (where D is expressed in ms and A_s in steradian degrees ($^\circ$) of visual angle).

Spatio-temporal profile: the temporal profile of saccadic speed is approximately Gaussian. We modelised the saccadic spatio-temporal profile by the following sygmoïdal function $F(t)$:

$$F(t) = -\lambda A_s + (A_s + 2\lambda A_s) / \left(1 + e^{(-2-\lambda)/(D_s * (D_s / 2 - t))} \right) \quad (1)$$
, where λ is a constant threshold fixed at 5%.

Saccadic direction: The direction of the movement was chosen randomly from a uniform $[0^\circ, 360^\circ]$ distribution. Since most saccadic paths present small drifts of directional angle during their execution (see Yarbus, 1967, Rucci & al, 2003). Since they are not well documented in the literature an adhoc sinusoidal variation of direction during the drift path was fitted visually to real recordings: $f(t) = \Delta\theta * \sin(2\pi t * \tau / D_s) \quad (2)$, where the amplitude in direction change ($\Delta\theta$) was chosen randomly between 0° and 4° , and the fraction of time during which it operated (τ) was chosen randomly in between 0.5 and 1 (relative to the full saccade duration).

3.5.8.3. Model of fixational movements: Drifts

Drifts amplitude: the drift amplitude was chosen randomly from a Gaussian distribution with a mean of 1.21° and a standard deviation of 0.63° , corresponding to measures obtained in the cat by Grantyn & al (1993).

Drifts duration: the duration (D_D) was derived from the best linear fit with the drift amplitude (A_D), on the basis of Grantyn & al (1993) measurements: $D_D = 41,7 * A_D + 53,7$, where D_D is expressed in ms and A_D in $^\circ$.

Spatiotemporal profile : We used the same sigmoidal function (1) as previously.

Drift direction: The direction of drift movement was chosen randomly from a uniform $[0^\circ, 360^\circ]$ distribution. Drift paths present smooth and very large variations of direction angle (see Yarbus, 1967, Rucci & al, 2003). Since they are not well documented in the literature the same adhoc sinusoidal variation of direction during the drift path (2) was fitted visually to real recordings, but with direction change ($\Delta\theta$) chosen randomly between 0° and 29° .

3.5.8.4. Model of fixational movements: Tremors (during drifts)

Tremors amplitude: Tremor eye-movements are typically of miniature amplitude, ranging from $0,005^\circ$ to $0,017^\circ$ ($0,006^\circ$ to $0,013^\circ$ in (Yarbus, 1967); with a mean amplitude of 0.007° in the cat (Pritchard, 1960). The simulation of tremor is constrained by the spatial pixel discretization of the screen ($1024*768$ pixels) and the viewing distance imposed to the cat (57 cm). In the present experiments, the smallest programmable distance between two neighbouring pixels was 0.039° .

Tremor modelisation and spectral characteristics: as a compromise, we chose to remove most of the tremor energy due to low amplitude micromovements while keeping its highest amplitude components. This was achieved by using a white noise signal and band-passing it through a Bessel filter, between 40 and 80 Hz (Eizenman & al, 1985). The obtained sequence movement was then discretised, using only 3 possible inter-pixel amplitude values (-1, 0, 1), and low-pass filtered at a frequency half the frame refreshment rate (75Hz) in order to avoid aliasing. One should note that the resulting impact of tremor on the full eye-movement sequence was underestimated when compared to realistic eye-movement trajectories.

Direction of tremors movements: four possible direction values were chosen randomly: 0, 90, 180, 270° , according to the limiting pixel grid of the screen.

3.5.8.5. Model of fixational movements: microsaccades

Microsaccades amplitude: microsaccades are particularly rare in cats (Kording & al, 2001) and our modelised eye movement sample sequence contains only 3 of them. The microsaccade amplitude was chosen randomly from a Gaussian distribution with a mean and

standard deviation set both at 1° , thresholded for amplitudes less than $0,02^\circ$, as found in Humans (Ditchburn,1973).

Inter-microsaccadic intervals: microsaccades were positioned at the end of a tremor.

Microsaccadic duration: an estimate of their duration (D_{ms}) was predicted on the basis of Ditchburn's observations in humans (1973), by using the best linear fit between microsaccadic amplitude and duration: $D_{ms} = 2.25 * A_{ms} + 20$, where D_{ms} is expressed in ms and A_{ms} in $^\circ$ of visual angle.

Spatiotemporal profile: the microsaccadic spatio-temporal profile was modelised by the same sigmoïdal function as previously (1).

Microsaccades direction: The direction of saccadic movement was chosen randomly from a uniform $[0^\circ, 360^\circ]$ distribution. Variation of angle during the microsaccade was modeled as for saccades.

3.5.9. Time-frequency estimation of Signal-to-Noise Ratio

3.5.9.1. General aims: atomic uncertainty decomposition and higher-order statistics revealing

Time-frequency representation allows the analysis of non-stationary signal containing multiple elementary components, to which traditional Fourier transform is not adapted. Time information is in fact encoded in the phase component of the Fourier transform, which is ignored by the energy spectrum. For non-stationary signal, a time and frequency representation is necessary to preserve the signal information. Time-frequency estimations are inherently bounded by the Heisenberg principle, and Gabor function, thanks to its Gaussian attenuation, minimizes conjointly this spectral and temporal uncertainty (Gabor, 1946). Moreover, time-frequency decomposition by Gabor functions can be understood as a multi-scale decomposition of the signal into a superposition of *atomic* signal elements, to which the ordered redundancies, entropies and complexity measurement previously introduced (and further detailed) can be applied.

From the physiological point of view, organisms rarely have the opportunity to compute the input statistics on long-lasting data sample to build their belief and behaviour; perception and action are mainly “on-line” computation and based on much more transient and short term statistics than classically considered. This on-Line computation implies very rapid or short term adaptation of the cortical network to those transient input correlations, wich is probably

simpler and easier to describe as short-term or working memory. Further, it appears obviously that those transient correlations are an essential component of the outside world “pertinent” information, and many organisms behaviour, such as gaze exploration, vibrissae sweeping, sniffing, or going to the museum, can be interpreted as “strategies” to increase those transient input correlations (or the redundancies and the logical depth of the input).

3.5.9.2. SNR, signal, noise and coherence time-frequency estimations

We thus use a classical wavelet decomposition method to estimate the instantaneous spectrum (the local second order statistics or fluctuations of a signal). Uncertainty in this time-frequency representation is related via the Heisenberg inequality and depends in this representation only on the frequency $\sigma^2 \cdot f = cste \geq 1$. The frequency uncertainty increases as the analysis frequency grows, and the temporal uncertainty decreases as the analysis frequency grows. Spike trains and subthreshold Vm waveforms are convolved for each trial (one repeat of the same movie presentation) with an array of complex-valued Gabors ($\Psi_{t,f}(\tau)$):

$$\Psi_{t,f}(\tau) = \sqrt{f} \cdot \exp(-2.\pi.i.f(\tau - t)) \cdot \exp\left(-\frac{(\tau - t)^2}{\sigma^2}\right)$$

To improve the readability of the time-frequency representation, the Gabor decomposition presented here is largely oversampled: the Gabor filter bank is non-orthogonal with frequency ranging from 1 to 100 Hz with 1 Hz linear steps, and the temporal sampling is of 1 ms. To allow a good temporal resolution (important for spike precision estimation), the Gabor function used in this example study had a Gaussian variance window of two Gabor period ($\sigma^2 \cdot f = 2$) and was normalized to an energy unity. The convolution of a signal $X(\tau)$ with this wavelet function is of the form:

$$S(t, f) = \int_{-\infty}^{+\infty} X(\tau) \cdot \Psi_{t,f}^*(\tau) d\tau$$

, where $*$ denotes the complex conjugate.

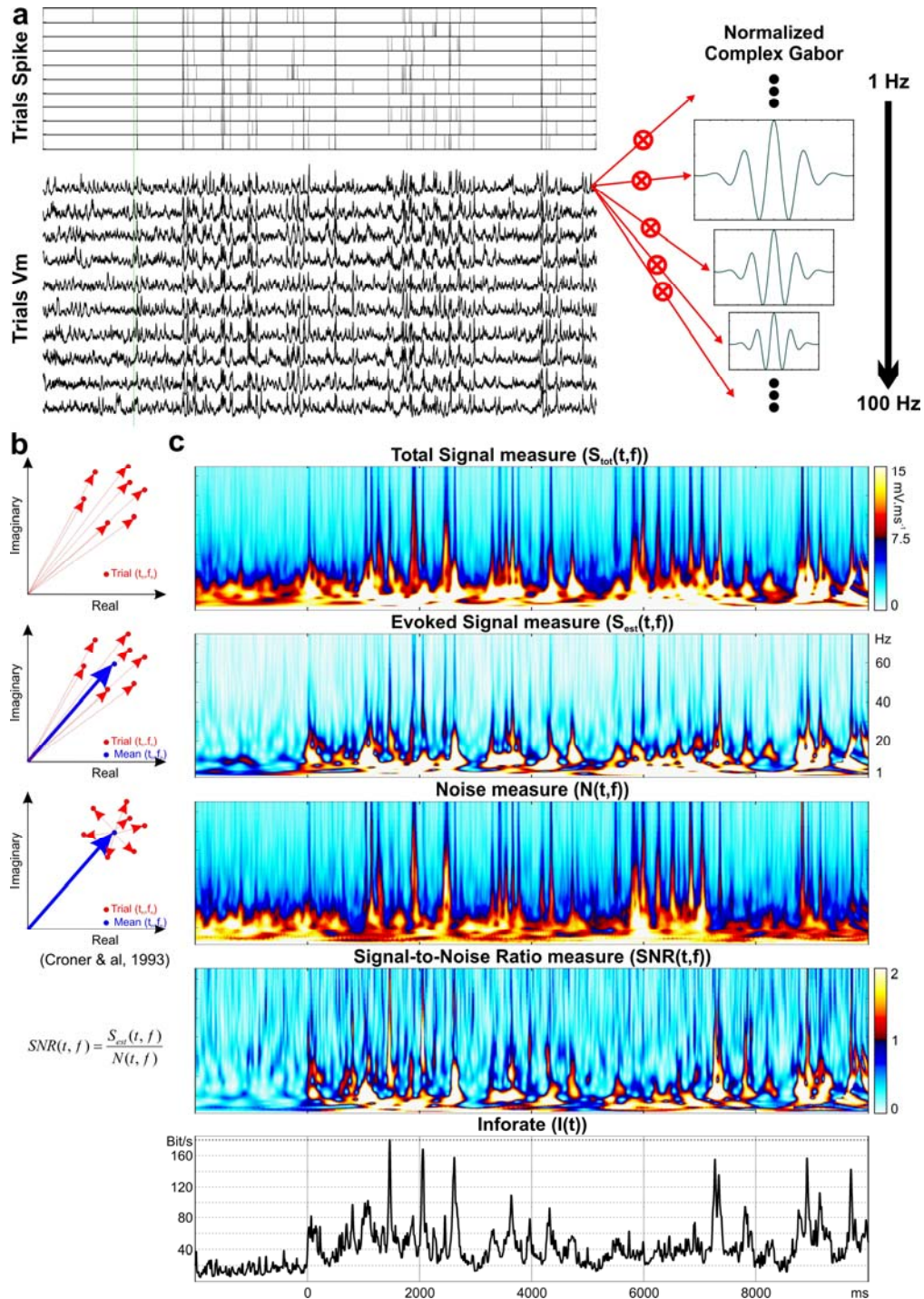


Figure 3.5.9: Time-frequency Signal-to-Noise Ratio estimation. *a*, another simple cell example of spiking and Vm response ($F1/F0 = 1.84$, different from figure 1 and 2) to grating animated by eye movement, and a schematic principle of Wavelet decomposition (wavelet are complex Gabor normalised to energy unity). *b*, Schematic principle of the measure of total signal, evoked signal, noise and SNR from the time frequency analysis. The red points represent the trials results of the wavelet convolution in the complex plane for one particular time and frequency. The Blue point represents the average trials vector which modulus gives the estimated signal. Noise is measured as the average distance of trials to this mean. *c*, The results of those measure when applied to the Vm responses presented in *a*.

From this time-frequency decomposition we derive several time-frequency dependent measures, signal power, noise power, total signal power, Signal-to-Noise Ratio (SNR this paper will mostly focus on), instantaneous coherence (phase dependent), and global coherence (phase independent). This method can be understood as an extension to the time-frequency domain and multiple frequency domain of the signal and noise estimation proposed by Croner & al (1993). For a given frequency and a given time, we define $S_i(t, f)$ as the complex result at time t and frequency f of the response and wavelet convolution for the trial i . The signal power S_{est} of the stimulus-locked waveforms is then measured as the squared modulus of the trials average vector of the wavelet transform in the complex domain (figure 3.5.9):

$$S_{est}(t, f) = \left| \langle S_i(t, f) \rangle_i \right|^2$$

Where angular brackets $\langle \rangle$ indicate the average across all trials and straight brackets $| |$ indicate the modulus. This measure when squared represent the energy of the stimulus related signal at a given frequency and time. The Noise power $N(t, f)$ is measured as the average distance between the trial vector and the trials average vector of the wavelet transform in the complex domain:

$$N(t, f) = \left\langle \left| S_i(t, f) - \langle S_i(t, f) \rangle_i \right|^2 \right\rangle_i$$

The total signal power $S_{tot}(t, f)$ is measured as the average modulus of the trials vector:

$$S_{tot}(t, f) = \left\langle \left| S_i(t, f) \right|^2 \right\rangle_i$$

Signal to Noise Ratio $SNR(t, f)$ is measured as:

$$SNR(t, f) = \frac{\left| \langle S_i(t, f) \rangle_i \right|^2}{\left\langle \left| S_i(t, f) - \langle S_i(t, f) \rangle_i \right|^2 \right\rangle_i} = S_{est}(t, f) / N(t, f)$$

$$SNR(t, f) = \frac{S_{est}(t, f)}{N(t, f)}$$

We made the important and reasonable assumption, only involved in the spike train decomposition, that in the case where no activity is evoked in all the trials at a given time and frequency ($S_i(t, f) = 0, \forall i$) the SNR value is nul.

Signal, Noise, and SNR power spectra are obtained averaging the function over time (the squared function in the case of SNR). The different power spectra are defined by:

$$F_{SNR}(f) = \int_{t_{start}}^{t_{end}} (SNR(t, f))^2 / (t_{end} - t_{start}) dt,$$

$$F_{Signal}(f) = \int_{t_{start}}^{t_{end}} (S_{est}(t, f))^2 / (t_{end} - t_{start}) dt ,$$

$$F_{Noise}(f) = \int_{t_{start}}^{t_{end}} (N(t, f))^2 / (t_{end} - t_{start}) dt .$$

Those measure represent the average energy of the signal, noise and SNR at a given frequency.

A Phase dependent coherence between pairs of signals recorded simultaneously is given by:

$$C(t, f) = \left\langle \frac{S_{xi}(t, f).S_{yi}^*(t, f)}{\sqrt{S_{xi}(t, f).S_{xi}^*(t, f).S_{yi}(t, f).S_{yi}^*(t, f)}} \right\rangle_i$$

This measure close to what exposed in Lachaux & al (1999), quantifies the level of synchronous activity in the two traces.

A two signal ($X(t)$ and $Y(t)$) global coherence (phase independent) measure is given by:

$$C(f) = \frac{\langle S_{xi}(t, f).S_{yi}^*(t, f) \rangle_t}{\sqrt{\langle S_{xi}(t, f).S_{xi}^*(t, f) \rangle_t \cdot \langle S_{yi}(t, f).S_{yi}^*(t, f) \rangle_t}}$$

This measure, corresponding to the classical coherence function, but estimated using time frequency wavelet decomposition instead of a Welch or other fixed time window Fourier decomposition, is measuring the level of similarity between two traces, as well as the level of linearity of the relation between the two traces.

3.5.9.3. SNR response comparison to a Rayleigh diffusion process: significance test

SNR measure significance is directly given by a comparison with a Rayleigh diffusion process, which corresponds to the most drastic signal fading process. The central limit theorem holds that, if there is sufficiently much scattering of the external input by the nervous system diffusion process, the channel impulse response will be pure noise (stochastic) and thus well-modelled as a Gaussian process. In this case without dominant component to the scatter, such a process will have zero mean and phase evenly distributed between 0 and 2π radians in the complex plane. The power, or envelope, of the channel response would therefore be Rayleigh distributed. The result of this process would have a cumulative

Rayleigh distribution function, given by: $f(x) = 1 - e^{\left(\frac{-1}{2}(\frac{x}{\sigma})^2\right)}$ that gives direct significant threshold values to our SNR power estimations.

3.5.9.4. Local time estimation of mutual-information

We propose a mutual-information upper-bound and time dependent estimation based on the classical Shannonian Gaussian channels. To do so, we consider that the neuronal response and neuronal noise have Gaussian probability distributions in the frequency domain for each time and that neuronal noise is additive. The information rate is given by (Shannon, 1948, Borst & Theunissen, 1999): $I_m(t) = \int_{f_0}^{f_{end}} \text{Log}_2(1 + (\text{SNR}(t, f))^2) df$ (figure 3.5.9). The possible presence of statistical dependencies or redundancy between the various times implies that the integral over time of this measure gives an upper bound estimate of the mutual information (that may be rectified by a redundancy estimation).

3.5.10. Evoked signal, noise, and total signal estimations as a function of the input complexity

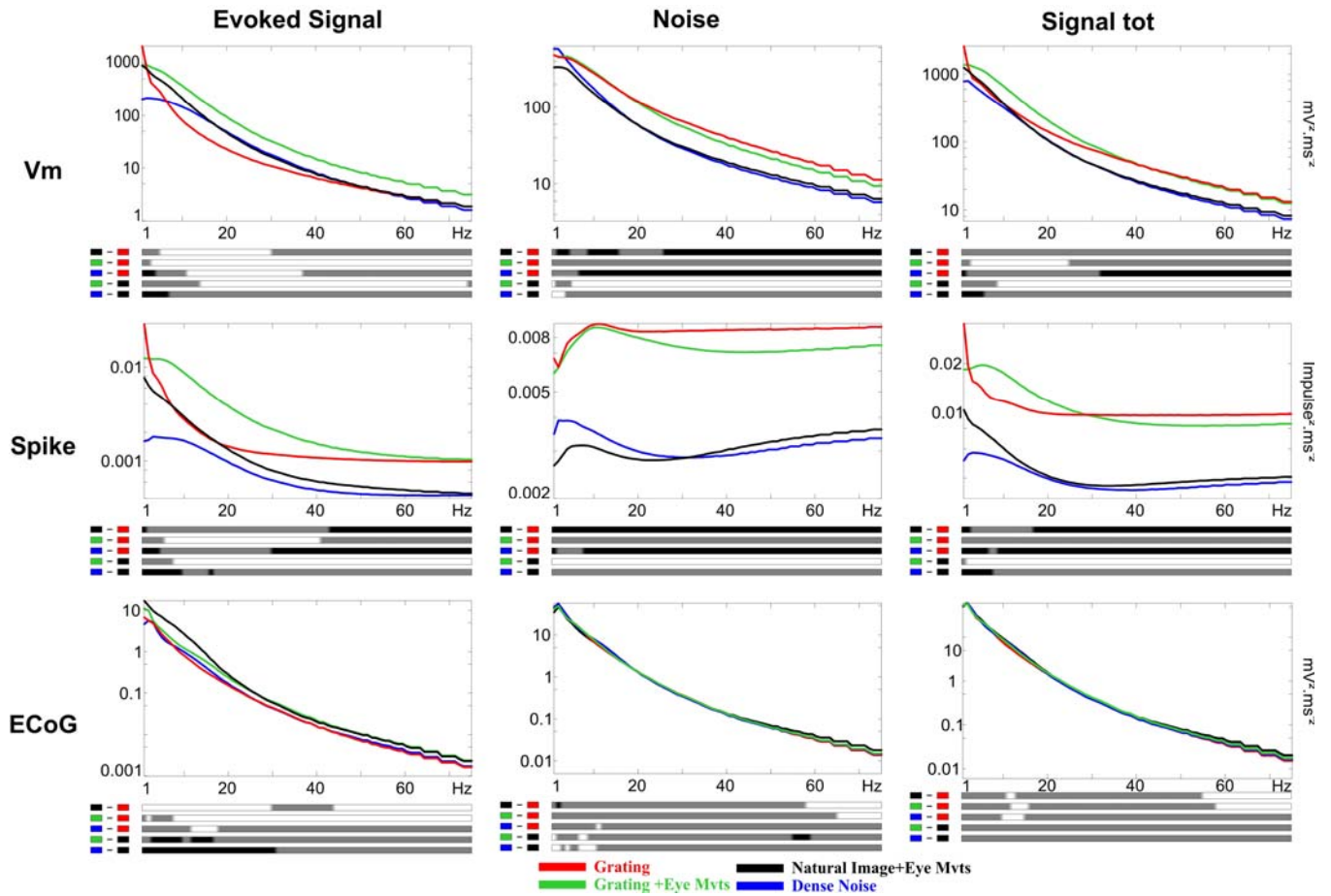


Figure 3.5.10: Evoked Signal, Noise and total Signal Power spectrum estimations for Vm, spiking and ECoG responses in the four conditions of stimulation. Each bar below abscissa expresses the result of a Wilcoxon paired test when comparing two stimulus conditions for each frequency (color code for “A” minus “B”, white : “A” significantly higher than “B”; grey : “A” not significantly different from “B”; black : “A” significantly lower than “B”, with $p < 0.05$).

3.5.11. Constrained cortical state and high SNR processing: a potential correlate to attentional and behavioral states

The internal ongoing states reflecting highly correlated cortical dynamic (Lampl & al, 1999), and probably produced by the cortical recurrence (Holcman & Tsodyks, 2006, Kenet & al, 2003) is manifested in intracellular recordings through stereotypical bistable Up and Down state synaptic activity sequences (Cossart & al, 2003, Shu & al, 2003) notably during rest or sleep phases (Steriade & al, 2001 for review). Those reverberating activity waves punctuated by silence states have been proposed to implement working memory states (Cossart & al, 2003). A common view considers that those internal reverberating activities reflecting “States of Mind” and expressing brain's autonomous internal context (Arieli, 2003, Fiser & al, 2004) are corrupting sensory responses and are further enhanced during vigilant states (Destexhe & Contreras, submitted). We recorded three cells presenting this peculiar spontaneous Up and down stereotyped dynamic during those particularly stimuli-irresponsible and highly-correlated cortical states (figure 3.5.11, cells analysed in this study including cell c of the figure 3.5.11 were recorded in more responsive cortical states for most of them). In the three cells, natural image animated by eye-movement stimulation induced long lasting Up-state responses. In contrast, for those peculiar bistable cortical state recordings, under dense-noise stimulation, two of the three cells presented a persistent UP and Down state internal dynamic unaffected by the sensory stimulation. In natural-like condition, the ECoG simultaneously recorded presented also an enhancement of high frequencies (ranging from 10 to 80 Hz depending on the cell) and an increase of the stimulus-locked trial-to-trial reliability of the overall ECoG signal and thus its SNR. In dense-noise condition, the sensory input had low or inexistent impact on the ECoG dynamic. The local (intracellular recording) and global (ECoG) cortical dynamic induced by natural-like stimuli remain the sleep-awake transition observed by Steriade & al (2001, figure 3.5.11d). Moreover such stimulus induced cortical state transition has already been reported in auditory system and in whisker-related barrel cortex. Complex dynamical sound sequences have been shown to have an alerting impact by clamping cortical activity into awake-like state and removing spontaneous ongoing correlations and slow-oscillations in auditory thalamus and cortex (Miller & Schreiner, 2000). In awake mice barrel cortex, the transition from rest to whisking exploration behavior induces a shift from low to high frequency EEG and from large slow to fast fluctuations in the Vm input (Crochet & Petersen, 2006).

figure 3.5.11: Natural-like condition induces prolonged cortical upstates correlated with an ECoG Beta-Gamma frequency enhancement. *a, b, c, present the three recorded cell with a spontaneous bistable activity (up and down states, a and b were not analysed in the present paper, because the four conditions could not be tested). 2 seconds of spontaneous activity followed by 4 seconds of stimulation are presented for, from top to bottom: single trial intracellular and simultaneous ECoG recordings in response to natural-like condition, superimposed Vm and ECoG trials (with their average in red), the total time-frequency spectrum (Phase independent) and SNR of the ECoG trials expressed as a z-score of the spontaneous activity. The bottom panels present the Vm, ECoG, signaltot(ECoG) and SNR(ECoG) responses obtained in dense-noise condition for those 3 cells. Only 8 and 4 trials could be recorded for cell a and b respectively, invalidating the time-frequency analysis for b. d, intracellular and EEG changes during sleep to awake transition recorded in the cat (taken from Steriade & al, 2001). e, EEG, whisker position and intracellular rest to whisking-behaviour transition in the awake mice barrel cortex (taken from Crochet & Petersen, 2006).*

The cortical states recorded in response to natural-like stimuli may be interpreted as approaching the awake state since they present:

- 1. sustained evoked up-state for the cells presenting a bistable during spontaneous activity (figure 3.5.11)
- 2. desynchronised ECoG in some cases
- 3. increase in beta-gamma range of the population response either observed in Vm or ECoG and notably at the time of the spike (figure 3.5.2 & 3.5.4)
- 4. a global desynchronisation during eye-movement period compared to on-going resting state and to saccadic period.

Those observation further sustain the vast literature on the implication of precise synchrony and high frequency oscillation mechanisms in the binding problem, visual feature integration, working memory activation (Singer, 2001, Engel & Singer, 2001, Singer & Gray, 1995, Gray 1999 for review) and studies relating large-scale transient desynchronisation to phenomenal perception (Rodriguez & al 1999). Moreover, SNR gain modulation or playing on the R_I / R_H cortical transfer, appear as a very simple mechanism to obtain attentional effects, either automatic (stimuli driven like in the pop-out effect) or supervised by feed-back or neuromodulation. In agreement, V1 receptive fields structure has been found to depend on the level of synchronisation of cortical states, leading to high resolution RFs in desynchronised states (with low spatial noise maps, Wörgötter & al, 1998). In psychophysics, Lu & Doshier (1998, 1998) have shown that attentional and learning mechanisms are consistent with a signal to noise ratio modulation of the cortical processing. At last, in the visual system visual imagery seems to be systematically correlated to eye-movement and “decorrelated” EEG states since those two criteria are the most obvious markers of the oniric REM sleep period. A complete and beautiful review on the possible link between phenomenological consciousness

and nervous system nonlinear dynamic can be found in (Cosmelli, Lachaux & Thompson, 2007).

3.5.12. Ordered redundancies, computational capacity and structural complexity definition

3.5.12.1. Ordered Redundancies and Entropies definition: Whole is less than the sum of its parts

Let consider a system S that can be decomposed or sampled into n variables S_1, S_2, \dots, S_n possibly taking N values. We emphasize that S has no predefined dimensions and can be considered in the general form of a spatio-temporal system (system with spatial memory of dimension n , and with temporal memory of dimension m , $S1_{t1}, S2_{t1}, \dots, Sn_{t1}, S1_{t2}, S2_{t2}, \dots, Sn_{t2}, \dots, S1_{tm}, S2_{tm}, \dots, Sn_{tm}$, or a m ordered Markov chain). In the case of cortex, the system is for example an area, the variables are the $n1$ neurons and their two possible state values during $n2$ discrete time bins (with $n = n1 * n2$), defining the cortical state and the ensemble is given by the several response trials. In genetic, the system is, for example, the DNA sequence, the variables are the n nucleotides and their four possible state values defining the genomic state and the ensemble is given by the several individuals of a generation (that share the same environment and initial conditions). The formalism is of course far more general. The entropy of S is given by:

$$H(S) = H(S_1, S_2, \dots, S_n) = \sum_{i=1}^{N^n} P_i(S) \text{Log}(1/P_i(S)) \quad (1).$$

Our aim of this chapter is to define rigorously redundancy, remarking that the information (entropy) of the system is less then the sum of its constitutive element, and quantifying the information between those elements that account for this difference (redundancy). This property, that we consider as a main characteristic of the world at our scale, is an important difference with the classical statistical physic framework. It implies that the system cannot be decomposed in sub-systems, or equivalently that the sub-systems are not a kind of absolute statistical equilibrium. It reflects the global out of equilibrium state of, at least, living organism world. Inspiring from Shannon and Weaver (1948) and Atlan (1979), we can define:

$$\boxed{H(S) = H_0(S)(1 - R(S))}, \quad (2).$$

Where $H_0(S) = n \text{Log} N$ (3), with N being the different possible values or state of S_i and where $R(S)$ is the redundancy present in the system. $H_0(S)$ is only defined by the intrinsic

dimensions of the system S (usually space and time), and is the system capacity. $H_0(S)$ is a constant of the system in the case of the nervous system, and is also the highest possible entropy, that can only be reached in the case where every component S_i are statistically independent (case where the S_i present random behaviour). Developing (1), redundancy R can be formulated into first and higher order redundancies:

$$R = \underbrace{\frac{1}{H_0} \left(H_0 - \sum_{i=1}^n H(S_i) \right)}_{\text{First-order-redundancy}} + \underbrace{\frac{1}{H_0} \left(\sum_{i=1}^n H(S_i) - H(S) \right)}_{\text{Higher-order-redundancy}} = R_1 + R_H = R_1 + R_2 + \dots + R_n, \quad (4)$$

It appears that : $H(S) = \sum_{i=1}^n H(S_i) - H_0 R_H$.., where

$$\sum_{i=1}^n H(S_i) = \sum_{i=1}^n P(S_i) \log(1/P(S_i)) = \sum_{i=1}^n \sum_{j=1}^N P_j(S_i) \log(1/P_j(S_i))$$

We can express ordered redundancies and ordered entropies as following: $H_1(S) = \sum_{i=1}^n H(S_i)$,

(6) the first order entropy of $H(S)$, $R_1 = \frac{H_0 - \sum_{i=1}^n H(S_i)}{H_0} = \frac{H_0 - H_1}{H_0}$, (7), and the general

form: $H_i = H_{i-1} - H_0 R_i$ and $R_i = \frac{H_{i-1} - H_i}{H_0}$ (8)

H_i decreases with i : $H_i \geq H_{i+1}$. It appears that $H(S) = H_n$ or equivalently for large n $\lim_{i \rightarrow n} H_i = H(S)$. R_n can be expressed in term of Mutual information between the n variables.

An expression of ordered redundancies can be proposed as:

$$H_0 R_1 = \frac{H_0 - \sum_{i=1}^n H(S_i)}{H_0} = 1 - \frac{\sum_{i=1}^n H(S_i)}{H_0}$$

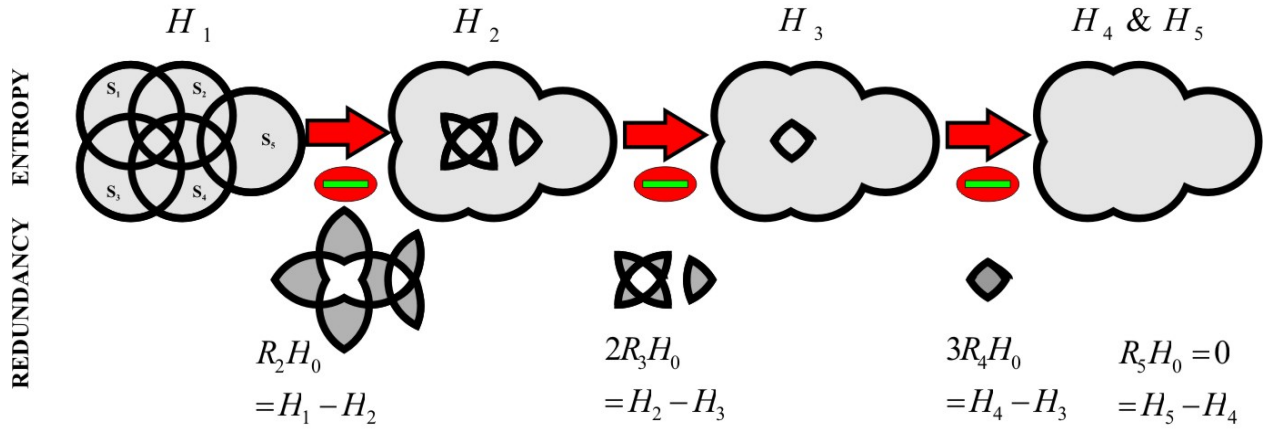
$H_0 R_2 = \sum_{j=1}^n \sum_{i=1}^n I(S_i; S_{j \neq i} | S_1, S_2, \dots, S_{a \neq i, j}, \dots, S_n)$ (sum of the mutual information between all pairs of variables knowing the other variable).

$\frac{H_0 R_3}{2} = \sum_{k=1}^n \sum_{j=1}^n \sum_{i=1}^n I(S_i; S_{j \neq i, k}; S_{k \neq i, j} | S_1, S_2, \dots, S_{a \neq i, j, k}, \dots, S_n)$ (sum of the mutual information between all triplets of variables knowing the other variable).

$$\frac{H_0 R_4}{3} = \sum_{l=1}^n \sum_{k=1}^n \sum_{j=1}^n \sum_{i=1}^n I(S_i; S_{j \neq i, k, l}; S_{k \neq i, j, l}; S_{l \neq i, j, k} | S_1, S_2, \dots, S_{a \neq i, j, k, l}, \dots, S_n)$$

etc... until $\frac{H_0 R_n}{n-1} = I(S_1; S_2; \dots; S_n)$

A simple representation of this redundancy decomposition is given using Venne diagrams:



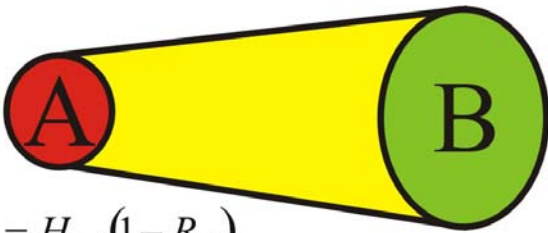
This paradigm, sharing many similarities with the holographic theory, notably its entropic bound (Bekenstein, 2003), can be applied to any system that can be decomposed into elementary probabilistic constituents. Moreover, this decomposition shares, at least in the spirit, an interesting similarity with the information geometry framework developed by Amari (1999, 2001) and the connected information measure proposed by Schneidman & al (2003), which may give a pragmatic way to estimate $H_0 R_H$ using maximum entropy principle). As reviewed recently (Amari & Nakahara, 2006), studies on nervous system correlations are embedded in a coding/decoding framework. In contrast, the framework proposed here, in agreement with the phenomenological point of view (Varela, 1989, 1999, O'Regan & Noe, 2001), only considers a single unsupervised and “non-representational” process. Coding-decoding paradigm implies intrinsically a Homunculus or dualistic paradigm: an autonomically predefined or self-generated code-language. Instead, our approach considers only the dynamic of the system states which holds at the same time the code and the meaning of the code.

3.5.12.2. Mutual information between systems

We can now consider the case of two systems exchanging information, and the focus on R_1 and R_H distinction is sufficient for our purpose here. Let's define an input system A, with an information $H(A)$, that exchanges information to a system B represented by an information $H(B)$, and consider the channel between A and B. Mutual information in between A and B is given by: $I(A, B) = H(A) - H(A/B) = H(B) - H(B/A)$, (9), where

$H(A/B)$ represent the equivocation and $H(B/A)$ represents the ambiguity. This relations is far more general than the classical application to channel with noise case (Shannon, 1948), and holds for the mutual information between objects case (Kolmogorov, 1968). $H(B/A)$ represents whatever entropy the system B has that did not come from the system A. In the case here the systems A and B can be considered as isolated, $H(B/A)$ represent the probabilistic behaviour of information transmission in between A and B corresponds to the entropy of noise H_{noise} . Considering the relation expressed in (5), $I(A;B)$ can be expressed as:

$$I(A;B) = \sum_{i=1}^n H(B_i) - H_{0B} R_{HB} - H(B/A) = \sum_{i=1}^n P(B_i) \text{Log}(1/P(B_i)) - H_{0B} R_{HB} - H(B/A), \quad (10)$$



$$H_A = H_{0A}(1 - R_A) \quad H_B = H_{0B}(1 - R_B)$$

$$I(A,B) = \sum_{i=1}^n H(B_i) - H_0 R_H - H(B/A)$$

This relation points out that noise or ambiguity and higher order redundancies are acting on mutual information in the same way. In fact, mutual information in between the two systems is already a redundancy. It gives also an interesting and intuitively satisfying definition of the efficiency of B to represent A:

$$\varepsilon = \frac{I(A;B)}{H_{0B}} = \frac{\sum_{i=1}^n H(B_i) - H_{0B} R_{HB} - H(B/A)}{H_{0B}} = 1 - R_B - \frac{H(B/A)}{H_{0B}}, \quad (11)$$

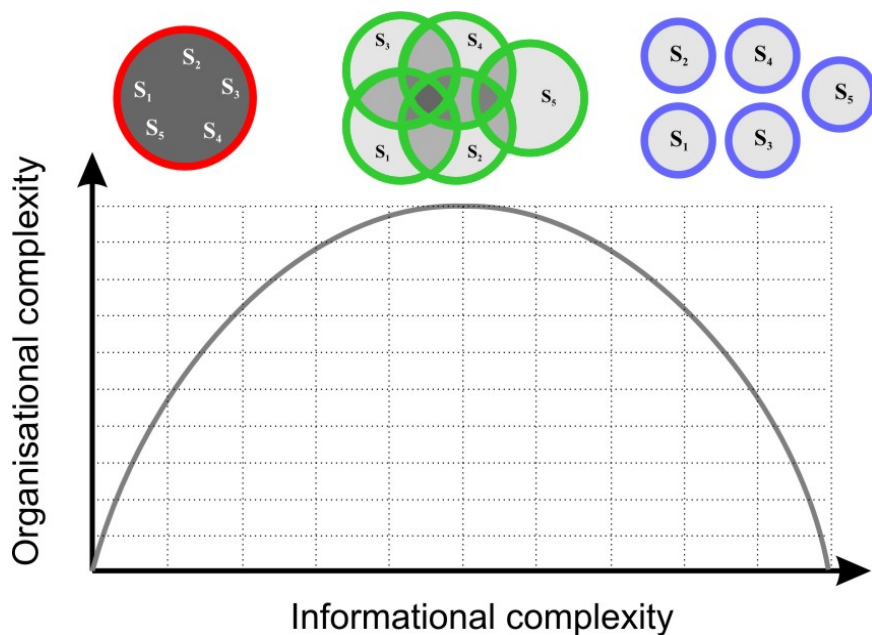
$H(B/A)$, ambiguity or noise, is participating to efficiency and mutual information exactly in the same way as redundancies. The efficiency measure classically used in neurophysiology (and we've been using in associated study, Rieke & al, 1997) is slightly different, but is also pertinent. Its expression in this framework is given by:

$$\varepsilon_1 = \frac{I(A;B)}{\sum_{i=1}^n H(B_i)} = \frac{1 - R_B - H(B/A)/H_{0B}}{1 - R_{1B}} = \frac{\varepsilon}{1 - R_{1B}} \quad (12) \text{ and thus represents a ratio in between}$$

the total redundancy with the first order redundancy ($\varepsilon_1 \rightarrow 0$ when $R_1 \ll R + \frac{H(B/A)}{H_{0B}}$ and $\varepsilon_1 \rightarrow 1$ when $R_1 = R$ and $\frac{H(B/A)}{H_{0B}} = 0$).

3.5.12.3. Logical depth measure or organisational complexity

Complementing the notion of Algorithmic Complexity, Bennett proposed the Logical Depth (Chaitin, 1977, Bennett, 1985, 1988) a measure of the time required by a universal Turing machine to generate the string or system from a random input (in number of computational steps, that is equivalent to a computational distance in between the uncompressed string or object and its maximally compressed form), to quantify the degree of organisation of a system. We propose to derive a related measure from the ordered redundancy expression. One could find in the simple measure $H_0 R$ an expression of the logical depth, but it do not catch the intuitive fact that repetitive systems (uniform, highly low order redundant system) are less organised or easier to compute compared to living systems which present a wide variety from local to long scale correlations and thus has a considerable logical depth (Bennett, 1988, Li & Vitanyi, 1997). Thus, logical depth would intuitively rather correspond to a diversity or disparity of the redundancy along the different orders. We propose a quantification of the organisational complexity that intuitively corresponds to Logical Depth. The proposed measure corresponds to the entropy of the R_i , and quantifies the dispersion of the structure among the different orders.

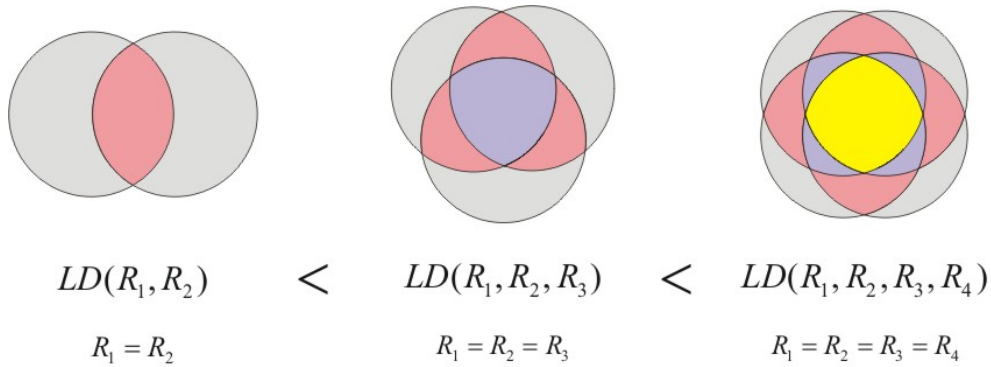


This measure is on our opinion important, since it considers that there is an “information” in the redundant part of a system (object etc...), and that this information is probably the one biologists and any observer are mostly interested in, since it quantifies organisation.

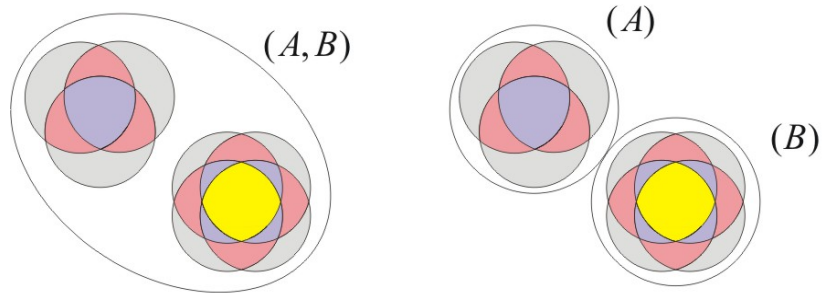
3.5.12.4. Proposition of Logical Depth measure

We propose the measure of logical depth introduced by Bennett to be a continuous function of the R_i . Using Shannon reasoning (1948), we propose a measure of LD to require the 3 following properties (monotonicity, independence, and branching):

1. If the n order redundancies are equal ($R_i = \frac{R}{n}$) then LD is a monotonically increasing function of n .



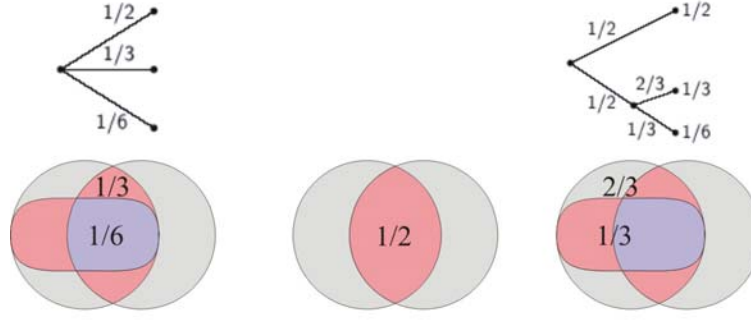
2. If the system, object or string is composed of two independent parts then the total LD of the string is equal to the sum of the two independent part LD's.



$$LD(A, B) = LD(A) + LD(B)$$

$$\Leftrightarrow A \& B \cdot \text{independent}$$

3. If redundancy is broken down into higher redundancies, the original LD should be the weighted sum of the individual values of LD .



$$LD(\frac{1}{2}, \frac{1}{3}, \frac{1}{6}) = LD(\frac{1}{2}, \frac{1}{2}) + \frac{1}{2} LD(\frac{2}{3}, \frac{1}{3})$$

The only function satisfying the 3 above assumptions is (Shannon, 1948):

$$LD(S) = -k \sum_{i=1}^{n-1} R_i \text{Log} R_i$$

From the everyday semantic point of view, the measure of logical depth appears more related to the intuitive and common notion of complexity (or biological complexity at least) that is neither maximal order nor disorder but something lying in between, whereas Descriptive complexity appear to us more closely related to the common notion of randomness. Logical depth is a measure of the level of organisation of a system, uniform or fully random systems are presenting low values of logical depth. Scale free systems are a class of systems that display obviously a large logical depth. It has to be noted the particularity of the redundancies compared to probabilities is residing in the fact that their sum can be less than one. However a sum equal to one is not required for the demonstration of the entropy as the only function satisfying the 3 exposed assumptions (Shannon, 1948 Appendix 2).

This measure is invariant to any transformation that conserves distance or mutual information. The fact that two systems present the same entropy is not sufficient to decide if the two systems are isomorphic (Falcioni & al, 2003). In this context it can be expressed by the fact that two systems presenting the same global amount of redundancy are not equivalent computationally or Algorithmically since their redundancy organisation or the computational work to generate them are not the same. An interesting idea, our intuition supports, would be that entropy combined with Logical Depth are sufficient to reveal isomorphism.

3.5.12.5. Logical depth increase ?

We can now ask what kind of behaviour Logical Depth is displaying across time. Let S_{t+1} and S_t included in a Markov chain $S_t \rightarrow S_{t+1}$:

$$\begin{aligned} LD(S_{t+1}) - LD(S_t) &= k \sum_{i=1}^{n-1} R_i(S_t) \text{Log} R_i(S_t) - k \sum_{i=1}^{n-1} R_i(S_{t+1}) \text{Log} R_i(S_{t+1}) \\ &= k \sum_{i=1}^{n-1} R_i(S_t) \text{Log} R_i(S_t) - R_i(S_{t+1}) \text{Log} R_i(S_{t+1}) \end{aligned}$$

We can only consider the sign of $R_i(S_t) - R_i(S_{t+1})$ whatever n. R_n are sums of various mutual information terms multiplied by a positive constant. Since relative entropy and Mutual information always decrease (to verify): $I(X_t, Y_t) \geq I(X_{t+1}, Y_{t+1})$ (Cover & Thomas, 1991 show it for relative entropy), we can write for any Markov chain:

$$LD(S_{t+1}) - LD(S_t) \geq 0$$

It would mean that the level of organisation of a system always increases. In fact, looking at the evolution of living systems on earth, it may appear plausible. If true, it is a justification of self-organising processes. In other word, the structure of a system is naturally getting more and more complex. Although it appears plausible from a global observation of the evolution of our world, and even tautological if this measure really corresponds to Bennet's logical depth (which is a measure of "time"), a simple experience of thought intuitively prones to the opposite conclusion, that this rule is false. The problem comes from the fact that redundancies sum is not equal to one and is decreasing as the entropy increases. In fact, this increase holds at least in the very specific case where the redundancy is conserved (equilibrium case). It would be interesting to know precisely under which condition such increase is observable. For example, one could expect a highly redundant homogeneous (redundancy represented in the highest orders) system to necessarily undergo a preliminary first phase of LD increase.

3.6. Non-linear control of the temporal precision of the neural code by eye-movements dynamics in visual cortex

(to be Submitted, Baudot, P., Levy, M., Marre, O., and Frégnac, Y.)

3.6.1. Summary

The stereotyped dynamics imposed on the retinal flow by eye movements, both during saccades and fixation, are a prerequisite for visual perception. However, their impact on the processing of visual information in primary visual cortex (V1) remains unclear. By recording intracellularly V1 neuron responses to various simplifications of the natural optic flow, we show that eye movements recruit nonlinearities which increase the temporal precision and reliability of membrane potential and spiking responses. Nonlinearities and gain control expression, involving center-surround interactions led to a temporal modulation of the natural input encoding. In eye-movements-like cases, cortical interactions strongly dominate the intracellular responses, and linear predictions greatly underestimate the measured response. This enhanced selectivity to natural statistics, which was associated with the recruitment of delayed inhibition and an amplification of the beta-gamma range frequencies, is further amplified by the spike threshold and translated into sparser, more precise spikes. Our results suggest that V1 nonlinearities, both facilitatory and suppressive, such as centre-surround interactions or contrast gain controls are adapted to the temporal and reliable encoding the saccadic and fixational eye-movement exploration of natural scenes.

3.6.2. Introduction

In recent years, natural stimuli have become a tool of choice for the characterization of sensory processing (Theunissen & al, 2001). The relative contribution of linear and non-linear processes in the response of V1 cells and notably in the integration of its synaptic input is still a matter of debate (Anderson et al. 2000; Jagadeesh et al. 1993, 1997; Lampl et al. 2001, Carandini & al. 2005). Discrepancies in the estimates of Receptive Fields (RFs) obtained under natural vs. artificial stimulation (David & al, 2004, Sharpee & al, 2006), and failures of linear or even elaborate static L-N-P models to correctly predict the actual response to natural images (Smyth & al, 2003, Felsen & al. 2005), suggest that even without eye movement dynamics, natural stimuli recruit V1 integrative non-linearities in some specific way, yet to be identified (see Felsen & Dan 2005 for a review). The concomitant stimulation of the “silent” surround and active visuomotor exploration seem to increase the sparseness of the cortical

representation and reduce activity correlation across neurons (Vinje & Gallant, 2000). Theoretical studies further suggest that efficient encoding of natural *spatial* statistics can account for V1 nonlinearities such as gain controls and surround suppression (Schwartz and Simoncelli 2001, Rao and Ballard 1999), even though the suppressive or facilitatory nature of centre-surround interactions remains controversial (Series & al, 2004). The processing of natural *temporal* statistics however has received less attention, since most thalamic and cortical studies on the functional impact of natural scenes have used randomized sequences of static scenes (but see Vinje and Gallant, 2000).

During natural vision, the retinal flow dynamics is dominated by eye-movements, whose abrogation leads to a rapid perceptual fading (Ditchburn & al, 1952). Microsaccades for instance, whose speeds are ideally suited to activate the early visual pathways, prevent Troxler fading (Martinez-Conde 2006) and elicit bursts of spikes in Macaque LGN and V1 cells (Martinez-Conde 2004). These fixational eye movements can remove a part of the correlation imposed by the spatial statistics of natural images on the response of linear spatiotemporal models of LGN cells (Rucci et al., 2000). Clues of a fit between eye movement dynamics and V1 processing are not limited to linear properties. The rapid adaptation observed in V1 complex cells (Muller et al. 1999), may enhance feature discrimination and encoding during saccadic exploration of a natural scene (Dragoi et al. 2002). Moreover, transient high-contrast stimuli induce quick, brisk (Gawne & al, 1996) and temporally coded spike responses (Mechler et al. 1998), presumably through the recruitment of a specific intracortical dynamic contrast gain control process (Albrecht and Geisler 1991, Bonds 1991).

In the previous chapter (Chapter 3.5), we presented evidence showing that the reliability and temporal precision of the response of any given cortical cell depend on the complexity and ecological relevancy of the input statistics present in the visual field and its similarity with the every-day experienced environment. Since the various visual input contexts we explored, i.e. luminance gratings (drifting or animated by eye movements), dense noise and natural movies, differ primarily by their spatiotemporal higher order statistics, nonlinearities in network-driven interactions appear as a likely substrate for the contextual-dependent modulation of the neural code we observed. The aim of the present study is to identify such non-linearities and their role in the control of the temporal precision of the neural response, and to precise their recruitment requirements in relation with the various classes of eye-movements which are used to explore our sensory environment.

3.6.3. Results

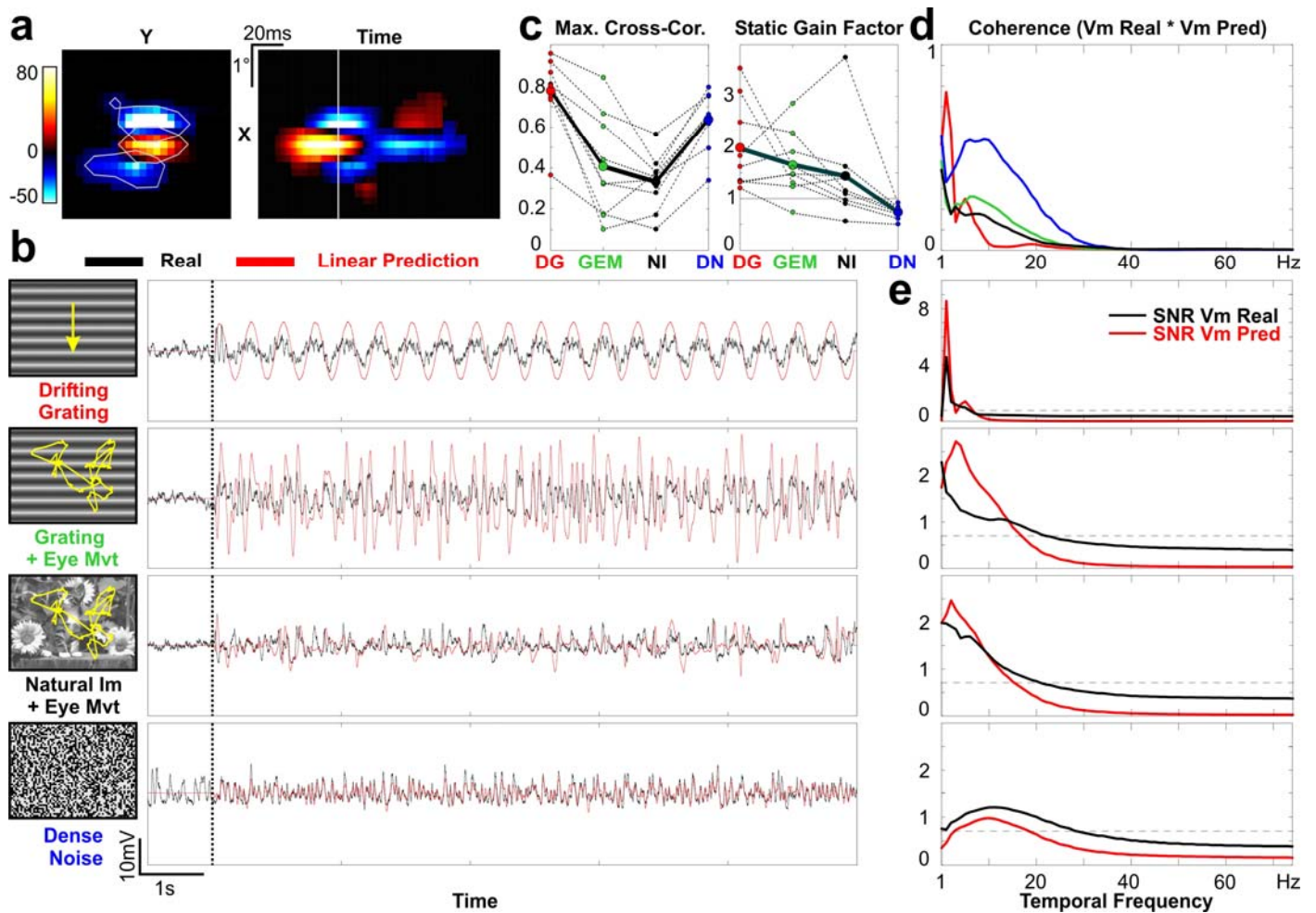


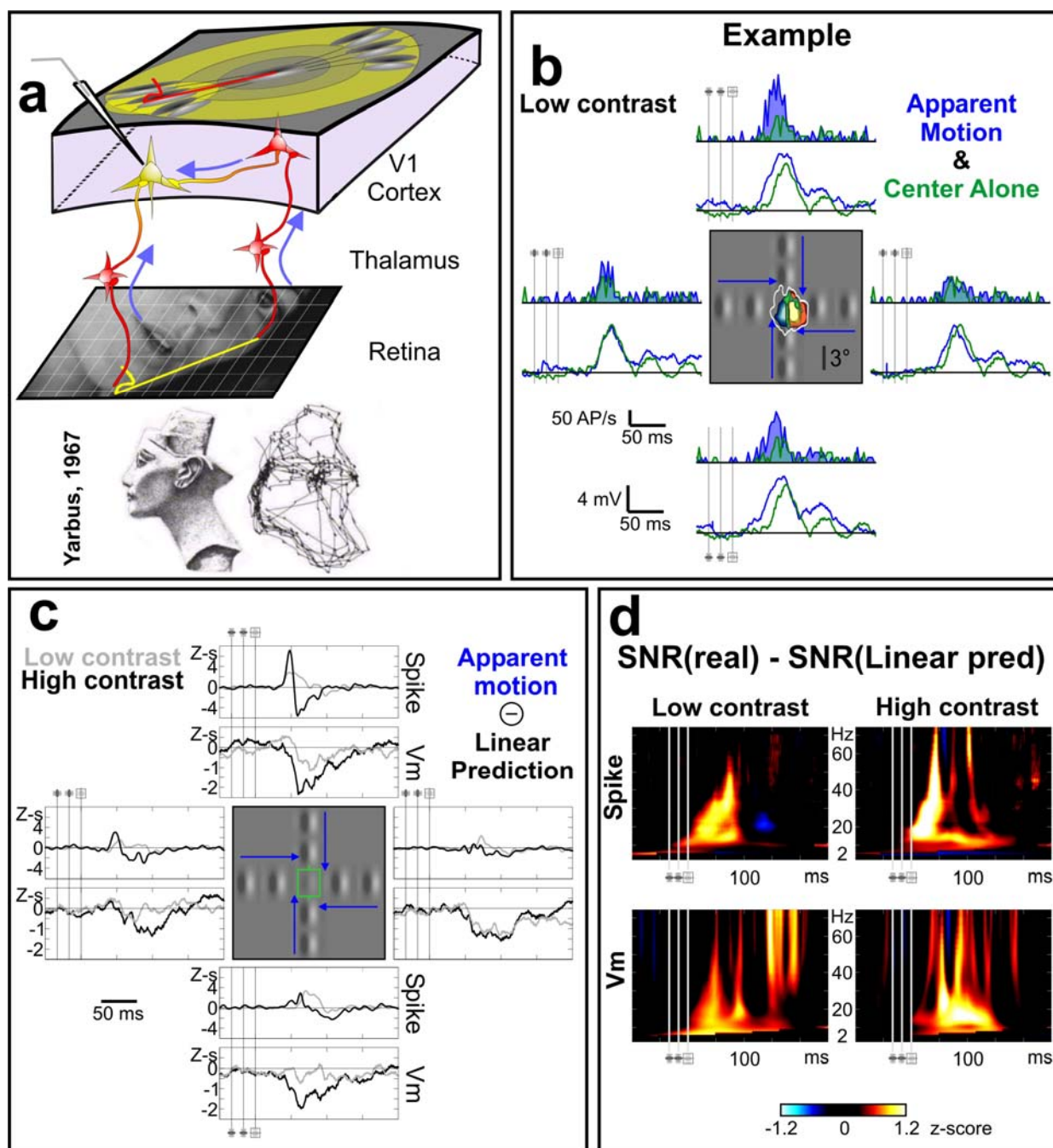
Figure 3.6.1: Nonlinearities induced by stimuli animated by eye-movements drastically reshape the Vm temporal waveform. **a**, Example of a simple cell subthreshold receptive field spatial map (X,Y) and spatiotemporal map (X,T), obtained using dense white noise stimulus and used to measure the linear prediction to the various stimulus movies (colour scale in z-score value against spontaneous activity). **b**, Example for the simple cell (a) of average Vm and linear prediction subthreshold (Vm) responses to four classes of stimuli of increasing complexity: a grating of optimal orientation and spatial frequency drifting at the optimal temporal frequency (here 2Hz), the same grating animated by a sequence of modelled eye-movement including saccade and fixational eye-movement, a natural image animated by the same eye-movements sequence, and a sequence of dense binary white-noise. **c**, Maximum of the cross-correlation and static gain factor (see Methods) between averaged Vm and the linear prediction of the response for the 9 simple cells (mean in bold). They quantify respectively the similitude of the waveforms shapes and the modulation of the average energy of the waveforms by the nonlinearities. **d**, Coherence between the linear prediction and the recorded average Vm averaged across cells, quantifying the waveform shape similitude and the consistency of the linear fit as a function of the frequencies. **e**, Nonlinearities suppress the low frequencies and increase the high frequency responses component: comparison of the temporal spectra of average Vm and the linear prediction averaged across cells (dashed line represents the $P=0.005$ significance threshold value given by the Rayleigh distribution). The bottom bars show in white the frequency range for which linear prediction is significantly higher than the observed average Vm and in black the opposite significant relation (Wilcoxon population cell paired test ($P<0.005$) on significant spectral values of individual cells ($P<0.005$, Rayleigh statistics)).

To do so, we predicted the intracellular response of Simple cells to the stimuli presented in the companion paper (drifting gratings, DG, gratings animated with eye movements, GEM, natural image animated with eye movements, NI and dense noise DN), from the spatiotemporal subthreshold receptive field obtained with DN stimulation (figure 3.6.1A, see methods). As could be expected from earlier studies, the recorded traces show deviations from linearity in all 4 conditions (figure 3.6.1bcd). However, the pattern and amplitude of these failures depend on the stimulus statistics: in the DG and DN conditions, nonlinearities affect the amplitude but preserve the time course of the predicted traces, whereas in the more natural conditions (NI and GEM), they drastically reshape the intracellular responses. Across the population, the peak of the cross-correlation between the observed and the predicted membrane potential confirms the greater impact of V1 nonlinearities on the dynamic of the responses to natural stimuli: it is minimal for the NI and the GEM, and maximal for the DG and DN. The coherence between the predicted and measured signals, which is an index of how linear is the transformation between the two signals, indicates that for stimuli animated by eye-movements, high temporal frequencies in the linear prediction undergo a strongly dynamic nonlinear processing (figure 3.6.1c, compare to DN condition).

To evaluate the contribution of these nonlinearities to the subthreshold response Signal to Noise Ratio (SNR(Vm)), we repeated the time-frequency analysis using the linear prediction as signal (SLPNR(Vm), see methods). Figure 3.6.1e shows that the SLPNR(Vm) spectra cross the measured SNR(Vm) spectra around 10-15Hz for the NI and GEM conditions, whereas such frequency dependency is less present for the stimuli having stationary statistics. We conclude that the nonlinear processing of natural statistics reduces the SNR at low temporal frequency, and increases it at high temporal frequencies.

Figure 3.6.2 : Center-surround directional selectivity for saccadic-like apparent motion and the temporal and SNR modulation of the response. *a*, Schematic representation of a visuo-oculomotor model of V1 processing, sequentially integrating visual information along spatial long range (saccade) and short range (fixational movement) eye-movements. During saccadic high speed long range movement, V1 neurons by the mean of their spatiotemporal association field integrate selectively the visual information iso-oriented to the saccadic motion along their collinear axis (co-aligned with the motion path), whereas during fixation they integrate the visual information on low spatial scales and low speed corresponding to their classical direction selectivity (classical direction preference axis across the discharge field width). Furthermore, the eye-movement scanpath is correlated to the image features, notably the contours for saccades path in this image exploration. The bottom cartoon, taken from Yarbus (1967), illustrates the eye-movement pattern of a Human observer (right panel) and the corresponding photograph (left panel). *b*, example of a simple cell response to apparent motion stimuli (blue colour) and center only control (green colour), for the low contrast center condition, exemplifying a collinear surround facilitation. Picture in the middle represent the four tested axis of apparent motion superimposed with the RF map obtained with sparse noise (ON responses in red scale colour, OFF responses in blue scale, depolarising field extent white line). Gabor patches were

sequentially flashed from the surround to the center. **c**, The biphasic temporal profile of center-surround apparent motion nonlinearity, and its directional collinear selectivity and modulation by the contrast (population analysis $n = 23$). The temporal waveforms of the nonlinearity are calculated for each cell by subtracting the linear predictor (Center alone + surround alone responses) to the real response observed to the full apparent motion sequence, both at the spiking levels (top panels) and at the Vm level (bottom panels). Here, we present the averaged across cells temporal waveforms of the nonlinearity expressed as a z-score of the spontaneous activity. The temporal profile of the nonlinearity is given for the low contrast center (grey colour) and the high contrast center (black colour). **d**, apparent motion nonlinear modulation of the SNR the responses. To measure the center-surround SNR modulation gain, each trials of the center alone condition are summed with those of the surround alone condition to obtain a pool of linear predictor trials, on which we could apply the SNR time-frequency analysis. The time-frequency apparent motion nonlinear SNR gain is then obtained by subtracting the apparent motion SNR to the linear predictor SNR, expressed as a z-score of the spontaneous activity (significant threshold calculated independently for each frequency z-score $p > 0.001$), and averaged across cells.



Taking into account the low-pass filtering occurring at the retina, the motion flow during saccade selectively and precisely preserves the spectrum of the image components which are iso-oriented with the motion path, whereas all the other orientation components are blurred (Geisler, 1999, 2001, Barlow & Olshausen, 2004). The correlation of the saccadic path with the image contours suggests that this selective blurring may be used as a strategy by the visual system to analyse and explore spatiotemporally the environmental scene (Yarbus, 1967, figure 3.6.2a). Moreover, saccadic displacements in the Cat (Collewijn, 1977), when projected in cortical coordinate space, have a speed similar to that of horizontal intracortical propagation as measured by intracellular (Bringuier et al. 1999) or imaging techniques (Grinvald et al, 1994).

We therefore elaborated an experimental protocol aiming specifically at demonstrating whether the apparent motion of an elementary oriented stimulus during a simulated saccade could indeed recruit centre-surround interactions in V1 cells along the unblurred collinear axis of the cell. Our prediction was that a facilitatory effect was likely to occur when the saccadic motion path was aligned with the orientation preference axis of the recorded receptive field. Three identical Gabor patches, with orientation, spatial frequency and phase optimized for the recorded cell, were flashed sequentially with their location progressively displaced from the “silent” surround of the receptive field towards its centre (apparent speed ranging from 175 to 475 °/s, mean 329°/s). The four polar axis of the cell RF (along the orientation and width axis defined by the discharge field) were explored, and the contrast of the centre patch was also varied (“low” or “high” contrast conditions in figure 3.6.2).

The center-surround interaction observed was found to be selective to the axis collinear with the receptive field orientation preference, and more particularly to one polar end-zone. This centre-surround nonlinearity presented a stereotyped biphasic temporal profile with an initial facilitation followed by a suppression. This effect can be visualized by subtracting the observed responses to the full sequence of apparent motion and the linear predictor given by the sum of the surround-only and the centre-only responses (figure 3.6.2bc). This nonlinear biphasic modulation, is contrast dependent both in its timing and amplitude, and leads to both a net time-average facilitation (example figure 3.6.2b, 41%) and suppression (59%) for of the center response when at low contrast, and to a net suppression when at high contrast.

The intracortical horizontal origin of this effect is further attested by the fact that it is selective to the iso-oriented surround condition (cf. chapter 3.3) which corresponds to the anatomical bias in the connectivity pattern between orientation-selective columns and the timing

requirements fit with that required by an in-phase relation between feedforward and horizontal activation (Series et al, 2002): the boosting of the center patch response is expressed only for centripetal (surround to center) but not for centrifugal (center to surround) conditions. Another important feature is that this effect is accompanied by a transient nonlinear increase of the Vm and spike SNRs expressed mostly in the beta-gamma frequency range. Thus, our results demonstrate a new form of directional selectivity of the cortical RF for high speed motion, mostly expressed along the collinear axis defined by the orientation preference of V1 RFs. The recruitment of such interactions during virtual saccades would notably increase the temporal frequency bandwidth of subthreshold dynamics and the reliability modulation of the evoked responses. Such a kind of center-surround dynamic nonlinearity is likely to generate in V1 an elementary form of temporal encoding of saccadic-induced motion, which may be used or further transformed at a higher stage of coordinate transformation and visuo-motor integration (Gawne & al, 1996, Victor & Pupura, 1996, Mechler & al, 1998, Reich & al, 2001).

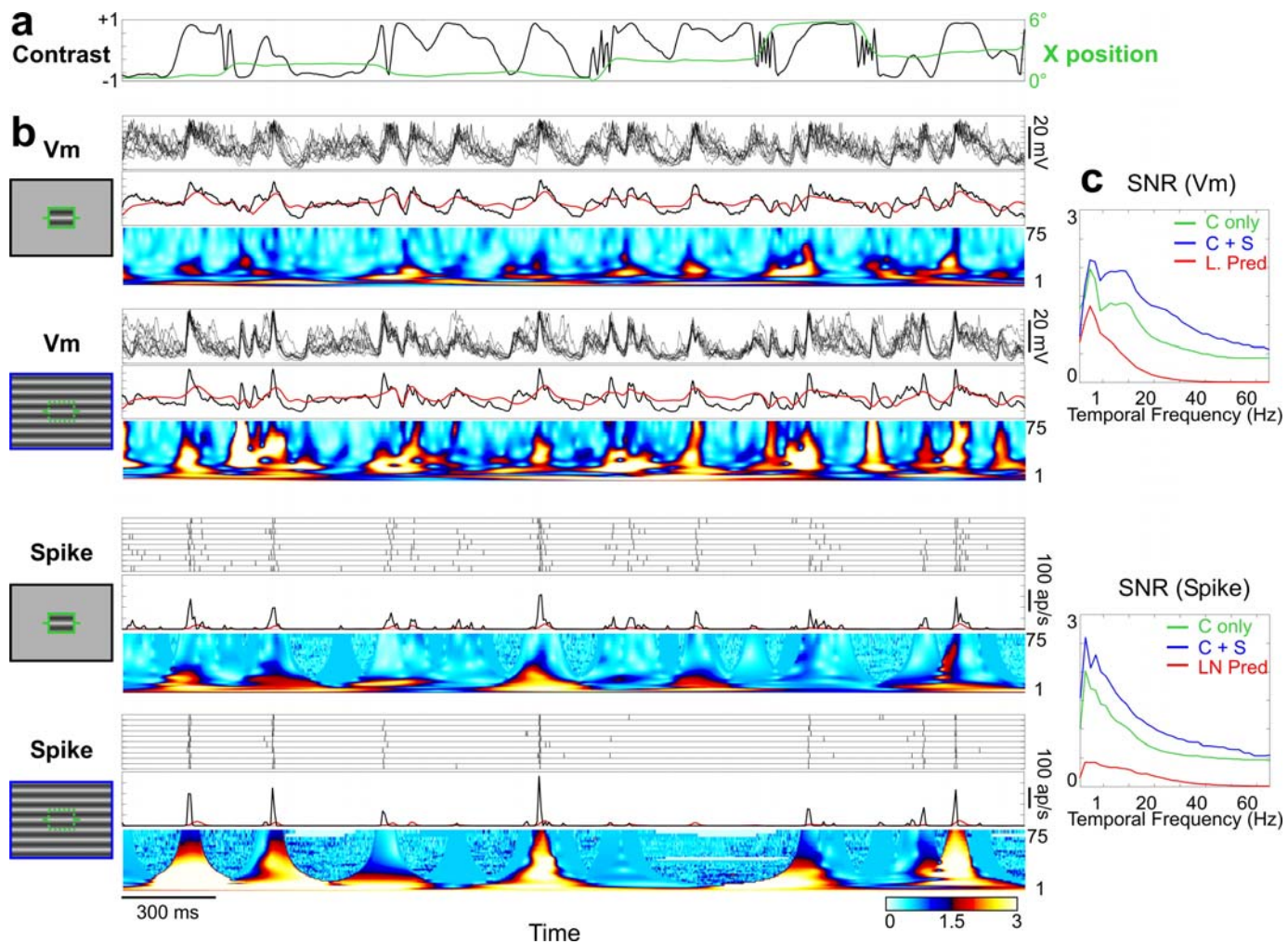


Figure 3.6.3 : Centre surround interactions and contrast gain control increase the trial-to-trial reproducibility and temporal precision of spiking responses and Vm trajectories. *a*, The stimulus (3s-long example) was a sinusoidal grating (of orientation, spatial frequency and phase optimized to fit precisely the spatial organization of the recorded Simple discharge field) whose contrast varied in time (black) such as to simulate the dynamics of the retinal flow produced by a realistic eye-movement trajectory (green, see Methods). In the centre-only condition, the stimulus was limited to the classical receptive field, whereas in the centre+surround condition, it extended over the non classical “silent” RF. *b*, The Vm and spiking responses for Center-only and center+surround responses (respectively shown in the 1st & 3rd rows vs. 2nd and 4th rows) are displayed for one simple cell ($F1/F0=1.26$) using three quantifications: individual trials, average (black) and prediction (red, Linear and L-N models for Vm and spike predictions respectively), and SNR time-frequency analysis (ordinates in Hz). *c*, Temporal frequency spectra of the integral over time of the SNR for the centre-only (green) and center+surround (blue) conditions, calculated from the observed and linearly predicted (red, see methods) spiking and Vm responses.

In order to further investigate the cellular mechanisms involved in the dynamic contrast gain control (CGC) during natural eye-movements and its centre surround dependency, we took advantage of the fact that a moving grating, can always be decomposed into the sum of two static, but contrast-modulated, gratings whose spatial and temporal phases are in quadrature (see Methods). We thus devised a new protocol, where a static grating corresponding to the cell preferred spatial phase was presented, and where its contrast was modulated in time such

as to simulate the local changes of contrast in the receptive field center produced by our virtual eye-movement sequences.

This new protocol was applied to one Simple cells, in two spatial contexts, either restricted to the classical discharge field or extending across both the centre and the “silent” surround of the RF. In the centre-only condition, the reliability and temporal precision of both intra- and extracellular responses depended on the stimulus history and were higher than those expected from the linear predictions. The recruitment of CGC by fast contrast dynamics (Mechler & al, 1998, Reid & al, 1992) was amplified when the surround of the receptive field was concomitantly stimulated: the membrane potential exhibited many more stimulus-locked events in the gamma temporal frequency range; most spike events became more precise (up to a few ms) while others, which were elicited in the center-only condition, were completely suppressed when costimulating the periphery, leading to sparser responses. The comparison with the linear predictions of the SNR, shown in Figure 3.6.3c, confirm that centre surround interactions nonlinearly increase the signal in the high temporal frequency range.

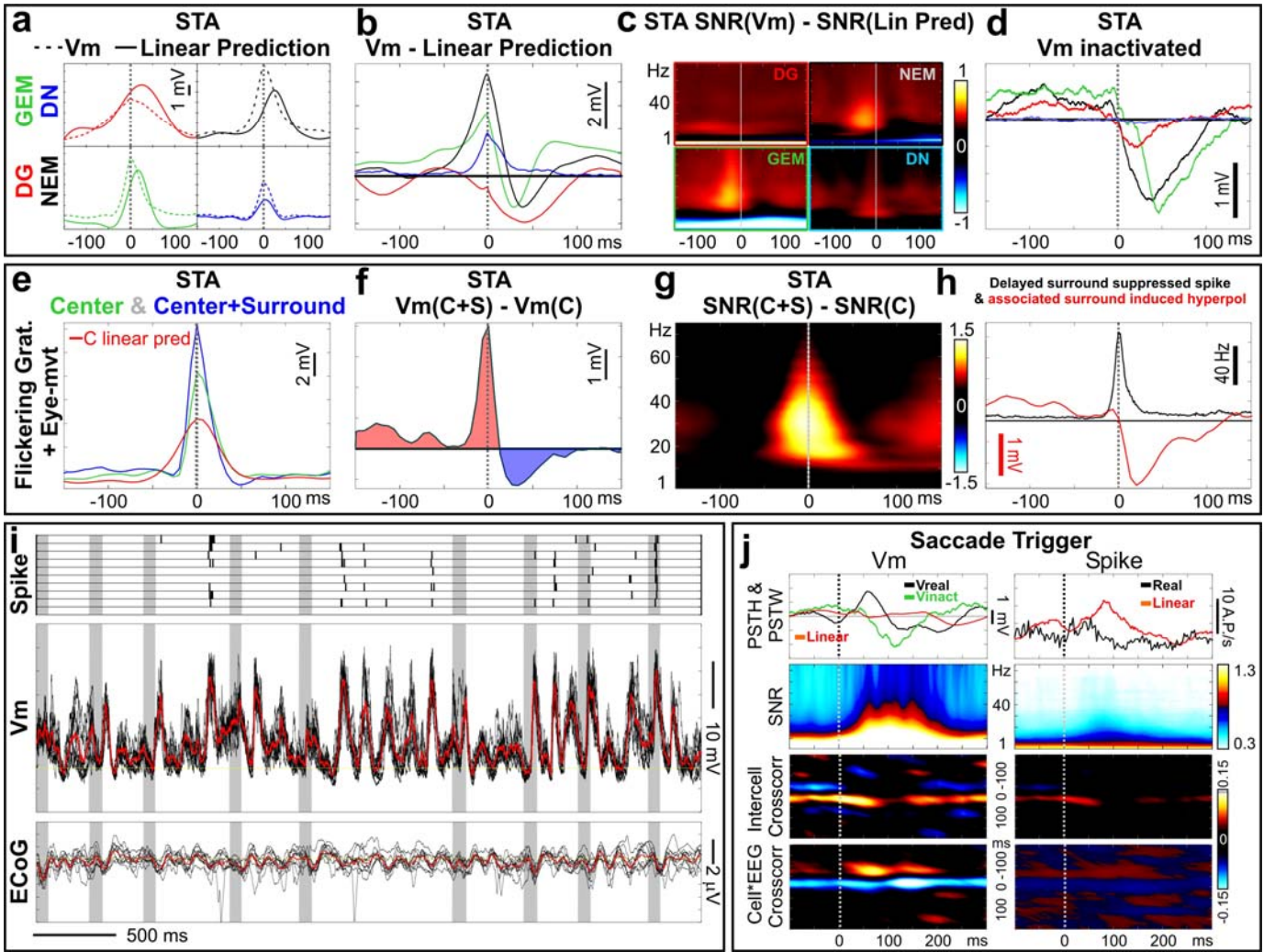


Figure 3.6.4 : Neuronal nonlinearity and delayed suppression-inhibition control the spike response timing and reliability of V1 responses, and the saccadic correlations removal of V1 resulting processing. .*abcd*, Characterisation of the spike timing dependent nonlinearity expression and dependency on the stimulus statistics and eye-movement dynamics, for the 9 simple cells presented in figure 3.6.1. **a**, Spike trigger averaging (STA) of the V_m time-locked averaged responses (plain lines) and of their respective linear prediction (figure 3.6.1, dashed lines)), averaged across cells, for the drifting grating (red), grating+eye-movement (green), Natural image+eye-movement (black), and dense noise (blue) conditions. **b**, STA of the difference between the V_m response and its linear prediction averaged across cells for the four conditions. Note that the temporal biphasic profile with an initial enhancement and a consecutive suppression is expressed only for condition, namely during animation by virtual eye-movements. **c**, Spike timing dependent nonlinear enhancement of the SNR(V_m) in the Beta-Gamma frequency range. We calculated the STA of the difference between the SNR(V_m) and the S_L NR(V_m) (obtained using the signal linear prediction of V_m) time-frequency matrices. **d**, To increase the visibility of the inhibition recruitment relative to the spike timing, we recorded the response of a cell while artificially depolarising it above the spike initiation threshold by the intracellular application of a constant current (V_m spike-inactivated = -40mV. The STA on average V_m across trials is represented for the four conditions. The quasi absence of spiking response may explain the flat STA in dense noise condition. *efgh*, Characterisation of the spike timing dependent nonlinearity expression and dependency on the contrast gain control and center-surround interaction, on the simple cell presented in figure 3.6.3. For *efg* the same measures are applied as in *abc* respectively but replacing the V_m linear prediction by the center only observed response. **h**, Surround

stimulation removes delayed spikes by a net hyperpolarising effect. STA of the spike of the center only stimulation on the subtract of the Vm in the centre only and centre + surround conditions (red), revealing a surround-specific, delayed post-spike hyperpolarization, which yields to the asymmetric STA between centre-only and centre+surround spike trains (black), presumably by suppressing the later spikes of each event when the surround is stimulated. i, An example of spiking, Vm and simultaneously recorded ECoG responses to fixational eye movements and saccades. The periods corresponding to the saccadic movements are presented in grey shaded regions. j, Decorrelation of the saccadic imposed correlations in the input by cortical processing in natural-like condition. The comparison of the spiking with the Vm responses and their correlation imposed by the saccade is assessed by a saccade trigger averaging (on the saccade onset $t=0$) on, from top to bottom: the average response (black), its linear prediction (red) and the nonlinearity (observed-predicted, blue) waveforms, the time-frequency SNR, the time-sliding normalised cross-correlogram (jPST) between each cells responses, and the time-sliding cross-correlogram (jPST) between each cells responses and the EEG (cf. methods). The result are averaged across the 9 simple cells recorded in this condition, and the Saccade TA Vm response recorded in one inactivated cell ($V_m=-40mV$, same cell as in d) is presented in green.

We could identify some obvious mechanisms sustaining the nonlinear processing common to the protocols studied here. The first one consist in an interplay between the spike nonlinearity and delayed inhibition. The large and fast depolarisations kinetics observed with eye-movement stimuli originate preferentially from a nonlinear processing. CGCs promote coincidence detection under centre only stimulation (compared to linear prediction), and this effect is further amplified by centre surround interactions (figure 3.6.4e). As a result, spikes evoked by eye-movement combined with surround stimulation specifically detect nonlinear amplifications of the input (figure 3.6.4b,f). The consecutive suppressive interaction, which is associated with a specific recruitment of inhibition by eye-movement (figure 3.6.4d,h), further shortened the linear prediction (4a), the center only (4e) depolarisation, and the spiking response (4h, black), constraining the spikes in a few ms window. The similar biphasic mechanism constraining the time course of the responses is observed in the center-surround apparent motion study (figure 3.6.2c). The resulting delayed inhibition control of the spike timing precision is reminiscent of what is observed in auditory cortex (Wehr & Zador, 2003), although it is governed here by interactions. The nonlinear control of the temporal precision of the synaptic excitation and inhibition sequence by the eye movement dynamic, leads in natural conditions to an increase in strength and reliability of beta gamma range frequencies. These nonlinear interactions are selectively represented in the spiking output (figure 3.6.4c,g).

Second, the neuronal nonlinearity is also modulated by the input statistics: it can improve the SNR not only by selectively amplifying the fast, reproducible, nonlinear events in the signal, but also by filtering out a proportionately greater amount of noise when the stimuli are animated by eye movements (figure 3.6.5). This is because Vm trajectories show less

dispersion in natural conditions (chapter 3.5), therefore decreasing the probability of spurious spikes, and yielding sparser, more precise and selective spiking responses. This result further point out that neuronal integration is intrinsically probabilistic and that this probabilistic component is stimulus dependent.

In agreement with the efficient coding and redundancy reduction (Barlow, 1961, Field, 1987, Atick, 1992, Nadal & Parga, 1994, Olshausen & Field, 1996, Bell & Sejnowski, 1996, Vinje & Gallant, 2000) general principle for sensory processing, the V1 RFs (both linear and nonlinear including the various gains controls previously described) appear specially suited to remove the redundancies imposed by eye-movements. First, the neuronal integration specially behaves as a nonlinear filter in natural conditions with eye-movements (figure 3.6.6): whereas, in drifting grating and grating with eye-movement condition, an important part of the information-fluctuations present in each Vm trials is transferred in the spike train, in natural and dense noise condition a predominant part of the input is filtered out. Saccades constitute the major source of common input to V1 in natural condition and all cells recorded responded to saccadic movement at the Vm level (figure 3.6.4j). This strong input correlations imposed by the saccadic movement (and probably related to the predominant blurring of the input) is detected in our recordings as an increase of the SNR(Vm) and of the average correlation between the Vm of each cell as well as between the Vm of each cell and the simultaneously recorded EEG in ipsilateral V1. In agreement with the efficient coding hypothesis, the average spiking response to saccades across cells as well as their SNR are almost flat, and the probability for a cell to respond to a given saccade at the spiking level is much lowered compared to the Vm level. The correlation of spike trains between neurons and with the EEG is also reduced. Suppressive nonlinearities, active at the time of the saccade, participate to the spike output removal of the saccadic input correlations and include supposingly the apparent motion high speed specific interaction previously described which only transfers the higher order “unexpected” correlations. The low correlation observed between spike trains confirms that the centre surround interactions exemplified in figure 3.6.2c are selective for the stimulus configuration. This temporal redundancy normalisation of the optic flow or informational flow constancy holding (figure 3.5.7) operated by the cortical processing is in agreement with the idea, originally proposed by Dong & al (2003) in the thalamus, that RF and its fast adaptation can account for eye-movement, notably saccadic, information removing, and thus to act as a alternative or synergetic mechanisms to the classical motor efferent copy suppression (Ross & al, 2001, Burr, 2004).

3.6.4. Conclusion

The main result of this study is that V1 nonlinearities participate to the temporal encoding of natural inputs. Centre surround interactions and dynamic contrast gain controls in particular, improve the reliability, the temporal precision, and, at the spike level, the sparseness of the responses. Our results also suggest that natural statistics nonlinearly improve the SNR(Vm) in the Beta-Gamma range by eliciting a strong synaptic inhibition just after the initial excitatory input (Wehr & Zador, 2003). This effect is further amplified by the neuronal integration function (Hirsch & al, 1991), and notably the spike threshold nonlinearity (Azouz & Gray, 2003). Both mechanisms remove V1 input redundancies and decrease noise in the output, yielding to an efficient encoding of natural stimuli in accordance with the companion paper.

Given its singular temporal biphasic shape, such kind of nonlinearities define a spike timing dependent associative short term adaptation or plasticity, and behave as a coincidence detector removing spatiotemporal correlations of the optic flow (and transmitting only unlikely correlations), as well as sustain a temporal coding in V1 (Gawne & al, 1996, Victor & Pupura, 1996, Mechler & al, 1998, Reich & al, 2001, Van Rullen & al, 2005) shortening responses latencies and duration. Moreover, the spatiotemporal specificity of center-surround interaction expression demonstrates the existence of a non-classical directional selectivity of the RF for high speed motion in the collinear axis of V1 cells. The remarkable fit of the spatiotemporal statistics of the ubiquitous saccadic and fixational eye-movements, and the two motion selectivities in V1, respectively the spatial long range and high speed demonstrated here and the short range and low speed of the classical RF, lead us to propose a simple visuo-oculomotor model of V1 cortical processing and function. According to this model, V1 operates a sequential and multiscale (local short range and global long range) analysis of the visual scene thanks to the convolution of environmental features with the various ballistic eye-movement exploration (figure 3.6.2a). Gain controls and adaptative decorrelation allowing an efficient coding (Laughlin, 1981, Barlow & Foldiak, 1989, Ruderman & Bialek, 1994, Bell & sejnowski, 1995, Schwartz & Simoncelli, 2001) are a well known computational principle for coordinate transformation (Salinas & Their, 2000). According to our result, it appears highly plausible that a preliminary form of eye-movement invariance could result from V1 process. Finally, since the increase of dynamic reliability by interactions is not a specific feature of the nervous systems (Becskei & Serrano, 2000), reproducibility of self-organised dynamic systems can be used as an heuristic to discover the full function and the pertinent dimensions the system is adapted to.

3.6.5. Methods

3.6.5.1. Preparation and recordings.

Cells in the primary visual cortex of anesthetized (Alfathesin) and paralyzed adult cats were recorded in vivo using sharp electrode recordings (n=12, average $V_{rest}=-67\text{mV}$, 0nA) as described elsewhere³². The electrocorticogram (EcoG) was simultaneously recorded using silver electrodes positioned homotopically or close to the recording site. Data processing and visual stimulation protocols used in-house software (G. Sadoc, Elphy, Biologic CNRS-UNIC/ANVAR).

3.6.5.2. Visual stimulation.

The stimuli presented in this study included the four presented in the accompanying paper (chapter 3.5) as well as two protocols designed to probe specifically the impact of V1 nonlinearities on the processing of eye movements.

Apparent motion stimuli are composed of 3 optimal Gabor patches successively flashed with 0.9 contrast in the surround and either a contrast eliciting the 1/3 of the maximum amplitude of the contrast response tuning (low contrast, mean=0.25) or the first maximum amplitude value of the contrast response tuning (high contrast, mean=0.75). The size of the patches was adjusted to the spiking RF measured using sparse noise. The distances between patches is set at 120% of the spiking RF length (5.9°) and the duration of the onset of each patch was 16 ms.

Center-surround stimuli animated by eye-movement contrast dynamic consisted in contrast-modulated gratings whose spatial and temporal phases are in quadrature: $C_{\max} \cdot \cos(SF \cdot 2 \cdot \pi \cdot (x + x_0(t))) = C_{\max} \cdot C_{\cos}(t) \cdot \cos(SF \cdot 2 \cdot \pi \cdot x) - C_{\max} \cdot C_{\sin}(t) \cdot \sin(SF \cdot 2 \cdot \pi \cdot x)$, where C_{\max} is the contrast of the original moving grating, SF its spatial frequency, x the spatial position along the axis orthogonal to the grating orientation, $x_0(t)$ the spatial position across time of the grating centre, $C_{\cos}(t)$ and $C_{\sin}(t)$ the time-varying contrasts of the cosine and the sine components, respectively equal to $\cos(SF \cdot 2 \cdot \pi \cdot x_0(t))$ and $\sin(SF \cdot 2 \cdot \pi \cdot x_0(t))$. We presented one of these components to a simple cell: the stimulus was a sinusoidal grating of optimal orientation, spatial frequency and spatial phase, whose contrast was varied in time as the cosine of the eye position (along the x axis) during a simulated oculomotor path. The grating presentation was either restricted to the classical (minimal) discharge field (mapped with sparse noise, “centre-only” configuration) or spatially extended such as to cover the “silent” surround part of the receptive field (“centre + surround” configuration).

3.6.5.3. Analysis.

Receptive field Vm first order kernel is estimated using the averaged across trials responses ($r(t)$, DC filtered) to dense white noise stimuli (50*50 shaker board of 0.39° pixels refreshed every 13.3 ms, 70 s long), with a multidimensional least square regression technique (Theunissen & al, 2001). This method minimises the estimation error $\langle \langle \hat{r} - r \rangle^2 \rangle$, where

$$\hat{r}(t) = \sum_{i=1}^{n_x * n_y * n_t} K(i)S(i)$$

is the linear response estimation, K(i) and S(i) represent the spatial and

temporal dimensions of the kernel and the stimulus respectively. To avoid overfitting effects, the spatial and temporal dimensions of the RF estimation are limited to the minimum size covering the full RF (typically $n_x * n_y = 8 * 8$ pixel definition). Prediction of the responses is achieved by resampling the stimulus movie at the kernel definition and convolving it with the linear kernel. Dense-noise linear prediction is based on a sequence of 10s stimuli consecutive to the one used for kernel estimation.

The resulting prediction present difference when compared to the observed waveform in the average energy and time course, respectively quantified by the Static-Gain-Factor: $SGF = \sigma^2(Vm_{pred}) / \sigma^2(Vm_{obs})$, and the maximum of the cross-correlation function. We also used a global wavelet coherence estimation to assess the level of similarity and linearity of the prediction as a function of the frequency (chapter 3.5.8, Theunissen & al, 2001).

In order to quantify the dependence of the response reproducibility on linear and nonlinear mechanisms, we computed the time-frequency wavelet transform of the linear (and LN for the spike of figure 3.6.3) model predictions $S_{lin}(t,f)$. This predicted signal matrix was divided by the observed noise matrix to yield $SNR_l(t,f)$. Average SNR vs. temporal frequency curves (SNR spectra) were obtained by averaging the SNR matrices over time. Significance of the result is assessed by testing SNR values against Rayleigh statistics (chapter 3.5.8).

The nonlinearity of center-surround interactions evoked by apparent motion stimulus is measured by adding the center-alone and surround-alone controls PSTHs and PSTWs, and then subtracting this linear prediction to the observed PSTHs and PSTWs. The resulting nonlinear waveform is expressed as a z-score of the spontaneous activity and then averaged across cells. For SNR non-linearity, the SNR linear predictor was obtained by summing all combinatory of trials responses to center-only and surround-only conditions, and the same

procedure as previous was then applied (Z-score values are calculated independently for each frequency).

Linear predictions of the Vm and spike responses of figure 3.6.3 cell were obtained by first convolving the contrast varying stimulus with the impulse response, and then by passing the predicted Vm to a static point nonlinearity. Both the impulse response and the static nonlinearity were fitted (least square regression) in the centre only condition, on a data set different from the one used for the predictions.

3.6.6. Supplementary figures

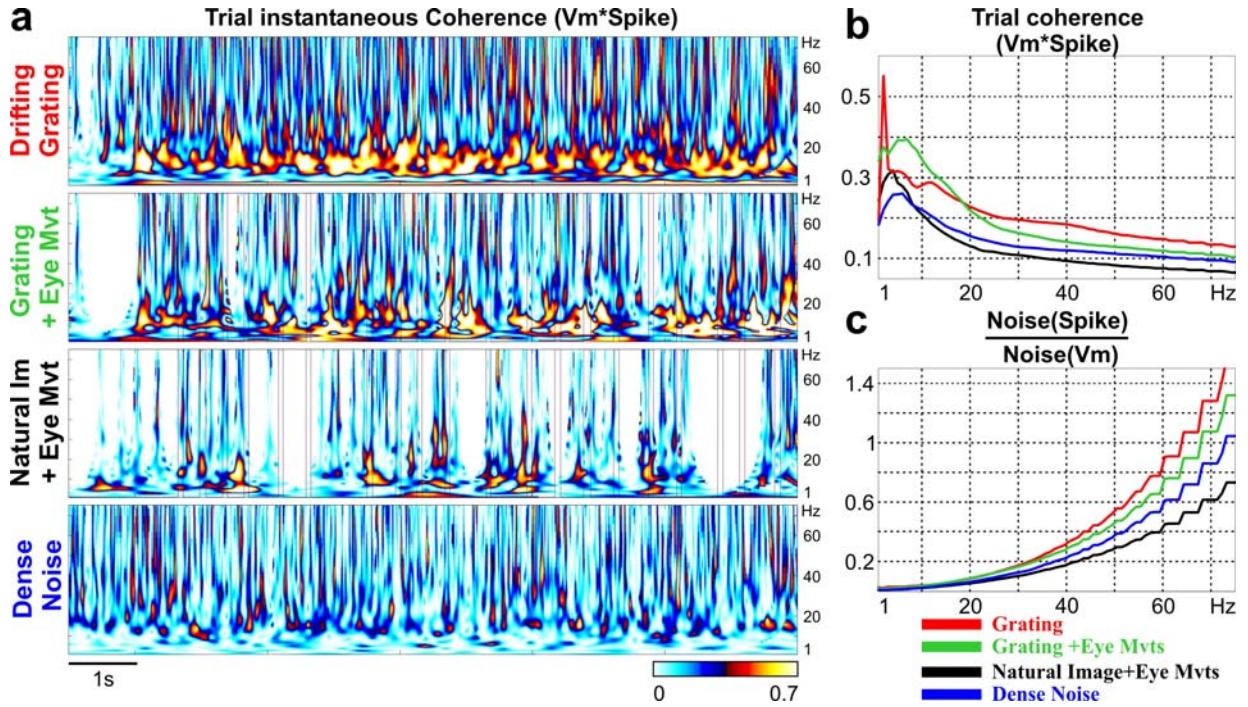


Figure 3.6.5: Modulation by the stimulus statistics of the neuronal integration filter function and of the input-output reliability relation: selective Vm input fluctuations-correlations removing and deterministic behaviour in natural-like condition. **a**, example of input correlation filtering for the four stimulus condition for the same simple cell as in figure 3.6.1. The neuronal filtering function is measured by the “instantaneous” coherence between the Vm and spike train of each trial and then integrated over trials. This measure quantifies the level of similarity between Vm and spike signals as well as the linearity of their temporally local relation. Note that in Drifting-grating condition (drifting at 2 Hz), an important fraction of the high-frequency components of single trials input signal is transferred to the output. **b**, population averaging of the time averaged trial local vm*spike coherence ($n=12$). **c**, The probabilistic component of the neuronal integration and its dependency to the stimulus condition are assessed by comparing the level noise in input to the level of noise in the output. To do so we divided the time-frequency measure of noise obtained for the spike trains to the one obtained for the Vm, and averaged across time and then across the whole pool of simple and complex cells ($n=12$), to obtain the frequency dependent function of this ratio. Note the power law frequency dependency of the ratio, which is also found for single neuron measure and for the time-frequency signal(spike) to signal(Vm) ratio.

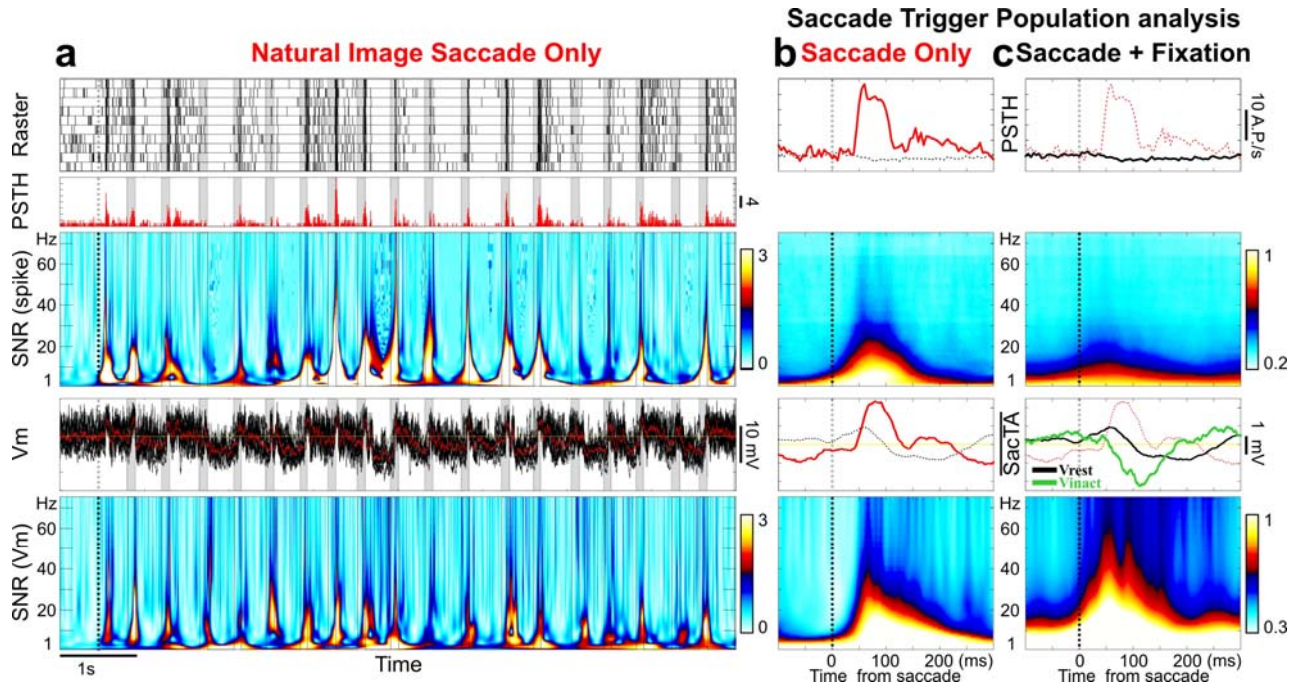


Figure 3.6.6: Comparison of Vm and spiking responses between natural image either animated by a saccade and fixational eye-movement sequence or by a saccade only sequence. a, example of responses recorded for a cell to a natural image animated by saccade interleaved by static periods. From top to bottom are represented the raster of spike trains, the PSTH, time-frequency SNR(spike), Vm trials (black) with their average (red), and SNR(Vm). The saccades are symbolised by the grey shaded period. **b & c**, Saccade trigger averaging for the saccade only condition (b, $n=6$) and for the saccade with fixational eye movement (c, same as figure 3.6.4, but for 22 cells, including cells only recorded for natural-like condition), average across cells. The dashed line marks the saccade onset. From top to bottom are represented the PSTH, time-frequency SNR(spike), Vm trials (black) with their average (red), and SNR(Vm) averaged across cells. For the saccade with fixational movement, the saccade trigger average Vm response recorded in inactivated state ($V_{inact} = -40\text{mV}$) is presented in green.

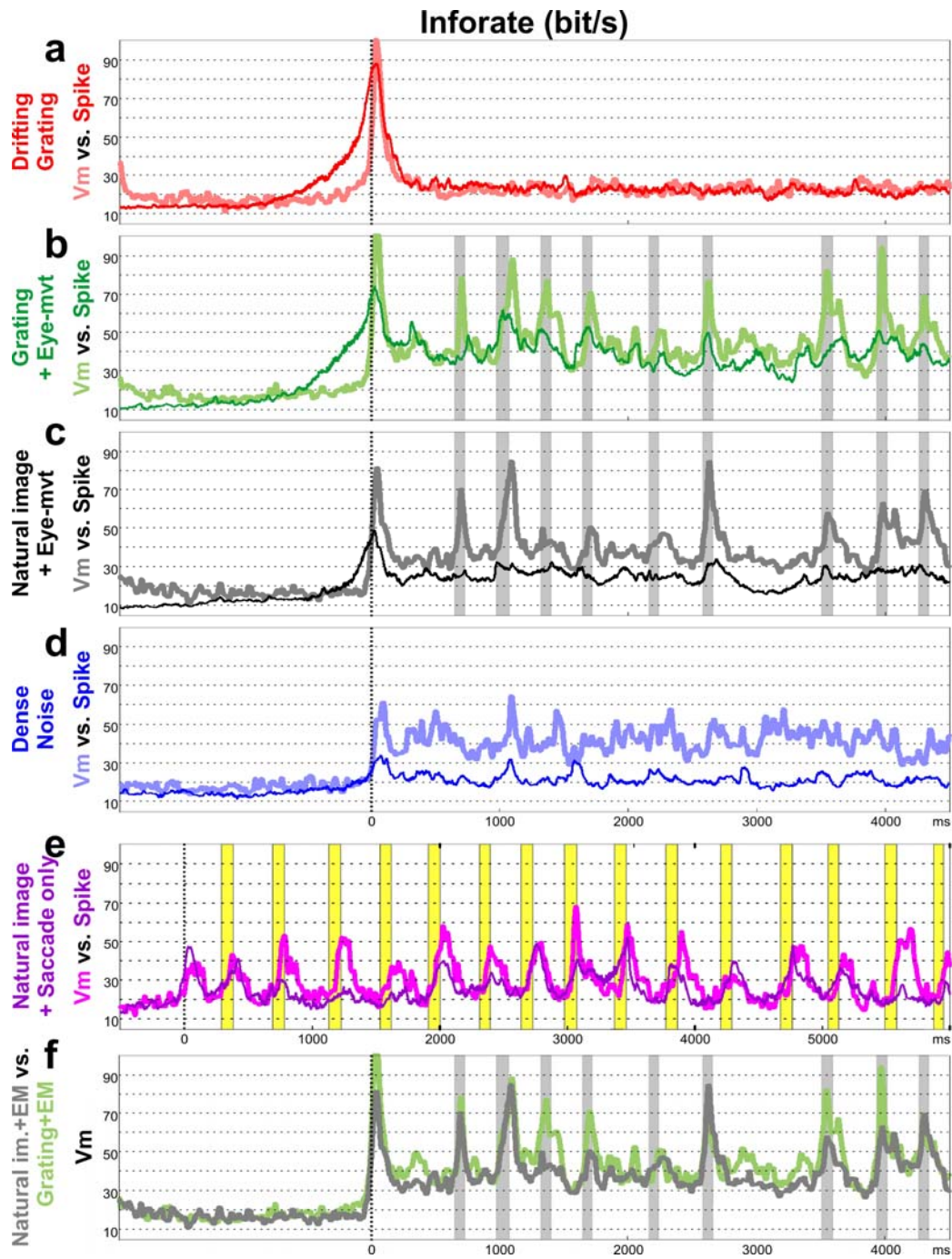


Figure 3.6.7: Temporal modulation of the informational flow of Vm and spiking responses. Comparison of the temporal profile of the estimated mutual-information rate between Vm and spiking responses averaged across cells for, from top to bottom: Drifting-grating (a), Grating with eye-movement (b), Natural Image with eye-movement (including fixational movement, c), dense-noise ($n=12$, d), natural image animated by saccade only ($n=6$, e), and a comparison of natural image vs grating both animated by the same eye-movement sequence for Vm responses (f).

The average mutual-information estimation using time-frequency method of spiking responses gives qualitatively the same result as the direct estimation presented in associated paper (Baudot & al, 2006, figure 3.6.3): drifting-grating, natural-like and dense-noise conditions present close mutual-information rate, whereas higher values are found for grating

with eye-movement condition. As expected also from the associated paper, Information rates are lower in the Vm response compared to the spiking response in natural-like condition and dense-noise condition, whereas they are approximately equivalent for the grating conditions. The information about the drifting is mainly concentrated in the transient initial increase corresponding to the non-stationary turning-on of the stimulus (recalling Mechler & al, 1998, results). In natural-like condition with fixational eye-movement, whereas the Vm mutual-information present large increases consecutive to saccades, at the spiking level the information remains approximately constant, probing the temporal informational flow normalisation by the cortical processing. This is neither observed in the grating with eye-movement nor in the saccade only condition, which shows saccade related information increase in the spiking response. The remarkable fit of the temporal profile and high values observed in the Vm responses to drifting and natural image with eye-movement further shows the importance of the information conveyed by the eye-movement dynamic on V1 input. The high DC values observed in both condition also probes the cortical responsiveness and the computational relevancy of the fixational eye-movements.

4. Conclusion

4.1. Much ado about nothing, still on the way of a thermodynamical theory of evolution and cognition: Knowledge is energy

4.1.1. Introduction

The aim of this chapter is to develop the previous model in detail and to give some physical and biological argumentation about its possible relevancy. The redundancy, entropy, logical depth (structural complexity) measures and natural dynamic of systems either isolated or in interaction, is exemplified in the semi-classical “minimal-scale” framework (for which quantum properties are considered roughly but simply in a classical representation), but is available for any scale and system definition (for any coarse grained precision). This minimal grained framework allows to define entropy and logical depth (structural complexity) as microscopic and non-relative variables, and compelling macroscopic “emergence” to a result of the Higher redundancy organisation.

4.1.2. Systems information and complexity

4.1.2.1. Ordered redundancies, entropies and absolute capacity definition

This chapter describes the general principle of redundancy and entropy decomposition, without defining the system and the probability laws associated, for which some example will be presented in the next chapters.

Let us consider a system S that can be decomposed or sampled into n probabilistic variables S_1, S_2, \dots, S_n possibly taking N values. We emphasize that S has no predefined dimensions and can be considered in the general form of a spatio-temporal system (system with spatial memory of dimension n , and with temporal memory of dimension m , $S1_{t1}, S2_{t1}, \dots, Sn_{t1}, S1_{t2}, S2_{t2}, \dots, Sn_{t2}, \dots, S1_{tm}, S2_{tm}, \dots, Sn_{tm}$, or a m ordered Markov chain). Let us imagine in fact that we have a large number of copies of the system S , a so called ensemble (M), on which the probabilities can be estimated. The entropy of S is given by:

$$H(S) = H(S_1, S_2, \dots, S_n) = \sum_{i=1}^{N^n} P_i \text{Log}(1/P_i) (1), \text{ where } P_i \text{ denotes the probability of the system}$$

to be in the i^{th} state in the ensemble M .

Our aim of this chapter is to define redundancy, remarking that the information (entropy) of the system is equal or less then the sum of its constitutive elements. Inspiring from Shannon and Weaver (1948) and Atlan (1979), we can define:

$$H(S) = H_0(S)(1 - R(S)), (2).$$

Where $H_0(S) = n \log N$ (3), with N being the different possible values or state of S_i and where $R(S)$ is the redundancy present in the system. $H_0(S)$ is only defined by the intrinsic dimensions of the system S (usually space and time), it's the system capacity. $H_0(S)$ is as a constant of the system and is also the highest possible entropy, that can only be reached in the case where every component S_i are statistically independent and each state equiprobable (case where the S_i present random behaviour). Developing (1), redundancy R can be formulated into first and higher order redundancies (see Atick, 1992), and further into n ordered redundancies:

$$R = \underbrace{\frac{1}{H_0} \left(H_0 - \sum_{i=1}^n H(S_i) \right)}_{\text{First-order-redundancy}} + \underbrace{\frac{1}{H_0} \left(\sum_{i=1}^n H(S_i) - H(S) \right)}_{\text{Higher-order-redundancy}} = R_1 + R_H = R_1 + R_2 + \dots + R_n, (4)$$

It appears that : $H(S) = \sum_{i=1}^n H(S_i) - H_0 R_H$, where

$\sum_{i=1}^n H(S_i) = \sum_{i=1}^n P(S_i) \log(1/P(S_i)) = \sum_{i=1}^n \sum_{j=1}^N P_j(S_i) \log(1/P_j(S_i))$, Where $P_j(S_i)$ represents the probability of the elementary constituents i to be in the state j in the ensemble M .

We can express ordered redundancies and ordered entropies as following:

$$H_1(S) = \sum_{i=1}^n H(S_i), (6) \text{ the first order entropy of } H(S), R_1 = \frac{H_0 - \sum_{i=1}^n H(S_i)}{H_0} = \frac{H_0 - H_1}{H_0}, (7),$$

and the general form: $H_i = H_{i-1} - H_0 R_i$ and $R_i = \frac{H_{i-1} - H_i}{H_0}$ (8)

H_i decreases with i : $H_i \geq H_{i+1}$. We can remark that $H(S) = H_n$.

$H_0 R_1$ quantifies the distance to equiprobability of all the elementary constituents, whereas $H_0 R_H$ quantifies the statistical dependency between the constituents.

Intuitively, quantifying the information in between the elementary constituents accounts for the system redundancy. In fact, as the information between the elementary constituents can be

shared between pairs, triplets (etc...), a precise counting have to be applied (figure 3.7.1). R_n can be expressed in term of Mutual information in between the n variables. An expression of ordered redundancies can be proposed as:

$$H_0 R_1 = H_0 - \sum_{i=1}^n H(S_i)$$

$$H_0 R_2 = \sum_{j=1}^n \sum_{i=1}^n I(S_i; S_{j \neq i} | S_1, S_2, \dots, S_{a \neq i, j}, \dots, S_n) \text{ (sum of the mutual information between all pairs of variables knowing the other variable).}$$

$$\frac{H_0 R_3}{2} = \sum_{k=1}^n \sum_{j=1}^n \sum_{i=1}^n I(S_i; S_{j \neq i, k}; S_{k \neq i, j} | S_1, S_2, \dots, S_{a \neq i, j, k}, \dots, S_n) \text{ (sum of the mutual information between all triplets of variables knowing the other variable).}$$

$$\frac{H_0 R_4}{3} = \sum_{l=1}^n \sum_{k=1}^n \sum_{j=1}^n \sum_{i=1}^n I(S_i; S_{j \neq i, k, l}; S_{k \neq i, j, l}; S_{l \neq i, j, k} | S_1, S_2, \dots, S_{a \neq i, j, k, l}, \dots, S_n)$$

etc... until $\frac{H_0 R_n}{n-1} = I(S_1; S_2; \dots; S_n)$

A simple representation of this redundancy decomposition is given using Venne diagrams:

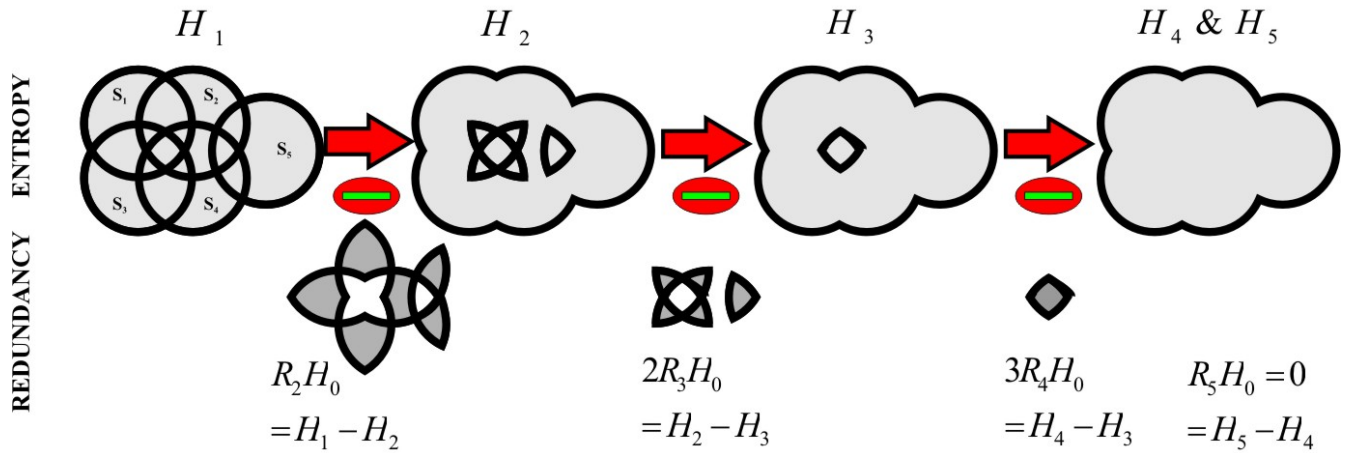


Figure 4.1.1: Schematic representation of the ordered redundancy and entropies decomposition using Venne diagrams. This drawing represent the various order of entropy (top panel) and redundancy (bottom panel), for a very small system composed of five elementary constituents (noted S_1, \dots, S_5). H_5 is equal to the classical entropy of the system.

A way to estimate $H(S)$ and $R_H(S)$, forgetting the decomposition into redundancy order is given by the following relation:

$$H(S) = H_1(S) - \sum_{\substack{i,j=1 \\ i \neq j}}^n I(S_i; S_j) + \sum_{\substack{i,j,k=1 \\ i \neq j \neq k}}^n I(S_i; S_j; S_k) - \sum_{\substack{i,j,k,l=1 \\ i \neq j \neq k \neq l}}^n I(S_i; S_j; S_k; S_l) \dots$$

$$\text{And } R_H = \sum_{\substack{i,j=1 \\ i \neq j}}^n I(S_i; S_j) - \sum_{\substack{i,j,k=1 \\ i \neq j \neq k}}^n I(S_i; S_j; S_k) + \sum_{\substack{i,j,k,l=1 \\ i \neq j \neq k \neq l}}^n I(S_i; S_j; S_k; S_l) - \dots$$

That we can summarize as $H(S) = I_1(S) - I_2(S) + I_3(S) - I_4(S) \dots \pm I_n(S)$

Since $\sum_{i=1}^n I(S_i; S_j) \geq \sum_{i=1}^n I(S_i; S_j; S_k) \geq \sum_{i=1}^n I(S_i; S_j; S_k; S_l) \geq \dots$, $H(S)$ is converging to its real value as the order of I increases.

In conclusion and to introduce the next chapter, Entropy can thus be intuitively understood as quantifying the whole world of possible microscopic states minus each constraints imposed by elementary interactions (elementary mutual informations, ponderated as a function of the level of sharing of this interaction in the whole population). For simplicity in a cognitive framework, those elementary interactions can be understood as elementary knowledge, monade or beliefs, whereas the rest is just uncertainty. They also can be considered geometrically as elementary distance between constituents and quantified by their Kullback-Leibler divergence (Cover and Thomas, 1991, Amari, 1999, although KL-divergence is not a symmetric measure and thus not directly assimilable to a distance). An important interest of this decomposition is to stress that entropy binds microscopic and macroscopic properties and accounts for emergent or macroscopic properties of systems.

4.1.2.2. Expression of redundancies in classical statistical physic

We now apply the previous definitions in the context of classical physics (figure 6.2.1). The system S is considered at a fixed time t without temporal dimension (as imposed by “classical” physics), and is composed or sampled of probabilistic constituents S_1, S_2, \dots, S_n , possibly taking N discrete state values. We further consider the ensemble of m copies of the system on which we define the probabilities. As usually, the entropy quantifies the uncertainty and the number of effective degrees of freedom the system displays. The component $H_0 R$ quantifies the constraints present in the system (suppressing some of the possible degrees of freedom). Moreover, Mutual-information between elementary constituents quantifies the entropic contribution of elementary interactions whatever their origin (gravitational,

electromagnetic, strong and weak). $H_0 R_H$ quantifies the renormalized impact of those elementary interactions on the entropy of the system.

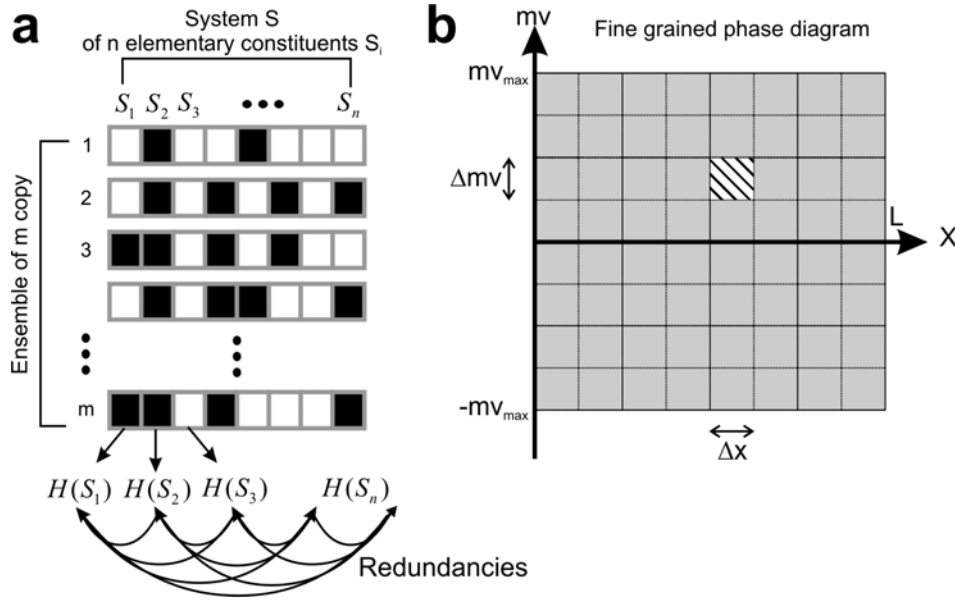


Figure 4.1.2: Schematic representation of the discrete system definition and fine-grained phase diagram: **a**, Schematic representation of our system definition in the classical statistical physics framework: The system S is composed of n elementary constituents S_i (for simplicity, here $N=2$, black or white). Classical entropy measure ($H(S) = \sum_{i=1}^{N^n} P_i \log(1/P_i)$) is based on the probability P_i of each possible global configuration in the ensemble (classically named microstate) illustrated here in each row of the ensemble of m copy. The proposed entropy estimation ($H(S) = \sum_{i=1}^n H(S_i) - H_0 R_H$) is based on the sum of each elementary constituents entropies minus the ordered redundancies component representing the statistical dependencies between each constituents. **b**, Schematic representation of the minimum grained phase diagram (reproduced from Ruelle, 1991). For simplicity, it is presented as two dimensional (X, mv_x), whereas a six dimensional space has to be considered (the 3 spatial dimensions and their associated impulsions). ΔX and Δmv represent the fundamental quantum uncertainty given by Heisenberg relations and the hatched square has a surface equal to the Planck constant h . mv_{\max} is the maximum possible speed (at most c) and L is the interval of length under consideration. Considering this example, the number of states each elementary constituent can take would be $N = \frac{2mv_{\max} \cdot L}{\Delta mv \cdot \Delta X} = \frac{2mv_{\max} \cdot L}{h}$ (See Ruelle, 1991). Entropy quantifies the dispersion of the system states in the phase diagram.

Whereas entropy quantifies the dispersion of the system states in the phase diagram (dispersion of its energy), $H_0 R_H$ is quantifying its level of compactness, of compression. We will base the quasi-classical statistical framework of entropy (a nice presentation can be found in Falcioni, Loreto & Vulpiani, 2003 and Landau, 1967). We can try to find the expression

H_0 and redundancy R using the general expression given by the quasi-classical case (Landau, 1967):

$$H = \text{Log} \frac{\Delta x \Delta p}{h^n} \quad (4.11)$$

Where n is the number of degrees of freedom of the system and h is the Planck constant, $\Delta x \Delta p$ is the volume the system occupies in the phase diagram, Δx is the variation of spatial coordinate of the system, and Δp is the variation of momentum coordinate of the system. The quantum constant can be understood as the minimal volume (spatio-temporal) of incertitude and is imposed by the quantum nature of mater (figure 3.7.1). In contrast with the mutual information that we imaged as an atomic knowledge, this in our paradigm the quantum of action is the minimal resolution of the system capacity, and if we aim at measuring a kind of absolute capacity it appears as the good and natural system resolution. This particular expression of entropy introducing the quantum constant is important, since it allows a non-relative expression of entropy (Landau, 1967). By identification (the precise framework has to be done rigorously, the following is just a logical trail to give ideas):

$$H = \sum_{i=1}^n H(S_i) - H_0 R_H = n \text{Log} \left(\frac{1}{2h} \right) - \text{Log} \left(\frac{1}{\Delta x \Delta p} \right) \quad (4.12)$$

The first member of the equation (4.12) depends only on constitutive variables of the system, the number of degrees of freedom of the system. We propose that:

$$\sum_{i=1}^n H(S_i) = n \text{Log} \left(\frac{1}{h} \right), \text{ and thus that, } H_0 R_H = \text{Log} \left(\frac{1}{\Delta x \Delta p} \right)$$

It gives the following definition of redundancy:

$$R_H = \frac{\text{Log}(\Delta x \Delta p)}{n \text{Log}(h)}$$

And the generalised uncertainty relation (that remind Heisenberg, 1927):

$$\Delta x \Delta p = (h)^{R_H n}$$

One can translate this relation by the fact that a system presenting some redundancy (structure) is more certain than if it was built of independent constituents. R is bounded between 0 and 1. When $R_H = 1$, $\Delta x \cdot \Delta p = (h)^n$ and gives the lower bound of uncertainty. When $R_H = 0$, $\Delta x \Delta p = 1$ and it is an upper bound to uncertainty (given by the finite system definition). This

upper bound, although obvious, is on our opinion very interesting since it gives an absolute limit to both momentum and position precision.

4.1.2.3. System absolute capacity and Bekenstein Upper bound.

Intuitively, the lower limit of entropy given by $R = 1$, gives an equivalence with the third thermodynamical principle stating that the entropy of each pure element or substance in a perfect crystalline form is zero at absolute temperature zero (Plank, 1913). This state corresponds to the maximal order of the system, and to a minimum of uncertainty. We can now focus on the other side upper bound given by $R = 1$. When $R = 1$, the system occupies the whole phase space. This corresponds to a maximal disorder and uncertainty state. We are referring to this state as the absolute statistical equilibrium (which is not the “classical” definition of equilibrium, an equilibrium state in classical thermodynamic can still present some redundancy, but which seems to find its physical implementation in black holes).

Since my knowledge is very limited in this following science field, the next paragraph tries to resume a paper of Bekenstein 2004. This upper bound may be related to the Bekenstein upper bound (1981, 2004), stating an absolute limit on how much information a region of space, or a quantity of matter and energy, can hold. This upper bound finding is coming from cosmological studies on black-holes which have been shown to reach the upper bound, and which dynamic has been found to follow a general form of the second law principle. The generalisation of this bound to any isolated physical gave rise to the so-called “Holographic” bound. The interesting nature of this informational capacity is that it depends on the surface, not the volume of the physical space under consideration, which is in deep agreement with the Holographic theory (which states that the 3-D physic of a space region is completely described by its 2-D boundary). In ergodic theory, probabilities and areas behave in the same way (“they have the same nature”, Arnoux & Chemla, 1992). It further argues about the intuition that the pertinent dimensions of our world is may be the probability or uncertainty (or h).

A second point of discussion can be proposed: as we will see further, the redundancy definition considered here for the space domain can be broadened to time dimension defining temporal redundancies. The redundancies defined previously have the form of energy (as discussed further), and in the cosmological field theory, energy imposes (is) the curvature of space and time. It is appealing, even at the sensory process level, to consider redundancies in the general geometrical form of space and time curvature (for DB).

4.1.2.4. Energy

In general, the concept of energy refers to "the potential for causing changes", and etymologically means "in work". In the context of natural sciences, all forms of energy: thermal, chemical, electrical, radiant, nuclear etc. can be in fact reduced to kinetic energy or potential energy. In physic, the strength of the link or interactions that bond physical systems (...molecules, atoms, nucleus, nucleons...) is measured in energy units. The previous definition of entropy/information ($H(S) = \sum_{i=1}^n H(S_i) - H_0 R_H$), which reminds Helmholtz Free energy definition ($F = U - TH$, where U is the internal energy, T the temperature), is explicit in energy terms, all the more when represented in the a phase diagram as in figure 3.7.2:

- $\sum_{i=1}^n H(S_i)$ is the entropic component of the "internal" energy of the system
- $H_0 R_H$ is the entropic component of the energy devoted to interactions (potential or free energy)
- $H(S)$ measure the energy of the system not involved into interactions.

Temperature is may be to be redefined, notably in non-equilibrium complex systems which, as exemplified in the paradigmatic studies of glasses present multiple temperatures on multiple time scales (Kurchan, 2005). Temperature is likely to be represented in the higher order redundancy component in this framework.

Moreover, the identification of h as the minimum grain may help to define the lowest level of elementary particle accessible to our knowledge (there is obviously one physical horizon here, but it is probably not new).

The probably most important point of all this: $H_0 R_H$ represent a general definition of "driving-force", encompassing the motion related Newtonian concept of force, and the concept of free energy in chemistry.

Until now we have only measured entropy in the minimum grained phase diagram, which comes somehow to measure the uncertainty of the uncertainty. One would prefer, and this was my basic original idea, to quantify directly uncertainty and energy, but it appears a hard task, necessarily modifying the informational framework developed previously. At last, to make all the previous entropies correspond directly to energy-like and physical uncertainty a change of the basis of the logarithm of the algorithm:

Entropies previously defined in base 2 $H_2(S) = K \sum_{i=1}^{N^n} P_i \ln(1/P_i)$ with $K = 1/\ln 2$, is converted into $H_p(S) = K \sum_{i=1}^{N^n} P_i \ln(1/P_i)$ with $K = (h)^m / \ln N$ where m is the physical dimensions under consideration (3 for classical physical space) and N is the number of possible states as before (cf. figure 3.7.2). It defines entropy as a physical information measure and knowledge or higher order redundancy as energy. However, the energy and uncertainty quantified this way do not correspond to the classical, but instead are measured on logarithmic scales. One can remark that the introduced constant $K = (h)^n / \ln N$ resembles to Boltzmann constant but in time unit instead of temperature unit. This unit change could fit well with the idea further developed of the quantum of action as a quantum of dissipation, and as a kind of unit of “relative or subjective” time.

The important point is that finding this direct expression of uncertainty and energy from the model proposed here (which is probably not correctly achieved here, but not so far) should logically lead to redefinition of the Boltzmann constant in term of other fundamental constant. The reason of this is that all the framework is only based on a pure informational paradigm (purely logical) and on microscopic states (the macroscopic emergence is a result of the Higher redundancy organisation), the Boltzmann constant is thus likely to be inside the formalism.

4.1.2.5. The wave side

The previous definition focus on the particle discrete aspect of systems. To investigate system as continuous wave, in the framework of undulating physique, the instantaneous spectra can be considered, as proposed in the Gabor wavelet analysis presented in the chapter 3.5.9. However, the rigorous framework has to be developed, and is more complicated than the simple SNR method exposed.

4.1.2.6. Gibbs paradox, elementary un-discernability, and non locality

The Gibbs paradox origins on the indistinguishability of particles of the same specie. For example, the entropy increase of the mixing of two gases (of same specie, volume, pressure and temperature) is null in reality whereas thermodynamical classical estimation leads to the false value of $\Delta_{mix} H = 2.n.R.\ln 2$ (where n is the number of particles and R the perfect gaz constant). The indistinguishability of particles is a peculiar property of quantum mechanic.

The paradigm proposed here intrinsically considers elementary constituents as indistinguishable (which are in fact elementary uncertainty) and is not affected by the Gibbs paradox: the system elementary constituents are interchangeable (they have not assigned number) without affecting the entropy or redundancy estimation.

Moreover, the paradigm proposed here also satisfies, in some way, the astonishing non-locality property of quantum mechanic: each minimal possible state grain of the phase diagram are interchangeable (they have not assigned number) without affecting the entropy or redundancy estimation.

In other words, the relevant and sufficient space for physical systems description (presenting all its information) may not be the classical, but the correlation or statistical space.

4.1.2.7. Relation to the Maxent inference and Minimum Description Length (MDL)

To obtain the probability distribution and the entropy of a system either in equilibrium or in non equilibrium with its environment, a general method consisting in maximising the Shannon information entropy under constraints is classically used (Maxent, Jaynes, 1957, 1957, 1979, Dewar, 2003, 2004, 2005). This method, prolonging Boltzmann and Gibbs work in the Shannonian information framework, is a statistical inference tool that reside naturally in the framework of Bayesian probability theory (Dewar, 2005). It can simply be understood as the inferring the system state and entropy taking into account the all the prior constraints applying to the system. It consists in maximising, using Lagrange multipliers λ_k

for each m constraints $\langle f_k \rangle = \sum_{j=1}^{N^n} P_j(S) f_{kj}(S)$, the function $-\sum_{j=1}^{N^n} P_j(S) \text{Log} P_j(S) - \sum_{k=1}^m \lambda_k \langle f_k \rangle$

(with an additive normalisation constraint). In fact, our formalisation, considering all the possible constraints expressions, can be found to justify the Maxent approach: there's nothing but constraints and "incertitude" in a system, and if you know all the relevant constraints applying to the system you automatically get the probability density and entropy by filling the remaining possibilities with incertitude.

It is also appealing to draw the correspondence between the entropy definition $H(S) = H_0(S)(1 - R(S))$ with the Minimum Description Length (MDL, Rissanen, 1978). MDL, following the Occam's razor principle and Bayes rule, aim at minimising both the size of the hypothesis and the size of the data when expressed in this latest basis. The definition of entropy $H(S) = H_0(S)(1 - R(S))$, is a special case of the MDL principle and measures the minimum size of the data without making hypothesis (in fact making the minimal hypothesis

of the minimum quantum graining of the phase diagram). Another way to express this is that from the physical theory developed here, the distinction between data and hypothesis do not appear relevant.

Moreover, the correspondence in between MDL and Maxent principles has already been established formally (Li and Vitanyi, 1997).

4.1.2.8. Relation to Kolmogorov-Chaitin complexity (or Algorithmic information)

Algorithmic information is the most formal definition of information and overcome the statistical probabilistic point of view. The algorithmic information is directly linked to mathematical foundations (Chaitin, 1977, Gödel, 1931) and to deductive logic. Algorithmic information quantifies roughly the level of randomness of a string, and by extension “the intrinsic information” of an “object”. It is rooted in automata theory notably universal Turing machines, and a brief paragraph is necessary to remind the Turing machine definition.

Turing (1937) reduced the formulation of theorem-proving problem to the problem of deciding whether or not a certain computing automaton can compute any given number or formula. The so-called Turing machine is defined formally as a “black-box”, used as formal biological system and brain model (McCulloch & Pitts, 1943) as well as the logical architecture for computers, having the following attributes:

- i) it possesses a finite number of states, $1, 2, \dots, n$
- ii) its operating characteristic comprises a description (program, short-code, “function”) of possible state transition
- iii) its environment consist of a potentially infinite tape divided into discrete fields that can be marked with 0 or 1 symbols, forming a sequence or pattern called configuration or string (or memory).
- iv) The automaton can inspect one field at a time and can move forward or backward one field at a time
- v) let the automaton be in the state $i(i=1, \dots, n)$ and let it see on the tape an input $e(=0,1)$. It will then print on to the tape an output $f(=0,1)$, move to the tape by p fields ($p=0,+1,-1$) and go over into the state $j(j=1, \dots, n)$. The specification of j , p , and f as a function of i and e comprises the program and is a complete definition of the functioning of such automaton.

Turing further defined the important concept of Universal automaton, as an automaton which can produce any configuration that can be produced by any automaton (which is

pragmatically an automaton with unspecified program, thus totipotent, and for which the program has to be added on the data tape).

Kolmogorov then defined the Algorithmic information (complexity, $K(S)$) of an object (string S) to be the length of the shortest program that produce (print) the object and halts on a given universal Turing machine T :

$$K(S) = \min \{|p| : S = C_T(p)\}$$

Where, $|p|$ denotes the length of the program in bits, and $C_T(p)$ is the result of running program p on Turing machine T .

A simple consequence is that regular string like 00000...0000 have a vanishing complexity (in the infinite string limit) and irregular or random strings such as the one produced by coin flip have a maximum complexity (for which $K(S) \approx |S|$).

Nonetheless, randomness like any general deductive or theorem proving problem must be undecidable (Gödel, 1931). The measure of complexity or “absolute” information of object is non-computable: no halting computation can possibly determine if a string is random simply because such a computation would render the string non-random (Chaitin, 1985). This is the counterpart for absolute things (pure object-subject or abstract).

However, in our physical world (which has an intrinsic probabilistic dimension), complexity of object may be statistically estimated under the copy ensemble framework previously exposed. Indeed the link between automata theory and information theory has been proven for a long while (Zvontin & Levin, 1970, Li & Vitanyi, 1997, and see the closely related reasoning in Adami & Cerf, 2000): in the limit of infinitely long strings, the average complexity $\langle K \rangle$ tends to the entropy of the copy ensemble M of the string or system S :

$$\langle K(S) \rangle_M = \sum_M P(S) K(S) \approx H(S) = - \sum_M P(S) \log P(S),$$

Where the string S appears in the ensemble M with probability $P(S)$. This relation is further made obvious by the entropy formulation $H(S) = H_0(S)(1 - R(S))$. Estimating the algorithmic information in physical systems is somehow leading to the consideration of a probabilistic automata framework, where the tape is replaced by an ensemble of tape and for which the computation is based on probability density and on statistical dependencies (Figure 3.7.1, in other word: probabilistic memory).

Turing machines have also allowed to define the important notion of efficiency or Algorithmic Complexity (AC or also dynamic complexity, or time complexity) of a program or algorithm. Essentially, the efficiency or AC is assessed by comparing the length of the input data (string, message...) with the time T in computational steps (cycle of the Turing machine) necessary for an universal Turing machine to produce the output (results...) and halt.

The P class, which correspond to efficient or feasible algorithms (realistically computable) is then defined as the ensemble of algorithm requiring a time which is a polynomial function of the data length L : $T \leq C(L+1)^n$ where C and n are constants. A similar definition but in space instead of time (in number string boxes or tape cells) is used to define the P-SPACE class of complexity (or space complexity).

The NP class, which correspond to inefficient or unfeasible algorithms (non realistically computable) is then defined as the ensemble of algorithm requiring a time which is a exponential function of the data length L : $T \geq 2^L$. An example NP hard problems (which are a special class of algorithm that do not necessities a yes or no output) is given by the spin glasses model energy optimisation.

In conclusion, and it is an already well established fact, the intrinsic information or complexity of an object or system can be well estimated by the entropy of the classical physical system previously proposed. However, this complexity measure is not reflecting the common conception of complexity, for which a complementing measure can be proposed.

4.1.2.9. Logical depth statistical measure or structural complexity

There has been many attempts to define organisation and its complexity (see Collier, 1999, Atlan, 1979, for review, Bialek & al, 2001, Adami & Cerf, 2000, Atlan & Koppel, 1990) each dealing with the same root problem clearly expressed in Bennett's definition of Logical depth that points out the insufficiency of the algorithmic information to uncover the notion of complexity, which one would like to be maximum for structures "in between crystal and smoke" (ie neither totally regular nor totally random, as our environment seems to be).

Complementing the notion of Algorithmic information, Bennett proposed the Logical Depth (Chaitin, 1977, Bennett, 1985, 1988) a measure of the time required by a universal Turing machine to generate the string or system from a random input (in number of computational steps, that is equivalent to a computational distance in between the uncompressed string or object and its maximally compressed form), to quantify the degree of organisation of a system. A related measure arise naturally from the ordered redundancy expression. One could find in

the simple measure $H_0 R$ an expression of the logical depth, but it do not catch the intuitive fact that repetitive systems (regular, highly redundant system, with all the redundancy at the same order i.e. in the R_n) are less organised or easier to compute compared to living systems which present a wide variety from local to long scale correlations and thus has a considerable logical depth (Bennett, 1988, Li & Vitanyi, 1997). Thus, logical depth would intuitively rather correspond to a diversity or disparity of the redundancy along the different orders. We can make this intuition more rigorous and propose the structural complexity to be measured as the dispersion of the redundancy across the various order. The proposed measure corresponds to the entropy of the R_i , and quantifies the dispersion of the structure among the different orders.

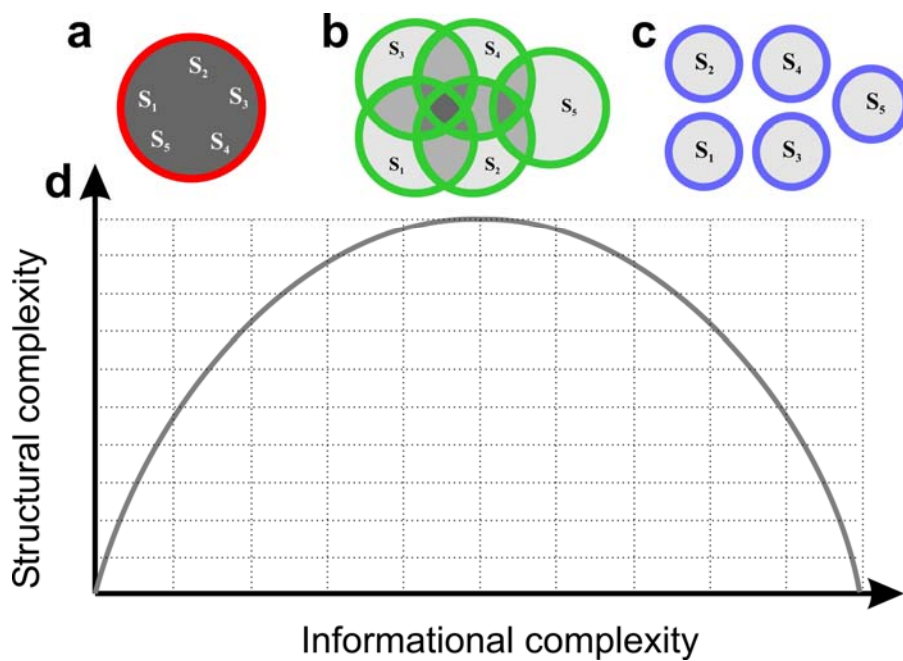


Figure 4.1.3: Schematic representation of the logical depth or structural complexity principle. Various level of structural complexity of systems (**a**, uniform, **b**, complex, **c**, independent) are exemplified using Venne diagrams. **d**, the proposed relationship between informational and structural complexity (inspired from Collier, 1999) represented here as a logarithmic function according to our proposition.

This measure is important, since it advances that there is an “information” in the redundant part of a system (object etc...), and since this information is the one biologists and more generally any observer are mostly interested in, as it quantifies organisation.

We propose that a measure of logical depth proposed by Bennett to be a continuous function of the R_i . The logical depth from its previous intuitive require the same properties as

information. Using Shannon reasoning (1948), we propose a measure of LD to require the 3 following properties (continuity & monotonicity, independence, and branching):

4. If the n order redundancies are equal ($R_i = \frac{R}{n}$) then LD is a monotonically increasing function of n and LD should be continuous in the R_i .

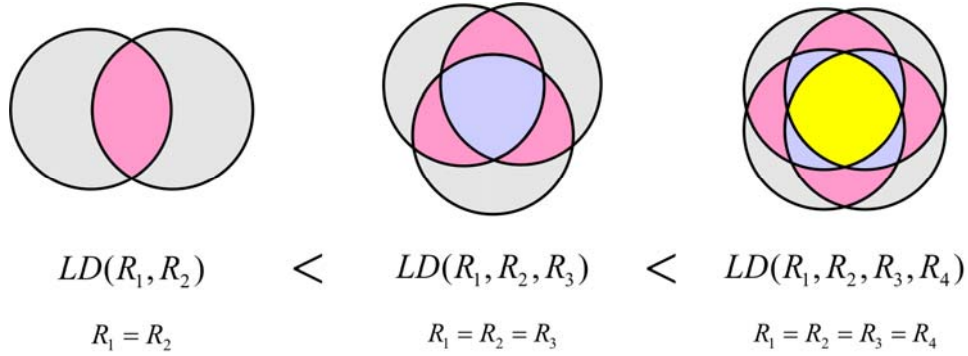


Figure 4.1.4: First postulate: LD is a monotonically increasing function of the order n .

5. If the system, object or string is composed of two independent parts then the total LD of the string is equal to the sum of the two independent part LD's.

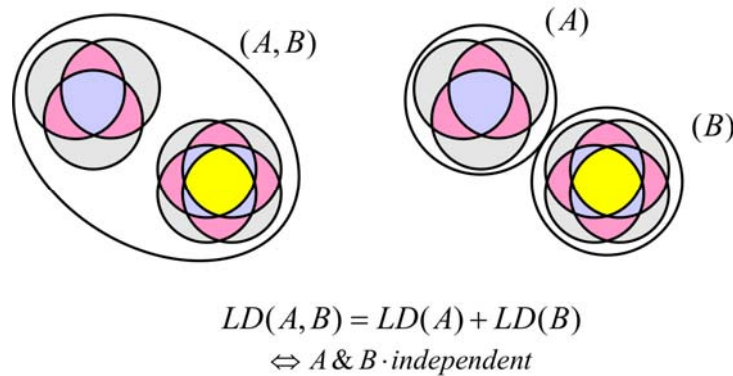


Figure 4.1.5: Second postulate: additivity of the LD for independent systems.

6. If redundancy is broken down into higher redundancies, the original LD should be the weighted sum of the individual values of LD.

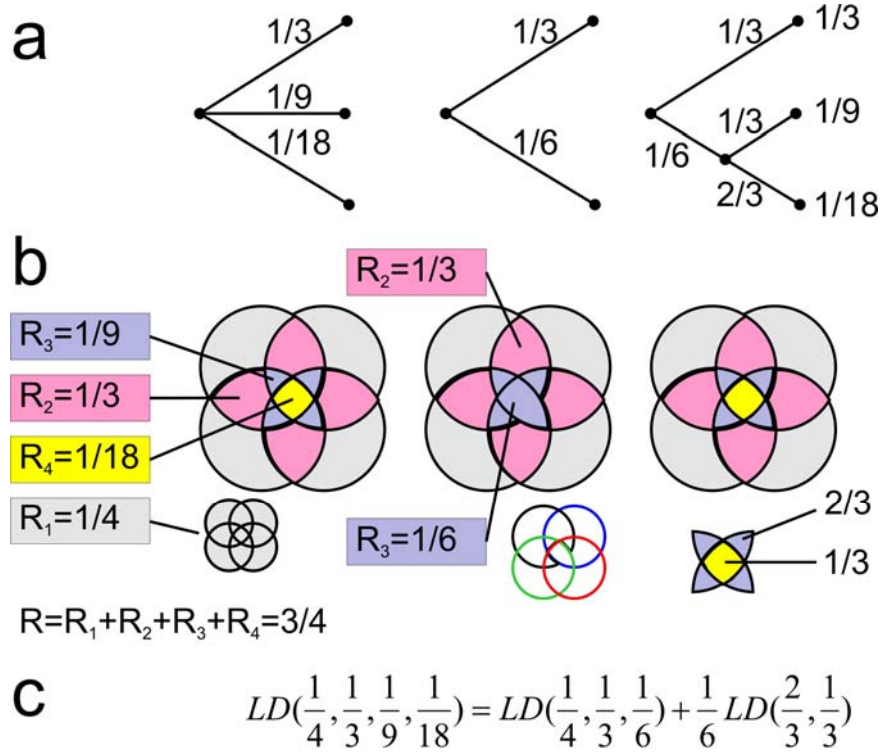


Figure 4.1.6: Third postulate: branching. *a*, schematic principle of redundancy branching (inspired from Shannon 1948). Each branch represent an ordered redundancy of the system under consideration (left: the full system, middle the same system with the fourth order redundancy omitted, right: the previous). *b*, schematic principle of redundancy branching represented using Venne diagram. *c*, The LD branching equality for this special case.

The only function satisfying the 3 above assumptions is (Shannon, 1948):

$$LD(S) = -k \sum_{i=1}^{n-1} R_i \log R_i$$

Logical depth is a measure of the level of organisation of a system, uniform or fully random systems are presenting low values of logical depth. Scale free system is a class of system that display obviously a large logical depth. It has to be noted the particularity of the redundancies compared to probabilities is residing in the fact that their sum can be less than one. However a sum equal to one is not required for the demonstration of the entropy as the only function satisfying the 3 exposed assumptions (Shannon, 1948 Appendix 2).

This measure by definition is invariant to any transformation that conserve distance or mutual information. The fact that two system present the same entropy is not sufficient to decide if the two systems are isomorphic (Falcioni & al, 2003). In this context it can be expressed by the fact that two systems presenting the same global amount of redundancy are not equivalent computationally or Algorithmically since their redundancy organisation or the computational

work to generate them are not the same. An interesting idea, our intuition supports, would be that entropy combined with Logical Depth are sufficient to reveal isomorphism (this property may be hold by the microscopic indistinguishability previously described).

4.1.3. Systems dynamic: Global “self-organisation” and local learning

Until now we only investigated the description of a system “statically”, at some fixed time. We have seen that whatever its past or future, its equilibrium or non-equilibrium state, it can be assigned an entropy function, statistically approximating its automata genesis complexity, and a structural complexity function, supposed to reflect the algorithmic Logical Depth. The aim of this chapter is to describe the temporal evolution of system (or dynamic), either isolated or in interaction with other system, in term of the previously defined redundancy. In other words, we saw in the previous chapter that it may possible to investigate systems in a geometrical way as surfaces, we will now try to investigate temporal carving, inflation or deployment of the surfaces, their natural evolution.

4.1.3.1. Isolated system evolution: entropy increase and energy conservation

According to Boltzmann second principle, which govern temporal evolution of physical systems, the entropy of an isolated system is always increasing or constant across time:

$\frac{dH(S)}{dt} \geq 0$. There is intrinsically a notion of evolution in the 2nd thermodynamical principle

proposed by Boltzmann: its basic statement is “The system of bodies goes always from a more improbable to a more probable state” (Boltzmann, 1877). This nature rule is intrinsically statistical, meaning that it is only based on a probabilistic assumption and suppose initial states to be very improbable. Indeed, the fact that “the early Universe was in a state of incredibly low entropy” is widely accepted (see “is our universe natural?” review in Nature on universe entropic and energetic evolution, Carroll, 2006). One has to note that the interpretation of entropy proposed here does not rely as classically on the ontological dichotomy between microscopic and macroscopic states: there are only microscopic states.

The first law of thermodynamic states that the energy is conserved. This natural rule is also deeply inscribed as a mathematical property of continuity or conservation. Noether's theorem relates the conservation of energy to the time invariance of physical laws, and is found in statistical physic in the Liouville theorem. Thus, energy cannot be made or destroyed; it can only be converted from one form to another, that is, transformed.

In the formalisation proposed here those two natural laws can be translated respectively in:

$$\frac{d \sum_{i=1}^n H(S_i)}{dt} = \frac{dR_1}{dt} = 0 \quad \text{for the first principle.}$$

$$\text{And } \frac{dR_H}{dt} \leq 0 \quad \text{for the second principle.}$$

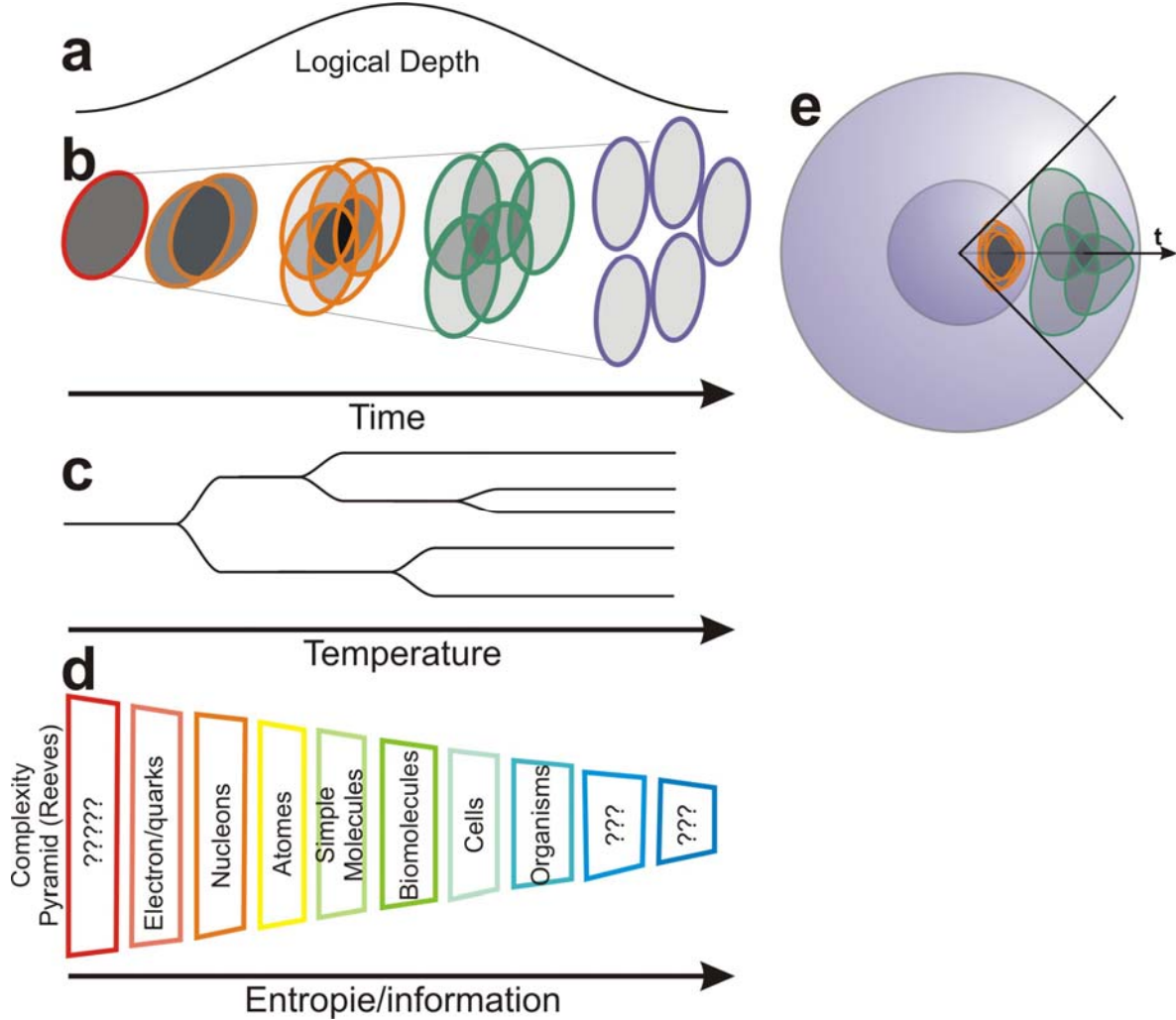


Figure 4.1.8: Schematic representation of an isolated system temporal evolution and complexity selforganisation. For this example the initial condition (**b**, red circle on the left) is arbitrarily set as totally redundant in the n th order (the five circles are completely superposed). Given the low entropy initial condition, the system undergoes a preliminary phase of self-organisation denoted by its increase of Logical depth (**a**), and a consecutive phase of self-disorganisation. First principle is depicted by the fact that the sum of the area of five circles is constant across time, whereas 2^{nd} principle is depicted by the decrease of the overall superposed area. **c**, schematic representation of the system dynamic as a tree (each line represent for example the center of each circle depicting the elementary H_i). This schema is proposed just to underline that the presented dynamic in **a** and **b** may be understood in the general framework of spatio-temporal singularities and symmetry breaking. **d**, the pyramid of complexity proposed by Reeves (1986) representing the temporal evolution and cooling of our universe and the relying structural complexity increase of the organisation levels. **e**, similar representation of isolated dynamic as in **a**, but schematized as a balloon inflation to emphasize the statistical inflation. As proposed in the next chapters the rate of entropy production may be non-homogenous and depend on the local redundancy (constraints) density, thus imposing a non-isotropic inflation. This representation is over-simplistic and more complex shapes than a sphere may have to be considered (it further argues about a potential link to physical relativity).

Under the plausible “realistic” assumption of highly redundant or very low entropy initial state, systems governed only by those two laws unavoidably undergo an initial phase of structural organisation with an increase of LD and a consecutive phase of disorganisation with an LD decrease (cf. Figure 4.1.8). This dynamic resume what can be predicted for the evolution of the universe organisation evolution from the state of knowledge in thermodynamic and complexity, however new undiscovered law, for example relating the $H_0 R_H$ component to the $H_0 R_I$ (which seems intuitively and logically plausible) may change or impose unexpected constraints on this predicted dynamic.

We can ask more rigorously what kind of dynamic Logical Depth is displaying across time in a general case without constraint on the initial conditions. Let S_{t+1} and S_t included in a Markov chain $S_t \rightarrow S_{t+1}$ (Simple Markov chains are probably non pertinent in dissipative systems or systems with memory, the following is just to understand better LD properties) :

$$\begin{aligned} LD(S_{t+1}) - LD(S_t) &= k \sum_{i=1}^{n-1} R_i(S_t) \text{Log} R_i(S_t) - k \sum_{i=1}^{n-1} R_i(S_{t+1}) \text{Log} R_i(S_{t+1}) \\ &= k \sum_{i=1}^{n-1} R_i(S_t) \text{Log} R_i(S_t) - R_i(S_{t+1}) \text{Log} R_i(S_{t+1}) \end{aligned}$$

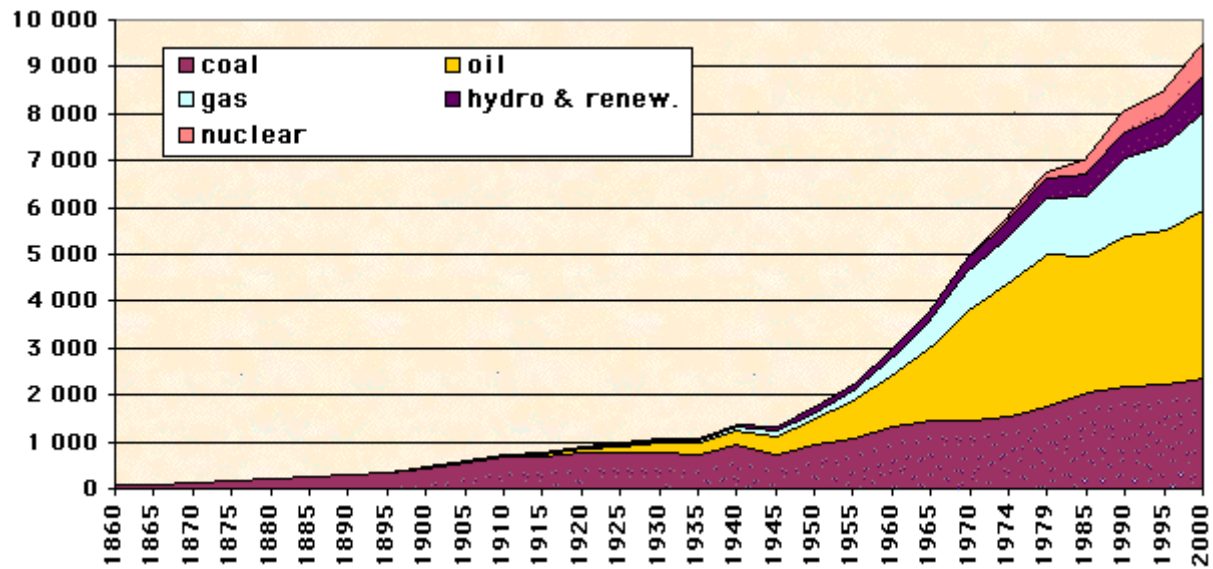
We can only consider the sign of $R_i(S_t) - R_i(S_{t+1})$ whatever n. R_n are sums of various mutual information terms multiplied by a positive constant. Since relative entropy and Mutual information always decrease: $I(X_t, Y_t) \geq I(X_{t+1}, Y_{t+1})$ (Cover & Thomas, 1991), we can write for any Markov chain :

$$LD(S_{t+1}) - LD(S_t) \geq 0$$

It would mean that the level of organisation of a system always increases. It appears plausible from a global observation of the evolution of our world, but contradicts the 2nd principle (the maximum entropy state have necessarily the lowest LD). The above equation failure come from the fact redundancies sum is not equal to one and is decreasing as the entropy increase. There is thus no systemetic increase of LD, as encountered with Mutual information, and initial conditions have to be considered to obtain some rule on the LD dynamic.

Interestingly, this framework may have a simple interpretation in term of symmetry breaking and singularity. As roughly schematized in figure 3.7.8.c, the natural system dynamic can give rise to singularity or bifurcation in the phase diagram (just a suggestion since i do not know those fields). Moreover, a tree, for biologist, is meaningful (and beautiful).

a



b

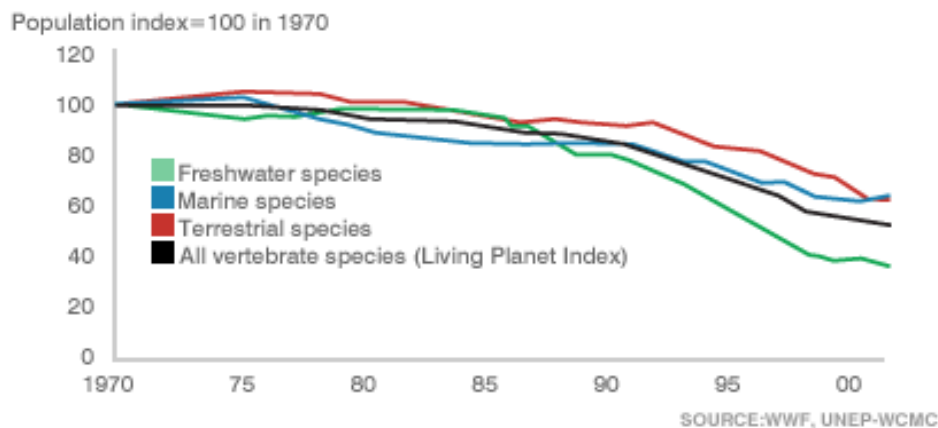


Figure 4.1.10: Actual evolution of Human energy consumption and earth biodiversity. *a*, The graphic represent the world industrial energy consumption since 1860. At the organisation level of Human societies, including an important part of its ecosystem, the equilibrium state is probably not so far. Y axis in million tonnes of oil equivalent (Mtoe) the upper value is equivalent to 7 million H bomb or 13 Hbomb.mn⁻¹. (Source: <http://www.manicore.com/> , From Schilling & Al. 1977, International Energy Agency, Observatoire de l'Energie). *b*, Evolution biodiversity on earth from 1970 to 2000. The Living Planet Index is a measure of the state of the world's biodiversity. It measures trends of vertebrate populations in terrestrial, freshwater and marine environments (Source WWF, UNEP-WCMC). This graphic does not account for vegetal diversity and biomass.

As stressed by the figure 3.7.8, isolated systems with low entropy initial condition necessarily undergo an initial phase of self-organisation and a consecutive phase of self-disorganisation. Cosmological studies in general seem to indicate that, at the scale of the universe, entropic potential is far from being consumed (for review, Carroll, 2006). However, at the scale of our planet, although the energy and the diversity (structural complexity, notably biodiversity) resources and circulation are hard to quantify, a colossal amount of scientific evidence (and even just the good sense of everyday observation) points out the extremely preoccupying and emergency of our actual state and dynamic (figure 3.7.10).

It is possible to try to exemplify intuitively such organisation process more locally and with a more common systems. When there's too much energy in a region of the phase space (high energy density, for example the sun), the only way to increase entropy is to radiate, to emit energy (usually photons) in the other region of the phase space. Organisation complexity development, or logical depth structural increase (and lastly life) requires a compromise in the energy density: enough energy-density to have structure and not too much energy-density to be complex (this is the energetical side of the “in between cristal and smoke” paradigm).

4.1.3.2. Maximum Entropy Production, Energy minimisation, constraint satisfaction, and hard problems

A central question arise from the previous description is “**what is controlling the speed of evolution, the dissipation rate? Or equivalently how to predict future in complex non equilibrium systems?**”. As always several trails given by literature can be followed. Obviously, in our environment, a whole range of system temporal dynamics can be encountered, from the extremely rapid to the very slow. Living systems dynamic seems on both slow and rapid temporal scales, they are very long-term and short-term memories.

According to the previous chapter, an isolated system natural evolution can be presented as an energy (interaction) or constraint minimisation problem, submitted to total energy conservation rule. Energy (interaction) or constraint minimisation problems have been long studied in physics and artificial intelligence and in some case has been proved to be NP hard, and a little reminder paragraph is needed.

A well known example of intractable energy optimisation problem is given by the paradigmatic spin glasses model. A Hebbian recurrent neuronal network model has been shown to present a dynamic isomorphic to those spin models (Hopfield, 1992). It consists in lattice (or matrix) of totally interconnected elementary constituents (n constituents X_i) that

can take two states -1 or +1. The values of the coupling interactions T_{ij} , which can be represented as a matrix of $n \times n$, can only take +1 or -1 values in a simple case (ising, T_{ij}

symmetric). The energy of such a system is given by: $E = -\frac{1}{2} \sum_{i=1}^n \sum_{j=1 \neq i}^n T_{ij} X_i X_j$. Finding the

minimum of this function requires considering case by case the 2^n possible configuration: no efficient polynomial time algorithm has been found for this task. In fact such kind of system possesses numerous local metastable (local minimal energy states) that brake considerably the evolution dynamic; and that explain the very long relaxation (dissipation) or very slow aging-evolution of glasses systems. In our terms, the obvious high R_H states of glasses systems present low rate dissipative dynamic. Interestingly, this type of dynamic appears closely related to Prigogine work in non-isolated systems, that have shown that in far from equilibrium conditions (in our framework high R_H states) the production of entropy is minimum.

Moreover, this problem has been found to have an equivalence in computer science under the very general constraint satisfying problem, more precisely to correspond to the “hard” phase of SAT problems where solutions clusters are splitting. The SAT problem formalisation has been shown to encompass many problems arising in a widespread range of scientific disciplines. Problems that can be expressed as constraint satisfaction problems are among others, the salesman travelling problem, the Boolean satisfiability problem, scheduling problems and the graph colouring problem (Mezard, 2003). Solving a constraint satisfaction problem on a finite domain is an NP complete problem, but researches have shown a number of tractable subcases. The major interest of this problem is that it presents a “phase transition” discontinuity: when the ratio of the number of constraints over the number of variables increases the solution landscape (at a precise given value of the ratio) splits into several local minima. I did not find yet the precise and relevant expression of the constraint to variable ratio in the present framework. It could be the absolute efficiency of a system:

$E(S) = 1 - R(S) = \frac{H(S)}{H_0(S)}$ or something like a ratio between free-energy and internal energy:

$$\frac{R_H(S)}{R_I(S)}$$

In any cases, constraints, in the framework we presented, are given by the elementary dependencies between the elementary constituents. Any regularity in the organisation of the constraints (that is measured by the LD of the system) may be used to solve efficiently the

SAT problem (this is in essence the principle of renormalisation, but much would have to be developed to make it formally clear).

For preliminary conclusion, it is appealing to draw the following rule: the evolution rate of a physical system is a function to the ratio of the number constraints over the number of degrees of freedom of the system. In other term the entropy production rate should be a function of the probability to find a microstate satisfying the constraints among all possible microstates. This, on my opinion, gives a general justification of space and time inseparability.

It is also appealing to consider the whole world as isomorphic to a glass system (at least partly), or equivalently to consider the initial conditions as a computational problem of energy minimisation. The evolution of the global system would give rise locally to a full range of problems ranging from simple problems rapidly solved, hard problems “still” present or may appear, and close to hard problems still converging where living systems lies.

But, let us come to what we think to be the best solution to this problem proposed in the litterature. As previously for space, the entropy maximisation under constraint have successfully formalised and solved the problem of temporal evolution for system either in equilibrium or in non equilibrium with its environment (Maxent, Jaynes, 1957 ,1957 ,1979, Dewar, 2005). Indeed, Dewar (2003, 2004, 2005) has extended the Maxent principle in the temporal dimension and by the way to non equilibrium systems, and thus established a new thermodynamical law that state that a system maximises its entropy at a maximal rate (Maximum Entropy Production). By the way, Dewar has shown that Fluctuation Theorem, emergence of Self-organised critically system, and Prigogine’s Minimum Entropy Production in far from equilibrium system, naturally follows from this principle. Those latest equivalence further prove the relevancy of the temporal Maxent paradigm. The idea is quite simple and consists in a generalisation of Jaynes maximum caliber principle: Dewar idea is that in order to take into account the history of the system and thus to predict the dynamic of any kind of system (in fact, systems with Gibbs distribution, but this may be generalised using our framework), the probability of the system paths in the phase diagram has to computed instead of the classical microstate probability (probabilities calculated on the dynamics instead of on the state). The maximisation of the entropy of the paths gives a direct and the best prediction of the future paths. This is the Boltzmann spatio-temporal generalisation to any system, and probably the physical horizon to our knowledge of the future. It consists in maximising the

function $-\sum_{\Gamma} P_{\Gamma} \text{Log} P_{\Gamma} - \sum_{k=1}^m \lambda_k \langle f_k \rangle$, where P_{Γ} are the probability of phase space path Γ (the

entropy is measured on the ensemble of possible paths) and λ_k the Lagrange multipliers for each m spatio-temporal constraints $\langle f_k \rangle = \sum_{\Gamma} P_{\Gamma} f_{kj}(S)$ (with an additive normalisation constraint).

We can inspire from this “dynamic Maxent” principle to develop the notion of spatio-temporal redundancy in the proposed framework, in order to describe the temporal evolution of any system (isolated or not and driven by any kind of force or energy). The consideration of time and space linked together is not classical in physic and imply a loss of correspondence with it. The ensemble on which we will compute the probabilities is now the ensemble of trajectories of the m copies of the systems trajectories in the phase space (figure 3.7.11). In fact, the consideration of spatio-temporal redundancies is particularly relevant for non-isolated interacting systems.

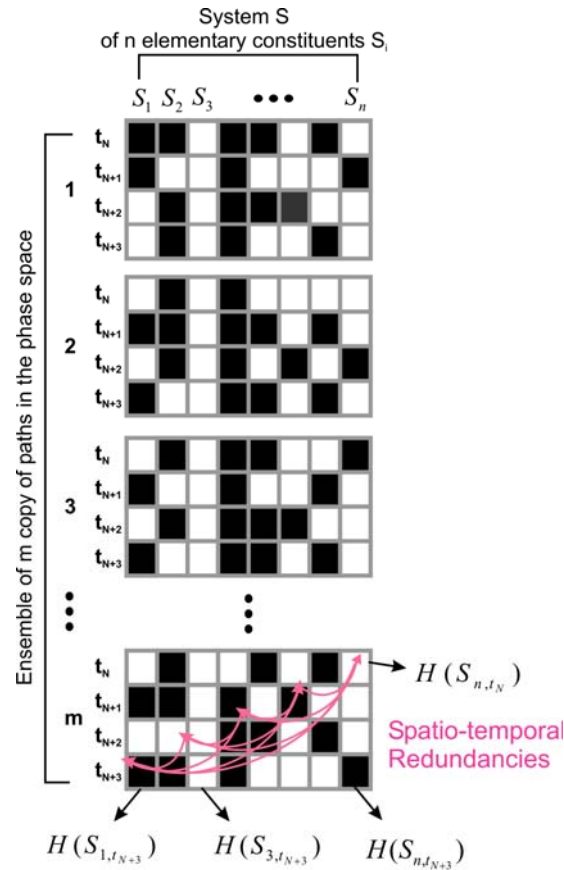


Figure 4.1.12: Proposition of a principle of measure of the entropy of the paths in the phase diagram (entropy of the dynamic). The convention of this graphic are the same as figure 3.7.2 but with system presenting a temporal dimension, and a measure of redundancy extended to spatio-temporal domain. Simply presented as here, this framework is only available for ergodic stationary systems, for which the temporal evolution is symmetric in time. To account for non stationary dynamic, a more complicated framework has to be considered that distinguishes and “numerates” each temporal slices. This development appears to be difficult and more time is necessary to investigate those problems correctly (since even the classical definition of time do not seem relevant).

4.1.3.3. Chaotic dynamic and deterministic quantum uncertainty amplification

As already suggested and proposed in various work (Ruelle, 1991, Zurek, 2003), our framework considers that various level of chaotic dynamic amplifies quantum uncertainty. This point of view has its deep roots in the Copenhagen school interpretation (on the irreducible non-deterministic/probabilistic dimension of the elementary constituents of our world), and states that the irreducible quantum non-determinism is amplified during system evolution by chaotic dynamic of various intensity (Zurek, 2003) that encompass the classical physic deterministic evolution equations. Chaotic systems are defined by the fact that the incertitude is exponentially increasing as a function of time, leading to a rapidly diluted determinism and thus to a deterministic limit to prediction and certainty. Chaotic dynamic can be understood as a dynamic that amplify uncertainty. The classical definition considers a dynamical system, represented by a n dimensional vector and defined by a deterministic function such as $\frac{dX}{dt} = f(X(t))$. The system is said chaotic if the evolution of the precision on X is a function of the type: $\Delta X(t) \approx \Delta X(t_0).e^{\lambda_1 t}$ when $t \rightarrow \infty$ and where $\Delta X(t) = |X(t) - X'(t)|$ is the divergence of two trajectories initially separated by a small imprecision ($\Delta X(t_0) \rightarrow 0$), and λ_1 is the first Lyapounov exponent (the dynamic is said to be chaotic if $\lambda_1 > 0$). In fact, to fully describe the dynamic, n Lyapounov exponent have to be considered for a system. Considering a ball of dimension n , of radius ε and center $X(t_0)$, according to function of evolution of X , the ball will be deformed into a n -dimensional ellipse with n axis $l_1(t) \geq l_2(t) \geq \dots \geq l_n(t)$. The different Lyapounov coefficients λ_i are then defined by: $\lambda_i = \lim_{t \rightarrow \infty} \lim_{\varepsilon \rightarrow 0} Ln(\frac{l_i(t)}{\varepsilon})$. (See Falcioni & al, 2003 for review).

The dynamic of uncertainty has a simple expression in term of higher order redundancy (considering the precision $\Delta x \Delta p = (h)^{R_H^n}$):

$$\Delta x \Delta p(t) = \Delta x \Delta p(t_0).h.e^{n(R_H(t) - R_H(t_0))}$$

Considering a system with initial condition $\Delta x \Delta p(t_0) \rightarrow 0$ (in fact the minimum of $\Delta x \Delta p(t_0) = h^n$ and thus $R_H(t_0) = 1$), which appears reasonable considering the physical history of our world (cf Carroll, 2006 and previous discussion), we can propose:

$$\Delta x \Delta p(t) = \Delta x \Delta p(t_0).h.e^{\lambda t} \text{ with } \lambda t = n(R_H(t) - R_H(t_0))$$

In other term, the ordered redundancy are the opposite of the Lyapounov exponents (for an isolated system of very low initial entropy), and quantify the dissipation “rate” of the system.

4.1.3.4. Interacting Systems : learning-adaptation

We can now consider the case of two systems exchanging information or energy, and we will focus on the simple particular case sufficient for our purpose, of a system S in its environment E considered as a reservoir. Let's define a system S represented by an information $H(S)$ which receives information or energy from the environmental system E with an information $H(E)$. This interaction or energy imposed by the environment to the system constitutes supplementary constraints that are added to the system evolution, and the two principles (energy conservation and entropy increase) still govern the temporal system evolution.

According to the previously exposed temporal Maxent principle (Dewar, 2003, 2004, 2005), the system in time will develop the maximum entropy dynamic compatible with the spatio-temporal constraints imposed by the environment. It is possible to express this dynamic in the framework of information theory, by considering the information channel between E and S and remarking that the maximum entropy under constraint principle is isomorphic to the maximisation of mutual information principle. This isomorphism has been several times underlined in computational sciences, where various Infomax principle implementations were shown to be equivalent to maximum likelihood density estimation algorithm (MLE, Pearlmutter and Parra 1996, Cardoso 1997, Mackay 1996). This correspondence can be expressed as the following: the maximisation of the mutual information between E and S comes to maximise the entropy of S and to minimise any other entropy source of S that do not come from E , since E constitute the only input to S in the channel framework and since all the constraints imposed by E have to be considered to make a valid Maxent inference, both come pragmatically to the same computation.

Mutual information in between E and S is given by: $I(E, S) = H(E) - H(E/S) = H(S) - H(S/E)$, where $H(E/S)$ represents the equivocation and $H(S/E)$ represents the ambiguity. $H(S/E)$ represents whatever entropy the system S has that did not come from the environment E . In classical interpretations, $H(S/E)$ represent the probabilistic behaviour of information transmission in between E and S , and

corresponds to what is classically named noise (H_{noise}). Considering the relation expressed in (5), $I(E;S)$ can be expressed as:

$$I(E;S) = \sum_{i=1}^n H(S_i) - H_{0S}R_{HS} - H(B/A) = H_{0S} - H_{0B}R_{1B} - H_{0B}R_{HB} - H(B/A),$$

This relation points out that noise or ambiguity and higher order redundancies are acting on mutual information in the same way. In fact, mutual information in between the two systems is already a redundancy and energy.

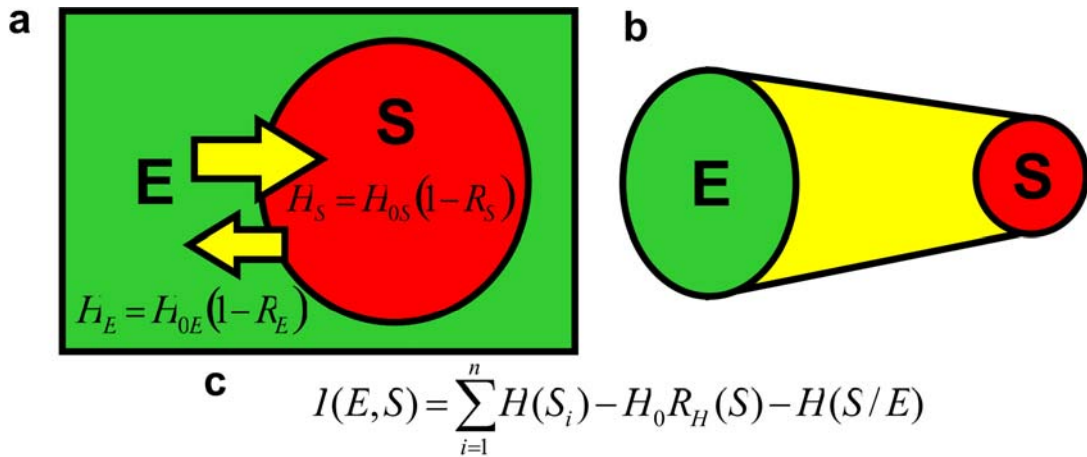


Figure 4.1.13: Schematic representation of the environmental system interaction formalisation from the informational point of view. *a*, Simplified representation of the system (S) interaction with its environment (representing all the sources of information-energy and all the output destination possible) The capacity of the system (H_{0S}) imposes a bound to the interaction. *b*, Representation of the information transmission from a more classical channel point of view. *c*, the mutual information formula in the proposed paradigm. Higher redundancy and ambiguity have the same reducing impact on the mutual information between E and S.

This relation is far more general than the classical application case of channel with noise (Shannon, 1948), and holds in the case of mutual Algorithmic Information between objects (or strings), or “shared complexity”: $K(E : S) = K(S) - K(S/E)$ (Kolmogorov, 1968).

As previously for the information-entropy, the Shannonian Mutual information is a statistical estimation of the Mutual Algorithmic Information, as demonstrated by Adami & Cerf (2000). According to their appellation, the mutual information of the system with its environment presented here is the “physical complexity” of the system, and $H_0(S)$ is the unconditional complexity of the system ($K_0(S)$ the Kolmogorov complexity in absence of any environment), and the measure of information presented above is the statistical analogue of mutual Kolmogorov-Chaitin complexity $K(E,S) = K(S) - K(S/E)$ which statistical quantification

is given by: $\langle K(E : S) \rangle_{S_M} = \sum_{S_M} p(S) K(E : S) \approx H(S_M) - H(S_M / E_m) \equiv I(E_m, S_M)$, where S_M

denotes the ensemble M of copies or trials of the system and E_m the ensemble m of copies or of the environment (our framework slightly differ from the one of Adami and Cerf and allows a definition of the environment ensemble).

In fact, Infomax is directly consistent with Bayes rule and is a little bit more sophisticated than the Maximum likelihood principle. It is possible to understand it intuitively by considering the Bayes rule: $P(S / E) = \frac{P(E / S)P(S)}{P(E)}$. Maximum Likelihood principle consists

in selecting the most probable hypothesis (or system S) generating the data (environment E) and thus in searching S such as $P(S / E)$ is maximal. Developing Bayes rule into informational term, we obtain: $-\text{Log}(P(S / E)) = -\text{Log}(P(E / S)) - \text{Log}(P(S)) + \text{Log}(P(E))$

and thus $\text{Log}(\frac{1}{P(S)}) - \text{Log}(\frac{1}{P(S / E)}) = \text{Log}(\frac{1}{P(E)}) - \text{Log}(\frac{1}{P(E / S)})$. Roughly information maximisation can be understood as both minimising the length S (optimal code) and as selecting the most probable hypothesis (system S) generating the data (the environment E).

From the automata point of view, and as stressed by Bennett, some type of computation can theoretically be made reversibly, instructions like *write*, *copy* (on a blank tape), *NOT* are conservative. However, the instructions *erase*, *overwrite* which correspond to the forgetting of the previous logical state are intrinsically dissipative (Bennett, 1982). In fact, the proportion of reversible compared to irreversible processes, in the physical world is not easy to evaluate and is directly assessed by the entropy production and chaotic coefficients previously discussed (and as always living systems seem to fall in between highly conservative and highly dissipative dynamic). This paradoxal state seems to be a direct consequence of the information maximisation process which signature is at the same time a redundancy minimisation and a maximisation of the environmental interaction.

It gives also an interesting and intuitively satisfying definition of the efficiency of S to “represent” E :

$$\varepsilon = \frac{I(E; S)}{H_{0S}} = \frac{\sum_{i=1}^n H(S_i) - H_{0S} R_{HS} - H(S / E)}{H_{0S}} = 1 - R_S - \frac{H(S / E)}{H_{0S}},$$

$H(S/E)$, ambiguity or noise, is participating to efficiency and mutual information exactly in the same way as redundancies. The efficiency measure classically used in neurophysiology (and that we have been using in associated study, Rieke & al, 1997) is slightly different, but is also pertinent. Its expression in this framework is given by:

$$\varepsilon_1 = \frac{I(A;B)}{\sum_{i=1}^n H(B_i)} = \frac{1 - R_B - H(B/A)/H_{0B}}{1 - R_{1B}} = \frac{\varepsilon}{1 - R_{1B}} \text{ and thus represents a ratio in between the}$$

total redundancy with the first order redundancy ($\varepsilon_1 \rightarrow 0$ when $R_1 \ll R + \frac{H(B/A)}{H_{0B}}$ and

$$\varepsilon_1 \rightarrow 1 \text{ when } R_1 = R \text{ and } \frac{H(B/A)}{H_{0B}} = 0).$$

It is possible to give some preliminary biological and cognitive interpretation of this phenomenon that will be further developed in conclusion. The maximisation of mutual information between a system and its environment, which can be also expressed in the fact that a system takes one of the most likely states compatible with the constraints imposed by its environment, can be considered as the driving force of system adaptation and evolution (in the Darwinian sense this time, and of course as in field physics force does not really exist). It may give a thermodynamical foundation for the adaptation and learning of systems to their environment. This adaptative dynamic is the same mechanism of self-organisation as the one exposed previously for a whole isolated system, but tackled relatively and locally from one system component taken as a referential in the whole system. It also gives some trail to understand how knowledge-energy is spreading in our environment (everyday examples are legion, and in fact everywhere, from ecosystem to human societies and cognition). Whenever energy or knowledge is more concentrated in some part of the system, it spreads and diffuses to the surrounding. This spread goes in hand with dissipation of a part of the energy-knowledge (that is the R_H), and in some case to a complexification of the structure. This dynamic can also be understood as a free-energy minimisation problem involving a widespread network at different resolution scale.

4.1.3.5. Discussion: space and time as product of dissipation

A proposition, far from being proved here, but appearing through this work is that time and space could be the result of energy consuming (at least, it seems to make sense at the psychophysical level). We saw in first chapters that the relevant spatial distances are probably statistical distances (mutual-information or KL-divergence), the creation of this space or distance implies dissipation. Fluctuation may not be the exception in our world but the generating rule. In more simple terms, the investigation of our world from the statistical dynamic point of view directly leads to the hypothesis of creative noise.

4.2. Global conclusion: convergence and principles of cortical computation

The results and model exposed in this thesis combined with neuroscience and computational literature, allows a convergence of the mains theories of brain computation:

- Receptive field functional theory
- Neural assembly theory and temporal binding
- Learning and adaptation theory
- Efficient coding, informational theory and fluctuation-dissipation
- Algorithmic and cybernetical theory
- Physical & thermodynamical theory of information and of cortical processing
- Active sensing theory.

4.2.1 Receptive field functional theory

Linear and nonlinear RFs **are** gain controls resulting from adaptative mechanisms. They operate a computation that can be resumed to two statistical processes, namely redundancy and noise removal (see Figure 3.6.5.c for empirical probe of the preferential noise removing regime of the neuronal integration process in natural condition). Those functions are generated by a wide range of physiological mechanisms, neuronal intrinsic non-linearity (including spike generation: Action Potential with its biphasic Na⁺ depolarising/K⁺ hyperpolarising voltage dependent dynamic is a generic primitive and widespread (evolutively the oldest) redundancy/noise reduction mechanism), and network dynamic (including excitatory inhibitory balance). The temporal biphasic nonlinearity observed for natural-like conditions can be considered as the generic cortical nonlinearity generating β - γ rhythms, emerging from STDP-like mechanisms (excitatory Hebbian-inhibitory antiHebbian STDP) and that increases the temporal precision and sparsness-selectivity of the code. Moreover, the temporal dependence and assymetry of the STDP rule provide to the cortical function the property of input temporal compression, a property often referred as predictive coding. In mature subjects, RFs refelect the highly specialised cortical memory, and even cells classically considered as “simple and linear cells” are found mostly non-linear in a natural context (“complex” and specific high dimensional feature). In natural condition and for cells that are considered classically as simple cells, the linear component could hardly explain 30% of the synaptic input response (figure 3.6.1), and the synaptic to spike output was further found to be specifically nonlinear in this condition (V_m*spike coherence is revealing

that at most 30% of the input-output process can be assigned to a linear process, cf figure 3.6.5 b). This specificity attests for the existence of specialised cortical microcircuits and neuronal properties, reflecting the wide diversity and variability of connectivity patterns, RF functions (eg. Center-Surround NL), neuronal morphology and phenotypes (depressing/facilitating synapses, fast-spiking/regular/bursting etc.) observed in the neocortex. A simple organisational rule can be proposed: cortical process maximises the RFs diversity (RFs are maximally different memories of the input). The cortical structural complexity corresponds to its functional diversity, and both are imposed by (or corresponds to) the structural diversity or complexity of the external environment. An important conclusion follows from this: the full description of RFs functions or equivalently of the whole cortical responses cannot be fully caught by one or few generic simple N-NL models as classically proposed (or equivalently, the enormous biological capacity and mechanism diversity of the cortex is irreducible to simple or small capacity model, thus imposing the allocation of an enormous computational power to faithfully simulate the neocortex corresponding to the enormous Logical depth of the environment and therefore of the cortical computation). Instead, to account entirely for cortical dynamic and responses, complex space and time NL functions and not monodimensional average contrast or luminance NL functions have to be considered (see for example the model presented in figure 3.3.9.2). Moreover, the content of the boxes should be different functions from one neuron to another in the same area, and reflects statistical biases of the environment (the most likely ones as we are in the first processing stages). In other terms, RF studies are a descriptive not a theoretical framework: a complete cortical function characterisation requires as many functions as the number of neurons and no simpler/shorter function can be found. Instead, and as further proposed (and already exposed in computational literature), informational theory provides simple general generative rule (algorithm improperly named “self-organising”, instead of “co-evolutive” dynamic), that given the environment characteristics (in fact, the organism complexity shall tend to be equal to the environment complexity (LD)), that shall be sufficient to modelise, simulate or predict the whole cortical function and dynamic.

An important conclusion concerning RFs and cortical selectivity (but which may be broadened to any physiological function), is that **selectivity is expressed in the precision, reliability and sparseness of the response rather than in the rate of discharge of the neurons** (see **figure 4.2.1**). Our thesis provides informational tool, notably time-frequency SNR measure, that can be used for a widespread range of signal analysis, and that allow to uncover

selectivity by taking into account the signal reliability and precision. Using the variability of the response (intersubject variability) to uncover cortical function has already been applied successfully at the macroscopic scale of cortical areas activation in fMRI (Hasson & al, 2004).

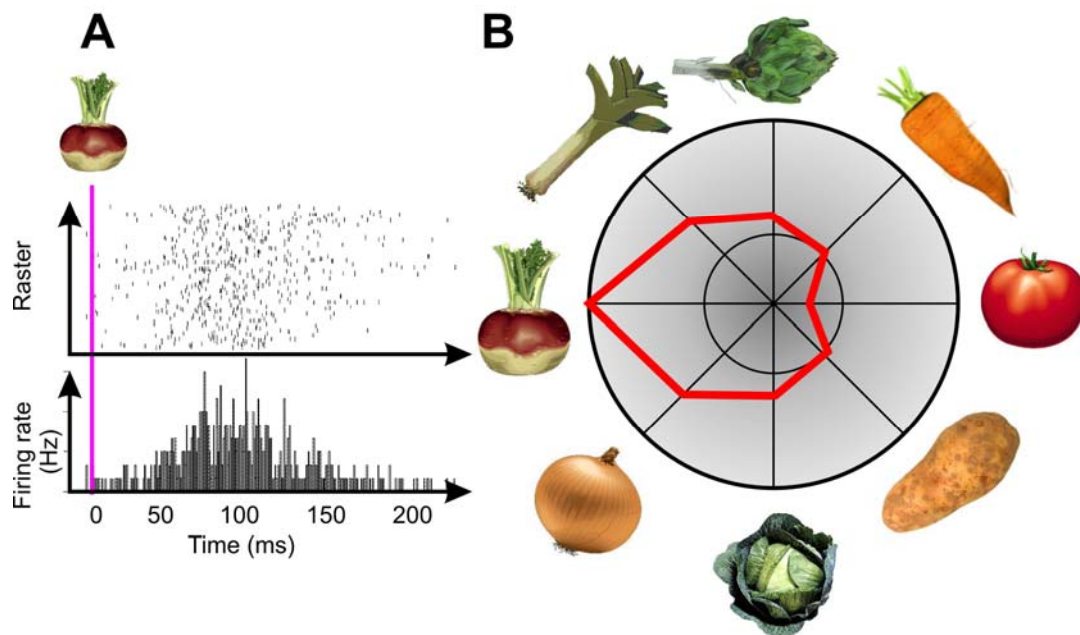


Figure 4.2.1: *What if Hubel had a turnip in this hand instead of a slide with straight edges when V1 selectivity was discovered?*

This new definition of selectivity is also supported, first in spirit by Vinje & Gallant study (2002) who have shown that some selectivity criterion is correlated with a sparseness criterion, and second, more precisely by Machens & al (2005), who have defined an “optimal stimulus ensemble” based on information criterion in the grasshoppers auditory receptor neuron. Defining selectivity and function as depending on the reproducibility is in deep rooted in the proposition of this thesis that learning-adapting unavoidably increase the determinism of the adapting system to its environment and reflects a causality axiom in physic (see also Dewar, 2004, for similar reasoning). If this new definition of selectivity is recognised as being more physically pertinent than the number of spikes (or rate of discharge), it would mean that a far predominant component of neuronal function in the cortex is still unknown since most of the studies base the function measure on the rate (such depicted in the figure 4.2.1) and that the cortical RFs complexity has been widely underestimated in most of the studies which have just uncovered a very partial and averaged approximation of the real function. Therefore, one would prefer, as proposed before, to forget about an exhaustive description of the cortical RFs and to focus on generative, dynamic, or adaptative rules.

As a leitmotiv appearing in all the chapters of this thesis, **this selectivity and RFs function of the neuron is shown to be generated by the Excitatory and Inhibitory balance provided notably by the intracortical recurrence** (carved/modulated by the cortical plastic mechanisms, as discussed in two chapters). This Excitatory-inhibitory balance was in fact shown to shape:

1. the spatiotemporal characteristics of the linear subthreshold RF
2. the orientation and direction selectivity of the neurons spiking output
3. the modulation notably temporal imposed by the center-surround interactions and their selectivity and their contrast dependence.
4. the sparseness and temporal precision of the spiking output in natural condition with eye-movement.

4.2.2 Neural assembly theory and temporal binding (synchrony, β - γ oscillations)

At the mature stage, and when immersed in its natural rearing environment, the cortical network presents a precise and sharp neural assembly dynamic (for the cortical systems involved in the analysis of the precise characteristics of the input at this time, other cortical areas non relevant for this peculiar context display a spontaneous internal dynamic without coherence with the “active” areas). In this condition, neurons work in a synchronous input or “coincidence” detection mode (the rate/temporal code, or frequency/coincidence integrator modes appear to form a continuum, see for example Theunissen & Miller, 1995). The information maximisation principle states that the number of neurons activated by a given input shall be the smallest possible, or equivalently that the neural assembly corresponding to a given cognitive task shall become as small as possible with learning-adaptation (this “sharp” assembly argument with the ultra-specialised functional microcircuit argument exposed in the previous paragraph, see also Deweese and Zador, 2006 for compatible empirical results). This optimal processing or neuronal assembly sharpening corresponds algorithmically to the Occam razor principle implementation (Schmidhuber, 1992), that is implemented by the mutual information maximisation process. Moreover, β - γ oscillations are often considered as carrier waves that sustain synchrony (W. Freeman, 1991) that depend crucially on GABA_A inhibition (in the olfactory system, see MacLeod and Laurent, 1996). Our results confirm and pursue these observations by further pointing out the origin of β - γ fast oscillations in the plastic STDP mechanisms (Hebbian excitatory and antiHebbian inhibitory, figure 3.6.4 b d & f).

The ordered redundancy formalism proposed in this thesis can be considered as a quantification-description-definition of neural assemblies in its largest definition, accounting for synchronous activity (or synfire chains), correlations among various number of neurons, and when applied in time, phase relationships and higher order temporal patterns (see Martignon & al, 2000, for an alternative definition).

4.2.3 Learning and adaptation theory

Learning-adapting reduces noise and redundancy (and therefore increases the precision of the code). This rule is proposed to be a universal property of learning in living systems (see Adami & Cerf, 2000 for the genomic adaptation) and is probably the most important empirical conclusion of this work. The resulting redundancy reduction can be understood as a fundamental and elementary cognitive or “intelligent” process. The biphasic nonlinearity profile presented in Figure 3.6.4 further argues about the relevance of **Hebbian excitatory and anti-Hebbian inhibitory** (the inverse of the classical STDP rule) Spike Timing Dependent Plasticity (STDP) as the generic cortical adaptive function (but which probably encompasses much more physiological mechanisms than the simple synaptic plasticity process). Moreover, we propose mutual information maximisation to be a formal definition of adaptation and learning.

4.2.4 Efficient coding, informational theory and fluctuation-dissipation

The interpretation of our empirical results and formalism proposed in this thesis is directly included into the mutual information maximisation principle (between the sensory input and the output of the cortical network) proposed in computational literature since the work of Barlow, Linsker, Bialek, Nadal & Parra, Bell & Sejnowski... However, the proposed formalism precise this computation in a physical framework and generalise it as an intrinsic computational/cognitive process. In the framework proposed, mutual information maximisation is an intrinsically irreversible and dissipative process rather than a conservative information transmission process. This holds on a central mechanisms: the resistance to fluctuations, and our formulation of the infomax process corresponds to the fluctuation-dissipation theorem in the non equilibrium case. This non-equilibrium case does not seem to be yet well formalised in Physics where the fluctuation-dissipation theorem has only derived for the general linear case. Application of the fluctuation-dissipation to out of equilibrium

system require the introduction of a still debated effective temperature, and therefore more work may have to be done on this topic notably using the model proposed here that in fact avoid the introduction of temperature.

In the cortical context, the sensory input imposes a complex energy flow, and information maximisation (or adaptation) process dissipates the energy. It corresponds to the receptive field function and “dynamic” that can be also viewed as an impulsional nonlinear system relaxation. On a more integrated scale, and to our opinion, it may correspond also to fMRI cortical activation that is well known to represent the metabolism (notably dioxygen consumption) and therefore energy consumption. A view inspired from Schrodinger could be that “living systems absorb environmental fluctuations and this plastic dynamic allows them to maintain their order from decaying (death)”.

We could identify empirically two neural mechanisms underlying this computation: on the one hand the cortical system, from the neuronal (figure 3.6.5) to the network level (dense noise input condition: figure 3.5.4 a & b, figure 3.5.2 b –spike, figure 3.5.1 d) resists to noise (or equivalently filters uncorrelated inputs), and on the other hand it transfers higher order redundancies into uncorrelated first order redundancies (figure 3.5.4 b, 3.6.2, and 3.6.4 j). The first mechanism corresponds to the previously exposed universal property that irregular or purely stochastic components are useless and wasted. The global function following from these 2 principles is a general fluctuation resistance and is a very general property of memory, an antichaotic or homeostatic principle (Ruelle, 1991), but also at the same time a chaotic principle. This is the essence of fluctuation-dissipation principle: a balance between two inseparable forces, one conservative and one dissipative.

This dissipative natural mechanism is proposed to generate the two classical notions of consciousness (Chalmers, 1995):

— **The reflexive consciousness:** The mutual information maximisation principle encompasses the reflexive aspects of consciousness such as the ability to represent environmental information (which is in fact more a processing than a passive representation) as well as the ability to access to its own internal state (meta-representation). Moreover, because of its dissipative aspect, mutual information maximisation can be proposed as a generic mechanism for any cortical area computation whatever its distance from the sensory input or motor output. Furthermore, as this mechanism intrinsically implies a loss of information (dissipated) and a simplification, it gives a very straightforward explication of the progressive abstraction of the cortical areas maps and cognitive associated function.

_ **The qualitative consciousness** (or the hard problem). It is appealing to propose, although probably not provable, that this dissipative process is giving rise to our qualitative perception, **notably to our subjective time**. Physiologically, this dissipative process is correlated with the main physiological markers of conscious or attentive states such as β - γ activity, cortical upstates and decorrelated cortical activity and EEG (cf. figure 3.5.11). Moreover, as probed with the apparent motion protocol (chapter 3.3), the cortical dissipation (redundancy reduction and SNR increase in the colinear condition) is correlated with an overestimation of the perceived speed in psychophysics (Georges & al, 2002). The proposition that redundancy dissipation is a qualitative process is directly inscribed in the monadic or panpsychic philosophical position briefly exposed in the next paragraph (semantic). I think this monist position is the only position compatible with theoretical physics axiomatic, and it makes the Hard problem of qualitative perception trivial. For

4.2.5 Physical/thermodynamical theory of information and of cortical processing

One of the aims of this work is to clarify the still widely debated notion of information/entropy and its application to cognition and the physical world. The information formalism proposed here differs from the classical Shannon point of view in three interrelated points:

_ Inspiring from Kolmogorov complexity, the information is defined not as an average measure but as an intrinsic object measure (a state function of the object). It considers any object as probabilistic by nature, and thus is directly inscribed into quantum physics (moreover our formalism relies on the smallest scale elementary and indistinguishable components of physical systems). It may inscribe perception as a quantum phenomenon, and the striking correspondence between quantum physics peculiarities such as indeterminacy, indistinguishability, non-locality, decoherence and this statistical/cognitive formalisation will be the subject of future investigation. Moreover, the formalism proposed does not consider any ontological distinction between microscopic and macroscopic scales or states, as classically done in statistical physics: a system is microscopic and the macroscopic scale is reduced to the microscopic constituent level and the microscopic interactions. In other words, emergent properties of a system (which are still in the scientific fashion, notably in the context of phase transition and renormalisation) are fully encompassed by the interaction component of the system (Higher order redundancy). As proposed further, this formalism avoids the ergodic and stationary hypothesis, and thus defines a physics with a direct concept

of time and an intrinsic concept of systems evolution and memory. Moreover, this formalism relies intrinsically on non-extensivity, and therefore offers a new paradigm for thermodynamic that still consider extensivity as an essential condition. It is also avoiding the important and restricting axioms of the classical thermodynamic that followed Gibbs work: the derivation of ensemble at the thermodynamic limit (infinitely many particles in the system) and homogenous system consideration. Instead our formalism considers a finite number of “particles” and nonhomogenous “complex” systems. This formalism should be particularly relevant for hard physical problems such as phase transition and out-of-equilibrium systems, and shall give, considering the structure of the Rh, an interesting formulation of the renormalisation problem.

_ In opposition to the original philosophy of Shannon, we are stating that information is directly linked to semantic: what makes sense is the redundancy (see also the work of Atlan for related reasoning). Consistently with Gestalt theory, atoms of sens are proposed to be the elementary interdependencies or interactions (they contain all contextual effects). More deeply, this philosophical position is directly rooted to the monadic concept of Leibnitz and avoids the subject-object duality (and thus is consistent with the axiomatic of Physic).

_ We have tried to go one step further the Landauer’s principle that states that “information is physical” by trying to show that information, in a physical context, is a very general form of energy (more precisely a dissipated energy, in joule.s) and higher redundancy is a very general form of free/potential energy. From this follows some potentially critically important results (if verified), that the Boltzmann constant can be expressed as depending on the Plank constant ($K = (h)^n / LnN$), and thus that temperature is the inverse of time. Moreover, this formalisation allows describing cognition in term of energy propagation and dissipation. It allows investigating the cortical computation by the estimation and comparison of the complex spatiotemporal wave energy (in the various high order redundancy) of the stimulus, of the cortical input (estimated by the Vm in our experiments) and the cortical output (cf. chapter 3.5). In other word, cortical areas are considered as closed non-isolated systems submitted to the energy flow of the input (and thus in non-equilibrium) According to our empirical results, the cortical computation was proposed to optimally and reliably dissipate the inputs energy for complex natural stimulus waveforms the cortex has been adapted to, and transmit only the higher redundancies which are left. The formalism we propose states that the efficiency of the dissipative process can be quantified by both the Rh/R1 ratio, which measures the higher order redundancy transfer to the purely stochastic first order redundancy component, and by the SNR measure that notably account for the reproducibility of the

process. Moreover, the formalism we propose allows to describe this process under well known physical principles such as belief propagation, which is a method to found factorial codes and to minimise free energy (elementary mutual information between elementary components are “beliefs”), and constraint propagation or entropy maximisation under constraints (elementary mutual information between elementary components are “constraints”). It also gives a very simple explanation of the sparse code observed in cortical systems in terms of energy: sparsity is the direct the consequence of the application energy conservation law to the overcomplete (High H_0) cortical system receiving an “energy-dense” but “undercomplete” (low R_1 , low H_0) sensory input (eg. thalamic input). In other words, this energy conservation universal constraint is necessary to generate a code of the input which is informationally optimal (minimum redundancy) but sparse (high R_1). This sparse code can be observed at all scales, from the level of the neuronal activation in the cortical area network as observed in our data, to the level of cortical area activation which has been found to be sparse in fMRI studies (see for example Hasson & al, 2004).

The information defined by Shannon semantically and physically corresponds to the uncertainty an observer have on the system state as already stressed by Jaynes (1957), and the concept of information in the common language and sometime in Physic, that we are referring as knowledge, is quantified by the mutual information. **In everyday words and philosophically, it means that the only certainty (knowledge, truth) in our world is the shared uncertainty (mutual information).** This “law” appears to be transversal to all levels of organisation and to apply from the elementary physical level to individual or even social knowledge/”truths”, and reflects the subject’s physical Horizon of knowledge. Unshared uncertainty is not-understandable, useless, wasted uncertainty or lost heat/energy (cf. Bennett, 1982 for similar reasoning). It further states thar any system (closed) operates as a natural Maxwell daemon and follows the logical/computational framework described by Bennett (1987, see also Cerf and Adami, 2000, for the genomic system analogy to Maxwell daemon). The diversity or complexity of this knowledge is quantified by the Logical Depth or structural complexity. In order to apply information/entropy to physical systems, notably living systems which are obviously evolutive systems (long term memory, or historical systems) the ergodic hypothesis has to be rejected: the temporal averages or probability densities are different from the averages and probability densities across an ensemble of copies of the system. Instead, only probability densities across a copy ensemble should be considered. We insist that the proposition that perception is based on non-ergodic instantaneous statistics constitute an important conceptual change, and that it embeds perception in a physical framework

surprisingly compatible to quantum physic (and its singular peculiarity). Moreover, Figure 3.5.7 shows that the stationarity hypothesis of the visual input signal, when considered for time scales encompassing perceptual phenomena (few seconds), is not verified in natural-like condition. This argues for the principle that perceptual phenomena are based on the analysis of probabilistic trajectories instead of states (probability densities have to be computed on trajectories in the phase space instead of states), since a system can only have access to one realisation of the copy ensemble and since there are strong temporal redundancy/correlations in the input (presence of a temporal memory in the input that carries the perceptual “information”).

A little digression can be done here on active-sensing: action can be understood as a way to increase the information flow, and by the way as an adaptative mechanism that maximise the cortex-environment mutual information and thus the understanding of the environment, the “fitness” of the organism to the environment (cf. conclusion 3.3.9.3 on active sensing). The inseparability of space and time redundancy-correlations may raise an important paradigmatic change in statistical Physic that classically consider an objective Newtonian linear time metric imposed by an absolute external referential, that assign to each system state a given fixed time. In classical terms, adaptation is a way for a system to maintain its dynamic in the environmental time; living systems are a kind of fashion victims☺.

4.2.6 Algorithmic and cybernetical theory

The statistical model of the cortical computation proposed in the previous chapter, as well as some work on neural encoders (Hinton & Zemel, 1994) state that the algorithm implemented by the cortex comes to a Minimum Description Length (MDL) algorithm, that both maximises the likelihood of the cortical states given the environment as well as minimises the resulting code length. Therefore, it encompasses the Bayesian and the entropy maximisation under constraints paradigms (see also Li & Vitanyi, 1991). This algorithm can be understood as computing a statistical approximation of the Kolmogorov-Chaitin complexity that was developed in the universal Turing machine paradigm. This compressive computation is the basis of the thermodynamical theory of computation reviewed by Bennett (1982), which proposed that the regularity of strings “can be used as fuel for computation. This regularity is caught according to the proposed statistical model in the higher order redundancy component or Free/potential energy of the input. Moreover, this computation is intrinsically an intelligent or cognitive computation that encompasses the whole Gestalt theory (simplicity goals) and the

Helmholtz likelihood principle (Chater & Vitanyi, 2003). The cognitive aspect of compression was originally proposed by Barlow (1961) in the field of neuroscience and Chaitin in the algorithmic field (“understanding is compression”). The spatio-temporal compression of the visual input demonstrated empirically in our thesis (implemented by gain controls/ nonlinearity) is consistent with the principle of gestalt spatiotemporal continuity (both electrophysiologically and perceptually as shown in the chapter 3.3.9 on apparent motion) and implement some preliminary cognitive computations such as (among others) the eye-movement invariance of the cortical responses (cf. chapter 3.6.4).

For the matter of the model implementation of this computation, our thesis strongly argues about the pertinence of fully recurrent Excitatory/Inhibitory models such as the Boltzmann or Helmholtz nets (derived from the Hopfield net, but with hidden layer). First, all our empirical results (Excitatory/inhibitory fields, orientation and direction selectivity genesis, center-surround interaction, and dense input/sparse output computation in natural conditions) point out the critical role of cortical recurrence and E/I balance in the cortical process (see the discussion of chapter 3.5.6). Second such networks automatically perform a free-energy minimisation (or energy descent) task: they are Rh removers, and are isomorphic to n-dimensional spin glasses model (Hopfield, 1982). Those fully recurrent nets can be understood as generic (totipotent-unspecialised) and universal data compressors (Amari & al, 1995). Combined with excitatory hebbian/ inhibitory antihebbian plasticity time dependent rules (STDP), such nets should be able to act as universal spatio-temporal compressors, and thus to present some predictive/anticipative properties (time anisotropy implies a temporal anisotropy of the redundancy reduction mechanism, as found for STDP rule). No doubt that those nets, when they will be implemented with sufficient computational power (Ho), will mark the beginning of the Artificial Intelligence age. However, some precise feature of those networks, such as for example the symmetric connectivity constraint, may have to be modified to be fully general, and some predefined constraints, such as for example free-scale (or small-world) connectivity (instead of fully recurrent), corresponding to the data/input structure may be added to improve the convergence rate of the network. The peculiar structure we observe for V1 can be simply understood as the result of the specialisation of those universal networks under the input environmental constraints.

From the cybernetic historical point of view, the Mutual information maximisation principle reconciles the two old-age antagonistic schools considering either that living systems “feed upon noise/disorder” (see Von Foerster, 1960, stochastic resonance paradigm, Gammaitoni & al, 1998, Heneghan & al, 1996 and see Atlan 1979 for review) or that living systems “feed

upon order/negentropy” and resist to noise/fluctuations (Schrodinger, 1944, Von Neumann, 1956, see Atlan 1979 for review). Moreover, this algorithmic point of view summarizes cognition and evolution to an optimisation process (a landscape minimum energy search, the evidence that genetic Darwinian adaptation and epigenetic cortical learning perform analogous computation is discussed in the next chapters) that is unsupervised and that is inscribed naturally in our world self-organisation. In other word, this paradigm presents the interesting advantages of not requiring the intervention of external goal, predefined function, notions such as pertinent or relevant information, and homonculi of any kind. The fact that external goal has to be evoked to explain the dynamic of the system only signifies that the system under consideration is not sufficiently large (but it is likely that in order to fully explain dynamic of complex systems such as Human, the whole world and its history has to be taken into account).

The other important concepts of cybernetic and biological system theory that are encompassed by the infomax principle are that it imposes a maximum diversity rule and a specialisation-differentiation process (see next chapters). It avoids the old dualism structure-function, and further state that organisms can be described as a wide diversity of gain control that are imbricated in different level of organisation (for example: molecular/cellular/organe (cortical area)/organism/society, see next chapters).

4.2.7 Active sensing theory

Active sensing theory states that the basis of sensory experience and of the notion of “self” consists in extracting and exercising laws of sensorimotor dependencies (O'Regan & Noë, 2001). It can be summarized by the original formulation of Merleau-Ponty (1960): "Mon corps mobile compte au monde visible, en fait partie, et c'est pourquoi je peux le diriger dans le visible. Par ailleurs il est vrai aussi que la vision est suspendue au mouvement. On voit que ce qu'on regarde. Que serait la vision sans aucun mouvement des yeux, et comment leur mouvement ne brouillerait-il pas les choses s'il était lui-même réflexe ou aveugle, s'il n'avait pas ses antennes, sa clairvoyance, si la vision ne se précédait en lui? Tous mes déplacements par principe figurent dans un coin de mon paysage, sont reportés sur la carte du visible. Tout ce que je vois par principe est à ma portée, au moins à la portée de mon regard, relevé sur la carte du "je peux". Chacune des deux cartes est complète. Le monde visible et celui de mes projets moteurs sont des parties totales du même être. Cet Extraordinaire empiètement, auquel on ne songe pas assez, interdit de concevoir la vision comme une opération de pensée qui

dresserait devant l'esprit un tableau ou une représentation du monde, un monde de l'immanence et de l'idéalité."

Our empirical data supports that the primary visual cortex is operating a visuo-motor dependent transformation and removes correlations imposed by eye-movements (that carry the environmental information, see conclusions in chapter 3.3.9.3). It thus operates a preliminary form of eye-movement invariant representation (activity or dynamic would have more faithful meaning, cf figure 3.6.4 & 3.6.6 & 3.6.7 and chapter 3.6.4). **This invariance property is just the functional correlate of the central physical property of the cortex of fluctuation resistance previously discussed.** Those results allow us to propose that V1 RFs, including linear and nonlinear components, are strongly shaped by the various Eye-movements kinematics. We have notably identified a striking spatiotemporal correspondence between the main and omnipresent two classes of eye-movements, saccadic and fixational, with the two cortical direction selectivities, respectively the center-surround/high-speed/collinear-axis motion selectivity demonstrated with apparent motion, and the classical short-range/low-speed/parallel-axis motion selectivity. Moreover, as V1 is directly projecting to the Superior Colliculus (eye-movement motor nucleus) and as evidence for motor activity in V1 is growing (Tehovnick & al, 2004 for review), we propose V1 to implement a preliminary visuo-motor transformation (a first stage visuo-motor loop, see conclusion of chapter 3.3.9.3).

Most of physiological studies base their logic on the principle that eye-movements (fixational, Murakami & al, 1998, or saccadic, Ross & al, 2001) have to be compensated by neuronal mechanisms (gain control or fast adaptation) to maintain perception stable. The other interpretation, more restricted to fixational eye-movement, is that their function is to avoid the neuronal mechanisms of adaptation (Martinez-Conde & al, 2004 for review). The point of view defended here is somehow the opposite and follows the phenomenological concept of action-perception inseparability: neural computation through gain controls is strongly adapted to eye movement statistics even at the first visual stages (either through a corollary efferent motor copy or through their impact on retinal spatio-temporal dynamic) and the resulting reduction of the spatiotemporal redundancy (that are eye-movement dependent) intrinsically constitutes the perceptual phenomena.

4.2.8 Conclusion

To summarize, the definition of the algorithmic information of a message or objects, has leaded G. Chaitin to the logical statement that **“understanding is compression”**, or in other words discovering the structure. We are claiming it in visual terms, finding the less redundant and noisy representation of visual input is what we call seeing. The world at our scale present a highly structured and diverse morphology, for example objects, concepts, words like Dog consist in a collection of “suspicious coincidence” of properties (bark, long tail, furry ...) that are also lower order highly correlated features (Barlow, 1985, Foldiak 1990). Given this structural diversity and enormous amount of redundancy of the photon flow falling on the retina or equivalently the huge Logical Depth of the visual input, finding such an efficient representation, can be considered as a Hard or close to Hard optimisation problem (probably NP according to Schmidhuber, 1992, but I would guess the opposite: the brain is not so huge) that is achieved in real time by the neo-cortical network. We would like to emphasize that in this context redundancy reduction is not just a matter of retinal, thalamic, or primary visual cortex network task nor to maximise a channel bandwidth, but the removing process of structural redundancy may appear as the general computational task of the whole sensory neo-cortex, and an intrinsic sensory perceptive computation. As argued in chapter 3.7, leaving the functional description, this computation is embedded in a natural dynamic process, which is unsupervised and does not require to appeal to goal function, finalism or aim. The relevant biological question is to ask how this process is implemented efficiently, what conditions and mechanisms are leading to efficient adaptation, and literature combined with our results already offers a wide palette of physiological implementation.

We can propose a simple neo-cortical implementation of the redundancy reduction occurring in neocortex that tries to point out the crucial required biological properties to achieve this computation efficiently. This model, voluntarily over-simplistic, is based on a huge literature of network models and empirical data, including ours, and is more fully detailed and justified in the associated paper.

4.3 Redundancy and noise removing mechanisms in cortical areas

In this section we will present in more details the physiological basis of the cortical redundancy and noise removing process. Therefore, we propose to define the neuron and the cortical area as the two pertinent cortical modules of information processing which defines two relevant structural/functional scale. It is a widespread belief in neuroscience field that one

or several intermediate processing modular level can be found in the neocortex, such as columns, minicolumns or hypercolumns (see Mountcastle, 1997 for review). However those modul identification mostly rely on functional characterisation with harsh thresholding rather than on direct anatomical evidence, and all the works on the cortical areas substructures convinced me of their physical irrelevance rather than the opposite. Opposingly, those publications, together with our results on the functional generative role of the intracortical reccurency, convinced me that cortical areas are continouous tissues or structurally/functionally indivisible organ. Therefor, we'll only consider as relevant the neuronal modules and the cortical areas modules with their layered organisation (but one as to keep in mind that even this minimum processing unit decomposition is an artefactual simplification).

4.3.1 A generic neo-cortical code

The results and model presented in this thesis state that the cortical code at mature adapted stage shall be the most reliable (high precision in the spike timing) and the less redundant possible. Neo-cortical optimal code is a binary reliable temporal code. Considering spatio-temporal statistics of our environment and cortical code, rate codes and pattern codes are unavoidably redundant codes (see Wennekers & Ay, 2005, for related reasoning). Patterns are necessarily present in the cortical code, they are the redundancy left by the cortical processing (and the neural assembly signature) that are removed by further cortical steps if already learned.

4.3.2 Cortical areas as redundancy reduction modules

Inhibitory connections present the ubiquitous particularity to be intra-area connections, inter-area connections being uniquely excitatory. This ubiquitous connectivity rules leads to the idea that cortical area behave as higher order redundancy reduction module. Another argument in favour of the redundancy reduction function of neo-cortical areas is the observation that the number of areas devoted to a given sensory modality appears roughly proportional to the Logical depth of the input. The olfactory system (which is philogenetically the oldest sensory system) that deals with very simple low redundancy external signals (an olfactory perceptive entity is due to a few molecule combinatory) presents only one devoted cortical area the pyriform cortex (and we're not even sure it is included in neo-cortex). Olfactory bulb acts as a first simple cortical structure that projects directly to pyriform cortex,

limbic system, amygdale and hippocampus paleo-cortex. Moreover, the results of Laurent's team on the olfactory code, oscillations genesis, sparsness and dynamic are deeply consistent with our own observation in the visual cortex.

Fodor (1987, 1988) has proposed that thoughts and thinking take place in a mental language thus defining the "language of thoughts hypothesis", and further proposed the modularity of mind hypothesis. We are precisising this view: the language that is used in the sensory cortex (at least) is the input language, a natural or environmental language. A simple model of cortical areas "self-organising" according to its input constraint can be proposed (figure 4.3.1). Each cortical area code or language consists in a simplification of the input code or language, leading to more and more abstract and simple representation (code or language).

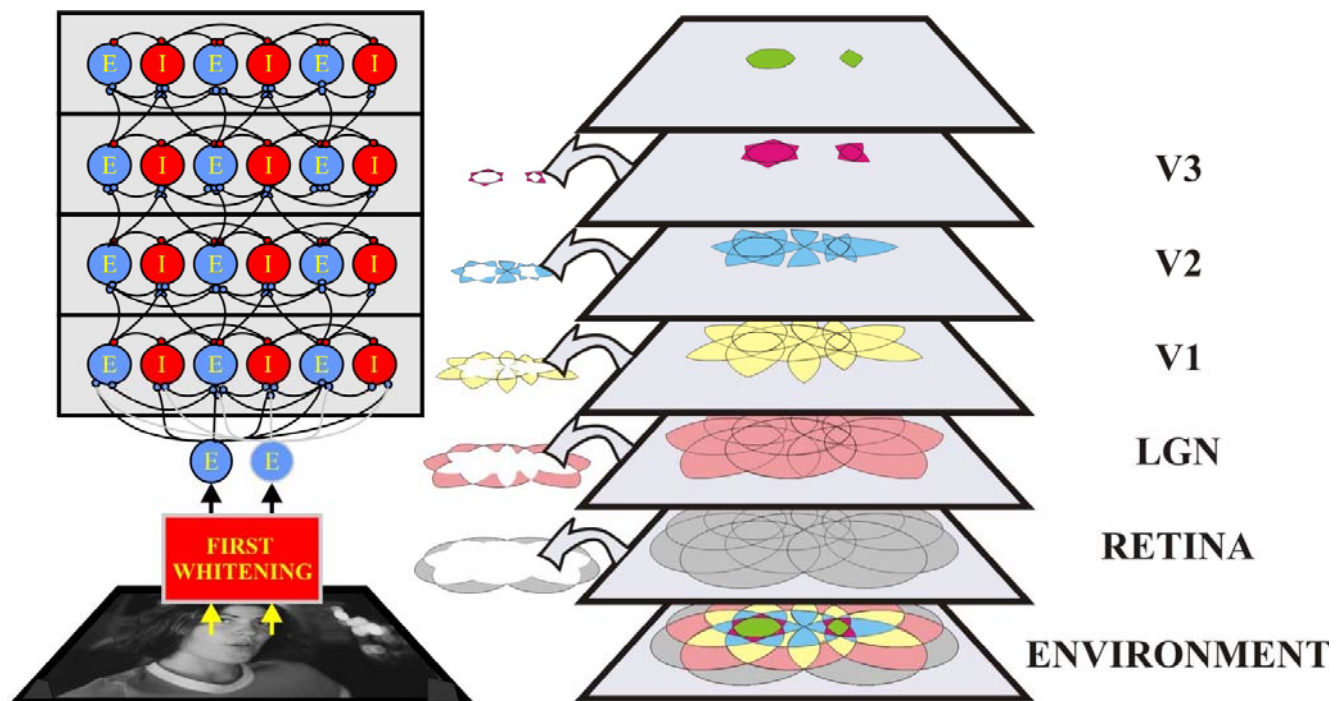


Figure 4.3.1: Canonical model of cortical computation and dissipation of input-driven complexity (cf. figure 3.5.5). Simplified model of cortical computation and dissipation of complexity along a hierarchy of visual cortical processing steps. At each stage of integration, higher order redundancies are transferred into first order redundancies that, because of their statistical independency, do not propagate further to the next cortical area (noise resistance property). This dissipation process represents the entropic cost of the cortical computation. Note the decrease in the logical depth of the environmental representation across cortical stages. The hierarchical feedforward schema presented here is of course an oversimplification: the redundancy minimisation and energy conservation principles applied to the cortical area level (\Leftrightarrow specialisation) should give rise to a complex inter-area wiring diagram (with divergent and convergent, parallel and serial pathways) such as the cortical visual arganisation found by Felleman and Van Essen (1991).

The very simplified following schema is emphasising the apparent cortical area informative filter function that transfers part of the remaining higher order redundancies in the input into first order redundancy in the output and remove uncorrelated (independent) activity present in the input. To simplify our purpose, it considers that redundancies are removed sequentially according to their order, which is not obligatory the case.

Cortical areas are presented here serially, but one can imagine an organisation with parallel modules (and convergence and divergence). A general and natural problem is to explicit the constraint that impose the cortical system to divide the redundancy reduction task into different specialised modules presenting a complex interconnectivity relationship (Felleman & Van Essen, 1991) instead of removing it at once with a single undifferentiated huge area. The same logic we have been applying to single neuron in a cortical area (specialisation increase computational efficiency) may apply to the functional organisation of cortical areas in the brain, at a higher population scale. Adaptation of brain structure to global macro structure of environment shall predict the functional specialisation of area (see Weber & Obermayer, 2000). Ultimately, this specialisation of areas is the direct consequence of both redundancy reduction and sensory input energy conservation at the macroscopic level of cortical areas. At some level of redundancy environment may split into general more or less independent class of feature (for example faces and buildings for vision) leading to distinct areas and divergence in the sensory stream. Reciprocally, for example in context of multimodal integration, at some level of redundancy removing, redundancy in between different sensory input may be represented sufficiently apparently to allow convergence in the sensory streams. This kind of macro-adaptation corresponds to the minimizing connection wiring length criterion observable in the inter-area connection biased scheme (Chklovskii & al, 2002), and is likely to be implemented genetically rather than epigenetically. This model is of course in direct affiliation with the general idea that evolution plays “Lego” by adding sequentially generic boxes that are progressively specified through adaptive process. Consistently with this point of view, 30% of the cortical surface, mainly corresponding to auditive and visual areas, has been found to present a reliable response activity in fMRI, even from one subject to another, during the presentation of a same natural complex movie (Hasson & al, 2003).

Moreover, the internal representation of cortical area in such a schema is oversimplified, notably it occults the layer organisation which as undoubtly some processing relevance. However, small and non substantial modifications have to be introduced to account for a more realistic layered anatomo-functional model, as proposed in the following schema (figure

4.3.2). As reviewed by Martin (2002, a), a canonical cortical circuit can be proposed on the basis of anatomical and functional studies as several recurrent E/I networks organised in serially in layers. As those E/I circuit (as further developed) act as a dissipative medium, an interesting analogy can be done with dissipative structures or patterns created by an anisotropic energy flow in various media.

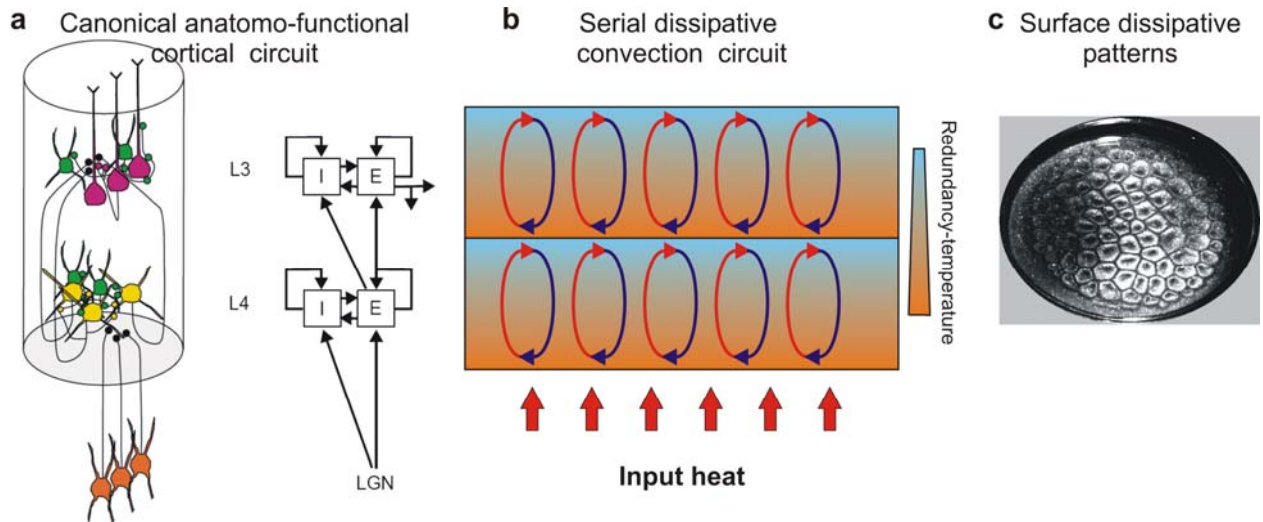


Figure 4.3.2: Canonical model of anatomo-functional cortical microcircuit and its proposed equivalent dissipative convection circuit. *a*, The layered canonical cortical circuit proposed by Martin (2002) on the basis of anatomic and functional literature. It represents layer 4 and layers 2-3 as excitatory-inhibitory recurrent circuits combined in series. Layer 5 and 6 are output layers not represented here and could be schematised by the same recurrent circuit. *b*, we propose an equivalent diagram from the thermodynamic computational point of view. It states that E/I recurrent circuit can be modelised as convection circuit that reduces the input redundancy (temperature), in two serial stages corresponding to the preceding layers (more complex and realistic convection scheme can be considered). *c*, the picture represent cells patterns produced by the Benard convection cells at the surface of the heated medium.

In fact we propose that E/I recurrent circuit to implement convection cells in which the input redundancy is partly dissipated. The resulting dissipative patterns could correspond to the cortical surface functional structures such as orientation domains and pinwheels observed notably with optical imaging technic. A preliminary speculative interpretation of our result can be proposed: on the one hand, the grating condition, for which we have shown that the cortical computation is in a low dissipative regime (cf. figure 3.5.4 b) and which give rise to orientation domains macrostructure activation at the cortical surface, could correspond to the low turbulent regime observed notably in the paradigmatic dissipative Benard convection cells example. On the other hand, the natural condition, for which we have shown that the cortical computation is in a high dissipative regime, could correspond to a fully developed turbulence regime with energy cascade at all scales (which would correspond to the existence of cortical

specialised microcircuit we inferred from our results, and shown notably empirically by Ikegaya & al, 2004, and may be also correspond to a scale-free organisation of the horizontal cortical connectivity).

4.3.3 Cortical implementation of redundancy and noise reduction

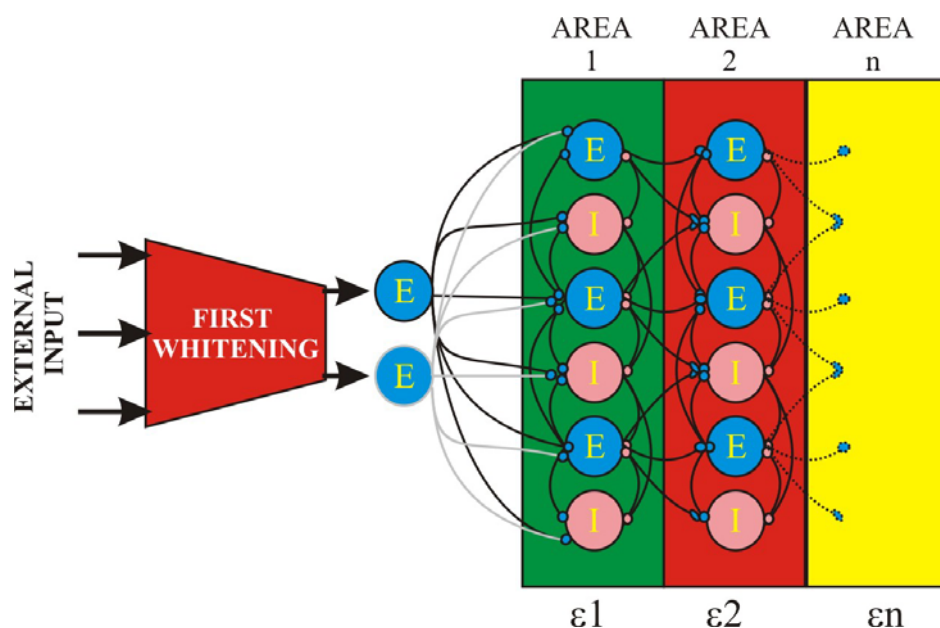
4.3.3.1 Recurrent E/I network

Most of the theoretical studies focusing on mutual information maximisation and by extension to independent component analysis using neural networks, have restricted their investigation to simple “perceptron” like feed forward models.

In physiological domains lateral inhibition appears as a leitmotif paradigm as a mechanism achieving contrast gain control, whitening or more generally redundancy reduction and selectivity sharpening (Barlow 1961, 1989, 1992, Laughlin, 1981, Srinivassan 1982, Foldiack 1990, Harpur & Prager, 1996, Olshausen and Field 1996, Schwartz & Simoncelli, 2001). Our results, showing that the V1 neurons in natural condition receive constantly reliable and silenced input trains that constrain the spiking output to very specific and rare time response, is strongly supporting this point of view. Inhibition in a network can be understood as the implementation of a competition in between the entities in the network, which is a strong motor of specialisation (dedifferentiation) of the entities. Competitive mechanism leading to higher order redundancy reduction or equivalently sparse population dynamic appears a widespread and already well documented phenomenon in Nature. For example, demographic dynamic of large number of interacting populations (predator prey dynamic that is governed by Volterra’s formalism, generalised to large number of populations using Gibbsian statistical development) is leading to sparse synchronous assemblies in the case complex (diverse) interactions (“the higher the complexity of interaction, the more spike-like do the oscillations become”, Cowan 1965). In previous study, we have shown a wide diversity of E/I micro-architecture and temporal phase between excitation and inhibition give rise to orientation and direction selectivity (Monier & al 2003). Studies in auditory cortex (Wehr & Zador, 2003), and in barrel cortex (Wilent & Contreras, 2005) show that either precise spike timing or selectivity emerge from a temporal shift of excitation relative to inhibition. The present study aims at generalising those results in the visual cortex to higher dimensional selectivity. Furthermore, the primary visual cortex capacity to remove environmental redundancy further

than the low order orientation or direction statistics, potentially explains the observed diversity of E/I micro-architecture for orientation selectivity (Monier & al 2003).

Foldiak (1990) with a pure inhibitory recurrent model with Hebbian excitatory and anti-Hebbian inhibitory connection, and Harpur & Prager (1996) with an excitatory-inhibitory two layer recurrent model have shown that recurrent inhibitory networks behave like redundancy removers which “self”-organisation in natural condition give rise to local band-passed oriented Gabor like filters. Further more, recurrent excitatory inhibitory network learning through simple Hebbian process develops topographic maps similar to those observed in optical imagery recording (ocular dominance, orientation, direction, and realistic patterned lateral connections between them, Bednar & al, 2003, Miikkulainen & al, 1997). Amari & al (1995), showed that a recurrent network with inhibition ruled by a generalised Hebbian/anti-Hebbian learning can achieve blind source separation, and Deco and Parra (1995) found that implementing information maximisation principle to Boltzmann Machine (generalised Hopfield recurrent network) is achieving optimal non-linear data compression and generate realistic Gabor-like receptive field. Even closer to the result presented here, Wennekers & Ay (2003,2005) extended the information maximisation principle to temporal domain in recurrent network (leading to time dependent learning rule) and observed reproducible functional cell assemblies. According to those studies, and our results, an E/I recurrent plastic network can be proposed to be a canonical self-organising circuit, or from the computational point of view a universal input encoder that learns input statistics and reduce higher order redundancy (Figure 5). This model can be understood as the simplest model giving rise to cortical function or reproducing cortical computation. It does not take into account layer structure and superior area feed-back connection etc. Layer structure appears to reflect a canonical inter-modules or inter area communication specialisation with specific feedforward input layer, feed-back input layer and output layer (see also figure 4.3.2). To develop functional maps such as observed in V1, local connectivity bias of feed-forward and recurrent connection must be added to the model (Ernst & al, 2001, Bednar & al, 2003, Miikkulainen & al, 1997), and that represent presumably a combination of epigenetical and genetical adaptation to external redundancy.



This model is also a generalisation of the simplex model (Debanne & al, 1998, Shulz & al, 1999), that allows to derive simple and complex receptive field from a single canonical connectivity scheme under Hebbian learning, and that explain the complexity of simple cells subthreshold depolarizing field observed in V1 (Chavane & al, 1998, Shulz & al, 1999, Priebe & al, 2004).

4.3.3.2 Neuronal non-linearity:

We've been focusing on the architectural E/I of neocortical that is carved by long term plasticity as an optimised structure for removing the environmental redundancy the organism has evolved in. This is of course a partial and simplified point of view. In fact, the neuronal unit individually behaves like a higher order redundancy remover, and its integration properties as well as the short term dynamic of its synapse appear widely optimised for this task. In this study we show that in natural condition, the neuron integrates input in a coincidence detection mode (Abeles, 1991), and thus acts as a higher order redundancy remover. This can be already found in Nadal's work (1994) that showed that the introduction of the spike threshold non-linearity in a perceptron infomax model shifts the statistical computation of the network from PCA like to ICA like. This neuronal informational compression is further more obvious when one consider that "neurons integrate thousands of inputs, each firing over a range of about 1-100 Hz" while keeping "their output firing rate within the same range" (Abbott & Regehr, 2004).

In fact, any mechanisms of adaptation or gain control (or homeostatic) implemented at the cellular level can be also invoked. Neuroscience literature already reveals such important mechanisms, non exhaustively:

_ Neuronal intrinsic non-linearity such as dynamic spike threshold (Azouz & Gray, 2000, 2003), activity dependent suppressive intrinsic K⁺ current (Wang & al, 2003, although they do not appear to be revealed in the sparse dynamic regime obtained with natural image opposingly to the drifting grating correlated regime or resting regime (in higher time scale correlation that are not present in our natural film, see also Castro-Alamancos 2004, for similar observation), or voltage dependent enhancement of recurrent lateral excitatory connections (Hirsch & Gilbert, 1991).

_ Short term synaptic plasticity (Koch & Segev, 2000, Destexhe & Marder, 2004, Abbott & Regehr, 2004 for review, Tsodyks & Markram, 1997) allows synapses to act like active filters at different time scales depending on its facilitating or depressing nature. For example, Goldman & al (2002) have shown that depressing synapse can remove redundancy in realistic natural activity regime. Short term plasticity concerns most of central synapses and thus our results show that amplitude and time course of those rapid plastic mechanisms if really present are widely reliable.

_ Shunting inhibition is narrowing the temporal filtering of the cell, by increasing the membrane time constant. Further more, Chance & Abbott (2000) show that divisive inhibition in a model with recurrently amplified feedforward responses can stabilize network activity for arbitrarily large excitatory coupling, and can eliminate the critical slowing down of a high-gain network without modifying its selectivity.

_ Input dynamic have strong influence on neuronal integration properties. Regime of high input conductance promoted by high synaptic bombardment that is observed *in vivo* and that are related to awake states, have been shown to enhance correlation detection, and to sharpen the temporal resolution of those coincidence detection up to the millisecond time scale by stochastic resonance like mechanism (Softky, 1994, Rudolph & al, 2001, Destexhe & al, 2003) and to generate a gain control (Chance, Abbott & Reyes, 2002).

4.3.4 Sharp neuronal assembly and redundancy reduction

The definition of redundancy we gave, when applied to central nervous system, can be understood as a quantification of neural assembly. A closed formalisation can be found in Martignon & al, 2000, taking the general form of correlation constraints on the joint distribution of the system (first and higher order constraint). Neural assemblies are defined by coherent patterns of activity, often considered as specific synchronisation of neuronal activity (or second order spatial correlations) or spatio-temporal patterns (higher order correlation) and intuitively represent a kind of redundancy of the code (or representation) in the network.

Martignon & al, 2000 proposed that the joint distribution of the system can be formulated according to entropy maximisation under constraint method as:

$$P(S_1, \dots, S_n) = \exp(\lambda_0 + \sum_{i=1}^n \lambda_i S_i + \sum_{i=1}^n \sum_{j=1}^n \lambda_{ij} S_i S_j + \dots + \lambda_{1\dots n} S_1 \dots S_n) , \text{ where } \lambda_i, \lambda_{ij} \text{ are first,}$$

second order correlation coefficient and so on. As

$$H(S) = H_0(1 - R) \propto - \int P(S_1, \dots, S_n) \log P(S_1, \dots, S_n) dP \text{ (there's no strict equality in this case}$$

because of the additional constraint on the sum of all probabilities normalised to 1 which gives λ_0 , that is not present in the redundancy method) correlation or neural assembly patterns are expressing redundancy in the code.

The aim of this chapter is to reveal the striking correspondence in between neural assembly theory and redundancy reduction computation, and by this way that the temporally precise and sparse code obtained in this study can be as well understood as the signature of precise and sharpened “synfire chains”. Neural assembly theory have its roots in Hebb work, and has find its formalisation in Abeles “synfire chains” and many experimental correlates in various investigation methods (Singer, Aertsen, Vaadia, Varela etc...). It can be understood as a study of activity propagation and clustering under associative learning rules in neural networks. Basing its thought on the observation that neuronal integration can behave in two stereotypical regimes, either as coincidence detector or input frequency integrator, it states that neuron at the same stage of information processing and coding for the same “perceptual” or “behavioural” entity shall synchronize their activity. Neural assemblies are the logical signature of the internal constitutive and unavoidable redundancy defining a cortical system, of cortical structure. They are also the indispensable redundancy for a system to generate a structured output or action. Imagine a cortical structure which output would be truly statistically independent (factorial), this activity would be stochastic (what we call noise in this paper) and would not propagate; statistical independence is a dead end: even more, true statistical independence implies a division of the system into independent systems, a split brain.

Our experiments present various scales of neural assembly, ranging from raw rate coding presenting high redundancy, expressed in the frequency integration regime (noisy or unreliable frequency codes are redundant codes, see Shalden & Newsome, 1998, for development), and the high level of correlation in the cortical state, to temporal code exhibiting low redundancy and precise correlation detection regime. More precisely, frequency vs temporal code, noisy vs reliable activity, redundant population code vs sparse

individual cell coding are just the expression (and can be summarized as) of different informational redundancy regimes (cf. the new definition of efficiency). Using this discontinuous fashion of describing neural activity, we are stating that the cortical network aims at finding the smallest (in term of number of neuron) or finest (taking into account temporal precision) neural assembly for a given input pattern. This is the direct consequence of the Occam's razor, automatically implemented by neural network aiming at removing statistical dependencies in the input (Schmidhuber, 1992). In this case of course the simplicity of the hypothesis is represented by the number of active neuron. Using the more general formalism and definition of neural assembly (Martignon & al, 2000), the cortical system aims at removing spatio-temporal patterns in the input, that is equivalent to find the spatio-temporal representation containing the less possible correlations (even at high order). It is easily understandable in this context that the temporal and spatial scale of the correlation removed by the brain is increasing with the stage of analysis. Going to higher stage of cortical processing shall increase the time and spatial constant of the engaged neuronal memories and increase the abstraction or simplicity of the environmental representation.

4.3.5 Information, redundancy reduction and qualitative perception or attention

Synchrony, and mechanisms potentially allowing the synchronisation such as transient high frequency oscillation (carrier waves, Singer 1993 for review) have often been invoked as a solution for the binding problem, and to be a signature of visual feature integration (Singer & Gray, 1995, example of Gestalt grouping, Gray 1999), a working memory activation or reactivation (Damasio, 1990, gamma oscillations, Howard & al, theta oscillation Lee & al, 2005), or more generally conscious process. This study, for condition approaching to natural stimulation, presents:

- A high synaptic bombardement that approaches awake state (long lasting stimulus induced upstate, see complementary figure).
- A global desynchronisation during eye-movement fixational period compared to on-going resting state and to saccadic period (that correspond to low perceptive state (Morrone & al, 2005))
- An SNR increase in the Beta-Gamma range in the ECG as well as in the input population of the cell.
- A sparse temporally precise spike timing that coincide with transient reliable high frequency input population activity.

Those result agrees with the point of view that desynchronisation of cortical activity is linked to phenomenal perceptive state (Rodriguez & al 1999) and to general cognitive process such as memory activation. This desynchronisation is a simple reflect of the input redundancy reduction occurring in the area. Of course, this is not in contradiction with role of temporal correlation in binding. Correlations that are left in the area output are removed at a higher level of processing, or learned if not already known by the network and repeatedly presented (and thus removed). Attention has been proposed as a global (arousal state) or more spatio-temporally local modulation (focal attention) of cortical activity. SNR modulation of cortical response implement rigorously a mechanism of gain control, and our results show that it is accompanied by a selectivity (or filtering) modulation. Thus playing on SNR appears a very simple mechanism to obtain attentional effects, either automatic (stimuli driven like pop-out) or supervised by feed-back or neuromodulation. In psychophysics, Lu & Doshier (1998, 1998) have shown that attentional mechanism (and even learning) are consistent with a signal to noise ratio modulation paradigm. We propose attention to reflect the level of computation occurring in an area and thus to result of simple work on R1 over Rh balance (computational efficiency). Simple mechanisms playing either on integration properties of neuron (excitability for example) or on E/I balance can be proposed as a target for neuromodulation, in the case of externally supervised attention or learning.

4.4 Natural computation: general self-organisation and adaptation physical laws

4.4.1 Redundancy, structure and organisational complexity (Logical Depth)

From the biological point of view, in the redundancy component H_0R lies all the structural and potentially “semantic” information of the environmental world. In other word, it is the only information available for a living system to learn (to evolve) and to perceive. Reciprocally, what is random or statistically independent is uncertain and non-understandable for any kind of observer either a human, a cortical area, or a genome. For example, although two sequences of random dense noise are the less correlated stimuli, any observer cannot distinguish one sequence from another (except if the noise is repeated, but it’s no more noise). Obviously, the world we are living in is highly structured, or equivalently is highly redundant and appear to strongly deviate from a pure chaotic dynamic.

In his essay “what is life” (1944), Schrodinger has proposed that living organism remarkable properties of non periodic but reproducible order (“aperiodic crystal”) could be measured as

the entropy with a negative sign. He also proposed that to maintain this order from decaying to the maximum disorder (entropic) equilibrium state (that is death), what biologist call homeostasis, organism has to “feed upon negative entropy” (order from order paradigm). A remarkable feature of (2) is that it shows that negentropy in its wide sense is equivalent to redundancy: $H_0 R$, allowing to reformulate Schrödinger’s adage into “organism feed upon environment redundancy”, that seems also to particularly fit to the neo-cortical function. Chaitin in 1970, consistently with the definition and reasoning proposed here, gave a first general mathematical definition of “life” based on complexity measure, remarking that “a living being a unity” and that “it is simpler to view a living organism as a whole than as sum of its parts”.

Moreover, high order redundancies are reflecting what complex studies are calling emergent properties macroscopic or collective behaviour. Phenomena of phase transition often described in physic correspond to drastic rehandling of the ordered redundancy distribution.

4.4.2 Toward a formal theory of evolution and cognition: reproducibility, differentiation, efficiency and diversity of living systems as a natural Maxent or Infomax process result

”God has chosen that which is the most simple in hypotheses and the most rich in phenomena” (Leibniz, *Discours de métaphysique*, VI, 1686).

The idea, supported in this thesis, that the 2nd principle drives evolution, is far from being new. In 1922, Lotka referred to Boltzmann as one of the first proponents of the proposition that available energy (also called exergy) can be understood as the fundamental object under contention in the biological, or life-struggle and therefore also in the evolution of the organic world. Lotka interpreted Boltzmann's view to imply that available energy could be the central concept that unified physics and biology as a quantitative physical principle of evolution. The work of Prigogine aimed at showing how in far from equilibrium systems dissipation could lead to the mergence of structure (minimum entropy production theorem).

This idea is further extended here to cognition: Darwinian evolution and cognition may result from a common and elementary process or computation, occurring at different spatial and temporal scales and on different system definition. They result from the adaptative capacity of respectively the species genome and the brain of individual to the environment.

Recent computational studies already exemplify this principle. In computational neuroscience, Laughlin (1981), Bell & Sejnowski (1995); Brenner, (2000) and Bialek (2002), and Sharpee & al (2006) have proposed that adaptation can be implemented by a simple mutual information maximisation in between the environment and the neuronal response (either an isolated neuron or the whole network). In fact, for organism, nervous system or at least neo-cortex can be considered as a powerful (huge capacity) extra genome adapting on multiple time scales. Genomic adaptation and natural selection can also be resumed by this simple information maximisation procedure. It can be understood from Adami and colleagues work (2000, 2000), that identifies genomic information with the amount of information a sequence stores about its environment. Adami and colleagues have further shown that this mutual information with the environment, or “physical complexity”, is increasing.

More simply, mutual information maximisation or entropy maximisation under constraint appears as logical and general formal definition of adaptation, and defines a simple and global knowledge homeostatic process.

We can now show the consequences of the mutual-information maximisation in term of the important and defining biological properties of efficiency, reliability and diversity/specialisation.

From equation, $I(E;S) = H_{0S} - H_{0S}R_S - H(S/E)$, it appears that maximising mutual information in between the system and its environment comes to minimising the redundancy and the ambiguity of the system (since as we showed before H_{0S} is a constant). Maximising mutual information in between the system and its environment by definition comes to optimise the efficiency of the system.

The alternative definition of mutual information is $I(E;S) = H_{0E} - H_{0E}R_E - H(E/S)$. Thus, maximising mutual information comes also to minimizing the equivocation $H(E/S)$. Several interpretations can be given to this equivocation minimisation: it can be considered as an error or representational failure minimisation, as well as the behavioural active quest of external information (active-sensing paradigm developed in chapter 3.3 and 3.6, Philipona & al, 2003).

Reproducibility-Reliability: Minimising the ambiguity is equivalent to increasing the reliability of the system in its environment. The reliability has been pointed out to be a singular particularity of living organism (Schrodinger, 1944, Cowan, 1965), and either the genetic code (genetic sequence is highly conserved from one Human to another for example) or the cortical code (that demonstrated empirically in chapter 3.5) are reliable code when

exposed to the environment it has been adapted to. Organism reliability is a consequence of, or maintained by, the environmental constraints (redundancies). This conclusion is already present in essence in Adami and Cerf (2000).

Redundancy reduction and differentiation: a system by adaptation to its environment tends to optimise its encoding or “representation” of its environment. We can directly derive, from the previous formulation of mutual-information, the conclusions of Nadal & Parga (1994), Bell & Sejnowski (1995, 1996), Deco & Obradovic (1998), obtained in the particular perceptron network case, that maximising mutual information in between the system and its environment comes to remove redundancy in the system (or partially tend to achieve ICA). This result is in fact, much more general than the perceptron case (Amari & al, 1995 for recurrent network generalisation). As explained before, information maximisation is closely related to the entropy maximisation under the constraints. The numerical simulation of Bell & Sejnowski (1995, 1996) is a maximisation of the network entropy considering the constraints imposed by the input. In fact, this Infomax principle is also closely related to maximum likelihood density estimation (MLE, Jaynes, 1988, Pearlmutter and Parra 1996, Cardoso 1997, Mackay 1996), reconciling two schools of thinking, and leading to the rough idea that predictive or generative coding (temporal or spatial) is equivalent to efficient coding. It follows from a very general rule: the most likely solution is also the simplest or shortest (Solomonoff, 1964, 1978, Vitanyi & Li, 1996, Chater & Vitanyi, 2003, Schmidhuber, 1997).

In evolutionary genetic, this redundancy reduction is also well described under the explicit term of compression selection. The work of Adami and colleagues on digital organisms may exemplify this redundancy minimisation principle (Edlund & Adami, 2004), although their theoretical context is much more sophisticated than the one presented here. For organisms evolving in a high mutation rate environment, they report a phenomenon of maximisation of independence in between the instructions composing the genomes (antagonistic epistasis removing, which is a particular kind of redundancy removing) which comes along in their context with an increase of ambiguity (or equivalently neutral fraction of the genome).

This redundancy minimisation can also be observed in other higher level systems such as human societies or ecosystems (interestingly, neo-cortex can be understood as a social genome). Individuals in societies are specialised into diverse tasks, such as farmer or researcher, herbivore and carnivore, and the redundancy in between a researcher brain and a farmer brain may be lowered by a social information maximisation process.

In artificial genetic, some results already exemplify such ecosystem influence on genome dynamic (Johnson & Wilke, 2004). Digital organism genome adapting to a single rich environment composed of two independent niches, nonetheless absorb environmental constraints, but irreversibly bifurcate into two distinct genome population each adapted to a given niche (White & Adami, 2004). Moreover, Johnson & Wilke (2004) have shown that two competing species evolve to a stable state that avoid synchronisation and by the way make maximal use of the available resources. Competitive mechanisms leading to higher order redundancy reduction or equivalently sparse population dynamic appears a widespread and already well documented phenomenon in Nature. For example, demographic dynamic of large number of interacting population (predator prey dynamic that is governed by Volterra's formalism, generalised to large number of populations using Gibbsian statistical development) is leading to sparse assemblies in the case complex (diverse) interactions ("the higher the complexity of interaction, the more spike-like do the oscillations become", Cowan 1965).

In the section dedicated to neo-cortical organisation, we propose that the specialisation of cortical areas is resulting from such a process. In fact constraints are present at many scales and their definitions depend on what is approximated as a system. And obviously, an "entity" like a human is participating to several systems (or networks) at various temporal and spatial scales. As we said before the Logical Depth is huge. In other word, "I" is a result of Human specie biological historical network that contain evolution and ecosystem, and of social network that contain family, schools and society etc... This is the essence of the holist physical view, when one considers pragmatically the various energy flows and exchange, the various interdependencies on all spatial and time scales, the notion of system (formally in statistical and mechanical physic), entity, or individual fades and a global system or holist network of elementary entities has to be considered.

The redundancy minimisation, imposed by the information maximisation process, is synonymous of specialisation (or differentiation) of the entity composing the system. It is intrinsically a rule that maximise diversity, that lead to maximally specialized entities. Two genes or two neurons have rarely the same structure and function. The introduction of the system capacity in the definition of mutual information ($I(E;S) = H_{0S} - H_{0S}R_S - H(S/E)$) shows that the amount of redundancy that can removed by adaptation is increasing with the system capacity. In other terms, increasing the number of entities of a system, in a given non-limiting energy (and structurally complex) environment is leading to an increase of the level differentiation, selectivity or specificity of the entities. As exposed further in the cortical

context which “strategy” is clearly to have a huge capacity, H_0 is a redundancy removing capacity, a computational capacity.

We can conclude simply that living systems, through their genetic patrimony and-or their nervous system, are dynamic memories optimising their fitness to the environmental context and modifying it the way.

4.4.3 System computational capacity increase

The absolute capacity of a system H_0 , is a computational capacity. Both Genomic (Cavalier-Smith, 1985) and neocortical capacity have been increasing on average along evolution. In the framework presented here, this increase may correspond to the increase in the structural complexity (LD) of the environment. However, the system capacity is not an absolute indicator of the system information or complexity, as number of exception, at least apparent, have been reported. Onion DNA contains for example 3 times more bases pair than Human one, and Dolphins relative brain size being superior to Human one (Jerison, 1973; Marino, 1996). In genetic, the absence of strict correlation between genome length and organismic complexity, due to various proportion of ambiguous neutral code, as led to the so-called C-value paradox. However, mean social group size is directly related to relative neocortical volume in primates (Sawaguchi & Kudo 1990, Dunbar 1992), carnivores (Dunbar & Bever 1998) and cetaceans (Marino, 1996), reinforcing the idea that neocortex act as a social genome, and that neocortical capacity is linked to a cognitive complexity.

4.4.4 Complex system modelisation and prediction

The model presented above have obviously a very simple analogue in cybernetics, in term of Turing machine. The algorithm of nature just looks like an entropy maximisation or redundancy minimisation process (which may be hard or close to hard problem). If so, there may be no simpler rule that can be used to explain or predict system dynamic. It would imply that, in order to predict complex system dynamic, an enormous amount of data and a huge computational capacity have to be employed. From the thermodynamical point of view, as noted by Bennett (1987) and Adami and Cerf (2000), this process defining a memory corresponds to the operation of a natural Maxwell daemon, “the population performs random measurements on its environment, and stores those “results” that decrease the entropy, but rejects all others. Thus, the process acts as a “semi-permeable membrane for information” (Adami & Cerf 2000).

4.4.5 Living systems as a function: gain controls diversity and non-linear systems.

So far from the line.

“The straight line leads to the downfall of mankind” Hundertwasser F., 1953.

According to the model presented here, the dynamic of living systems is not a singular dynamic and is common to any system dynamic. From the functional point of view, information maximisation can be achieved by gain control (Laughlin, 1981, Bell & Sejnowski, 1995). Furthermore, as shown in chapter 3.6, non-linear interaction, or gain control, increase the reliability of the cortical response. Similar results have also been obtained considering gene expression, showing that negative feedback loop increases the reliability of genetic expression (Becskei & Serrano, 2000, Gardner & Collins, 2000). Living systems can be viewed as a collection of gain controls (at mature adapted stage): they’re intrinsically non-linear systems. Consistently, the response observed in primary visual cortex to natural movie (with eye-movement) is poorly explained by the linear classical receptive field (chapter 3.6). This wide and compact superposition of gain controls, corresponding physically to a complex network structure, explains the striking difficulty of the functional characterisation of organisms (just look at the diversity of result on the center-surround interaction in the cortex or on the control of protein expression or intracellular signalisation in cell-biology). This complexity also explains the omnipresence of large variability in experimental results when the system is dissected into isolated elementary mechanisms or function.

In such complex systems, computational models can have critical role not only in reproducing or validating empirical results, but in predicting them. Artificial life and intelligence should even abstract from the function, and increase the still widely underestimated computational capacity (Ho) of their model and environmental informational richness of the input (LD, cf. chapter cybernetic).

Reciprocally, reproducibility of the results shall be used by experimentalists as an heuristic to discover the full function and the pertinent dimensions the system responds to. Philosophically, adaptative process may be sufficient to explain the antagonistic apparent role of “hazard” and the apparent purpose, functionality or “necessity” of the living dynamic (Democrite, Monod, 1970). In other terms, apparent function or goals naturally arise from adaptive processes. This is on our opinion why “anthropic principles” widespread from biology to physic, although hardly justified logically, may appear pragmatically relevant.

4.4.6 Natural language and Human language: linguistic generalisation

Another important point can be proposed from this model. Many theories stress that Human specificity is due to his peculiar linguistic competence. It seems to us that this definition that most nowadays ethologist would laugh about has to be discussed. We can give a very intuitive and simple expression of the model presented above (that most of the poets already claimed): nature is a language (or a code, see Reeves, 1986, for a simple physical and general argumentation), and organisms learn this language and speak or express themselves in this language (it's not restricted to organisms, anything learns or evolves). Human languages are just very compact natural language allowed by the high human brain computational capacity (neo-cortex). As Barlow already noticed, Human languages are probably one of the highest ordered (abstract) and less redundant representation of the world. The simple fact that all human languages are approximately equivalent, meaning they can be translated in one another with very low "information" loss, can be interpreted as a signature of this natural origin of Human languages, world being essentially the same for any-culture, and language translation fails mainly where the environmental content differs. This consideration in turn moderate Chomsky proposal, with all the respect and admiration we have for his work on generative grammars, that "linguistic competence", the unconscious knowledge of grammatical rules, are innate features of the human mind (Chomsky, 1965). This idea that grammatical rules are genetically encoded is still supported in psycholinguistic (Sakai, language acquisition review, 2005). Hidden laws can be understood as processes that generate or explain redundancy or structure, learning the outside or internalising external constraints leads to a hidden or non-representative internalisation of this law. A more obvious example of hidden law is gravity, most organism implicitly know this rule and even play with it without having the explicit or representative expression that culminated with Newton and which necessities a high level of generalisation of integration to be formulated. More generally, the debate innate vs. acquired information appears obsolete since both are experience learned competence either genetically or epigenetically. Furthermore, both genetic and epigenetic learning implement the same algorithm at different scale. Some studies in psychology are already probing that subject can learn implicitly simple rules and that this ability can simply be explained by a powerful associative memory capacity, globally leading to a more and more founded critic of Chomsky's genetical proposition (Richardson & al, 1990, Perruchet & al, 1997, Redington & Chater, 1998). Furthermore, recent modelisation studies show that prototypic languages can emerge in population of interacting adaptative agents (Steels, 2003 for review). In genetic

field, universal genetical code can be understood in this context as hidden rules (grammatical rules, not code), that are simply represented by associative memory like tARN (more precisely, amino-acyl ARN_t synthétase).

4.4.7 Evolutionary Epistemology, history, and intelligence

Redundancy is an elementary definition of knowledge. Intelligence, when considered as the amount of knowledge a system display can be quantified by its Logical depth; intelligence, when considered as the process that generate the knowledge, can be quantified by its Algorithmic information (unfortunately noncomputable). As already emphasized in algorithmic and statistical literature, it also gives a formal framework for epistemology and scientific production, a good theory being defined by the shortest possible expression (low complexity) and the largest possible amount of data explanation (large logical depth) (Parisi, 2003, for review).

The mutual information maximisation or maxent pragmatically corresponds to the most classical empirical principle in science. This paradigm can be understood as a pragmatical formalisation of observation.

Interestingly, H_0R is also the elementary logical definition of the system memory, since the presence of mutual information in between two entities of the system notably in time implies the presence of a memory (Ashby, 1967).

4.4.8 Philosophical and epistemological debates

We can also investigate how this model may participate to philosophical and epistemological debates (but a whole book would be necessary). Of course, one of the main consequences of this work is a re-naturalisation of the conception we have of Humans, of their thoughts and beliefs, culture and societies. It is also a criticism of Cartesianism, and we are opposing to Descartes' (1644) "I think therefore I am", Rimbaud's (among others, and they are many) point view: "It is wrong to say: I think. One ought to say i am thought. Pardon the pun. I is someone else. No matter for the wood that find itself a Violin, and scoff at thoughtless, who argue about something they completely ignore!".

A first remark concerning the philosophical aim of biological definition (Canguilhem, 1968) follows from this: any rigorous definition of Human or Life is probably doomed to fail. Secondly, any science field studying structure and its dynamic or the following apparent function can be translated into physical terms: there's no hard or weak/soft science: Human sciences are hard sciences just classically expressed in less formal ways than physics.

Coherently, an example of the economical sciences attempt of formalisation in mathematical terms, the gambling theory, is leading to an equivalent formalism to the informational one, the best gambler being also the best data compressor (Cover & Thomas, 1991). We can even go a step forward, considering that scientific concepts are just beliefs generated by the same brain and the same process as any other beliefs like artistic or religious ones. From this point of view, those three families of beliefs are just natural sciences (or natural arts, or natural religions) sharing many similarities (further more phylogenetically, those knowledge are parents) and expressed in different specialised languages, none of them being more legitimate than another, and all of them having to be considered concerning the conception we have of the world. This can be related to the basement of anthropological and ethnological studies (Lévi-Strauss, 1972, Latour, 1979), and many principles developed here are consistent with those science field conclusions. It has to be emphasized that what is defended here is not a pure relativism or idealism (nor of course pure objectivism), brain beliefs are legitimated, and if our beliefs and percept may be just illusions, the whole world is intrinsically included in this same illusion (i think therefore the world is). In other terms, the paradigm proposed in this thesis, in the direct affiliation with Leibnitz, avoid the subject-object dualism. There are many ways of interpreting this work; at least, to finish on an optimistic considerations, it appears as a natural conclusion that Life, Time, and Energy are precious, that a realistic definition of a system is in fact a great-widespread family and history, and one can interpret the minimisation of constraint ongoing in the world and systems both as a freedom, a creativity and a consciousness quest.

“Peacock makes the wheel
 Chance makes the rest
 God sit inside
 And Man pushes it”

“Le paon fait la roue
 Le hasard fait le reste
 Dieu s’assoit dedans
 Et l’homme le pousse. »

*The wheelbarrow or the great inventions,
 La brouette ou les grandes ineventions*
 Prevert (Paroles, 1946)

Vers dorés

« Eh quoi tout est sensible! »

Pythagore

Homme, libre penseur! Te crois-tu seul pensant
Dans ce monde où la vie éclate en toutes choses?
Des forces que tu tiens ta liberté dispose,
Mais de tous tes conseils l'univers est absent.

Respecte dans la bête un esprit agissant:
Chaque fleur est une âme à la Nature éclore;
Un mystère d'amour dans le métal repose;
"Tout est sensible!" Et tout sur ton être est puissant.

Crains, dans le mur aveugle, un regard qui t'épie:
A la matière même un verbe est attaché...
Ne la fait pas servir à quelque usage impie!

Souvent dans l'être obscur habite un Dieu caché;
Et comme un oeil naissant couvert par ses paupières,
Un pur esprit s'accroît sous l'écorce des pierres.

Gérard de Nerval

5. Bibliography

- Abeles M., 1991, *Corticonics: Neural Circuits of the Cerebral Cortex*, Cambridge University Press, Cambridge.
- Abbott LF, Regehr WG., *Nature* 2004, Synaptic computation, VOL 431 | 14 OCTOBER 2004. 796-803.
- Adami, C., & Cerf NJ, *Physica D* 2000. Physical complexity of symbolic sequences. 137, 62--69.
- Adami, C., Ofria, C. & Collier, T. C., *Proc. Natl. Acad. of Sci.* 2000. Evolution of biological complexity. U.S.A. 97, 4463–4468.
- Adorjan, P., Levitt, J.B., Lund, J.S. and Obermayer, K., *Visual Neurosci.* 1999. A model for the intracortical origin of orientation preference and tuning in macaque striate cortex. 16, 303-318.
- Aertsen AM, Smolders JW, Johannesma PI., *Biol Cybern.* 1979, Neural representation of the acoustic biotope: on the existence of stimulus-event relations for sensory neurons. Mar 19;32(3):175-85.
- Ahmed, B., Anderson, J.C., Douglas, R.J., Martin, K.A.C. and Nelson, J.C., *J. Comp. Neurol.* 1994. Polyneuronal innervation of spiny stellate neurons in cat visual cortex. 341, 39-49.
- Albrecht, DG, & Geisler WS. *Vis Neurosci* 1991. Motion selectivity and the contrast-response function of simple cells in the visual cortex. 7: 531–546.
- Albrecht DG & Hamilton DB. *J Neurophysiol* 1982. Striate cortex of monkey and cat: contrast response function. 48: 217–237.
- Amari S., Cichocki A. and Yang H. H., *Proc. Int. Symposium on Nonlinear Theory and its Applications - NOLTA'95*, 1995, Recurrent neural networks for blind separation of sources, Las Vegas, Dec.10-15, vol.1, pp. 37-42.
- Amari, S. 1999. Information geometry on hierarchical decomposition of stochastic interactions. Citeseer preprint.
- Amari, S. *IEEE Transactions on Information Theory* 2001. Information geometry on hierarchy of probability distributions. 47(5), 1701–1711.
- Amari S, Nakahara H., *Neural Comput.* 2006, Correlation and independence in the neural code. Jun;18(6):1259-67. Review.
- Anderson, J., Lampl, I., Reichova, I., Carandini, M. and Ferster, D.. *Nat. Neurosci.* 2000a. Stimulus dependence of two-state fluctuations of membrane potential in cat visual cortex. 3, 617-621.
- Anderson, J.S., Carandini, M. and Ferster, D. *J. Neurophysiol.* 2000b., Orientation tuning of input conductance, excitation, and inhibition in cat primary visual cortex. 84, 909-926.
- Anderson, J.S., Lampl, I., Gillespie, D.C. and Ferster, D., *Science* 2000c. The contribution of noise to contrast invariance of orientation tuning in cat visual cortex. 290, 1968-1972.
- Anzai A, Ohzawa I, & Freeman RD. *J Neurophysiol* 1999. Neural mechanisms for processing binocular information. I. Simple cells. 82: 891–908.
- Arieli A, Sterkin A, Grinvald A, Aertsen A., *Science.* 1996, Dynamics of ongoing activity: explanation of the large variability in evoked cortical responses. Sep 27;273(5283):1868-71.
- Arnoux P., & Chemla K. , 1992, Systèmes dynamiques et théorie ergodique, in *Chaos et déterminisme*, sous la direction de Dahan Dalmedico, Chabert, & Chemla, eds seuil, p46-49.
- Ashby WR., *Curr Mod Biol.* 1967, The place of the brain in the natural world. May;1(2):95-104.
- Atlan H., 1979, *Entre le cristal et la fumée*. Seuil, Paris.

- Atlan H. & Koppel M. *Bul. Math. Biol.* 1990, The cellular computer DNA: program or data. 52(3) 335-348.
- Atick, J.J., *Network: Computation in Neural Systems*, 1992, Could information theory provide an ecological theory of sensory processing. 3 213-251.
- Atick J. J., Redlich A.N., *Neural Comput* 1992, “What does the retina know about the natural scenes?”. 4, 196–210.
- Attneave, F., 1954. Some informational aspects of visual perception. *Psych. Rev.* 61, 183–193.
- Ay N, Wennekers T., *Neural Netw.* 2003, Dynamical properties of strongly interacting Markov chains. Dec;16(10):1483-97.
- Azouz R, Gray CM. *J Neurosci.* 1999, Cellular mechanisms contributing to response variability of cortical neurons in vivo. Mar 15;19(6):2209-23.
- Azouz R, Gray CM., *Neuron.* 2003, Adaptive coincidence detection and dynamic gain control in visual cortical neurons in vivo. Feb 6;37(3):513-23.
- Azouz R, Gray CM., *Proc Natl Acad Sci U S A.* 2000, Dynamic spike threshold reveals a mechanism for synaptic coincidence detection in cortical neurons in vivo. Jul 5;97(14):8110-5.
- Barlow, H.B., 1961. Possible principles underlying the transformation of sensory messages. In *Sensory Communication*, W.A. Rosenblith, ed. (Cambridge, MA: MIT Press), pp. 217–234.
- Barlow HB, Blakemore C & Pettigrew JD, *J Physiol* 1967. The neural mechanism of binocular depth discrimination. 193, 327-342
- Barlow HB, 1985. Cerebral cortex as model builder. In: Rose D, Dobson VG (eds) *Models of the visual cortex*. Wiley, Chichester, P37-46.
- Barlow H.B., Kaushal T.P., and Mitchison G. J., *Neural Computation* 1989, Finding minimum entropy codes. 1:412-423.
- Barlow H. B. *Neural Computation* 1989, Unsupervised learning. vol. 1, pp. 295-311.
- Barlow H., *Network.* 2001, Redundancy reduction revisited. Aug;12(3):241-53. Review.
- Barlow H.B., Olshausen B., *J. Of Vision* 2004, Convergent evidence for the visual analysis of optic flow through anisotropic attenuation of high spatial frequencies. 4 . 415-426.
- Basole A, White LE, Fitzpatrick D., *Nature* 2003, Mapping multiple features in the population response of visual cortex. Jun 26;423(6943):986-90.
- Becskei A, Serrano L., *Nature.* 2000, Engineering stability in gene networks by autoregulation. Jun 1;405(6786):590-3.
- Bednar J.A., Miikkulainen R., *Neurocomputing* 2003. Self-organization of spatiotemporal receptive fields and laterally connected direction and orientation maps.52-54:473-480..
- Bekenstein J.D., *Scientific American* 2003, Information in the Holographic Universe. Vol. 289, n 2, p. 61.
- Bell AJ, Sejnowski TJ., *Vision Res.* 1997, The "independent components" of natural scenes are edge filters. Dec;37(23):3327-38.
- Bell AJ, Sejnowski TJ., *Neural Comput.* 1995, An information-maximization approach to blind separation and blind deconvolution. Nov;7(6):1129-59.
- Benevento, L.A., Creutzfeldt, O.D. and Kuhnt, U., *Nature* 1972. Significance of intracortical inhibition in the visual cortex. 238, 124-126.
- Bennett, C.H., *Int. J. Theoret. Phys.* 1982. The thermodynamics of computation, 21, 905-940.
- Bennett C.H., *Sci. American* 1987, Demons, engines, and the second law. November, 108-116.
- Bennett C.H., 1988, Logical Depth and Physical Complexity, *The Universal Turing Machine— a Half-Century Survey*, edited by Rolf Herken, Oxford University Press , 227-257.
- Bennett C.H., 1985, “Information, Dissipation, and the Definition of Organization”, in *Emerging Syntheses in Science*, David Pines ed. (Santa Fe Institute, Santa Fe, NM) 297-313.
- Ben-Yishai, R., Bar-Or, R.L. and Sompolinsky, H., *Proc. Natl. Acad. Sci. USA* 1995. Theory of orientation tuning in visual cortex. 92, 3844-3848.

- Benzi R., Sutera A. & Vulpiani A., J. Phys. A 1981. The mechanism of stochastic resonance. 14, 453
- Berman, N.J., Douglas, R.J., Martin, K.A.C. and Whitteridge, D., J. Physiol 1991. Mechanisms of inhibition in cat visual cortex. 440, 697-722.
- Bekenstein JD., Sci Am. 2003, Information in the holographic universe. Aug;289(2):58-65.
- Bialek W, Rieke F, de Ruyter van Steveninck RR, Warland D., Science. 1991, Reading a neural code. Jun 28;252(5014):1854-7.
- Bialek W., 2001, Thinking about the brain. Based on lectures at Les Houches Session LXXV, July 2001. To appear in Physics of Biomolecules and Cells, H. Flyvbjerg et al., eds. EDP Sciences, Les Ulis; Springer-Verlag, Berlin, 2002.
- Bialek W, Nemenman I, Tishby N., Neural Comput. 2001, Predictability, complexity, and learning. 2001 Nov;13(11):2409-63.
- Bialek, W., Nemenman, I. & Tishby, N. Physica A 2001. Complexity through nonextensivity. 302:89-99.
- Bishop, P.O., Coombs, J.S. and Henry, G.H., J. Physiol 1973. Receptive fields of simple cells in the cat striate cortex. 231, 31-60.
- Boltzmann L., Graz Sitzb. d. Kaiserlichen Akademie der Wissenschaften, mathematisch-naturwissen 1877, On the relationship between the second main theorem of mechanical heat theory and the probability calculation with respect to the results about the heat equilibrium. Cl. LXXVI, Abt II, pp. 373-435.
- Bonds AB., Vis Neurosci. 1991, Temporal dynamics of contrast gain in single cells of the cat striate cortex. Mar;6(3):239-55.
- Bonhoeffer, T., Kim, D.-S., Malonek, D., Shoham, D., and Grinvald, A., Eur J Neurosci 1995. Optical imaging of the layout of functional domains in area 17 and across the area 17/18 border in cat visual cortex. 7, 1973-1988.
- Borg-Graham, L. J., Nature Neurosci 2001. The computation of directional selectivity in the retina occurs prior to the ganglion cell. 4, 176-182.
- Borg-Graham, L., Monier, C. and Frégnac, Y., J. Physiol. (Paris) 1996. Voltage clamp measurement of visually evoked conductances with whole-cell patch recordings in primary visual cortex. 90, 185-188.
- Borg-Graham L.J., Monier C., Frégnac Y., Nature 1998, Visual input evokes transient and strong shunting inhibition in visual cortical neurons, 393, 369-373.
- Borst A, Theunissen FE., Nat Neurosci. 1999, Information theory and neural coding. Nov;2(11):947-57. Review.
- Braddick, O.J., Philosophical Transactions of the Royal Society of London 1980. Low-level and high-level processes in apparent motion. Series B (Biological Sciences). 290, 137-151.
- Brenner N., Bialek W, de Ruyter van Steveninck R., Neuron 2000, Adaptive Rescaling Maximizes Information Transmission. Vol. 26, 695-702, June.
- Brillouin L., 1956, Science and Information Theory. New York: Academic Press.
- Bringuier, V., Chavane, F., Glaeser, L. and Frégnac, Y., Science 1999. Horizontal propagation of visual activity in the synaptic integration field of area 17 neurons. 283, 695-699.
- Britten KH, Shadlen MN, Newsome WT, Movshon JA., Vis Neurosci. 1993, Responses of neurons in macaque MT to stochastic motion signals. Nov-Dec;10(6):1157-69.
- Buracas GT, Zador AM, DeWeese MR, Albright TD., Neuron. 1998, Efficient discrimination of temporal patterns by motion-sensitive neurons in primate visual cortex. May;20(5):959-69.
- Burr D., Curr Biol. 2004, Eye movements: keeping vision stable. Mar 9;14(5):R195-7. Review.

- Burt, H.E., *Journal of Experimental Psychology* 1917a. Auditory illusions of movement - A preliminary study. 2, 63-75.
- Burt, H.E., *Journal of Experimental Psychology* 1917b. Tactile illusions of movement. 2, 371-385.
- Bush, P.C. and Sejnowski, T.J. J., *Neurophysiol* 1994. Effects of inhibition and dendritic saturation in simulated neocortical pyramidal cells. 71, 2183-2193.
- Buzas, P., Eysel, U.T., Adorjan, P. and Kisvarday, Z.F., *J. Comp. Neurol* 2001. Axonal topography of cortical basket cells in relation to orientation, direction, and ocular dominance maps. 437, 259-285.
- Carandini, M. and Ferster, D., *J. Neurosci.* 2000. Membrane potential and firing rate in cat primary visual cortex. 20, 470-484.
- Carandini M, Heeger DJ, & Movshon JA. *J Neurosci* 1997. Linearity and normalization in simple cells of the macaque primary visual cortex. 17: 8621– 8644.
- Carandini M, Heeger DJ, & Movshon JA., 1999. Linearity and gain control in V1 simple cells. In: *Cerebral Cortex. Models of Cortical Circuits*, edited by Ulfink PS, Jones EG, and Peters A. New York: Kluwer Academic/Plenum, vol. 13, p. 401–443.
- Carandini M, Demb JB, Mante V, Tolhurst DJ, Dan Y, Olshausen BA, Gallant JL, Rust NC., *J Neurosci.* 2005, Do we know what the early visual system does? Nov 16;25(46):10577-97. Review.
- Cardoso J.F., *IEEE Signal Processing letters* 1997, Infomax and maximum likelihood for blind source separation. 4: 112-114.
- Carroll SM., *Nature* 2006, Is our Universe natural?, Apr 27;440(7088):1132-6.
- Castro-Alamancos M.A., *Neuron* 2004, Absence of rapid sensory adaptation in neocortex during information processing states. 41, 455-464.
- Cavalier-Smith, T. (1985). Eukaryote gene numbers, non-coding DNA and genome size. In: *The Evolution of Genome Size* (T. Cavalier-Smith, Ed.) pp. 69–103. New York, NY: Wiley.
- Cavanaugh J.R., Bair W., Movshon J.A., *J Neurophysiol* 2002. Nature and interaction of signals from the receptive field center and surround in macaque V1 neurons, 88, 2530–2546.
- Chaitin G., 1970, To a mathematical definition of “life”, *ACM SIGACT News* N°4 p12-18.
- Chaitin G., 1977, Algorithmic Information Theory, *IBM J. Res. Develop.* 21, 350-359, 496.
- Chaitin G., *Sci. Am.* 1985, Randomness and mathematical proof. 232(5). 47-52.
- Chalmers D., *Journal of consciousness* 1995. Facing up the problem of consciousness. 2(3): 200-19.
- Chance FS, Abbott LF., *Network.* 2000, Divisive inhibition in recurrent networks. May;11(2):119-29.
- Chater N, Vitanyi P., *Trends Cogn Sci.* 2003, Simplicity: a unifying principle in cognitive science? Jan;7(1):19-22.
- Chavane F, Monier C, Bringuier V, Baudot P, Borg-Graham L, Lorenceau J, Fregnac Y., *J Physiol Paris.* 2003. Shunting inhibition, a silent step in visual cortical computation. Jul-Nov;97(4-6):441-51.
- Chavane F, Monier C, Bringuier V, Baudot P, Borg-Graham L, Lorenceau J, Fregnac Y., *J Physiol Paris.* 2000, The visual cortical association field: A Gestalt concept or a psychophysiological entity? 94 333–342
- Chavane, F., Monier, C., Baudot, P., Borg-Graham, L. and Frégnac, Y. (1998). Dynamics of the on/off balance of subthreshold versus spike receptive fields in cat area 17. In "28th Annual Meeting of the Society for Neuroscience". Society for Neuroscience Abstracts. 24: 897. Los Angeles, USA.
- Chavane, F., 1999, Diversité d'expression fonctionnelle du champ d'intégration synaptique. Thèse.

- Chen C.C., Kasamatsu T., Polat U., Norcia A.M., *Neuroreport* 2001. Contrast response characteristics of long-range lateral interactions in cat striate cortex, 12, 655–661.
- Chklovskii DB, Schikorski T, Stevens CF., *Neuron*. 2002, Wiring optimization in cortical circuits. Apr 25;34(3):341-7.
- Chomsky N., 1965. *Aspects of the Theory of Syntax*. MIT Press, Cambridge.
- Chow SS, Wilke CO, Ofria C, Lenski RE, Adami C., *Science*. 2004, Adaptive radiation from resource competition in digital organisms. Jul 2;305(5680):84-6.
- Collier J., 1999, *Information Theory*, Stanford Encyclopedia of Philosophy, <http://www.kli.ac.at/theorylab/jdc/information/information.html>
- Collins JJ, Chow CC and Imhoff TT. , *Nature* 1995, Stochastic resonance without tuning. 376: 236-238.
- Collewyn H., 1977, Gaze in freely moving subjects, in *Control of Gaze by brain stem Neurons*, Developments in Neuroscience Volume 1. Elsevier (13-22).
- Comon P., *Signal Processing* 1994, Independent Component Analysis -- A new concept ? 36:287--314.
- Coppola D, Purves D., *Proc Natl Acad Sci U S A*. 1996. The extraordinarily rapid disappearance of entopic images. Jul 23;93(15):8001-4.
- Cosmelli D., Lachaux J.P., and Thompson E., 2007, *Neurodynamics of Consciousness*, Forthcoming in Philip David Zelazo, Morris Moscovitch, and Evan Thompson, eds., *The Cambridge Handbook of Consciousness*.
- Cossart R, Aronov D, Yuste R., *Nature*. 2003, Attractor dynamics of network UP states in the neocortex. May 15;423(6937):283-8.
- Cowan JD., *Prog Brain Res*. 1965, The problem of organismic reliability. 17:9-63.
- Creutzfeldt, O.D., Kuhnt, V. and Benevento, L.A., *Exp. Brain Res*. 1974. An intracellular analysis of visual cortical neurons to moving stimuli: responses in a co-operative neuronal network. 21, 251-274.
- Crochet S, Petersen CC., *Nat Neurosci*. 2006, Correlating whisker behavior with membrane potential in barrel cortex of awake mice. May;9(5):608-10.
- Croner LJ, Purpura K, Kaplan E., *Proc Natl Acad Sci U S A*. 1993, Response variability in retinal ganglion cells of primates. Sep 1;90(17):8128-30.
- Crook, J.M., Kisvarday, Z.F. and Eysel, U.T., *Visual Neurosci*. 1997. GABA-induced inactivation of functionally characterized sites in cat striate cortex: effects of orientation tuning and direction selectivity. 14, 141-158.
- Crook, J.M., Kisvarday, Z.F. and Eysel, U.T. (1998). Evidence for a contribution of lateral inhibition to orientation tuning and direction selectivity in cat visual cortex: reversible inactivation of functionally characterized sites combined with neuroanatomical tracing techniques. *Eur. J. Neurosci*. 10, 2056-2075.
- Crook , *Experimental Brain Research*. 1990. Directional tuning of cells in area 18 of the feline visual cortex for visual noise, bar and spot stimuli: a comparison with area 17. 80, 545-561.
- Crook, J.M., Worgotter, F. and Eysel, U.T., *Exp. Brain Res*. 1994. Velocity invariance of preferred axis of motion for single spot stimuli in simple cells of cat striate cortex. 102, 175-180.
- Dan Y, Atick JJ, Reid RC., *J. Neurosci*. 1996, Efficient coding of natural scenes in the lateral geniculate nucleus: experimental test of a computational theory. 16(10):3351-62.
- Das, A. and Gilbert, C.D., *Nature* 1999. Topography of contextual modulations mediated by short-range interactions in primary visual cortex. 399, 655-661.

- Daugman JG., J Opt Soc Am A. 1985. Uncertainty relation for resolution in space, spatial frequency, and orientation optimized by two-dimensional visual cortical filters. Jul; 2(7): 1160-9.
- David SV, Vinje WE, Gallant JL., J Neurosci. 2004, Natural stimulus statistics alter the receptive field structure of v1 neurons. Aug 4;24(31):6991-7006.
- Dayan P, Hinton GE, Neal RM, Zemel RS., Neural Comput. 1995, The Helmholtz machine. Sep;7(5):889-904.
- Dean, A.F., Exp. Brain Res. 1981. The variability of discharge of simple cells in the cat striate cortex. 44, 437-440.
- Dean AF, Tolhurst DJ., J Physiol. 1983. On the distinctness of simple and complex cells in the visual cortex of the cat. Nov;344:305-25.
- DeAngelis, G.C., Robson, J.G., Ohzawa, I. and Freeman, R.D., J. Neurophysiol. 1992. Organization of suppression in receptive fields of neurons in cat visual cortex. 68, 144-163.
- DeAngelis G.C., Freeman R.D., Ohzawa I., J Neurophysiol 1994. Length and width tuning of neurons in the cat's primary visual cortex, 71, 347-374.
- DeAngelis GC, Ghose GM, Ohzawa I, Freeman RD., J Neurosci. 1999, Functional micro-organization of primary visual cortex: receptive field analysis of nearby neurons. May 15;19(10):4046-64.
- Debanne D, Shulz DE, Fregnac Y., J Physiol. 1998. Activity-dependent regulation of 'on' and 'off' responses in cat visual cortical receptive fields. Apr 15;508 (Pt 2):523-48.
- Debarre C., 2003, Joe Bar Team 2, Vent d'ouest editions.
- Dehaene S, Izard V, Pica P, Spelke E., Science. 2006, Core knowledge of geometry in an Amazonian indigene group. Jan 20;311(5759):381-4.
- de Ruyter van Steveninck RR, Lewen GD, Strong SP, Koberle R, Bialek W., Science. 1997 Reproducibility and variability in neural spike trains. Mar 21;275(5307):1805-8.
- Descartes, R., 1644, Les Principes de la philosophie.
- Destexhe A, Marder E., Nature 2004, Plasticity in single neuron and circuit computations. Oct 14;431(7010):789-95.
- Destexhe A. & Contreras D. Neural computations during irregular network states, submitted to science.
- De Valois RL, Yund EW, Hepler N., Vision Res. 1982. The orientation and direction selectivity of cells in macaque visual cortex. ;22(5):531-44.
- Dewar RC, J. Phys. A, 2003, Information theory explanation of the fluctuation theorem, maximum entropy production and self-organized criticality in non-equilibrium stationary states. 36:631-641.
- Dewar RC, 2004, Maximum entropy production and non-equilibrium statistical mechanics. Kleidon A, Lorenz R (eds) Non-equilibrium thermodynamics and the production of entropy: life, Earth, and beyond. Springer Verlag.
- Dewar RC, J. Phys. A: Math, 2005. Maximum entropy production and the fluctuation Theorem. Gen. 38 L371-L381.
- Deweese MR, Zador AM., J Neurophysiol. 2004, Shared and private variability in the auditory cortex. Sep;92(3):1840-55.
- DeWeese MR, Zador AM., J Neurosci. 2006, Non-Gaussian membrane potential dynamics imply sparse, synchronous activity in auditory cortex. Nov 22;26(47):12206-18.
- Ditchburn R.W. (1973). Eye-movements and visual perception. Oxford: Clarendon Press.
- Ditchburn R.W., Ginsborg BL., Nature. 1952, Vision with a stabilized retinal image. Jul 5;170(4314):36-7.
- Doi E, Lewicki: M, NIPS 2004, Sparse Coding of Natural Images Using an Overcomplete Set of Limited Capacity Units. http://books.nips.cc/papers/files/nips17/NIPS2004_0757.pdf

- Dong DW, Atick JJ., Netw. Comput. Neural Syst.1995. Statistics of natural time-varying images. 6:345–58.
- Dong, J. Vision 2004, No suppression only dynamic decorrelation, saccadic effect on visual responses to natural time Varying image. <http://dove.ccs.fau.edu/talks/03VSS-2/>
- Doshier BA, Lu ZL. Proc Natl Acad Sci U S A. 1998, Perceptual learning reflects external noise filtering and internal noise reduction through channel reweighting. Nov 10;95(23):13988-93.
- Douglas, R., Koch, C., Mahowald, M. & Martin, K., 1999. The role of recurrent excitation in neocortical circuits. In *Cerebral Cortex: Models of cortical circuits*, pp. 251-282. Edited by P. S. Ulinsky, E. G. Jones & A. Peters. New York: Kluwer Academic : Plenum Publishers.
- Douglas, R.J., Koch, C., Mahowald, M.A., Martin, K.A.C. and Suarez, H.H., Science 1995. Recurrent excitation in neocortical circuits. 269, 981-985.
- Douglas, R.J., Martin, K.A.C. and Whitteridge, D., Nature 1988. Selective responses of visual cortical cells do not depend on shunting inhibition. 332, 642-644.
- Douglas, R.J., Martin, K.A.C. and Whitteridge, D., J. Physiol.1991. An intracellular analysis of the visual responses of neurones in cat visual cortex. 440, 659-696.
- Dow, B.M., Snyder, A.Z., Vautin, R.G. and Bauer, R., Exp. Brain Res. 1981. Magnification factor and receptive field size in foveal striate cortex of the monkey. 44, 213-228.
- Dragoi, V., Rivadulla, C., and Sur, M., Nature 2001. Foci of orientation plasticity in visual cortex. 411, 80-86.
- Dragoi V, Sharma J, Miller EK, Sur M., Nat Neurosci. 2002, Dynamics of neuronal sensitivity in visual cortex and local feature discrimination. Sep;5(9):883-91.
- Dunbar, R. I. M., Journal of Human Evolution 1992. Neocortex size as a constraint on group size in primates. 20, 469–493.
- Dunbar, R. I. M. & Bever, J., Ethology 1998. Neocortex size predicts group size in carnivores and some insectivores. 104, 695–708.
- Edlund JA, Adami C., Artificial Life. 2004, Evolution of robustness in digital organisms. Spring;10(2):167-79.
- Einstein A., *Investigations on the Theory of Brownian Movement*, ed. R. Fürth, translated by A.D. Cowper (1926, reprinted 1956); Einstein, *Collected Papers*, vol. 2, 170-82, 206-22.
- Eizenman M, Hallett PE, Frecker RC., Vision Res. 1985, Power spectra for ocular drift and tremor. 25(11):1635-40.
- Engel AK, Singer W., Trends Cogn Sci. 2001, Temporal binding and the neural correlates of sensory awareness. Jan 1;5(1):16-25.
- Evans DJ, Cohen EGD., Moriss GP., Phys Rev Let 1993, Probability of second law violations in shearing steady states. Vol 71 N°15. 2401-2404.
- Evans DJ, Searles D., Advance in physics, 2002, The fluctuation theorem, Vol. 51, No. 7, 1529±1585
- Eysel, U.T., Crook, J.M. and Machemer, H.F., Exp. Brain Res. 1990. GABA-induced remote activation reveals cross-orientation inhibition in the cat striate cortex. 80, 626-630.
- Eysel, U.T. and Shevelev, I.A., NeuroReport. 1994. Time-slice analysis of inhibition in cat striate cortical neurones. 5, 2033-2036.
- Fairhall AL, Lewen GD, Bialek W, de Ruyter Van Steveninck RR., Nature. 2001, Efficiency and ambiguity in an adaptive neural code. Aug 23;412(6849):787-92.
- Falcioni M., Loreto V., Vulpiani A., 2003, Entropie, Chaos & Complexité. In « L'héritage de Kolmogorov en physique », R. Livi, A. Vulpiani, eds Belin.
- Felleman DJ, Van Essen DC., Cereb Cortex. 1991, Distributed hierarchical processing in the primate cerebral cortex. Jan-Feb;1(1):1-47.

- Felsen G, Dan Y., Nat Neurosci. 2005, A natural approach to studying vision. Dec;8(12):1643-6. Review.
- Felsen G, Touryan J, Han F, Dan Y., PLoS Biol. 2005, Cortical sensitivity to visual features in natural scenes. Oct;3(10):e342. Epub 2005 Sep 27.
- Ferster, D., J. Neurosci. 1986. Orientation selectivity of synaptic potentials in neurons of cat primary visual cortex. 6, 1284-1301.
- Ferster, D. and Jagadeesh, B., J. Neurosci. 1992. EPSP-IPSP interactions in cat visual cortex studied with in vivo whole-cell patch recording. 12, 1262-1274.
- Ferster, D. & Koch, C., Trends Neurosci. 1987. Neuronal connections underlying orientation selectivity in cat visual cortex. 10, 487-492.
- Ferster, D. and Miller, K.D., Ann. Rev. Neurosci. 2000. Neural mechanisms of orientation selectivity in the visual cortex. 23, 441-472.
- Field DJ., J Opt Soc Am A. 1987, Relations between the statistics of natural images and the response properties of cortical cells. Dec;4(12):2379-94.
- Field, D.J., Hayes, A. and Hess, R.F., Vision Res 1993. Contour integration by the human visual system: evidence for a local "association field". 33, 173-193.
- Fiser J, Chiu C, Weliky M., Nature. 2004, Small modulation of ongoing cortical dynamics by sensory input during natural vision. Sep 30;431(7008):573-8.
- Fitzpatrick, D., Current Opinion in Neurobiology 2000. Seeing beyond the receptive field in primary visual cortex. 10, 438-443.
- Foldiak P., Biological Cybernetics 1990. Forming sparse representations by local anti-Hebbian learning, vol. 64, pp. 165-170.
- Fodor J., 1987. Psychosemantics. Cambridge, Mass.: Bradford Books.
- Fodor, Jerry and Zenon W. Pylyshyn. 1988. "Connectionism and Cognitive Architecture: A Critical Analysis." In Connections and Symbols, ed. Pinker, Steven and Jacques Mehler, MIT Press, 1988.
- Frégnac Y., 2002. Hebbian synaptic plasticity. In The Handbook of Brain Theory and Neural networks, 2nd edition, M. Arbib, ed. (MIT Press). pp. 512-522.
- Freeman W., Scientific American 1991, The physiology of perception. 264 (2) 78-85.
- Fusi S, Drew PJ, Abbott LF., Neuron. 2005, Cascade models of synaptically stored memories. Feb 17;45(4):599-611.
- Gabor D., Journal of IEE London 1946. Theory of communication. Vol.93, No.3, Nov.,
- Gammaitoni L., P. Hanggi, P. Jung, and F. Marchesoni, Rev.Mod.Phys. 1998. Stochastic Resonance, 70, 223.
- Gardner TS, Collins JJ., Nature. 2000, Neutralizing noise in gene networks. Jun 1;405(6786):520-1.
- Gardner JL, Anzai A, Ohzawa I, & Freeman RD. Vis Neurosci 1999. Linear and nonlinear contributions to orientation tuning of simple cells in the cat's striate cortex. 16: 1115–1121.
- Gawne TJ, Kjaer TW, Richmond BJ., J Neurophysiol. 1996. Latency: another potential code for feature binding in striate cortex. Aug;76(2):1356-60.
- Geisler W.S., Nature 1999. Motion streaks provide a spatial code for motion direction, 400, 65–69.
- Geisler W.S., Albrecht D.G., Crane A.M., and Stern L., Vis Neurosci 2001. Motion direction signals in the primary visual cortex of cat and monkey, 18, 501–516.
- Geisler WS, Albrecht DG., Vision Res. 1992. Cortical neurons: isolation of contrast gain control. Aug; 32(8):1409-10.
- Georgopoulos AP., Neuron 1994, New concepts in generation of movement. Aug;13(2):257-68. Review.

- Georges S, Series P, Fregnac Y, Lorenceau J., Vision Res. 2002. Orientation dependent modulation of apparent speed: psychophysical evidence. Nov;42(25):2757-72.
- Gilbert, C.D. and Wiesel, T.N., J. Neurosci. 1989. Columnar specificity of intrinsic horizontal and corticocortical connections in cat visual cortex. 9, 2432-2442.
- Goethe J. W. V., 1808, from the Preface to his 'Scientific Studies' ed. Douglas Miller, New York, Suhrkamp, 1988.
- Gödel K., Mschr. Math. Phys. 1931, Über formal unentscheidbare sätze der principia Mathematica und verwandter systeme I. 38, 173-189.
- Goldman MS, Maldonado P, Abbott LF., J Neurosci. 2002, Redundancy reduction and sustained firing with stochastic depressing synapses. Jan 15;22(2):584-91.
- Gray CM., Neuron. 1999, The temporal correlation hypothesis of visual feature integration: still alive and well., Sep;24(1):31-47, 111-25.
- Grinvald A, Lieke EE, Frostig RD, Hildesheim R., J Neurosci. 1994, Cortical point-spread function and long-range lateral interactions revealed by real-time optical imaging of macaque monkey primary visual cortex. May;14(5 Pt 1):2545-68.
- Harpur GF and Prager RW., Network 1996. Development of low entropy coding in a recurrent network. 7:277-284.
- Harris CM, Hainline L, Abramov I, Lemerise E, Camenzuli C. Vision Res 1988. The distribution of fixation durations in infants and naive adults. 28:419-432.
- Hasson U, Nir Y, Levy I, Fuhrmann G, Malach R., Science 2004, Intersubject synchronization of cortical activity during natural vision. Mar 12;303(5664):1634-40.
- Hahnloser, R.H., Kozhevnikov, A.A. & Fee, M.S. Nature 2002, An ultra-sparse code underlies the generation of neural sequences in a songbird. Sep 5;419(6902):65-70.
- Heeger DJ., Vis Neurosci 1992. Half-squaring in responses of cat striate cells. 9: 427-443.
- Heeger DJ., J Neurophysiol 1993. Modeling simple-cell direction selectivity with normalized, halfsquared, linear operators. 70: 1885-1898.
- Heggelund P, Albus K., Exp Brain Res. 1978. Response variability and orientation discrimination of single cells in striate cortex of cat. Jun 19;32(2):197-211.
- Heneghan C, Chow CC, Collins JJ, Imhoff TT, Lowen SB and Teich MC. Physical Review E 1996. Information measures quantifying aperiodic stochastic resonance. 54: R2228-R2231.
- Hennig M., Kerscher N., Funke K., Worgotter F., Neurocomputing, 2002, Stochastic resonance in visual cortical neurons: does the eye-tremor actually improve visual acuity?, 44-46C.115-121
- Henry, G.H., Bishop, P.O., Tupper, R.M. and Dreher, B., Vision Res. 1973. Orientation specificity and response variability of cells in the striate cortex. 13, 1771-1779.
- Hess R.F., Beaudot K.H.A., Mullen K.T., Vision Res 2001. Dynamics of contour integration, 41, 1023-1037.
- Hinton G.E. and Sejnowski. T.J. 1986, Learning and relearning in Boltzmann machines. In Parallel distributed processing, eds Rumelhart and McClelland, MIT press, Cambridge 282-317.
- Hinton G.E. and Zemel. R.S. 1994, Advances in neural information processing systems 6, 1994, Autoencoders, Minimum Description Length and Helmholtz Free energy. Cowan, Tesauro & Alspector (Eds.), Morgan Kaufmann: San Mateo, CA.
- Hirsch, J.A., Alonso, J.M., Reid, R.C. and Martinez, L.M., J. Neurosci. 1998. Synaptic integration in striate cortical simple cells. 18, 9517-9528.
- Hirsch JA, Gilbert CD., J Neurosci. 1991, Synaptic physiology of horizontal connections in the cat's visual cortex. Jun;11(6):1800-9.
- Hoffmann K.P., Stone J., Brain Res. 1971. Conduction velocity of afferents to cat visual cortex: a correlation with cortical receptive field properties, 32, 460-466.

- Holcman D, Tsodyks M., PLoS Comput Biol. 2006, The emergence of Up and Down states in cortical networks. Mar;2(3):e23.
- Hopfield JJ., Proc Natl Acad Sci U S A., 1982, Neural networks and physical systems with emergent collective computational abilities. Apr;79(8):2554-8.
- Hubel D.H., Wiesel T.N., J. Physiol. 1962, Receptive fields, binocular interaction and functional architecture in the cat's visual cortex, 160 106–154.
- Ikegaya Y, Aaron G, Cossart R, Aronov D, Lampl I, Ferster D, Yuste R., Science. 2004, Synfire chains and cortical songs: temporal modules of cortical activity. Apr 23;304(5670):559-64.
- Innocenti, G.M. and Fiore, L., Brain Res. 1974. Post-synaptic inhibitory components of the responses to moving stimuli in area 17. 80, 122-126.
- Jagadeesh, B., Wheat, H.S., Kontsevich, L.L., Tyler, C.W. and Ferster, D., Journal of Neurophysiology 1997. Direction selectivity of synaptic potentials in simple cells of the cat visual cortex. 78, 2772-2789.
- Jagadeesh B, Wheat HS, Kontsevich LL, Tyler CW, Ferster D. J Neurophysiol. 1997, Direction selectivity of synaptic potentials in simple cells of the cat visual cortex. Nov;78(5):2772-89.
- James W., 1890, The principles of psychology , New York, 1890, 2 vol, available on-line at <http://psychclassics.yorku.ca/James/Principles/index.htm>
- Jaynes ET, Phys Rev 1957, Information theory and statistical mechanics. 106:620–630.
- Jaynes ET, Phys Rev 1957, Information theory and statistical mechanics II. 108:171–190.
- Jaynes ET, 1979, The Maximum Entropy Principle. Eds Levine RD and Tribus M (Cambridge MA : MIT) p 15.
- Jenkins, J. B., & Dallenbach, K. M., American Journal of Psychology, 1924, Oblivescence during sleep and waking, 35, 605–612.
- Jerison, H. J., 1973, Evolution of the brain and intelligence. New York: Academic.
- Johnson TJ, Wilke CO.. Artificial Life 2004, Evolution of resource competition between mutually dependent digital organisms. Spring;10(2):145-56.
- Jones JP, Palmer LA., J Neurophysiol. 1987. An evaluation of the two-dimensional Gabor filter model of simple receptive fields in cat striate cortex. Dec;58(6):1233-58.
- Jones H.E., Wang W., Sillito A.M., J Neurophysiol 2002. Spatial organization and magnitude of orientation contrast interactions in primate V1, 88, 2796–2808.
- Jones LM, Depireux DA, Simons DJ, Keller A. Science. 2004, Robust temporal coding in the trigeminal system. Jun 25;304(5679):1986-9.
- Jutten C., and Herault J., Signal Processing 1991, Blind separation of sources,.24:1-10.
- Jung C. G., 1953, Two Essays on Analytic Psychology, Collected Works, v. 7.
- Kaiser M, Lappe M., Neuron 2004. Perisaccadic Mislocalization Orthogonal to Saccade Direction. Vol. 41, 293–300,
- Kapadia, M., Westheimer, G. and Gilbert, C.D., Journal of Neurophysiology 2000. Spatial distribution of contextual interactions in primary visual cortex and in visual perception. 84, 2048-2062.
- Kapadia, M.K., Ito, M., Gilbert, C.D. and Westheimer, G., Neuron 1995. Improvement in visual sensitivity by changes in local context: Parallel studies in human observers and in V1 of alert monkeys. 15, 843-856.
- Kara P, Reinagel P, Reid RC., Neuron. 2000, Low response variability in simultaneously recorded retinal, thalamic, and cortical neurons. Sep;27(3):635-46.
- Kayser C, Salazar RF, Konig P., J Neurophysiol. 2003, Responses to natural scenes in cat V1. Sep;90(3):1910-20.

- Kenet T, Bibitchkov D, Tsodyks M, Grinvald A, Arieli A., *Nature*. 2003, Spontaneously emerging cortical representations of visual attributes. Oct 30;425(6961):954-6.
- Kisvarday Z.F., Toth E., Rausch M., Eysel U.T., *Cereb. Cortex* 1997. Orientation specific relationship between populations of excitatory and inhibitory lateral connections in the visual cortex of the cat, 7, 605–618.
- Kisvarday, Z.F., Buzas, P. and Eysel, U.T., *Cereb. Cortex* 2001. Calculating direction maps from intrinsic signals revealed by optical imaging. 11, 636-647.
- Kisvarday, Z.F., Kim, D.S., Eysel, U.T. and Bonhoeffer, T., *Eur. J. Neurosci.* 1994. Relationship between lateral inhibitory connections and the topography of the orientation map in cat visual cortex. 6, 1619-1632.
- Knierim J.J., Van Essen D.C., *J Neurophysiol* 1992. Neuronal responses to static texture patterns in area V1 of the alert macaque monkey, 67. 961–970.
- Koch C., Segev I., *Nature Neuroscience* 2000, The role of single neurons in information processing. • volume 3 • november 1171-1177.
- Kolmogorov A.N., *IEEE Trans Inform Theory* 1968, Logical basis for information theory and probability theory. IT-14, 662-664.
- Kording KP, Kayser C, Betsch BY, Konig P., *J Neurosci Methods*. 2001, Non-contact eye-tracking on cats. Sep 30;110(1-2):103-11.
- Kubo R., *Rep. Prog. Phys.* 1966. The fluctuation-dissipation theorem. **29** 255-284.
- Lachaux JP, Rodriguez E, Martinerie J, Varela FJ., *Hum Brain Mapp.* 1999, Measuring phase synchrony in brain signals. ;8(4):194-208.
- Lampl I, Reichova I, Ferster D., *Neuron*. 1999, Synchronous membrane potential fluctuations in neurons of the cat visual cortex. Feb;22(2):361-74.
- Lampl I, Anderson JS, Gillespie DC, Ferster D. *Neuron*. 2001, Prediction of orientation selectivity from receptive field architecture in simple cells of cat visual cortex. Apr;30(1):263-74.
- Landau & Lifchitz, 1967. *Physique statistique*, Mir.
- Laughlin S.B., *Z. Naturforsch* 1981, A simple coding procedure enhances a neuron's information capacity. 36c, 910–912.
- Lempel A. and Ziv J., *IEEE Trans. Inform. Theory* 1976. On the complexity of finite sequences. Vol. IT-22, no. 1, pp. 75--81, January.
- Lenski RE, Ofria C, Pennock RT, Adami C., *Nature*. 2003, The evolutionary origin of complex features. May 8;423(6936):139-44.
- Levitt, J.B. and Lund, J.S., *Nature* 1997. Contrast dependence of contextual effects in primate visual cortex. 387, 73-76.
- Li M. and Vitanyi PMB, 1997, *An Introduction to Kolmogorov Complexity and Its Applications*. Springer-Verlag, New York, second edition.
- Linsker R., *Computer* 1988, Self-organization in a perceptual network,, vol. 21, pp. 105--117.
- Livingstone M., *Neuron* 1998. Mechanisms of direction selectivity in macaque V1, 20 509–526.
- Lotka A.J., *Proc Natl Acad Sci* 1922. Contribution to the energetics of evolution., 8: pp. 147–51.
- Lotka A.J. *Proc Natl Acad Sci* 1922 Natural selection as a physical principle. 8, pp 151–54.
- Lu ZL, Doshier BA., *Vision Res.* 1998, External noise distinguishes attention mechanisms. May;38(9):1183-98.
- Machens CK, Wehr MS, Zador AM. *J Neurosci.* 2004, Linearity of cortical receptive fields measured with natural sounds. Feb 4;24(5):1089-100.
- Machens CK, Gollisch T, Kolesnikova O, Herz VM, *Neuron*. 2005. Testing the efficiency of sensory coding with optimal stimulus ensembles. 47. 447-456.

- MacKay, D. J. C., 1996. Maximum likelihood and covariant algorithms for independent component analysis (Tech. Rep.). Cambridge University, Cavendish Laboratory.
- Maex, R. and Orban, G.A., J. Neurophysiol. 1996. Model circuit of spiking neurons generating directional selectivity in simple cells. 75, 1515-1545.
- Maldonado, P. E., Godecke, I., Gray, C. M. & Bonhoeffer, T., Science 1997. Orientation selectivity in pinwheel centers in cat striate cortex. 276, 1551-1555.
- Malach, R., Amir, Y., Harel, M. and Grinvald, A., PNAS USA. 1993. Relationship between intrinsic connections and functional architecture revealed by optical imaging and in vivo targeted biocytin injections in primate striate cortex. 90, 10469-10473.
- Mainen ZF, Sejnowski TJ., Science. 1995, Reliability of spike timing in neocortical neurons. Jun 9;268(5216):1503-6.
- Marino, L., Evolutionary Anthropology 1996. What dolphins can tell us about primate evolution. 5, 81-86.
- Martignon, L., Deco, G., Laskey, K., Diamond, M., Freiwald, W. A., & Vaadia, E. Neural Computation 2000. Neural coding: Higher-order temporal patterns in the neurostatistics of cell assemblies. 12(11), 2621-2653.
- Martin K. AC, Curr. Opinion in Neurobiology 2002. Microcircuits in visual cortex. 12, 1-9.
- Martinez, L. M., Alonso, J. M., Reid, R. C. & Hirsch, J. A., J Physiol 2002. Laminar processing of stimulus orientation in cat visual cortex. 540, 321-33.
- Martinez-Conde S, Macknik SL, Hubel DH. Proc Natl Acad Sci U S A. 2002, The function of bursts of spikes during visual fixation in the awake primate lateral geniculate nucleus and primary visual cortex. Oct 15;99(21):13920-5. Epub 2002 Oct 02.
- Martinez-Conde S, Macknik SL, Hubel DH., Nat Rev Neurosci. 2004, The role of fixational eye movements in visual perception. Mar;5(3):229-40.
- Martinez-Conde S, Macknik SL, Troncoso XG, Dyar TA., Neuron. 2006. Microsaccades counteract visual fading during fixation. Jan 19;49(2):297-305.
- Maunsell, J.H.R. and Newsome, W.T., Annual Review of Neuroscience 1987. Visual processing in monkey extra striate cortex. 10, 363-402.
- McCulloch W.S. & Pitts W.H., Bull. Mathemat. Biophys. 1943, A logical calculus of the ideas immanent in nervous activity. 5, 115-113.
- McLaughlin, D., Shapley R., Shelley, M. and Wielaard, D.J., Proc. Natl. Acad. Sci. USA. 2000. A neuronal network model of macaque primary visual cortex (V1): orientation selectivity and dynamics in the input layer 4Calpha. 97, 8087-8092.
- Mechler F, Ringach DL., Vision Res. 2002. On the classification of simple and complex cells. Apr;42(8):1017-33.
- Mechler, F., Victor, J.D., Purpura, K.P. and Shapley, R., J. Neurosci. 1998. Robust temporal coding of contrast by V1 neurons for transient but not for steady-state stimuli. 18, 6583-6598.
- Merleau-Ponty, 1960, L'oeil et l'esprit . Paris: Gallimard.
- Mezard M., Science. 2003, Physics/computer science. Passing messages between disciplines. Sep 19;301(5640):1685-6.
- Miller LM, Schreiner CE., J. Neurosci. 2000, Stimulus-based state control in the thalamocortical system. Sep 15;20(18):7011-6.
- Miikkulainen R., Bednar J.A., Choe Y., and J. Sirosh J., 1997. Self-Organization, Plasticity, and Low-level Visual Phenomena in a Laterally Connected Map Model of the Primary Visual Cortex. In R. L. Goldstone, P. G. Schyns and D. L. Medin (editors), Psychology of Learning and Motivation, volume 36: Perceptual Learning, 257-308. San Diego, CA: Academic Press.
- Mikami, A., Newsome, W.T. and Wurtz, R.H., Journal of Neurophysiology 1986. Motion selectivity in macaque visual cortex II. Spatiotemporal range of directional interactions in MT and V1. 55, 1308-1339.

- Mizobe K., Polat U., Pettet M.W., Kasamatsu T., *Vis Neurosci* 2001. Facilitation and suppression of single striate-cell activity by spatially discrete pattern stimuli presented beyond the receptive field, 18, 377–391.
- Monier C, Chavane F, Baudot P, Graham LJ, Fregnac Y., *Neuron*. 2003, Orientation and direction selectivity of synaptic inputs in visual cortical neurons: a diversity of combinations produces spike tuning. Feb 20;37(4):663-80.
- Monier C., 2002, Diversité fonctionnelle de l'intégration synaptique dans le cortex visuel primaire. Thesis.
- Monod J., 1970: Le hasard et la nécessité. Essai sur la philosophie naturelle de la biologie moderne. Paris, Le Seuil.
- Moore C.I., Nelson S.B., *J. Neurophysiol.* 1998. Spatio-temporal subthreshold receptive fields in the vibrissa representation of rat primary somatosensory cortex, 80, 2882–2892.
- Morrone, M.C., Ross, J., and Burr, D.C. (1997). Apparent position of visual targets during real and simulated saccadic eye movements. *J. Neurosci.* 17, 7941–7953.
- Morrone MC, Ross J, Burr D., *Nat Neurosci.* 2005. Saccadic eye movements cause compression of time as well as space. Jul;8(7):950-4.
- Mountcastle V.B., *Brain*, 1997. The columnar organisation of the neocortex. 120, 701-722.
- Movshon J.A., *J Physiol.* 1975. The velocity tuning of single units in cat striate cortex. Aug;249(3):445-68.
- Murakoshi T., Guo J.-Z., Ichonose T., *Neurosci. Lett.* 1993. Electrophysiological identification of horizontal synaptic connections in rat visual cortex in vitro, 163 211– 214.
- Nadal J.-P. and Parga N, *Network: Computation in Neural Systems* 1994. Nonlinear neurons in the low-noise limit: a factorial code maximizes information transfer, 5(4):565-581.
- Nelson J.I., Frost B.J., *Exp Brain Res* 1985. Intracortical facilitation among co-oriented, co-axially aligned simple cells in cat striate cortex, 61, 54–61.
- Nelson, S., Toth, L., Sheth, B. and Sur, M., *Science* 1994. Orientation selectivity of cortical neurons during intracellular blockade of inhibition. 265, 774-777.
- Newsome, W.T., Britten, K.H. and Movshon, J.A., *Nature* 1989. Neuronal correlates of a perceptual decision. 341, 52-54.
- Nowak L.G., Bullier J., *Cereb. Cortex* 1997. The timing of information transfer in the visual system, 12 205–241.
- Nowak LG, Sanchez-Vives MV, McCormick D.A., *Cereb Cortex.* 1997, Influence of low and high frequency inputs on spike timing in visual cortical neurons. Sep;7(6):487-501.
- Obradovic, D. & Deco, G., *Neural Computation* 1998. Information Maximization and Independent Component Analysis: Is There a Difference?, 10:8, 2085-2101.
- Olivier E., Grantyn A., Chat M., Berthoz A., *Exp. Brain Res.*, 1993, The control of slow orienting eye movements by tectoreticulospinal neurons in the cat: behavior, discharge patterns and underlying connections, 93: 435-449.
- Olshausen BA, Field DJ., *Nature* 1996, Emergence of simple-cell receptive field properties by learning a sparse code for natural images. Jun 13;381(6583):607-9.
- Ofria C, Adami C, Collier TC., *J Theor Biol.* 2003. Selective pressures on genomes in molecular evolution. Jun 21;222(4):477-83.
- O'Regan JK, Noe A., *Behav Brain Sci.* 2001, A sensorimotor account of vision and visual consciousness. Oct;24(5):939-73; discussion 973-1031. Review.
- Palmer L.A., Davis T.L., *J. Neurophysiol.* 1981, Receptive field structure in cat striate cortex. 46(2):260-276.
- Pack CC, Conway BR, Born RT, Livingstone MS., *J Neurosci.* 2006. Spatiotemporal structure of nonlinear subunits in macaque visual cortex. Jan 18;26(3):893-907.

- Parra L, & Deco G., Neural Netw. 1997, Non-linear Feature Extraction by Redundancy Reduction in an Unsupervised Stochastic Neural Network. Jun;10(4):683-691.
- Paré, D., Shink, E., Gaudreau, H., Destexhe, A. and Lang, E., J. Neurophysiol. 1998. Impact of spontaneous synaptic activity on the resting properties of cat neocortical pyramidal neurons in vivo. 79, 1450-1460.
- Parisi G., 2003, complexité et intelligence. In « L'héritage de Kolmogorov en physique », R. Livi, A. Vulpiani, eds Belin
- Pearlmutter BA, Parra LC, Actes ICONIP'96, 1996, A context-sensitive generalisation of ICA. pp. 151-157, Hong-Kong.
- Perruchet, P., Pacteau, C. & Gallego, J. British Journal of Psychology 1997. Abstraction of covariation in incidental learning and covariation bias. 88, 441-458.
- Petrov Y, Zhaoping L., J Opt Soc Am A Opt Image Sci Vis. 2003, Local correlations, information redundancy, and sufficient pixel depth in natural images. Jan;20(1):56-66.
- Philipona D, O'Regan JK, Nadal JP., Neural Comput. 2003, Is there something out there? Inferring space from sensorimotor dependencies. Sep;15(9):2029-49.
- Prevert J., 1949. Paroles. Edition revue et augmentée. Sl, Gallimard.
- Pritchard RM, Heron W., Can J Psychol. 1960, Small eye movements of the cat. Jun;14:131-7.
- Polat, U. and Sagi, D., Vision Res. 1994. The architecture of perceptual spatial interactions. 34, 73-78.
- Polat, U. and Sagi, D., Vision Res. 1993. Lateral interactions between spatial channels: suppression and facilitation revealed by lateral masking experiments. 33(7):993-9.
- Polat, U., Mizobe, K., Pettet, M.W., Kasamatsu, T. and Norcia, A.M., Nature 1998. Collinear stimuli regulate visual responses depending on cell's contrast threshold. 391, 580-584
- Polat, U. and Sagi, D., Vision Res. 2006. Temporal asymmetry of collinear lateral interactions. Mar;46(6-7):953-60.
- Priebe NJ, Mechler F, Carandini M, Ferster D., Nat Neurosci. 2004. The contribution of spike threshold to the dichotomy of cortical simple and complex cells. Oct;7(10):1113-22.
- Prigogine E., 2002. in « La complexité, vertiges et promesses" Réda Benkirane eds Le Pommier - octobre 2002. Paris.
- Rao RP, Sejnowski TJ., Philos Transact A Math Phys Eng Sci. 2003, Self-organizing neural systems based on predictive learning. Jun 15;361(1807):1149-75.
- Rao RP, Ballard DH., Nat Neurosci. 1999, Predictive coding in the visual cortex: a functional interpretation of some extra-classical receptive-field effects. Jan;2(1):79-87.
- Ratliff F., Mach Bands: Quantitative Studies on Neural Networks in the Retina, Holden-Day Inc, San Francisco, 1965, p. 365.
- Reeves H., 1986, L'heure de s'ennivrer, l'univers a-t-il un sens. Seuil, Paris.
- Redington, M. & Chater, N. Language and Cognitive Processes 1998. Connectionist and statistical approaches to language acquisition: A distributional perspective. 13, 129-191.
- Redlich AN, Neural Computation 1993, Redundancy reduction as a strategy for unsupervised learning, 5:289--304.
- Reichardt, W., 1961. Autocorrelation, a principle for the evaluation of sensory information by the central nervous system. In "Principles of Sensory Communication", eds. W. A. Rosenblith (New-York: J. Wiley and Sons), 303-317.
- Reich DS, Mechler F, Victor JD., Science. 2001 Independent and redundant information in nearby cortical neurons. Dec 21;294(5551):2566-8.
- Reich DS, Mechler F, Victor JD., J Neurophysiol. 2001, Temporal coding of contrast in primary visual cortex: when, what, and why. Mar;85(3):1039-50.
- Reid, R. C., Soodak, R. E., and Shapley, R. M., Proc Natl Acad Sci USA 1987. Linear mechanisms of directional selectivity in simple cells of cat striate cortex. 84, 8740-8744.

- Reid RC, Victor JD, Shapley RM., *Vis Neurosci.* 1992, Broadband temporal stimuli decrease the integration time of neurons in cat striate cortex. Jul;9(1):39-45.
- Reinagel P, Reid RC. *J Neurosci.* 2000. Temporal coding of visual information in the thalamus. Jul 15;20(14):5392-400.
- Reinagel P, Zador AM., *Network.* 1999, Natural scene statistics at the centre of gaze. Nov;10(4):341-50.
- Richardson, K. & Carthy, T., *British Journal of Psychology* 1990. The abstraction of covariation in conceptual representation. 81: 415-438.
- Riehle A, Grun S, Diesmann M, Aertsen A., *Science.* 1997, Spike synchronization and rate modulation differentially involved in motor cortical function. Dec 12;278(5345):1950-3.
- Rieke F, Bodnar DA, Bialek W., *Proc Biol Sci.* 1995, Naturalistic stimuli increase the rate and efficiency of information transmission by primary auditory afferents. Dec 22;262(1365):259-65.
- Rieke F., Warland D., de Ruyter van Steveninck R., and Bialek W., 1997, *Spikes: Exploring the Neural Code.* MIT Press, Cambridge.
- Rimbaud Arthur, 1871, Première lettre du Voyant (à Georges Izambard, 13 mai)
- Ringach, D. L., Bredfeldt, C. E., Shapley, R. M. & Hawken, M. J., *J Neurophysiol* 2002. Suppression of neural responses to non-optimal stimuli correlates with tuning selectivity in macaque V1. 87, 1018-27.
- Rissanen J., 1978, Modeling by shortest data description. *Automatica*, vol. 14, pp. 465-471.
- Rodriguez E, George N, Lachaux JP, Martinerie J, Renault B, Varela FJ., *Nature.* 1999, Perception's shadow: long-distance synchronization of human brain activity. Feb 4;397(6718):430-3.
- Ross, J., Morrone, M.C., Goldberg, M.E., and Burr, D.C. (2001). Changes in visual perception at the time of saccades. *Trends Neurosci.* 24, 113-121.
- Roerig, B. and Kao, J.P., *J. Neurosci.* 1999. Organization of intracortical circuits in relation to direction preference maps in ferret visual cortex. 19, RC44.
- Rucci M, Edelman GM, Wray J., *J Neurosci.* 2000. Modeling LGN responses during free-viewing: a possible role of microscopic eye movements in the refinement of cortical orientation selectivity. Jun 15;20(12):4708-20.
- Rucci M, Desbordes G., *J Vis.* 2003. Contributions of fixational eye movements to the discrimination of briefly presented stimuli. Dec 19;3(11):852-64.
- Ruderman DL, Bialek W., *Phys Rev Lett.* 1994, Statistics of natural images: Scaling in the woods. Aug 8;73(6):814-817.
- Ruelle, D., 1991, *Hazard et chaos*, edition Odile Jacob Paris France.
- Ruff, P.I., Rauschecker, J.P. and Palm, G.A., *Biol. Cybern.* 1987. Model of direction-selective "simple" cells in the visual cortex based inhibition asymmetry. 57, 147-157.
- Rust NC, Schwartz O, Movshon JA, Simoncelli EP., *Neuron.* 2005. Spatiotemporal elements of macaque v1 receptive fields. Jun 16;46(6):945-56.
- Sabatini, S.P. and Solari, F., *Biol. Cybern.* 1999. An architectural hypothesis for direction selectivity in the visual cortex: the role of spatially asymmetric intracortical inhibition. 80, 171-183.
- Sakai KL., *Science.* 2005, Language acquisition and brain development. Nov 4;310(5749):815-9.
- Sato, H., Daw, N.W. and Fox, K., *Brain Res.* 1991. An intracellular recording study of stimulus-specific response properties in cat area 17. 544, 156-161.
- Sawaguchi, T. & Kudo, H., *Primates* 1990. Neocortical development and social structure in primates., 31, 283-290.

- Sceniak M.P., Ringach D.L., Hawken M.J., Shapley R., *Nature Neurosci* 1999. Contrast's effect on spatial summation by macaque V1 neurons, 2; 733–739.
- Schiller PH, Finlay BL, Volman SF., *J Neurophysiol.* 1976, Quantitative studies of single-cell properties in monkey striate cortex. V. Multivariate statistical analyses and models. Nov;39(6):1362-74.
- Schmidhuber, J. (1992). Learning factorial codes by predictability minimization. *Neural Computation*, 4(6):863--879.
- Schmidhuber J., *Neural Networks* 1997, Discoverin neural nets with low Kolmogorov complexity and high generalisation capability. 10(5) 857-873.
- Schmidt, K.E., Goebel, R., Lowel, S. and Singer, W., *Eur J Neurosci.* 1997. The perceptual grouping criterion of colinearity is reflected by anisotropies of connections in the primary visual cortex. 9, 1083-9.
- Schneidman, E., Bialek, W., Berry, M.J. II. *J. Neurosci.* 2003 Synergy, redundancy, and independence in population codes. Dec 17;23(37):11539-53.
- Schrodinger E., 1944, *What is Life ?* Cambridge University Press, 1967.
- Schuett, S., Bonhoeffer, T., and Hubener, M., *Neuron* 2001. Pairing-induced changes of orientation maps in cat visual cortex. 32, 325-337.
- Schummers, J., Marino, J. and M. Sur, *Neuron* 2002. Synaptic integration by V1 neurons depends on location within the orientation map. 36, 969-978.
- Schwartz O, Simoncelli EP., *Nat Neurosci.* 2001, Natural signal statistics and sensory gain control. Aug;4(8):819-25.
- Sclar, G. and Freeman, R.D. *Exp. Brain Res.* 1982. Orientation selectivity in the cat's striate cortex is invariant with stimulus contrast. 46, 457-461.
- Sclar G, Maunsell JH, & Lennie P., *Vision Res* 1990. Coding of image contrast in central visual pathways of the macaque monkey. 30: 1–10.
- Series P, Lorenceau J, Fregnac Y., *J Physiol Paris.* 2003. The "silent" surround of V1 receptive fields: theory and experiments. Jul-Nov;97(4-6):453-74. Review.
- Series P, Georges S, Lorenceau J, Fregnac Y., *Vision Res.* 2002. Orientation dependent modulation of apparent speed: a model based on the dynamics of feed-forward and horizontal connectivity in V1 cortex. Nov;42(25):2781-97.
- Series P, Latham PE, Pouget A., *Nat Neurosci.* 2004, Tuning curve sharpening for orientation selectivity: coding efficiency and the impact of correlations. Oct;7(10):1129-35.
- Shadlen MN, Newsome WT., *J Neurosci.* 1998, The variable discharge of cortical neurons: implications for connectivity, computation, and information coding. May 15;18(10):3870-96.
- Shannon C.E., 1948 ``A mathematical theory of communication," *Bell System Technical Journal*, vol. 27, pp. 379-423 and 623-656, July and October,.
- Shannon C.E & Weaver, W, 1949. *The Mathematical Theory of Communication.* The University of Illinois Press, Urbana, Illinois, 1949.
- Sharpee TO, Sugihara H, Kurgansky AV, Rebrik SP, Stryker MP, Miller KD., *Nature* 2006, Adaptive filtering enhances information transmission in visual cortex. Feb 23;439(7079):936-42.
- Shmuel, A. and Grinvald, A., *J. Neurosci.* 1996. Functional organization for direction of motion and its relationship to orientation maps in cat area 18. 16, 6945-6964.
- Shu Y, Hasenstaub A, McCormick DA., *Nature.* 2003. Turning on and off recurrent balanced cortical activity. May 15;423(6937):288-93.
- Sillito, A.M., *J. Physiol.* 1979. Inhibitory mechanisms influencing complex cell orientation selectivity and their modification at high resting discharge levels. 289, 33-53.
- Sillito, A.M., Grieve, K.L., Jones, H.E., Cudeiro, J. and Davis, J., *Nature* 1995. Visual cortical mechanisms detecting focal orientation discontinuities. 378, 492-496.

- Sillito, A.M., Kemp, J.A., Milson, J.A. and Berardi, N., *Brain Res.* 1980. A re-evaluation of the mechanism underlying simple cell orientation selectivity. 194, 517-520.
- Singer W. *Ann N Y Acad Sci.* 2001, Consciousness and the binding problem. Apr;929:123-46. Review.
- Singer W, Gray CM., *Annu Rev Neurosci.* 1995, Visual feature integration and the temporal correlation hypothesis. ;18:555-86.
- Skottun BC, De Valois RL, Grosof DH, Movshon JA, Albrecht DG, Bonds AB., *Vision Res.* 1991. Classifying simple and complex cells on the basis of response modulation. ;31(7-8):1079-86. Review.
- Smolders JW, Aertsen AM, Johannesma PI., *Biol Cybern.* 1979, Neural representation of the acoustic biotope. A comparison of the response of auditory neurons to tonal and natural stimuli in the cat. Nov;35(1):11-20.
- Solomonoff, R., 1964. A formal theory of inductive inference i and II. *Information and Control*, 7 (pp. 1-22 and 224-254).
- Somers, D.C., Nelson, S.B. and Sur, M., *J. Neurosci.* 1995. An emergent model of orientation selectivity in cat visual cortical simple cells. 15, 5448-5465.
- Somers D.C, Todorov E., Siapas A.G., Toth L.J., Kim D., Sur M., *Cereb Cortex* 1998, A local circuit approach to understanding integration of long-range inputs in primary visual cortex, 8 204–217.
- Schneidman E, Still S, Berry MJ 2nd, Bialek W., *Phys Rev Lett.* 2003, Network information and connected correlations. Dec 5;91(23):238701.
- Smyth D, Willmore B, Baker GE, Thompson ID, Tolhurst DJ., *J Neurosci.* 2003, The receptive-field organization of simple cells in primary visual cortex of ferrets under natural scene stimulation. Jun 1;23(11):4746-59.
- Snodderly DM, Kagan I, Gur M. *Vis Neurosci.* 2001, Selective activation of visual cortex neurons by fixational eye movements: implications for neural coding. Mar-Apr;18(2):259-77.
- Srinivasan MV, Laughlin SB, Dubs A., *Proc R Soc Lond B Biol Sci.* 1982, Predictive coding: a fresh view of inhibition in the retina. Nov 22;216(1205):427-59.
- Steels L., *Trends Cogn Sci.* 2003, Evolving grounded communication for robots. Jul;7(7):308-312.
- Stemmler M., Usher M., Niebur E., *Science* 1995. Lateral interactions in primary visual cortex: a model bridging physiology and psychophysics, 269: 1877– 1880.
- Steriade M., *J Neurophysiol.* 2001, Impact of network activities on neuronal properties in corticothalamic systems. 2001 Jul;86(1):1-39. Review.
- Stevens CF., *Nature.* 2001, An evolutionary scaling law for the primate visual system and its basis in cortical function. May 10;411(6834):193-5.
- Strong, S., Koberle, R., de Ruyter van Steveninck, R. and Bialek, W., *Physical Review Letters* 1998. Entropy and information in neural spike trains, 80, 197-200.
- Schwartz O, Simoncelli EP., *Nat Neurosci.* 2001, Natural signal statistics and sensory gain control. Aug;4(8):819-25.
- Tehovnick E., Slocum W., Carvey C., Schiller P., *J. Neurophysiol* 2004, Phosphene induction and the generation of saccadic eye movements by striate cortex. Jan;93(1):1-19. Review.
- Theunissen FE, David SV, Singh NC, Hsu A, Vinje WE, Gallant JL., *Network.* 2001, Estimating spatio-temporal receptive fields of auditory and visual neurons from their responses to natural stimuli. Aug;12(3):289-316.
- Theunissen, F. and Miller, J. P., *J. Comput. Neurosci* 1995, Temporal encoding in nervous systems: a rigorous definition, 2:149-162.

- Thompson, K. G., Leventhal, A. G., Zhou, Y. F. & Liu, D., Visual Neurosci. 1994. Stimulus dependence of orientation and direction sensitivity of cat LGNd relay cells without cortical inputs: a comparison with area 17 cells. 11, 939-951.
- Thorpe S, Delorme A, Van Rullen R., Neural Netw. 2001, Spike-based strategies for rapid processing. Jul-Sep;14(6-7):715-25. Review.
- Timofeev, I., Grenier, F. and Steriade, M., Proc. Natl. Acad. Sci. USA. 2001. Disfacilitation and active inhibition in the neocortex during the natural sleep-wake cycle: an intracellular study. 98, 1924-1929.
- Toth L.J., Rao S.C., Kim D.S., Somers D., Sur M., Proc Natl Acad Sci USA 1996. Subthreshold facilitation and suppression in primary visual cortex revealed by intrinsic signal imaging, 93, 9869-9874.
- Touryan J, Felsen G, Dan Y., Neuron. 2005, Spatial structure of complex cell receptive fields measured with natural images. Mar 3;45(5):781-91.
- Touryan J, Lau B, Dan Y., J Neurosci. 2002. Isolation of relevant visual features from random stimuli for cortical complex cells. Dec 15;22(24):10811-8.
- Troyer, T.W., Krukowski, A.E., Priebe, N.J. and Miller, K.D., J. Neurosci. 1998. Contrast-invariant orientation tuning in cat visual cortex: thalamocortical input tuning and correlation based intracortical connectivity. 18, 5908- 5927.
- Tsodyks M, Kenet T, Grinvald A, Arieli A. Science 1999. Linking spontaneous activity of single cortical neurons and the underlying functional architecture. Dec 3;286(5446):1943-6.
- Tsodyks M, Gilbert C., Nature. 2004, Neural networks and perceptual learning. Oct 14;431(7010):775-81. Review.
- Tsodyks M, Markram H., PNAS 1997. The neural code between neocortical pyramidal neurons depends on neurotransmitter release probability. 94, 719-723.
- Turing A.M., Proc. Lond. Math. Soc. Ser. 1937, On computable numbers, with an application to the Entscheidungsproblem. 42, 230-265.
- Tusa R.J., Palmer L.A., Rosenquist A.C., J. Comp. Neurol. 1978. The retinotopic organization of area 17 (striate cortex) in the cat, 177 213-236.
- Vaadia E, Haalman I, Abeles M, Bergman H, Prut Y, Slovin H, Aertsen A., Nature. 1995, Dynamics of neuronal interactions in monkey cortex in relation to behavioural events. Feb 9;373(6514):515-8.
- Varela F., 1989, Autonomie et connaissance, Paris, Seuil.
- Varela F.J., Riv Biol. 1999, Cognition without representations. Sep-Dec;92(3):511-2.
- Van Hateren J.H., Ruderman D.L., Proc.R.Soc.Lond. 1998, Independent component analysis of natural image sequences yields spatio-temporal filters similar to simple cells in primary visual cortex. B, 265:2315-2320.
- Van Hateren JH., Biol Cybern. 1992, A theory of maximizing sensory information. 68(1):23-9.
- Victor JD, Purpura KP., J Neurophysiol. 1996, Nature and precision of temporal coding in visual cortex: a metric-space analysis. Aug;76(2):1310-26.
- Vinje WE, Gallant JL., Science. 2000, Sparse coding and decorrelation in primary visual cortex during natural vision. Feb 18;287(5456):1273-6.
- Vinje WE, Gallant JL., J Neurosci. 2002, Natural stimulation of the nonclassical receptive field increases information transmission efficiency in V1. Apr 1;22(7):2904-15.
- Volgushev, M., Pei, X., Vidyasagar, T.R. and Creutzfeldt, O.D. (1993). Excitation and inhibition in orientation selectivity of cat visual cortex neurons revealed by whole-cell recordings in vivo. Visual Neurosci. 10, 1151-1155.
- Volgushev, M., Pernberg, J. and Eysel, U.T., J. Neurosci. 2000. Comparison of the selectivity of postsynaptic potentials and spike responses in cat visual cortex. Eur. J. Neurosci. 12, 257-263.

- Von der Malsburg C., 1981, The Correlation Theory of Brain Function. Technical Report 81-2, Biophysical Chemistry, MPI.
- Von Foerster, H., 1960. On Self-Organizing Systems and Their Enviroments, in: Yovits, M. C., Cameron, S.; Self-Organizing Systems, London: 31-50.
- Von Neumann J., 1956, Probabilistic logics and the synthesis of reliable organisms from unreliable components. In Automata studies, CE. Shannon & J. McCarth eds, Princeton University press p 43-98.
- Von Neumann J., 1966, Theory of self-reproducing automata, AW. Burks eds, Urbana Illinois, University of Illinois Press.
- Wagner A., 2005, Robustness and evolvability in living systems. Princeton University press.
- Wang G. M., Sevick E. M., Mittag E., Searles D.J., Evans Denis J, Phys. Rev. Lett., 2002, Experimental Demonstration of Violations of the Second Law of Thermodynamics for Small Systems and Short Time Scales. (5) 89, 050601.
- Wang XJ, Liu Y, Sanchez-Vives MV, McCormick DA., J Neurophysiol. 2003, Adaptation and temporal decorrelation by single neurons in the primary visual cortex. Jun;89(6):3279-93.
- Watanabe S., 1981 “Pattern recognition as a quest for minimum entropy,” Pattern Recognition 13, 381–387 .
- Weaver W., & Shannon C. E., The Mathematical Theory of Communication 1949, Urbana, Illinois: University of Illinois Press.
- Weber C., Obermayer K., IJCNN (4) 2000. Structured Models from Structured Data: Emergence of Modular Information Processing within One Sheet of Neurons. 608-613
- Weber C., Obermayer K., Proc. 7th Int. Conf. Neur. Inf. Proc. 2000. Emergent neural computational architectures based on neuroscience: towards neuroscience-inspired computing. Springer-Verlag New York, Pages: 53 - 67
- Wehr M, Zador AM., Nature. 2003. Balanced inhibition underlies tuning and sharpens spike timing in auditory cortex. Nov 27;426(6965):442-6.
- Wennekers T, Ay N., Neural Comput. 2005 Finite state automata resulting from temporal information maximization and a temporal learning rule. Oct;17(10):2258-90.
- Wertheimer, M. (1912). Experimentelle Studien über das Sehen von Bewegung. In "Zeischrift für Psychology", eds. T. T. Shipley (New-York). Pp. 161-265
- Wiener MC, Oram MW, Liu Z, Richmond BJ., J Neurosci. 2001, Consistency of encoding in monkey visual cortex. Oct 15;21(20):8210-21.
- Wilent WB, Contreras D., Nat Neurosci. 2005, Dynamics of excitation and inhibition underlying stimulus selectivity in rat somatosensory cortex. Oct;8(10):1364-70. Epub 2005 Sep 11.
- Wilke CO, Adami C., Mutat Res. 2003, Evolution of mutational robustness. Jan 28;522(1-2):3-11.
- Winograd S. and Cowan J.D., 1963, Reliable Computation in the Presence of Noise. MIT Press.
- White J.S. and Adami C., Artificial life 2004, Bifurcation into Functional Niches in Adaptation. Vol. 10, Issue 2 - Spring 2004
- Wörgötter, F. & Eysel, U. T., Biol. Cybern. 1987. Quantitative determination of orientational and directional components in the response of visual cortical cells to moving stimuli. 57, 349-355.
- Wörgötter, F. and Koch, C., J. Neurosci. 1991. A detailed model of the primary visual pathway in the cat: comparison of afferent excitatory and intracortical inhibitory connection schemes for orientation selectivity. 11, 1959-1979.
- Worgötter, F. and Eysel, U.T. Experimental Brain Research. 1989. Axis of preferred motion is a function of bar length in visual cortical receptive fields. 76, 307-314.

- Wörgötter, F. and Eysel, U.T. Exp. Brain Res. 1991. Axial responses in visual cortical cells: spatio-temporal mechanisms quantified by Fourier components of cortical tuning curves. 83, 656-664.
- Worgotter F, Suder K, Zhao Y, Kerscher N, Eysel UT, Funke K., Nature. 1998, State-dependent receptive-field restructuring in the visual cortex. Nov 12;396(6707):165-8.
- Wolfe J., Brodie III E.D., and Wade M.J. (eds), 2000, Epistasis and the Evolutionary Process. Oxford University Press, Oxford, U.K..
- Yarbus, A. L. 1967. Eye movements during perception of complex objects. In L. A. Riggs (Ed.), Eye Movements and Vision (p. 171-196). New York:Plenum Press.
- Yoshioka, T., Blasdel, G.G., Levitt, J.B. and Lund, J.S., Cerebral Cortex. 1996. Relation between patterns of intrinsic lateral connectivity, ocular dominance and cytochrome oxidase-reactive regions in macaque monkey striate cortex. 6, 297-310.
- Yousef, T., Bonhoeffer, T., Kim, D. S., Eysel, U. T., Toth, E. & Kisvarday, Z. F., Eur. J. Neurosci. 1999. Orientation topography of layer 4 lateral networks revealed by optical imaging in cat visual cortex (area 18). 11, 4291-4308.
- Zar, J. H., 1974. Biostatistical analysis, fourth edition. New Jersey: Prentice-Hall Inc.
- Ziv J., and Lempel A., IEEE Trans. Info. Theory 1977, A Universal Algorithm for Sequential Data Compression. VOL. IT-23, NO. 3, MAY, p377-384.
- Zurek W.H., Rev. Mod. Phys., 2003, Decoherence, einselection, and the quantum origins of the classical. **75**, 715.
- Zvontin A.K., Levin L.A., Russ. Math. Surv. 1970, The complexity of finite objects and the development of the concepts of information and randomness by means of the theory of algorithms. 256, 83-124.